

AD-A273 003



2

NAVAL POSTGRADUATE SCHOOL Monterey, California

S DTIC
ELECTE
NOV 22 1993
A



THESIS

DESIGN, FABRICATION AND TEST
OF A VERTICAL ATTITUDE TAKEOFF AND LANDING
UNMANNED AIR VEHICLE

by

Robert B. Stoney

June 1993

Thesis Advisor:

Richard M. Howard

Approved for public release; distribution is unlimited.

93-28386



93 11 19 044

Unclassified

Security Classification of this page

REPORT DOCUMENTATION PAGE

1a Report Security Classification: Unclassified			1b Restrictive Markings		
2a Security Classification Authority			3 Distribution/Availability of Report		
2b Declassification/Downgrading Schedule			Approved for public release; distribution is unlimited.		
4 Performing Organization Report Number(s)			5 Monitoring Organization Report Number(s)		
6a Name of Performing Organization Naval Postgraduate School		6b Office Symbol (if applicable) AA/HO	7a Name of Monitoring Organization Naval Postgraduate School		
6c Address (city, state, and ZIP code) Monterey CA 93943-5000			7b Address (city, state, and ZIP code) Monterey CA 93943-5000		
8a Name of Funding/Sponsoring Organization		8b Office Symbol (if applicable)	9 Procurement Instrument Identification Number		
Address (city, state, and ZIP code)			10 Source of Funding Numbers		
			Program Element No	Project No	Task No
			Work Unit Accession No		
11 Title (include security classification) DESIGN, FABRICATION AND TEST OF A VERTICAL ATTITUDE TAKEOFF AND LANDING UNMANNED AIR VEHICLE.					
12 Personal Author(s) Stoney, Robert B.					
13a Type of Report Engineer's Thesis		13b Time Covered From To	14 Date of Report (year, month, day) 1993, June	15 Page Count 234	
16 Supplementary Notation The views expressed in this thesis are those of the author and do not reflect the official policy or position of the Department of Defense or the U.S. Government.					
17 Conati Codes			18 Subject Terms (continue on reverse if necessary and identify by block number)		
Field	Group	Subgroup	Unmanned Air Vehicle (UAV), Vertical Attitude Takeoff and Landing (VATOL), Tailsitter, Design, Fabrication, Test, Simulation		
19 Abstract (continue on reverse if necessary and identify by block number) Future fleet needs for real-time intelligence require an unmanned platform capable of operations from small surface combatants without the need for extensive support personnel and equipment and without causing disruption to the operations of the ship from which it operates. A candidate must not only takeoff and landing vertically but also be capable of high forward flight speeds and efficient on-station performance. The design and initial fabrication of a Vertical Attitude Takeoff and Landing (VATOL) Unmanned Air Vehicle (UAV) airframe was completed at the Naval Postgraduate School. The vehicle, called Archytas, was a combination of two existing UAV's--the AROD and Aquila--as well as locally manufactured components, including a canard and wing spar. The objective of creating Archytas was to provide a proof-of-concept platform for research to explore performance trade-offs and stability augmentation. A three-degree-of-freedom simulation was used as the focus of the design efforts, to validate design decisions made in the fields of propulsion, aerodynamics, structures and flight mechanics. Engine tests were conducted to determine thrust and control power. Structural components were designed, fabricated and then tested, making modifications where necessary to ensure sufficient airframe strength. A longitudinal control system was designed, validated by simulation, and tested structurally.					
20 Distribution/Availability of Abstract __ unclassified/unlimited __ same as report __ DTIC users			21 Abstract Security Classification Unclassified		
22a Name of Responsible Individual Professor Richard M. Howard			22b Telephone (include Area Code) 408 656 2870	22c Office Symbol AA/HO	

DD FORM 1473, 84 MAR

83 APR edition may be used until exhausted

security classification of this page

Unclassified

Approved for public release; distribution is unlimited.

Design, Fabrication and Test
of a Vertical Attitude Takeoff and Landing
Unmanned Air Vehicle

by

Robert Brian Stoney
Lieutenant Commander, United States Navy
B.S., Iowa State University, 1980

Submitted in partial fulfillment of
the requirements for the degree of

Aeronautical and Astronautical Engineer

from the

NAVAL POSTGRADUATE SCHOOL
June, 1993


Author:

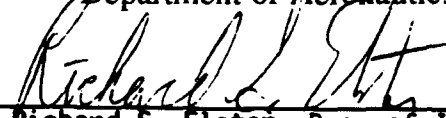

Robert Brian Stoney

Approved by:


Richard M. Howard, Thesis Advisor


Gerald H. Lindsey, Second Reader


Daniel J. Collins, Chairman
Department of Aeronautics and Astronautics


Richard S. Elster, Dean of Instruction

ABSTRACT

Future fleet needs for real-time intelligence require an unmanned platform capable of operations from small surface combatants without the need for extensive support personnel or equipment and without causing disruption to the operations of the ship from which it operates. A candidate must not only takeoff and land vertically but also be capable of high forward flight speeds and efficient on-station performance. The design and initial fabrication of a Vertical Attitude Takeoff and Landing (VATOL) Unmanned Air Vehicle (UAV) airframe was completed at the Naval Postgraduate School. The vehicle, called Archytas, was a combination of two existing UAV's--the AROD and Aquila--as well as locally manufactured components, including a canard support structure and wing spar. The objective of creating Archytas was to provide a proof-of-concept platform for research to explore performance trade-offs and stability augmentation. A three-degree-of-freedom simulation was used as the focus of the design efforts, to validate design decisions made in the fields of propulsion, aerodynamics, structures and flight mechanics. Engine tests were conducted to determine thrust and control power. Structural components were designed, fabricated and then tested, making modifications where necessary to ensure sufficient airframe strength. A longitudinal control system was designed, validated by simulation, and tested structurally.

ACKNOWLEDGEMENTS

This work is essentially the result of life-long advice, instruction, nurturing and motivation from people too many to thank. I am certainly thankful to my parents, William and Nancy. My father showed me by example the skills and thought processes of an "Ingegnere". I could have no better example of an engineer, or a father. My mother raised me to believe in myself--I draw from her nurturing every day of my life. And to my other mom, Lenore, who's insistence on education as a means to an end has not been lost on me.

My work at NPS would not have been possible without the strong support of Professor Rick Howard, a gifted mentor who exemplifies the type of teacher we all need....we all want to be.

But above all I am indebted to my family: Anne, William and Allison for the daily support, patience and motivation without which this thesis would not have been possible. They reminded me of what the most important thing in life is: love of family.

Accession For	
NTIS CRA&I	<input checked="" type="checkbox"/>
DTIC TAB	<input type="checkbox"/>
Unannounced	<input type="checkbox"/>
Justification	
By	
Distribution /	
Availability Codes	
Dist	Avail and/or Special
A-1	

DTIC QUALITY INSPECTED

TABLE OF CONTENTS

I. INTRODUCTION	1
A. MISSION NEED.....	1
B. LIMITATIONS OF CURRENT SYSTEMS.....	2
C. MOTIVATION	3
II. BACKGROUND.....	5
A. VERTICAL ATTITUDE TAKEOFF AND LANDING (VATOL).....	5
1. General.....	5
2. VATOL historical designs.....	7
B. NAVAL POSTGRADUATE SCHOOL UAV PROGRAMS	12
1. General.....	12
2. Aquila UAV.....	13
III. ARCHYTAS DESIGN--GENERAL.....	17
A. DESIGN OBJECTIVES	17
1. General.....	17
2. Specific.....	17
B. DESIGN TEAM.....	18
C. DESIGN PROCESS--ARCHYTAS AIRFRAME.....	20
D. THESIS ORGANIZATION.....	22
IV. ENGINE EXPERIMENTS	23
A. PURPOSE OF TESTS	23
B. DESCRIPTION OF TEST EQUIPMENT.....	24
1. Engine description and installation.....	24
2. Support and control equipment.....	25

3. Test stand	25
C SCOPE AND METHOD OF TESTS	27
D. RESULTS AND DISCUSSION	27
1. General.....	27
2. Thrust measurements.....	28
3. Vane control power measurements.....	29
a. General.....	29
b. Dual-vane roll-control power.....	32
c. Four-vane roll-control power	32
d. Pitch control power modelling.....	34
4. Effect on thrust from blockage in AROD duct.....	38
5. Impact of propwash on vane position.....	39
a. Noise.....	43
b. Fuel flow.....	44
c. Acceleration/deceleration characteristics	45
d. Reliability.....	45
V. WING SPAR DESIGN, FABRICATION AND TEST.....	46
A. GENERAL.....	46
B. WING SPAR DESIGN AND FABRICATION	46
1. Design load	46
2. Forward spar design and attachment.....	48
3. Aft spar design and attachment.....	50
4. Integration of NPS spars with Aquila wing spars.....	50
C WING SPAR EXPERIMENTS	52
1. Initial component testing.....	52

2. Redesign of basic spar structure.....	58
3. Testing of modified spar.....	59
4. Comprehensive structural test.....	61
VI. CANARD DESIGN, FABRICATION AND TEST	66
A. GENERAL.....	66
B. WING MODELING	68
C. CANARD SIZING AND LOCATION.....	73
1. Static Margin.....	73
a. General.....	73
b. Computer modelling.....	73
2. Longitudinal trimmability.....	74
3. Results.....	77
D. CANARD BOOM STRUCTURAL DESIGN.....	85
1. General.....	85
2. Shear stress derivation.....	86
3. Tensile stress derivation.....	90
4. Failure criteria.....	90
5. Canard boom loading model.....	93
6. Material selection.....	95
7. Structural testing of boom support structure.....	97
VII. SIMULATION	101
A. GENERAL.....	101
B. EQUATIONS OF MOTION--LINEAR MOMENTUM.....	101
1. Derivation of equations.....	101
2. Modeling of linear momentum equation elements.....	105

a. Thrust modeling.....	105
b. Lift modeling.....	106
C EQUATION OF MOTION--ANGULAR MOMENTUM.....	110
1. Derivation of equation.....	110
2. Modeling of angular momentum equation elements.....	112
a. Pitching Moment due to wing.....	112
b. Pitching Moment due to canard deflection.....	113
c. Pitching Moment due to vane deflection.....	114
d. Pitching moment due to pitch rate.....	116
D. COMPUTER CODE.....	117
1. Program features.....	117
2. Program description.....	117
E. RESULTS AND DISCUSSION	122
1. Time step determination.....	122
2. Takeoff, transition to forward flight.....	123
a. Thrust-to-weight envelope.....	123
b. Takeoff transition tradeoffs.....	125
3. Horizontal flight.....	131
a. Trim conditions.....	131
b. Cruise flight short period characteristics.....	132
c. Predicted short period characteristics.....	132
d. Long period.....	136
4. Transition from horizontal flight to vertical landing.....	139
a. General.....	139
b. Level deceleration profile.....	140

c. "Zooming" profile	142
VIII. CONCLUSIONS.....	144
A. GENERAL.....	144
B. SPECIFIC	145
1. Engine tests.....	145
2. Wing spar design, fabrication and test.....	145
3. Canard design.....	145
4. Simulation.....	146
C. ARCHYTAS CONFIGURATION.....	147
IX. RECOMMENDATIONS.....	148
A. GENERAL.....	148
B. SPECIFIC	148
1. Engine tests.....	148
2. Wing spar design.....	149
3. Canard design.....	150
4. Simulation.....	150
5. Weight control.....	151
6. Lateral and directional flight mechanics.....	152
7. Flight test.....	152
LIST OF REFERENCES.....	154
APPENDIX A	
TABLES.....	159
APPENDIX B	
PHOTOGRAPHS OF FABRICATION AND TEST	164

APPENDIX C

VORTEX-LATTICE CAMBER PROGRAM AND DATA	169
--	-----

APPENDIX D

CODE FOR PROGRAMS "XPLOT" AND "INCIDENCE"	171
---	-----

APPENDIX E

SIMULATION ASSUMPTIONS.....	180
-----------------------------	-----

APPENDIX F

FLOWCHART FOR SIMULATION PROGRAMS	185
---	-----

APPENDIX G

CODE FOR SIMULATION PROGRAMS	192
------------------------------------	-----

APPENDIX H

SIMULATION PROFILES	216
INITIAL DISTRIBUTION LIST.....	222

I. INTRODUCTION

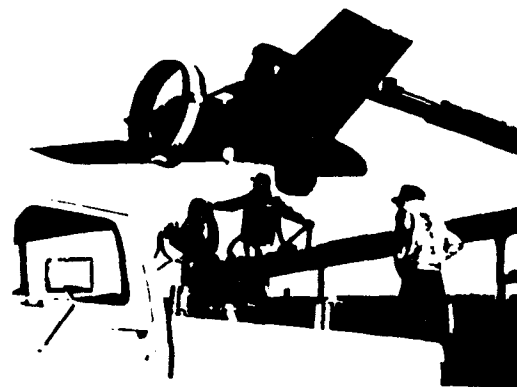
A. MISSION NEED

Among the many news stories reported during Desert Storm was that of a group of Iraqi soldiers waving a white flag to a Unmanned Air Vehicle (UAV). This particular UAV, the Pioneer, had been providing targeting information to a battleship firing 16 inch shells from over the horizon. As the Pioneer helped refine the battleship's aim, the Iraqis knew that the small craft which flew over their position and the ship raining metal upon them were a team. Lacking any direct contact with those operating the big guns, they surrendered to the small package of hardware and electronics orbiting above them. The utility of the UAV, long known to military commanders, was graphically demonstrated on world-wide TV.

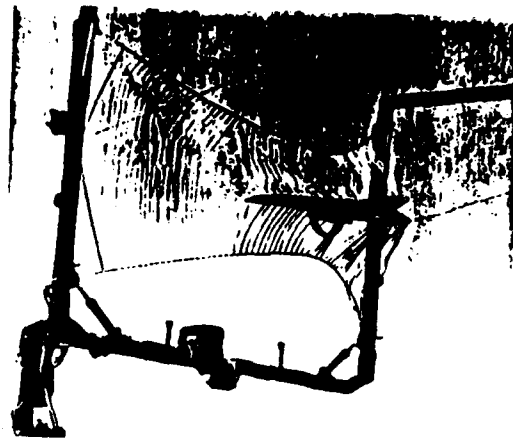
UAV's, formerly known as Remotely Piloted Vehicles (RPV's) can serve military commanders in a variety of missions. Carrying optical and/or infrared (IR) sensors, they provide targeting, intelligence and reconnaissance information. They can also be equipped with communications intelligence (COMINT) and electronics intelligence (ELINT) packages for relay to a ground or sea-based user. Other systems that can be carried aloft by UAV's include: radar, communications relay, electronic countermeasures (ECM), laser designators, nuclear/biological/chemical (NBC) contamination sensors, and even weapons, all without sending military personnel in harm's way.

B. LIMITATIONS OF CURRENT SYSTEMS

The utility, then, for the UAV is great but there are limitations. Many systems, such as the Pioneer, Sky Owl, and the Aquila shown in Figure 1.1, require special equipment or procedures for launch and recovery. This equipment includes pneumatic rail-launchers or rocket assist for takeoff, and nets for capture at the completion of the UAV's mission. The landborne systems require a fairly large area for



LMSC YMQM 105A Aquila and its truck mounted launch rail



Aquila being retrieved in vertical ribbon net

Figure 1.1

Aquila UAV Shown With Special Launch and Recovery Equipment

takeoff and landing. Seaborne UAV's can impact the battlegroup's operations due to stringent wind and sea state envelopes for launch and recovery. Because of these disadvantages, other concepts have been explored as alternatives to the classic fixed-wing UAV.

Rotary wing UAV's, such as unmanned helicopters and ducted-fan types, have the advantage that they can operate from small forward-deployed areas or ship decks without special equipment. However, systems with exposed rotors present a formidable safety hazard to nearby personnel. Additionally, vertical-only UAV's are limited by their relatively slow forward flight speeds and generally shorter endurance times once on-station. They simply cannot get to the target area fast enough or stay there long enough.

C. MOTIVATION

Another class of UAV's that has recently received renewed attention are those with vertical takeoff and landing (VTOL) capability and the ability to transition to wing-borne forward flight. These vehicles conceptually have the strengths of both fixed and rotary wing vehicles: able to takeoff and land vertically but with higher forward flight speeds. This class of aircraft is comprised of several types, including: lift fan (eg: Ryan XV-5), tilt rotor (eg: Bell XV-15 and V-22), tilt wing (eg: LTV XC-142A), vectored thrust (eg: Harrier), Lift engines plus cruise engines (separate engines for each function, eg: Dassault Mirage IIIV), and Vertical Attitude Takeoff and Landing (VATOL), also known as "Tailsitters" [Ref. 1].

The goal, then, for the next generation of UAV's will be to retain the capabilities of current systems but to provide this capability in a more flexible form.

II. BACKGROUND

A. VERTICAL ATTITUDE TAKEOFF AND LANDING (VATOL)

1. General

As discussed in the introduction, one of the VTOL concepts capable of wing-borne flight is the VATOL type. It is this type which is the subject of this thesis. In 1949 the first "convertible aircraft congress" was held and from this meeting came several designs, as depicted in Figures II.1 and II.2 [Ref. 2]. Some of the advantages of the VATOL design [Ref. 3] are:

1) Simplicity of design. The same engine is used for vertical lift and forward flight, normally with only simple modifications to allow hovering control. This simple design generally results in less weight penalty because there are no pivoting wings, nozzles or engine nacelles with the accompanying structural weight.

2) High thrust-to-weight ratio for mission use. VATOL aircraft, with lower structural weight, have more excess thrust which can be utilized during takeoff and landing as well as in the mission area.

3) Reduced or eliminated degradation of vertical lift capability due to "suckdown" or exhaust ingestion.

4) In general, better control at high angles of attack.

In a 1978 study of several generic designs, the David Taylor Research Center [Ref. 4] concluded that VATOL was the best VTOL configuration, with a 12% higher payload/operating weight ratio than

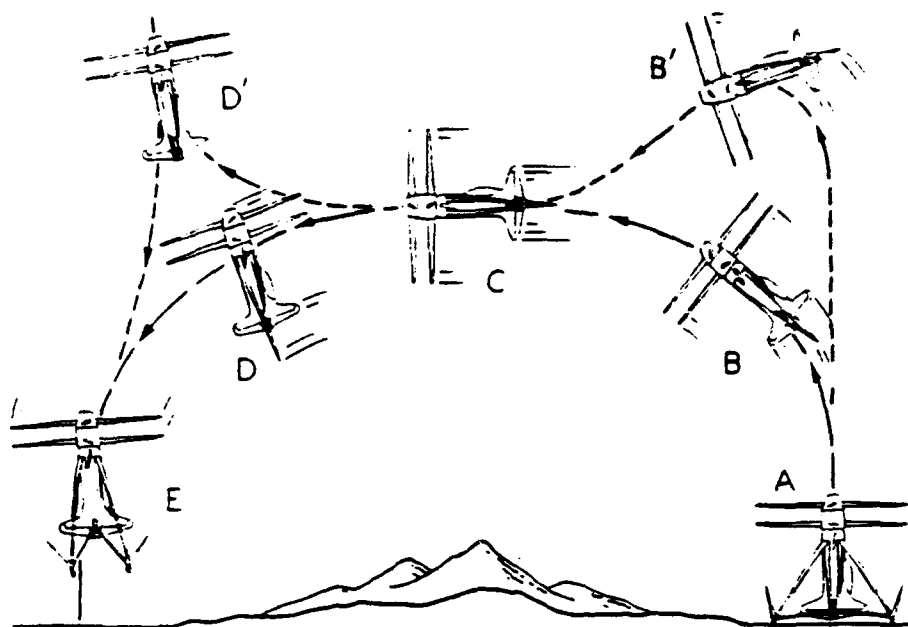


Figure II.1: Early VATOL concept

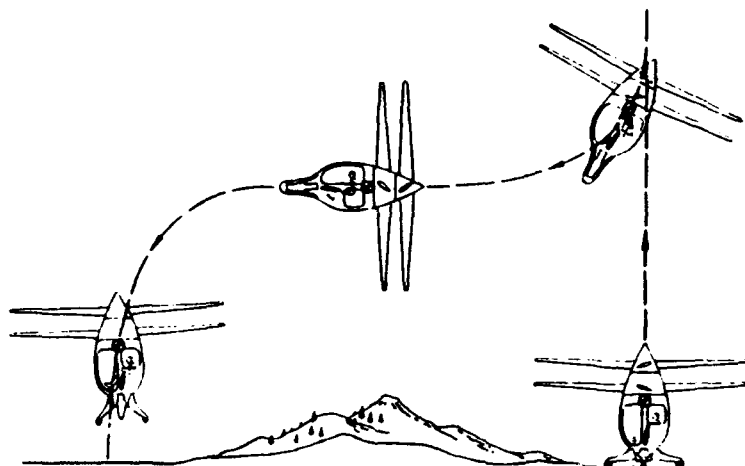


Figure II.2: Early VATOL concept

the next best configuration, as shown in Figure II.3.

The disadvantages of the VATOL concept in general include:

- 1) In the case where special launch-and/or-recovery platforms or equipment are required, there is a reduction in the operational flexibility compared with conventional fixed wing aircraft.

- 2) Most VATOL designs have no STOL capability, limiting their ability to handle increased takeoff weight.

2. VATOL historical designs

During the 1950's and early 1960's and then again during the Carter administration, there was much research on VATOL designs, including several successful manned and unmanned programs. The prop-driven Convair XFY-1, Figure II.4, was a successful design flown in 1953. Over 400 flights were made, all with transitions to and from horizontal flight. Later came the jet-powered Ryan XV-13, Figure II.5, which completed 136 flights, of which 104 were VATOL [Ref. 1]. Both programs were completed without serious incident. It is important to note the configurations of these experimental aircraft: all, except for the least successful Lockheed XFV-1 about which less has been written, had highly-swept delta wings and most had reaction control augmenting aerodynamic control. A review of the many documents concerning these and other VATOL studies revealed several potential problem areas for VATOL designs. These include:

- 1) Longitudinal trim. The jet designs all suffered from a

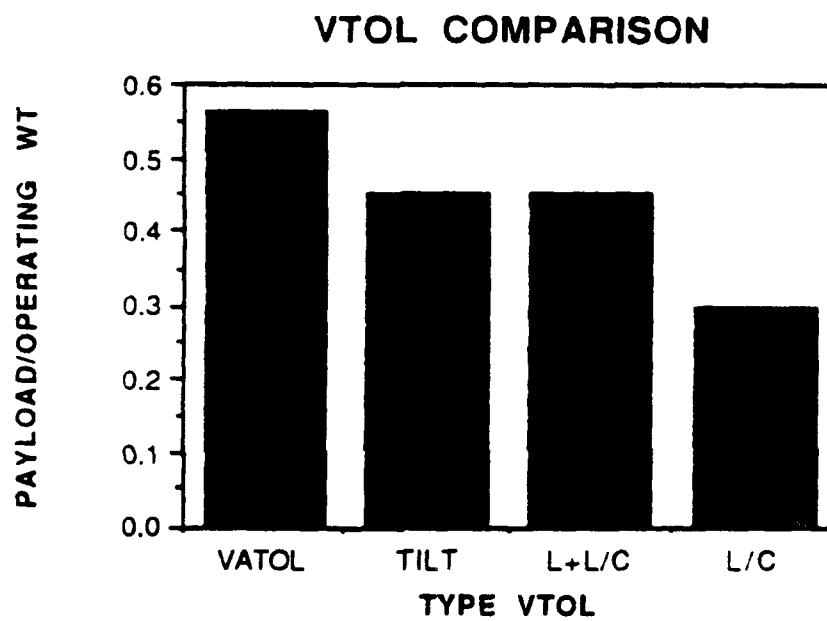


Figure 11.3
Payload comparison of several VTOL types.

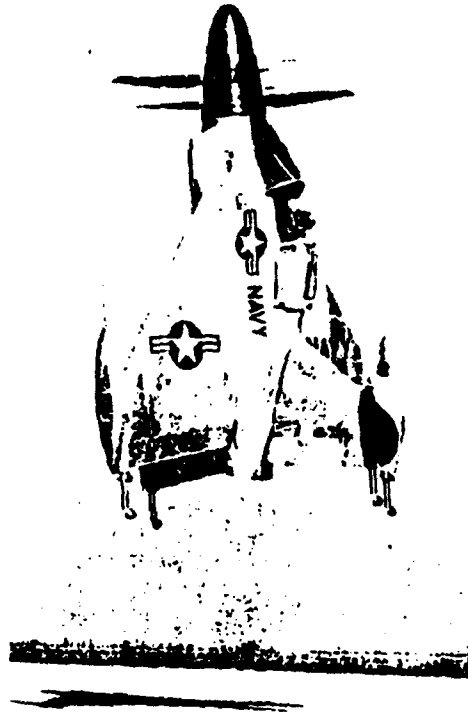


Figure II.4: CONVAIR XFY-1--Propeller-Driven VATOL Research
Airplane

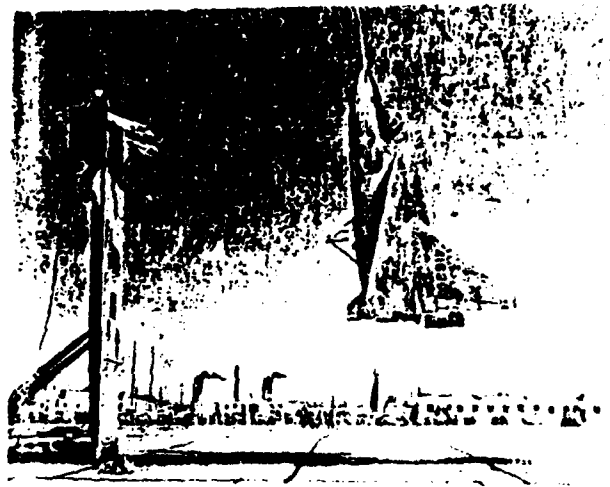


Figure II.5: Ryan XV-13 VERTIJET--Jet -powered VATOL research
airplane

significant pitch-trim problem, encountered during constant-altitude decelerating transitions. According to Girard and Everett [Ref. 5], the XV-13 "could not be flown steady state at attitude angles between 32 and 70 deg due to an incompatibility between thrust required for constant altitude, and that required for longitudinal control, the latter requirement being the greater." The XV-13 utilized a gimbaled nozzle, much like that on a rocket, to vector thrust. The solution to the problem was to simply pitch through this region by "following a memorized schedule of engine rpm versus airplane angle" (to avoid excessive altitude gain) [Ref. 5].

2) Longitudinal flying qualities. Because the VATOL design is often operated at relatively high angles of attack, it is desirable that the vehicle have a high coefficient of lift and a post-stall region that is as free of abrupt changes in the aircraft's stability derivatives as possible. Longitudinally, this means desiring benign stall characteristics. The typical approach has been to utilize fairly low-aspect-ratio delta wings, trading off a lower coefficient of lift for good high-alpha flying qualities. Not all programs experienced longitudinal flying qualities problems, however. In 1961 NASA performed tests on a 1/5-scale RPV very similar in configuration to the XV-13. A three-view of the model is shown in Figure II.6. The report on this vehicle stated: "Transitions from hovering to normal forward flight and back to hovering flight could be made smoothly and easily in the full-scale tunnel, and the model seemed to have stability of angle of attack over most of the speed range. These

flights...represented slow, constant-altitude transitions and covered a range of angles of attack from about 20 deg to 90 deg." [Ref 6].

3) Lateral/directional flying qualities. Another problem encountered in the high angle of attack regime is marked changes in aircraft lateral-directional flying qualities. In many airplanes at AOA's just a few degrees above stall, the sign of directional stability can

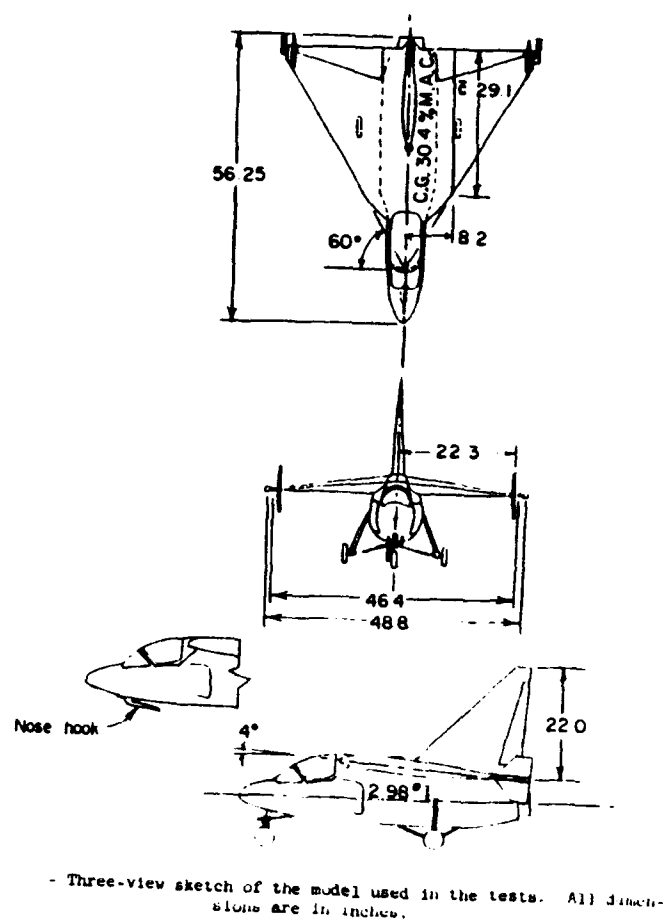


Figure II.6

NASA 1/5 Scale Model of a Jet Powered VATOL Research Airplane

change and aerodynamic roll control power can be drastically reduced. The XV-13 experienced this problem. Roll control required to "handle extreme sideslip angles exceeds the control available in level flight by a considerable margin at and just beyond the stall. Adequate control is available at full power [the XV-13 utilized reaction roll control to augment aerodynamic control] but then the airplane would begin to climb." [Ref 5].

The preceeding review of flight test reports for both manned and unmanned VATOL research projects suggests an additional design objective: to design the vehicle to be flown with an angle of attack (α) in regions of predictable airplane response. This means either keeping the α low--not more than a few degrees beyond stall--or exploring higher α behavior in wind tunnel or flight test.

B. NAVAL POSTGRADUATE SCHOOL UAV PROGRAMS

1. General

UAV research at the Naval Postgraduate School (NPS) is conducted by the UAV Flight Research Laboratory (FRL). Members of this lab have experience in several UAV projects and have obtained assets for use in future proof-of-concept designs. Additionally, the FRL has facilities to manufacture and test UAV's. Resident skills include metalworking, composite manufacturing and model building.

2. Aquila UAV

Developed by the U.S. Army in the 1970's as a surveillance platform, the Lockheed MQM-105 is a flying wing design with a shrouded pusher propeller, as shown in Figure II.7. The Aquila was made from Kevlar composite material which resulted in a strong, lightweight airframe. The Aquila was launched by pneumatic rail and captured in a net, as shown in Figure I.1. Lateral and longitudinal flight control was achieved through wing-mounted elevons. The Aquila had no sustained vertical flight capability. Several Aquila airframes were obtained by the FRL for use in UAV research.

3. Airborne Remotely Operated Device (AROD)

Designed and fabricated by Sandia Research Laboratory under a contract for the Naval Ocean Systems Center (NOSC), the AROD, shown in Figure II.8, was a ducted-fan UAV built of graphite and Kevlar composites. It was powered by a two-cylinder, two-cycle engine developing approximately 26 BHP. The engine is more fully described in Section IV. Capable of hovering and limited forward flight, the AROD was controlled by four vanes mounted in the wake of the engine driving a three-bladed composite propeller. Stabilization was performed by an onboard computer fed by rate sensors and gyros. AROD characteristics are shown in Table II.I. All remaining AROD assets were obtained in 1993 by the FRL for UAV flight research.

4. Archytas UAV Notional Concept

The work of theses by Blanchette, Ellwood, Brynstead, Merz and Kress [Refs. 7-11] have led to the development of a VATOL UAV concept combining the assets of Aquila and AROD with locally manufactured components. Figure II.9 shows the notional concept for FRL's VATOL UAV, named Archytas. It is designed to be flown in a hover in the same manner as the AROD, by using the vanes immersed in the wake of the propeller, and then transitioned into forward flight and flown as a conventional fixed-wing airplane, much like the Aquila. Following return to the landing site it will be designed to transition back to a vertical attitude and land from a hover.

In his thesis, Lieutenant Kress designed the spar to connect the AROD to the Aquila wing, designed and built an engine test stand, and performed initial engine tests [Ref. 11].

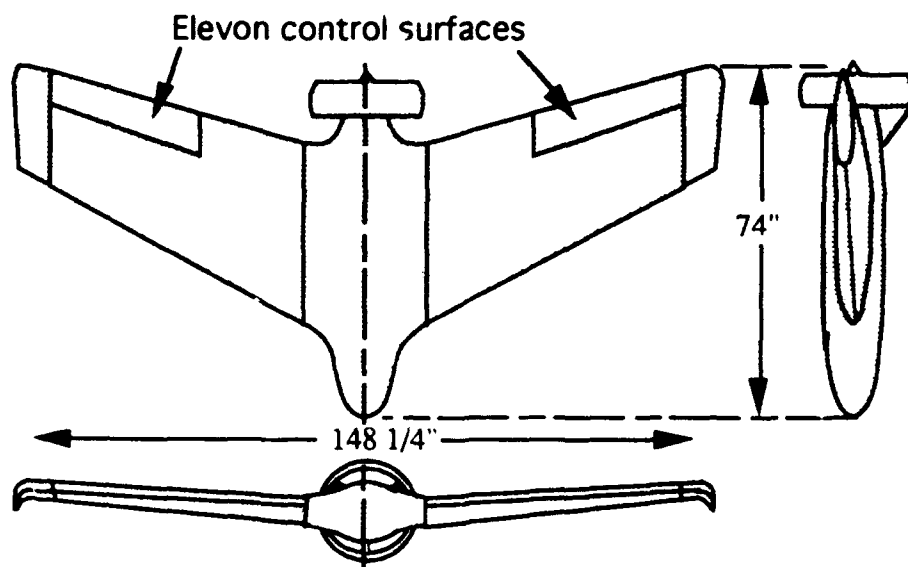


Figure II.7: Lockheed/US Army MQM-105 Aquila UAV

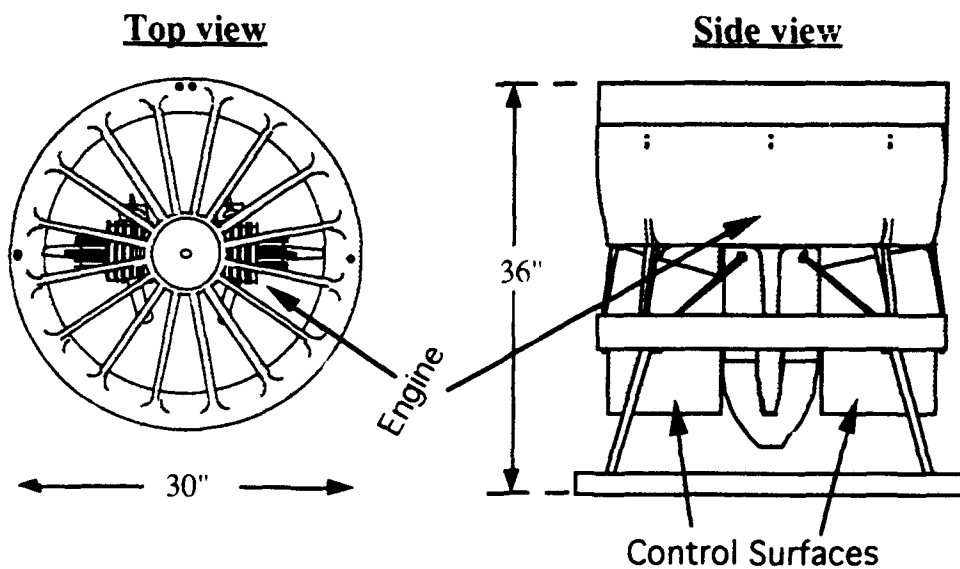


Figure II.8: Sandia Lab/NOSC AROD Ducted-Fan UAV

Table II.I AROD CHARACTERISTICS

Inlet diameter	29.25 inches
Propeller diameter, D	24 inches
Exit diameter	26.75 inches
Number of blades	3
Tip clearance	0.031 ± 0.005 inches
Engine speed, maximum	8000 rpm
Engine speed, nominal	7000 rpm
Tip speed, maximum	838 fpm
Tip speed, nominal	733 fpm
Weight (approx)	70 lbf

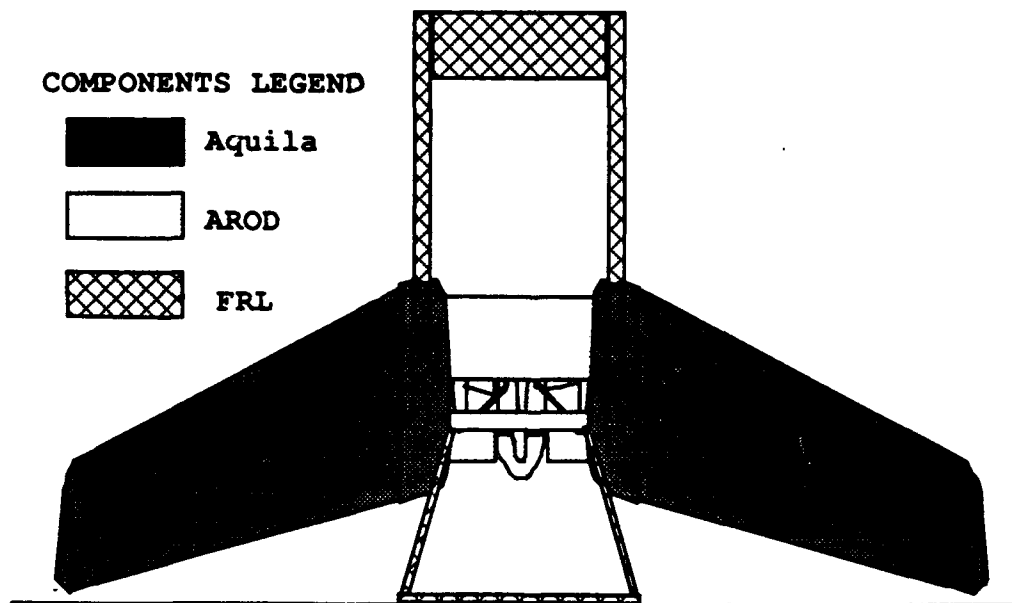


Figure II.9: NPS VATOL UAV Notional Concept, the Archytas

III. ARCHYTTAS DESIGN--GENERAL

A. DESIGN OBJECTIVES

1. General

The objectives of the Archytas program are to design, produce and test a proof-of-concept VATOL UAV. This vehicle will be used to examine the technologies and techniques applicable to a military UAV. A conceptual follow-on UAV to the Archytas program would be capable of carrying a variety of military payloads. A key feature of this future military UAV must be the ability to conduct operations with minimal support equipment and personnel. Additionally, these operations must be conducted without adversely impacting the operations of other components of the war-fighting team.

2. Specific

As in any design effort, there are constraints which the designer strives to meet. In the case of the Archytas, the primary specific design objectives were:

- Minimum weight. To increase the maneuver margins during hovering flight, high thrust to weight (T/W) is desirable. Clearly, a T/W less than one will prevent flight for a VATOL airplane. Historical information [Refs 12, 13, 14] suggest that the minimum acceptable T/W is in the range of 1.05 to 1.08 with a desirable T/W of 1.15. The thrust of the Archytas was considered to be fixed. In

other words, the AROD's propulsion system--the duct, inlet, propeller and engine--would be incorporated into the Archytas design with few modifications. This left weight as the design variable--low weight was a significant design goal.

- Low angle-of-attack flight. As a result of the review of the historical VATOL programs another design goal emerged: that of operating the Archytas, if possible, at maximum angles of attack of a few degrees beyond stall when at flight speeds beyond slow hover. This limit on angle of attack was to ensure that the problems and uncertainties of high angle of attack flight were avoided, most notably in the area of longitudinal and lateral/directional flying qualities.

- Structural support for a 100 lb vehicle at 8 g's ultimate normal load factor. This requirement resulted from the work of Kress [Ref. 11].

- Minimum modification of AROD duct, to prevent loss of structural integrity of the AROD.

- Favorable static longitudinal stability for forward flight.
- Favorable longitudinal control power for forward flight.
- Minimum special equipment to launch or recover the vehicle.

- Minimum modification of Aquila wing.

B. DESIGN TEAM

The subject of this thesis, design and fabrication of the Archytas airframe, is one part of a larger effort at NPS to produce a

controllable VATOL UAV capable of autonomous flight, as shown in Figure III.1. Research is ongoing by members of the NPS Aeronautical Engineering, Electrical Engineering and Weapons Systems curricula to achieve this goal. The topics of the research work include:

- Control, including advanced six degree of freedom simulation.
- Navigation; sensors and integration.
- Communication and data acquisition. Up-link and down-link.

Design of the airframe, therefore, required interaction with these other disciplines. The areas of most interest to all parties included: weight and center of gravity management, configuration, vehicle performance, aircraft control power and aircraft flying qualities.

C. DESIGN PROCESS--ARCHYTAS AIRFRAME

Design is by its nature an iterative process. Design of the Archytas was no exception to this rule. Several disciplines interacted closely in the airframe design process. As depicted in Figure III.2, the disciplines included:

- Aerodynamics research included wing placement and orientation. This involved a strong interaction with Flight Mechanics to achieve proper longitudinal characteristics. Additionally, strong interaction with the Structures discipline was necessary to supply predicted flight loads.

- Flight Mechanics theory was utilized for proper sizing and placement of the canard control surface.

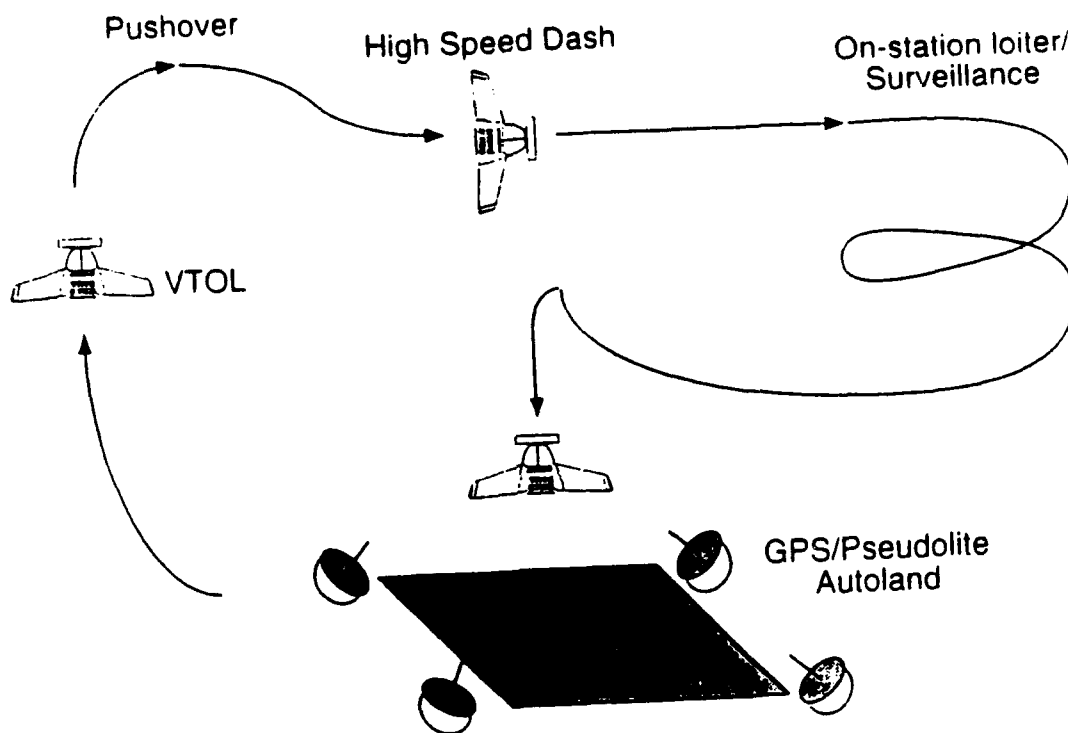


Figure III.1
Archytas Mission Profile

- Simulation was used to predict results of all disciplines' effects on design.

- Structural analysis was performed to achieve a lightweight structure capable of supporting predicted aero-loads. This portion of the project included test of key structural components.

- Propulsion tests were conducted to characterize the installed propulsion system.

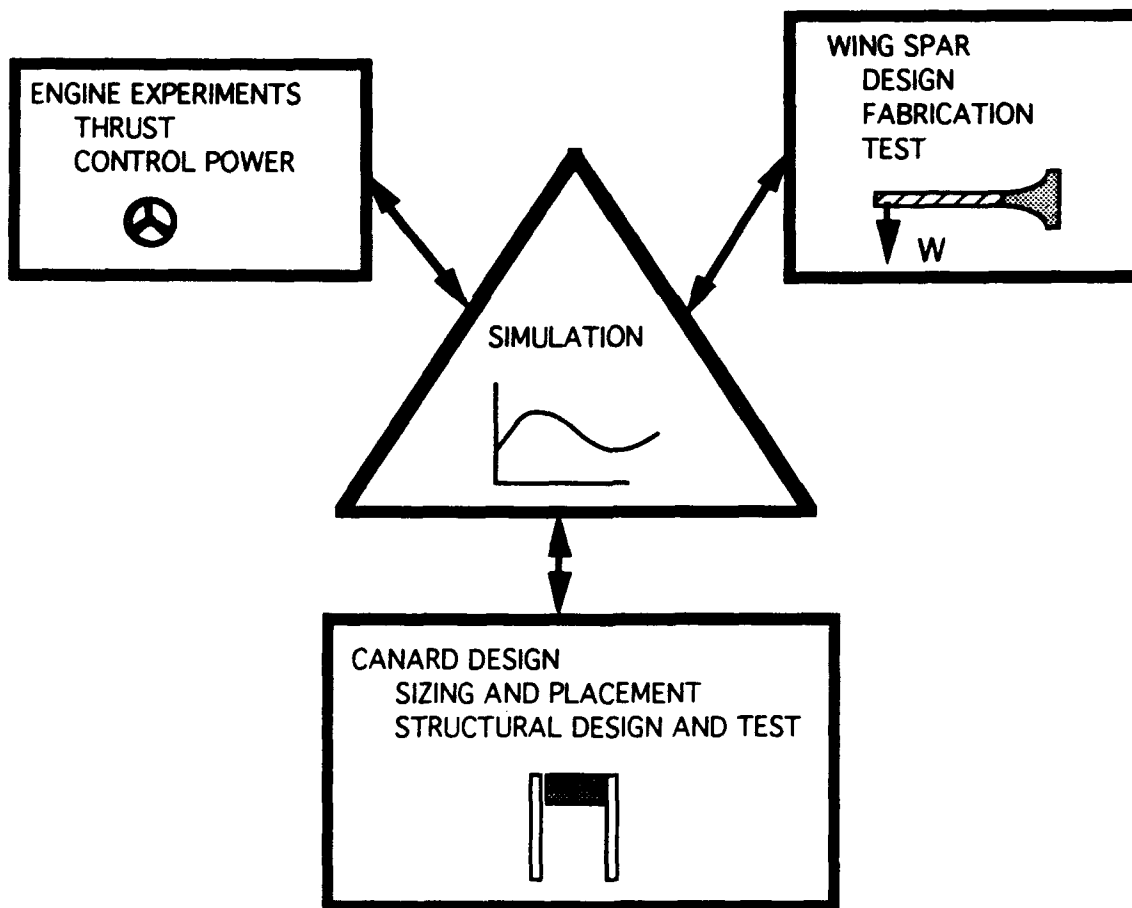


Figure III.2

Archytas Airframe Design Process

D. THESIS ORGANIZATION

This thesis is organized by subject area as shown in the preceeding figure. A chapter is devoted to each of the following subjects:

- Section IV: Engine Tests
- Section V: Wing spar Structural Design, Fabrication and test
- Section VI: Canard Design and test
- Section VII: Simulation

Sections VIII and IX follow with conclusions and recommendations.

IV. ENGINE EXPERIMENTS

A. PURPOSE OF TESTS

The purposes of performing engine tests included:

- Characterization of thrust versus throttle position for use in simulation program's equations of motion. This led directly to estimation of desirable thrust to weight ratios for vertical takeoff and landing--which in turn led to a directed weight management effort.
- Measurement of noise and comparison of thrust with and without factory-installed muffler system.
- Determination of roll control power for use by other design team members. These data were also used to model pitch control power in the simulation program.
 - Characterization of engine acceleration and deceleration.
 - Determination of fuel flow rates.
 - Survey of flow velocity at AROD duct exit for possible use in control power modeling.
 - Measurement of the effects on thrust of deflecting the vanes--called "Blockage effect".
 - Characterization of "blowback effect"--changes in vane position caused by propeller wash.
 - Gaining of experience in starting and running AROD in anticipation of flight test.

B. DESCRIPTION OF TEST EQUIPMENT

1. Engine description and installation

The engine, manufactured by Herbrandson Enterprises, was a two-cylinder, two-stroke, horizontally-opposed, air-cooled engine with a displacement of 290 cc (17.4 cu in) developing approximately 26 BHP, driving a graphite-composite three-bladed, fixed-pitch propeller. The uninstalled engine with its ignition electronics and without mufflers weighed 15.5 pounds. [Ref 15]. Installation characteristics were previously stated in Table II.I. The engine was fueled with a mixture of two-cycle engine oil and unleaded supreme gasoline at a ratio of 80:1.

The propeller blade angle could be varied by the loosening of a blade retaining assembly. Propeller blade angle was left at the position in which it was received--14 degrees at the tip. Four vanes were immersed in the wake of the propeller and were designed to be used for control of the AROD in hovering flight. Each of the four vanes had a ten-inch span and eight-inch chord. End-caps approximately two inches high were placed on each end of the vanes, presumably to reduce spanwise loss of lift.

Self-contained electrical power was designed to be delivered from an engine driven generator. For engine testing purposes, an external power source was also available [Ref 16]. The engine and engine installation in the test AROD, named "Annie", were considered representative of the eight vehicles obtained by NPS.

2. Support and control equipment

Control of vane and throttle servos was affected by pulse width modulated signals in one of two ways: (1) via an umbilical line connected to an IBM PC running a "C" software code, or (2) via radio frequency control from an off-the-shelf Futaba[®] radio control (R/C) transmitter sending signals to a receiver mounted inside the vehicle. Ignition was also provided in two different manners: (1) external power through a 28 VDC power source, or (2) on board engine driven generator. Several problems with electronics and ignition were encountered during engine tests. These problems and the control set-up are described in thesis work by Lieutenant Commander Moran [Ref. 16].

3. Test stand

The test stand was designed to measure thrust and rolling moment of the AROD. Test stand design and manufacture was accomplished in work by Lieutenant Kress [Ref.11]. Modifications to the original design concerned improvement in accuracy of force and moment by replacement of the original "fish scale" apparatus with sensitive mechanical force gages. Three force gages were obtained. Two gages, with a combined capacity of 175 lb, were used in parallel to measure force and one 50 lb capacity gage was mounted to measure rolling moment at the end of of a nine-inch moment arm. for a moment capacity of 37.5 ft-lbf. Figure IV.1 shows the engine test stand, force and moment measuring equipment, and the test article, an AROD. Force was measured by adding the pair of force

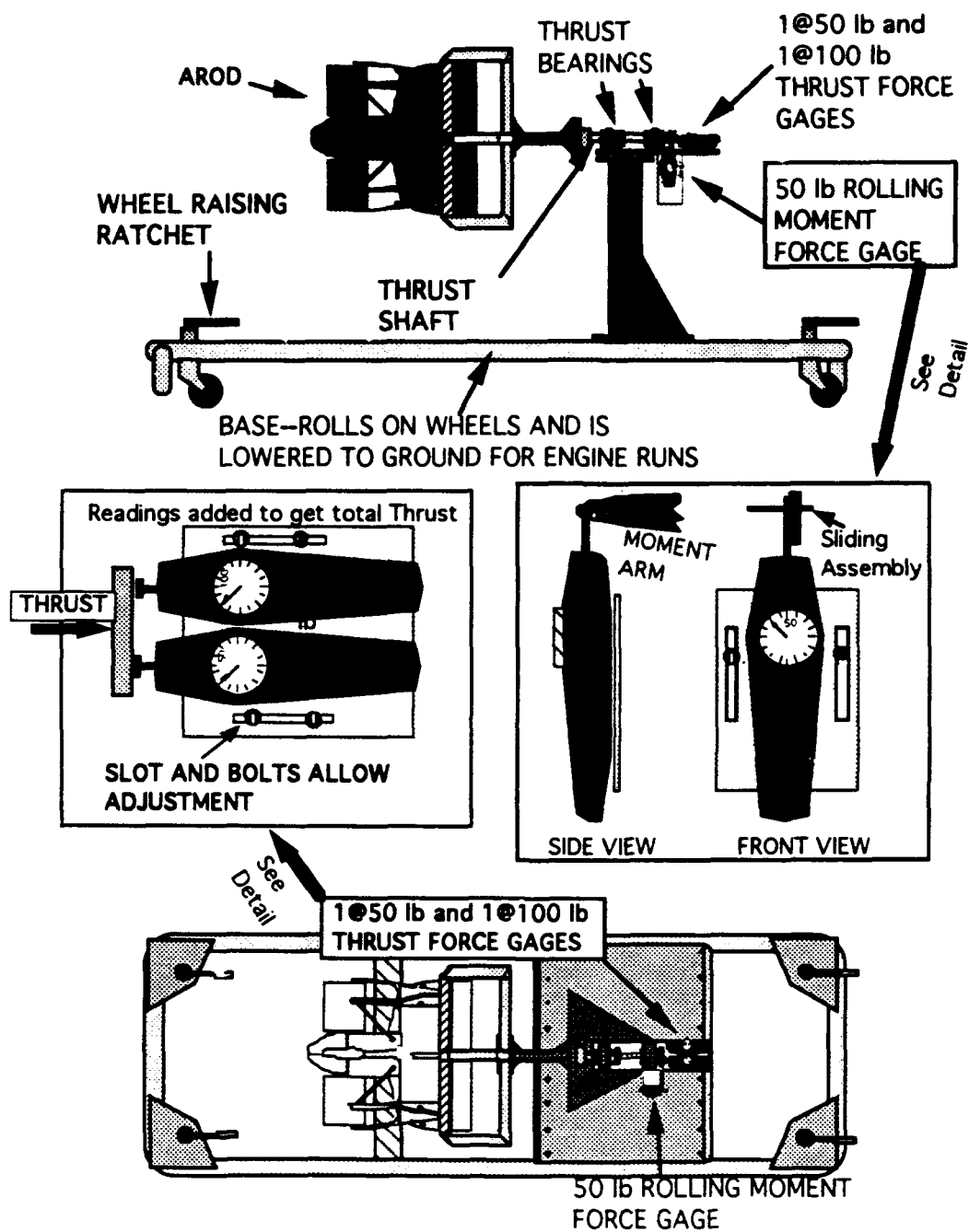


Figure IV.1: Engine Test Stand for AROD Thrust and Rolling Moment measurement

gages mounted on an adjustable plate which was in-line with the thrust shaft.

C. SCOPE AND METHOD OF TESTS

The tests were conducted on two separate occasions for a total engine run time of approximately four hours. Tests were performed at the engine run block-house located at the NPS Laboratory. Tests were conducted in accordance with the test matrix shown in Appendix A, Table A.I. Data included temperature, pressure, thrust, engine speed in rpm, vane position, moment reading, and--when applicable--computer inputs. Vane deflection was read directly off protractors mounted at the base of each vane and calibrated in one-degree increments. Further discussion of vane numbering and deflection convention follows. Rpm was measured by an oscilloscope connected to the ignition source or by a sensor mounted on the side of the R/C transmitter which essentially detected light oscillations caused by propeller passage. Velocity of airflow in the area of the vanes were measured with a hand-held digital wind-speed meter. Double hearing and eye protection were worn by all test personnel. Data were recorded on pre-printed data sheets and by a video camera.

D. RESULTS AND DISCUSSION

1. General

The data for engine tests completed are shown in Appendix A, Tables A.II and A.III.

2. Thrust measurements

The first task was to determine what effect the mufflers had on thrust and noise output. The engines were apparently operated by the previous user with mufflers off and a straight-tube exhaust installed. In their production configuration, the Herbrandson mufflers would not fit inside the AROD duct. Several sets of brand-new mufflers were contained in the spare parts obtained by NPS. FRL personnel built an exhaust manifold adapter that allowed installation of the mufflers in the constrained AROD duct. Thrust reading at a full throttle rpm of 7595 with the mufflers on was 118 lbf. The engine was shut down and the mufflers replaced by the original straight tube exhaust system. Upon restart and re-establishment of full throttle, again at 7595 rpm, the thrust had increased over four percent to 123 lbf. Temperature and pressure for both runs--separated by less than five minutes--were the same. Noise was substantially increased by removal of the mufflers, as discussed in a later paragraph, but since initial simulation results had showed a need for the highest available thrust-to-weight ratio (T/W), the decision was made to conduct subsequent tests with the straight-tube exhausts. This test was repeated twice to verify a consistent result. The surprisingly large difference in thrust at the same temperature, rpm and blade angle may have been due to drag on the mufflers, which were in the wake of the propeller. The frontal area and blockage effect of the mufflers was approximately 32 square inches total.

Thrust measurements were considered accurate to within 1/2 lbf. Engine speed versus thrust is shown in Figure IV.2. A second order polynomial curve fit is overlaid and shows good correlation. Figure IV.3 shows the thrust that resulted at different throttle settings as well as a polynomial curve fit. The throttle position on this plot was arrived at by taking the computer's throttle position and mapping it linearly to a zero to 100 percent scale. This thrust versus throttle position curve fit was used in the simulation program, as discussed in Section VII. As shown in Figure IV.3, the thrust output at idle was over 20 lbf. This relatively high minimum thrust setting may cause the vehicle to be more difficult to slow down in horizontal flight. Further testing may be required with the idle adjustment set for a lower rpm.

3. Vane control power measurements

a. General

The rolling moment imparted by deflection of vanes was measured on the test stand. Moment readings tended to "wander" over a range of approximately ± 3 lbf force gage reading which, through a nine-inch test stand moment arm, converted to approximately ± 2 ft-lbf accuracy for rolling moment. This range of readings was inconsistent and at times the readings wandered 5 ft-lbf from the nominal reading. The source of this relatively large variation in readings could not be determined. Engine speed fluctuations were ruled out in that aural and measured rpm were constant, as were the thrust readings. Wind in the test area was light

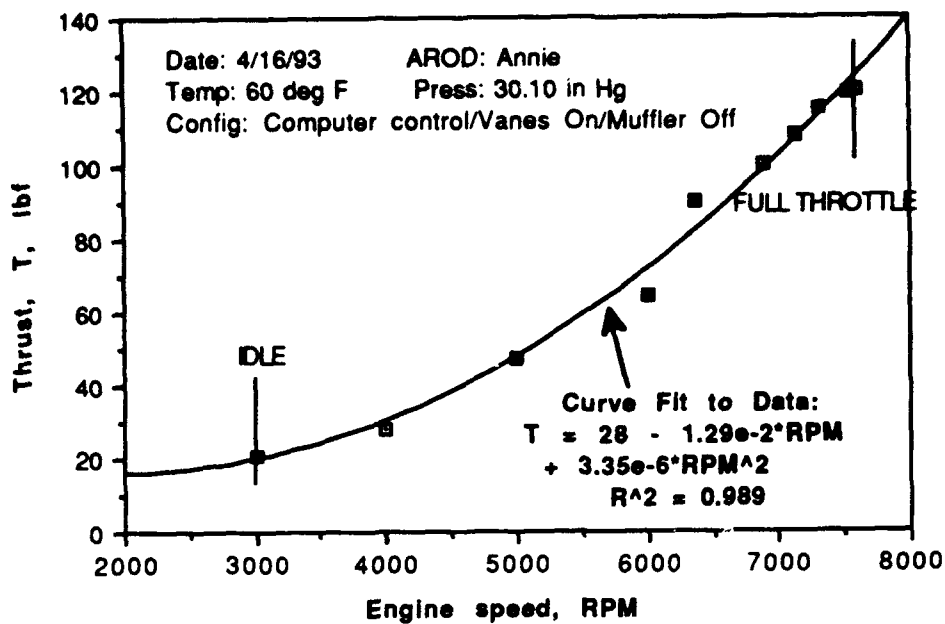


Figure IV.2: AROD Engine Test Results--Thrust Versus Rpm

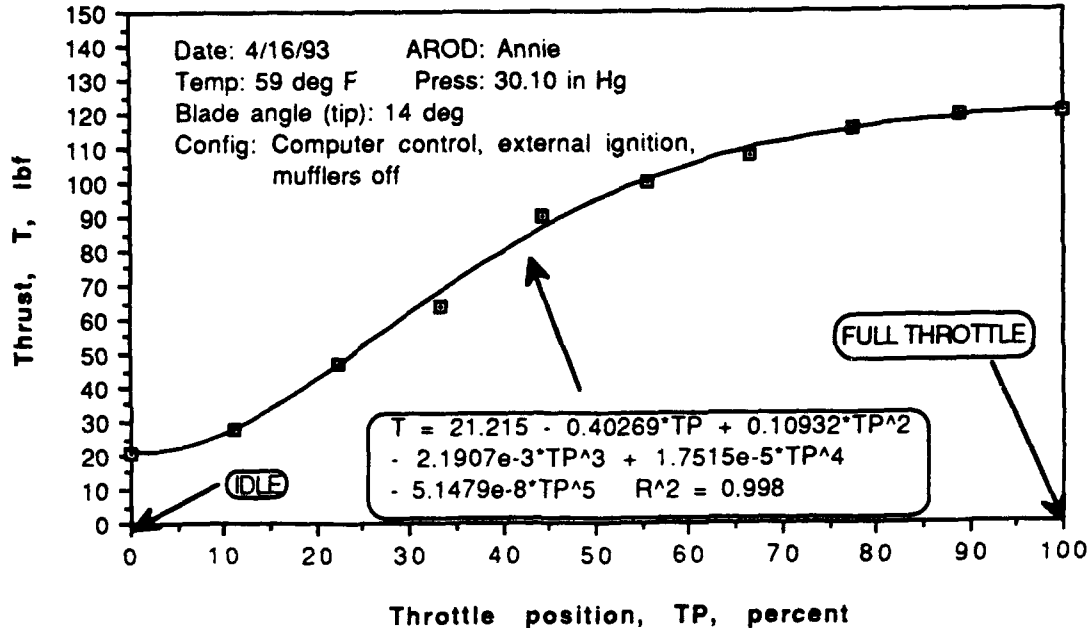


Figure IV.3: AROD Engine Modelling--Thrust Versus Throttle Position

and variable. The control vane positions were visually checked as steady. One possible explanation for the variable moment readings would be unsteady flow within the duct--flow over the engine and its support structure is downstream of the propeller but just upstream of the vanes.

In keeping with MILSPEC convention for roll control deflection [Ref 17] positive vane deflections--clockwise when viewed from the vane tip--were those which produced positive rolling moments--clockwise viewed from the rear of the AROD. Zero vane deflection was defined as the deflection at which a vane was aligned with the longitudinal axis of the AROD. The "top" of the AROD when mounted on its side in the test stand as shown in Figure IV.1 was considered to be the point where two fuel vents were next to each other. Vanes were then numbered according to Figure IV.4 below.

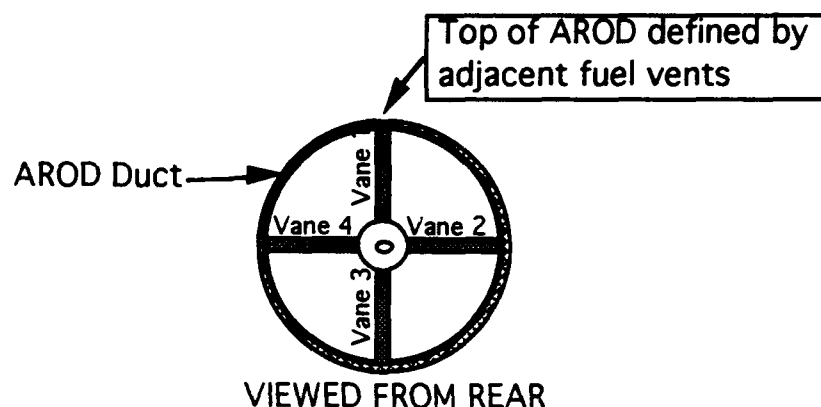


Figure IV.4:AROD Vane Numbering Convention for Engine Tests

b. Dual-vane roll-control power

Dual-vane roll-control power was obtained by deflection of vanes two and four, while one and three were set to zero deflection. The rolling moment response to this vane deflection, shown in Figure IV.5, was fairly linear and showed no propensity to drop off at high deflection angles. The combined effects of engine and propeller torque were overcome, for the two-vane case, by approximately 18 deg of deflection.

c. Four-vane roll-control power

Four-vane roll-control power was obtained by deflection of all vanes in the same direction so as to produce a rolling moment. The response to this vane deflection with throttle set to full open (7520 rpm) is shown in Figure IV.6 and, as with dual vane power, was fairly linear and showed no propensity to drop off at high deflection angles. The combined effects of engine and propeller torque were overcome, for the four-vane case, by approximately 12 deg of deflection.

The change in four vane roll control power with changes in throttle setting was investigated for two additional rpm settings: 7240 and 6580. These rpm levels corresponded to approximately 93 and 75 percent of full throttle *thrust*, respectively. As shown in Figure IV.7, there was little effective change in roll control power as throttle was reduced, even though the thrust was decreased by 25 percent. As discussed in Figure VII, this surprising result was researched and it was discovered that the AROD manufacturer,

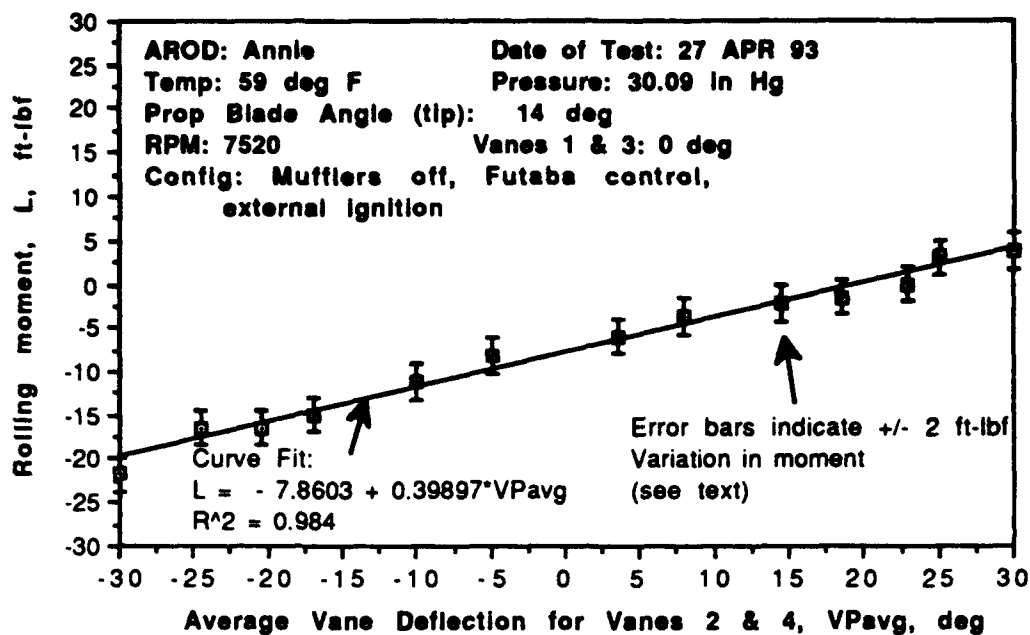


Figure IV.5: AROD Engine Test--Dual Vane Roll Control Power

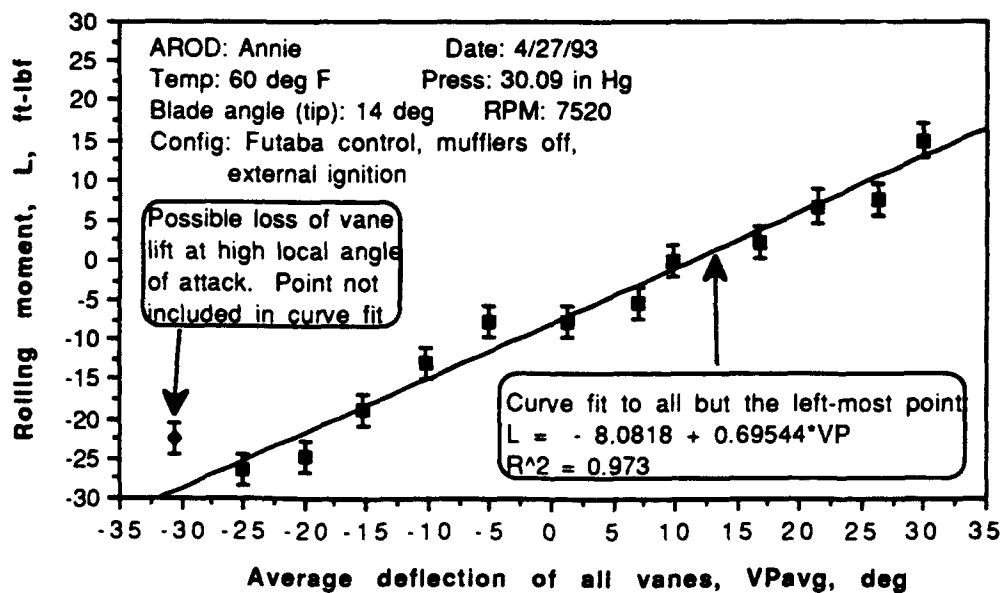


Figure IV.6: AROD Engine Test--Four-Vane Roll-Control Power

Sandia National Lab, had similar results during testing [Ref 18].

d. Pitch control power modelling

Data from the engine tests were used by other team members to model roll control power [Ref 19]. Additionally, the data were used to model the pitch control power due to vane deflection for use in the 3-DOF simulation, discussed in Figure VII. Details of this transformation from roll control power to pitch control power follow.

Pitch control power from the vanes in the Archytas airframe will be implemented by deflection of vanes two and four as shown in Figure IV.4. They will both be deflected so as to cause pitching motion. In other words, to pitch the "nose" of the Archytas down vane two will be rotated counter-clockwise (negative for the roll control convention) while vane four will be rotated clockwise (positive under the roll control convention). Since this will involve deflection of two vanes, the data from the dual-vane roll-control power tests were used to model pitch control power.

Dual-vane roll control was assumed to occur from the lift of the two vanes at mid-span, as shown in Figure IV.8, with each vane producing an equal lifting force, F .

The rolling moment generated by these pair of vanes, then, is:

$$L = 2F\left(\frac{9}{12}\right) \quad (L = \text{rolling moment in ft} \cdot \text{lbf}) \quad (\text{IV.A})$$

Equating this rolling moment model to the curve fit of dual vane rolling moment test data from Figure IV.5:

$$L = 1.5F = -7.86 + (0.400)(VP)$$

(Recall that VP is vane deflection) (IV.B)

Solving equation IV.B for F:

$$F = -4.24 + (0.267)(VP) \quad (IV.C)$$

Pitching moment will then be a result of twice this same lifting force applied over a moment arm from the vane quarter chord to the longitudinal center of gravity, as depicted in Figure IV.9:

Which gives a pitching moment due to vane deflection of:

$$M_{vane} = -2F(xcg_v)$$

or, substituting for F from equation IV.C:

$$M_{vane} = -2\{-4.24 + (0.267)(VP)\}(xcg_v) \quad (IV.D)$$

The number -4.24 in ft-lbf from equation IV.C represents the rolling moment zero-vane-deflection position, as shown on Figure IV.5. Because the propwash characteristics will be different when vanes are deflected for pitching moment, and to simplify user input to the simulation program--i.e. user will not be

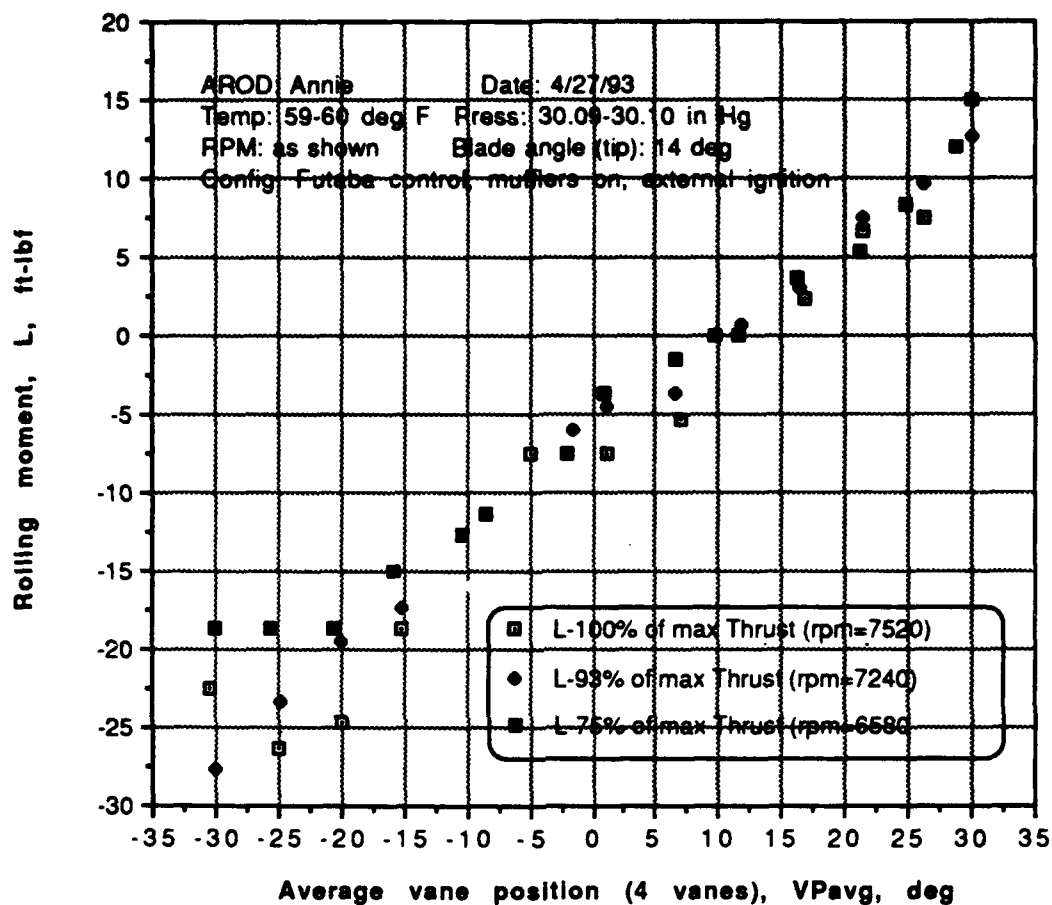


Figure IV.7

AROD Engine Tests--Change in Roll Control Power With Throttle

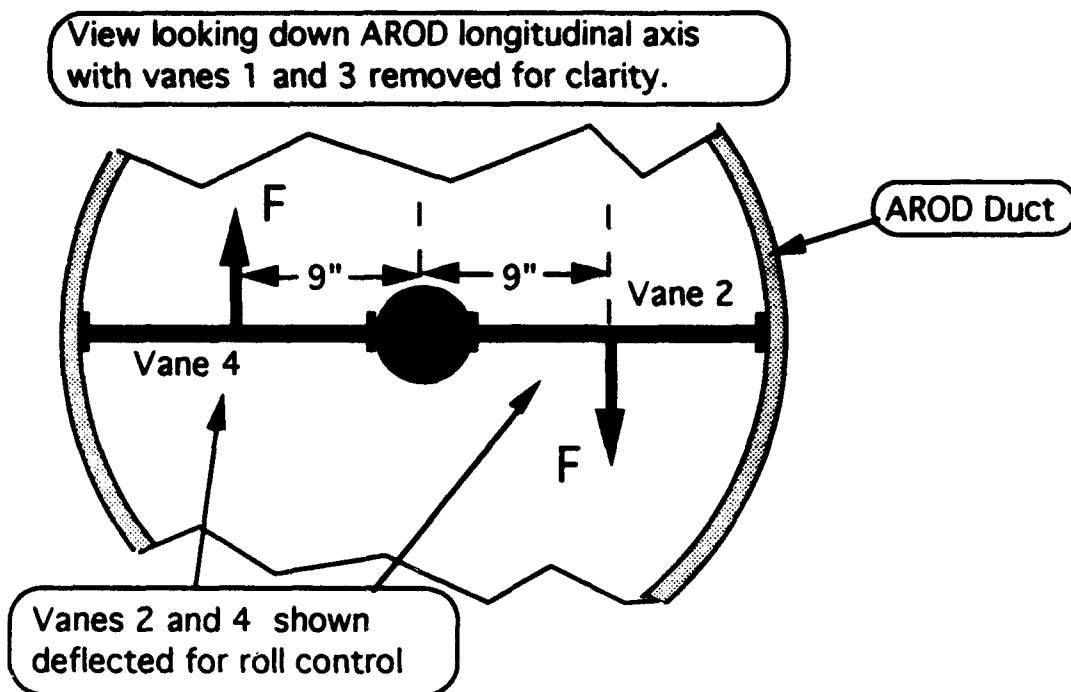


Figure IV.8: AROD Roll Control Functional Model

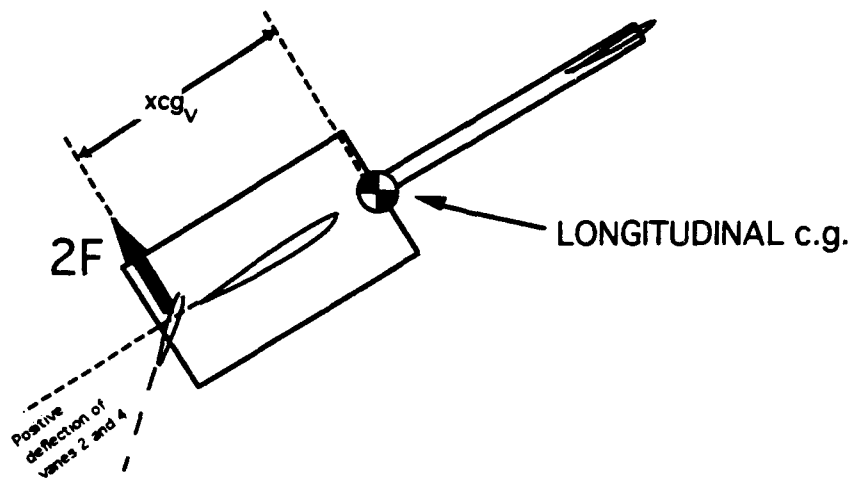


Figure IV.9: Pitch Control Functional Model

required to know that a certain number of degrees of vane deflection are required to counter the swirl of propwash in the duct--this quantity was eliminated from the analysis. Note that equation IV.D accounts for the sign change required to reflect the difference in sign convention between the roll axis--where positive deflections produce positive moments--and the pitch axis--where positive deflections produce *negative* moments [Ref 17]. Note also the change in variable from VP to δ_v , used to define vane deflections in a pitching sense for the simulation program. Making these two changes to equation IV.D as well as inserting the final value for x_{cg_v} of 1.5 ft, which was arrived after considering issues discussed in Figure VI, the final model for pitching moment due to vane deflection, used in Figure VII, was:

$$M_{vane} = -(0.80)(\delta_{vane})$$

$$\text{where } \delta_{vane} \equiv \text{vane deflection in degrees} \quad (IV.E)$$

4. Effect on thrust from blockage in AROD duct

The changes in thrust due changes in vane deflection, termed "blockage effect", were documented by noting changes in thrust due to vane deflection at three throttle settings. This analysis was performed primarily to predict the change in thrust with vane deflection for improved computer modeling of thrust, particularly in

a hover, where engine thrust levels are critical. A secondary goal of these tests was to attempt to characterize the swirl of propwash in the duct. The effect on thrust due to vane deflection is shown in Figure IV.10. Regardless of throttle setting, the maximum thrust was achieved at about -5 deg of vane deflection. The differences in indicated thrust were likely a result of changes in the local angle of attack, and hence vane drag, due to swirl in the duct. Apparently the local velocity at the vanes was approximately in-line with the vane's symmetrical airfoil section when the vanes were at -5 deg. At vane deflections off this peak-thrust-value the thrust fell off steadily, decreasing approximately ten percent at full throw in each direction. Incorporation of these results will increase the fidelity of future simulations.

5. Impact of propwash on vane position

Early in engine testing it was observed that, when using computer control of vane position, the vanes would be at a different deflection when the engine was running than they had been during position calibration with the engine shut down. Furthermore, as throttle--and presumably local velocity at the vanes--was increased the vane position would change with no change in the commanded position. This effect, which came to be known as "blowback effect", was documented during testing completed on April 16, 1993. Vane position was calibrated with the engine off through a program written in "C" and run on an IBM PC 386. Reference 16 describes the computer control set-up. Figure IV.11 shows the change in vane

deflection with the engine running. A general trend in the errors is apparent in Figure IV.11, with errors approximately linear from minus 15 to plus ten degrees and then dropping off at higher commanded vane positions.

Engine tests performed on April 27, 1993 were conducted using a Futaba[®] R/C set to command vane and throttle positions. When using radio control, this blowback error did not occur.

6. Flow speed at vane locations

The speed of airflow at two locations near the vanes was measured with a hand-held digital wind meter for future use in duct aerodynamic modeling and/or control power prediction. Readings fluctuated approximately ± 2 ft/sec. These fluctuations, which may have been due to actual fluctuations in flow speed or to wind meter inaccuracies, were considered insignificant to the goal of the analysis. Flow speed was gathered over a range of speeds at two different locations as shown in Figure IV.12. Rotor theory predicts an induced velocity at the disk-plane of a rotor according to the following formula [Ref 20]:

$$v_a = \sqrt{\frac{T}{2\rho A}} \quad (\text{IV.F})$$

where:

$v_a \equiv$ Induced velocity in ft/sec

$T \equiv$ Thrust in lbf

$\rho \equiv$ density in slugs/ft³

$A \equiv$ Rotor area in ft²

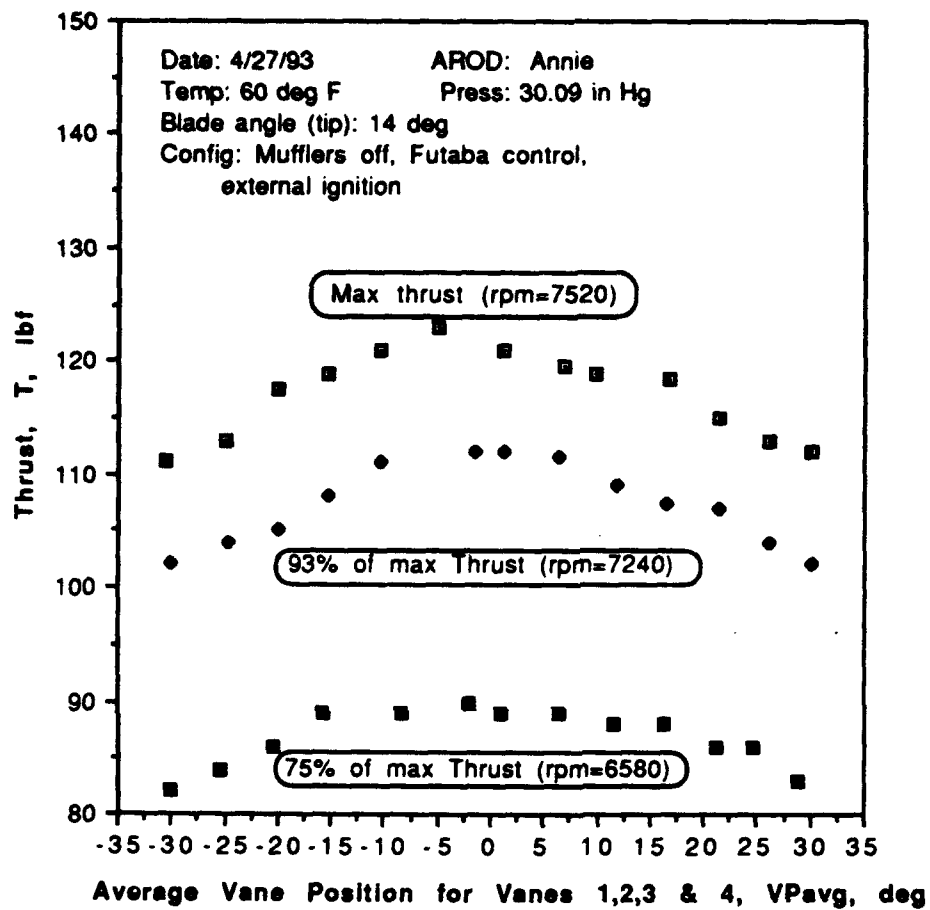


Figure IV.10:AROD Engine Tests--Vane Deflection's Effect on Thrust

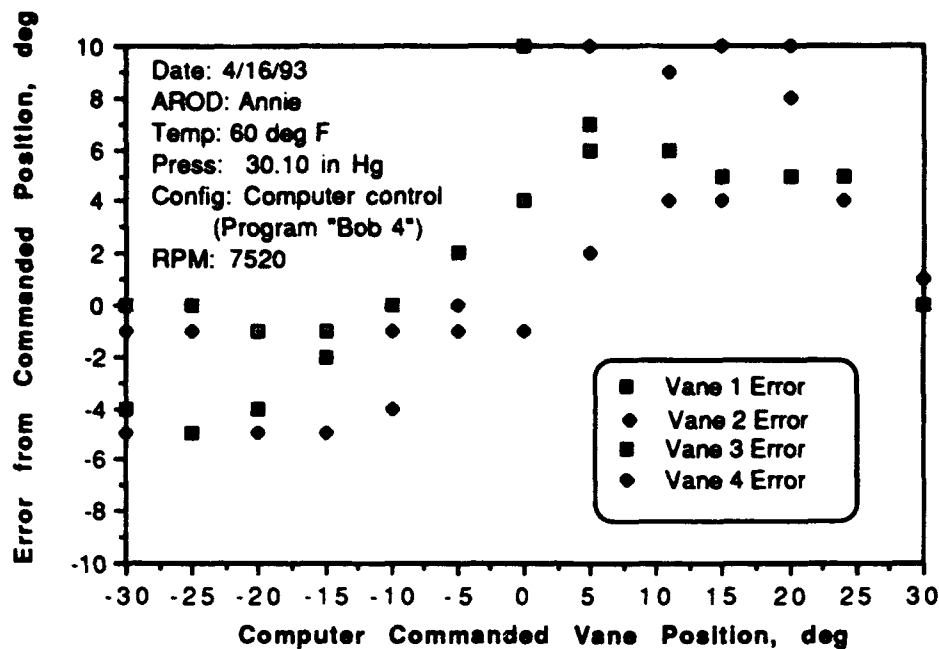


Figure IV.11
AROD Engine Test--Blowback Effect

Survey results are shown in Figure IV.13, with a second order polynomial curve fit displayed for survey position #1. Also shown in Figure IV.13 is the rotor theory prediction for a 12-inch radius rotor at the test day density of 0.002382 slugs/ft³. The data followed the slope predicted by theory but with an approximate average increase in velocity of 12 ft/sec. This velocity above prediction was probably due to a combination of three factors:

- The duct was not accounted for by rotor theory but would have the effect of containing and speeding the flow.
- The value for thrust, T , used in equation (IV.F) was not

actual thrust but rather engine thrust minus drag from the engine and its supports as well as duct wall and vanes.

- The hub of the propeller, at approximately 15 percent of the propeller diameter, was larger than that on most rotor systems.

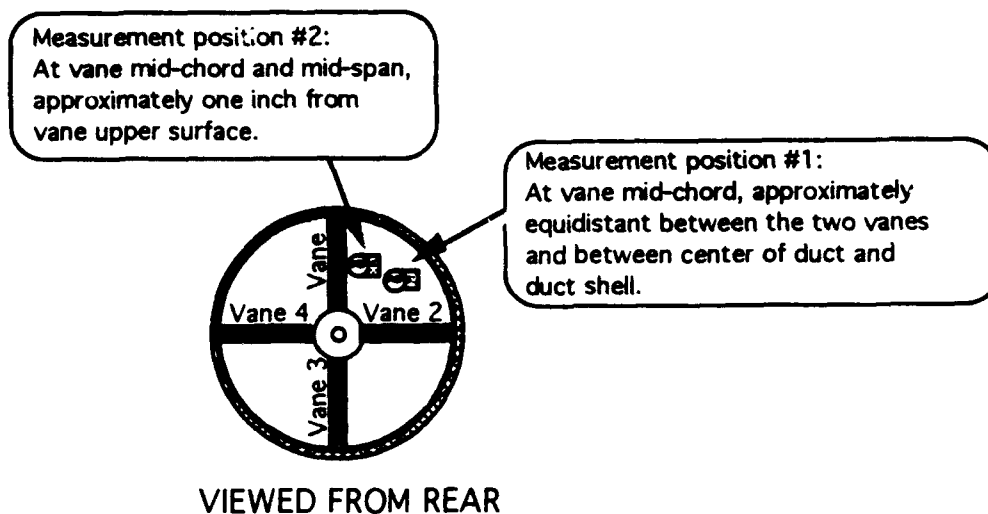


Figure IV.12:AROD Engine Tests--Locations of Flow Velocity Survey

7. Miscellaneous engine tests

a. Noise

The sound level was measured for the purpose of determining hearing protection required for test personnel. Additionally, the noise level figured into the decision on whether to operate the AROD with or without its mufflers, as discussed in a previous paragraph. Double hearing protection must be worn in areas with sound levels higher than 90 dB. With mufflers not installed, and when within about 20 ft of the AROD at full power, the noise level exceeded the noise meter limit of 120 dB. Installation of

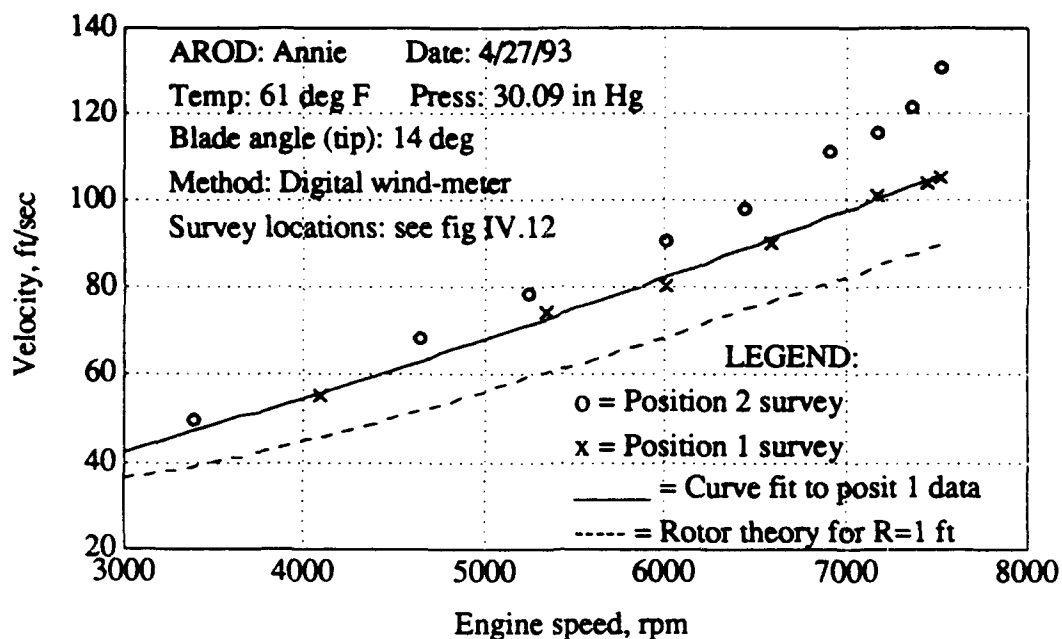


Figure IV.13:AROD Engine Tests--Flow Velocity Survey

mufflers reduced the sound levels by about 6 dB. For the mufflers-off case, a separation distance of greater than 100 ft was required to bring sound levels below the double-hearing-protection limit. These measurements were taken with the AROD positioned at the FRL test cell, which is surrounded by earth berms. Further testing will be required to determine sound levels for flat areas, such as that expected for flight test.

b. Fuel flow

Fuel usage was recorded for three separate engine runs at sustained high power, at or above 80 percent of maximum rpm. The average fuel consumption for these high power conditions, approximately representative of hovering flight, was 3.6 gallons per

hour. Qualitatively, fuel usage at reduced power was significantly less. No attempt was made to lean the engine to reduce fuel flow.

c. Acceleration/deceleration characteristics

The acceleration and deceleration characteristics were evaluated by attempting to record rpm versus time during rapid throttle movements. The response of the engine was too fast to allow observation/recording of the rpm on an oscilloscope. Qualitatively, by listening to engine response, the spool up and down characteristics were first order, with a time constant less than one third of a second.

d. Reliability

During the three data periods and several other practice and engine familiarization sessions, no engine related failures occurred. However, several failures occurred with the electronics which caused the engine to shut down. These failures generally occurred as a result of the AROD's high vibration levels. The failures included broken solder joints and wiring, and damaged circuit board components. Electronics failures and related issues are discussed in the thesis by LCDR Moran [Ref.16].

V. WING SPAR DESIGN, FABRICATION AND TEST

A. GENERAL

The purpose of designing a spar was to connect the existing Aquila wing, and the wing root support structure, which came to be known as the "shoulder", to the AROD duct. Previous work by Kress had specified a general design of two composite spars in the shape of rings that would surround the AROD duct [Ref. 11]. Initial work with cardboard mock-ups showed this design to be impractical for installation on the AROD duct, due to the AROD's longitudinal struts and landing gear, and so the spar was redesigned. The new design consisted of a two spar configuration with a shape similar to the previous design but spanning only 90 deg of the AROD duct, instead of the original design's 360 deg.

Several structural tests were conducted to determine component strength. A final, full configuration test was then conducted to determine the strength of a production-like installation.

B. WING SPAR DESIGN AND FABRICATION

1. Design load

The spar was designed to withstand 8 g's ultimate load factor and 5.33 g's limit load factor for a 100 lbf vehicle. This converted to 400 lbf of lift load per wing for ultimate strength and

267 lbf for design limit. For purposes of spar design and test, this lift load was assumed to occur as a point force at the quarter chord of the mean aerodynamic chord, as shown in Figure V.1. The moment at the wing root, then, was this lift load times the distance from the mean aerodynamic chord (MAC) to the wing root, 30.5 inches. This resulted in a predicted moment of 12,200 and 8,128 in-lbf for ultimate and design limits, respectively. The load for each of the two spars was then assumed to be carried as a function of its longitudinal distance from the point lift force. Ultimate and design limits for each spar are detailed in Table V.I. A sample calculation for the aft spar is presented below:

$$\begin{aligned}
 \text{AFT SPAR}_{\text{design moment}} &= \frac{(Wt)(Nz)(\bar{y})}{(\# \text{ WINGS})} \left(\frac{X_{\text{spar}} - \bar{X}}{X_{\text{spar}}} \right) \\
 &= \frac{(100 \text{ lbf})(5.33)(30.5 \text{ in})}{2} \left(\frac{16 - 5}{16} \right) \\
 &= 5588 \text{ in} \cdot \text{lb}_f
 \end{aligned}$$

where :

Wt = design weight

Nz = load factor

\bar{y} = y coordinate distance to MAC

X_{spar} = longitudinal distance between spars

\bar{X} = longitudinal distance from design spar
quarter chord of MAC

Table V.I
ARCHYTAS WING SPAR STRUCTURAL DESIGN LIMITS

SPAR	ULTIMATE MOMENT		DESIGN MOMENT	
	(8 g's)	in-lbf	(5.33 g's)	in-lbf
Forward		3812		2540
Aft		8388		5588
TOTAL		12200		8128

2. Forward spar design and attachment

Figure V.1 depicts the two-spar system conceived for use on the Archytas flight article [Ref. 21]. The basic structure consisted of a combination of graphite and fiberglass in an epoxy matrix surrounding a foam core. The two spars were connected to the AROD in different ways. The forward spar was affixed to the duct's exterior by three methods (refer to Figure V.1):

- The spar was cut to fit the duct surface as closely as possible and was attached with a special structural adhesive to the outside of the duct. Adhesive thickness varied depending on the quality of the fit between the spar and the duct--approximately 1/32 to 1/8 inch. The load path for this connection method--termed "peel strength"--was from the surface of one composite component (the AROD and the forward spar), through the structural adhesive and into the other component.

- Grip plates were manufactured from 0.053-inch thick 6061-00 aluminum and configured with 0.25 in nut plates. These grips were attached to the forward spar surface with the structural adhesive, with a targeted adhesive thickness of 5.0 mm. As specified in industrial references, to ensure a good bond between the aluminum grip plates and the composite/epoxy spar, the aluminum was bead-blasted and then cleansed by a commercially available trichloroethane product ("Brake Clean") [Ref 22 and 23]. Research was conducted to determine the feasibility of first etching the aluminum plates with chromic acid and then phosphoric anodizing them, in an attempt to optimize the bonding surface [Ref 22]. Discussions with personnel in the NPS Physics department as well as commercial anodizing contractors revealed that this process was environmentally risky and required special equipment and chemicals not readily available [Ref 24 and 25]. A decision was made to utilize a mechanical abrasion method (bead blasting). Additionally, the grip plates had number 25 holes drilled in them so that the structural adhesive could flow through for improved bonding [Ref 26]. The grips were attached to the AROD duct by 0.25 in bolts passing through their own load-bearing plates, which were adhered to an AROD strut with the structural adhesive, then through the strut and into the grip's nut plate, as shown in Appendix B, Figure B.1

- The last connection made between the forward spar and the duct was through a aluminum grip plate of the same material as above but oriented radially. In other words, the base of the grip

plate (with an integral 0.25 in nut plate) rested on the duct's exterior surface and this plate was attached to the forward spar at a 90-deg angle to the previously described grips. A single 0.25 in bolt was passed through a plate mounted on the *inside* of the AROD duct, as shown in Appendix B, Figure B.2, and into the nut plate on the grip. The bolt was positioned below the propeller to avoid Foreign Object Damage (FOD) to engine and propeller components. The purpose of this last connection was to improve the spar's "peel strength".

3. Aft spar design and attachment

The aft spar was similar in construction to the forward spar except that, owing to reduced area available for mounting in the wing root, it was 2.0 in thick, 1.0 in thicker than the forward spar. The aft spar had aluminum grips mounted in the same manner as the forward spar. These grips were bolted to the AROD's aluminum landing gear legs and constituted the entire mounting strength for the aft spar. Appendix B, Figure B.3 shows grips installed on both spars.

4. Integration of NPS spars with Aquila wing spars

The forward and aft spars manufactured at the FRL were mated to the Aquila wing's root by a combination of bolts, plates and structural adhesive as shown in Figure V.2. The Aquila wing was then attached to its wing root by its original system of bolts and nut-plates.

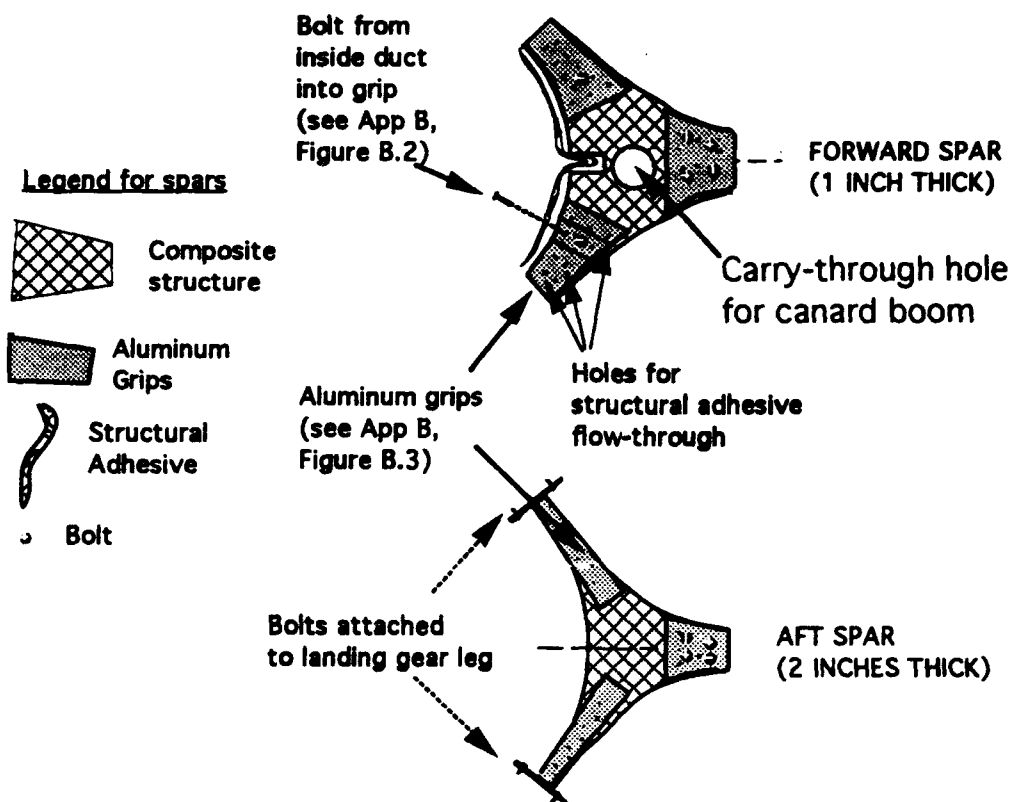
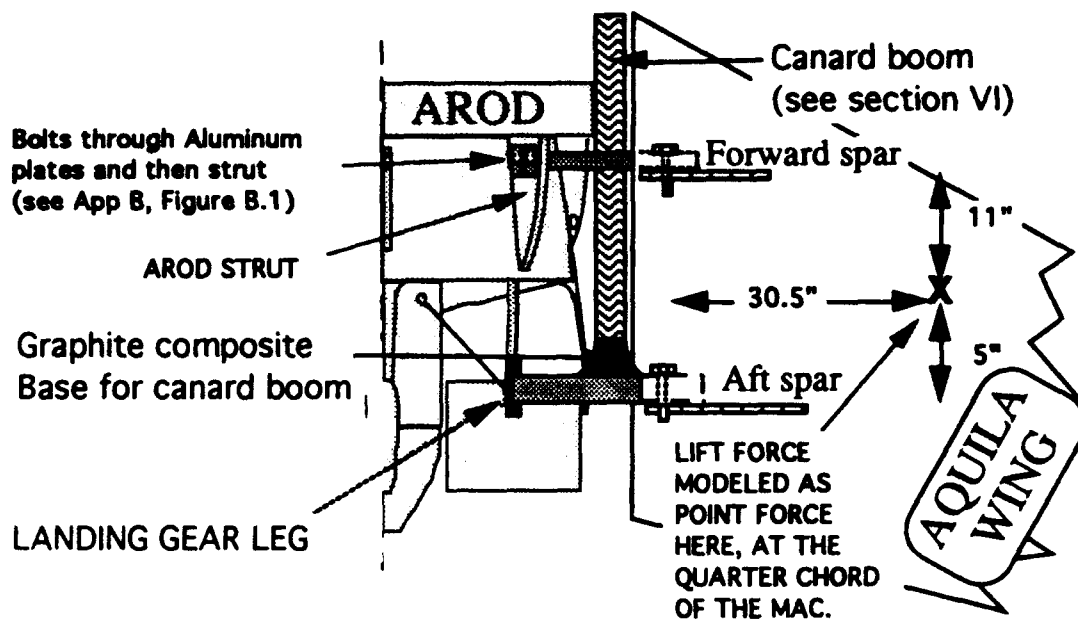


Figure V.1: Archytas Wing Spar Design

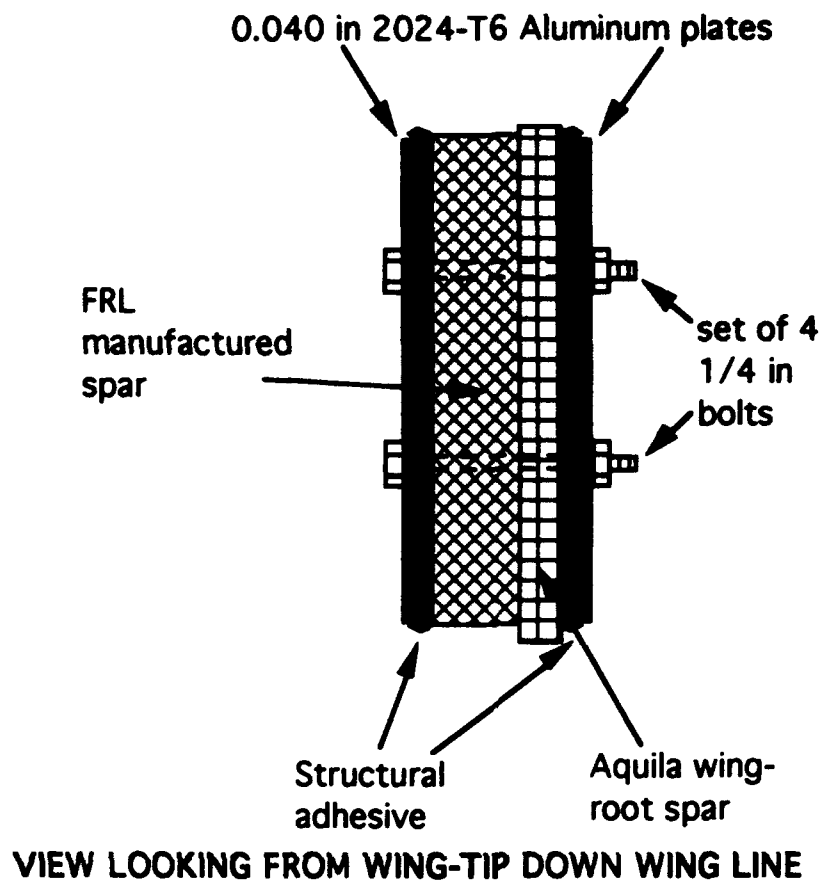


Figure V.2

Archytas FRL/Aquila Wing Spar Integration

C. WING SPAR EXPERIMENTS

1. Initial component testing

Forward and aft spars were first fabricated as detailed in previous work [Ref 11], at which point a structural test was performed on these test specimens to compare actual strength with those predicted in the finite element analysis of the previous thesis work. The structural test at this point of development was on the individual spar component. Figure V.3 depicts the set-up for the

structural test on an individual spar. The upper part of the figure, part a, shows the spar in a notional installation. The lower part of Figure V.3 depicts the experiment to test spar strength. The test spar was mounted in a supporting fixture designed to test the narrow area of the spar and the bonding of the structural adhesive to the aluminum plate, as depicted in Figure V.2. The test spar was mounted upside down so that the weight placed on the beam would simulate a lift load. Appendix B , Figure B.4 is a photograph of the test set-up.

The 215 lbf weight, a stainless steel bar, was set in place by a hand forklift at known distances marked on the steel beam. The 42 lbf steel tube was then placed on the steel beam and progressively moved farther out the beam. Once the steel tube was at the beam's end it was removed, and the 215 lbf weight was then moved out enough to produce the same total moment that had existed when the bar was in its former location with the tube at beam's end. The tube was then replaced on the beam, near the test spar, and then again progressively moved out the beam. The weight of the steel beam was also accounted for and was assumed to act as a point force at half its length. This process continued until either a failure occurred or a desired moment value was reached.

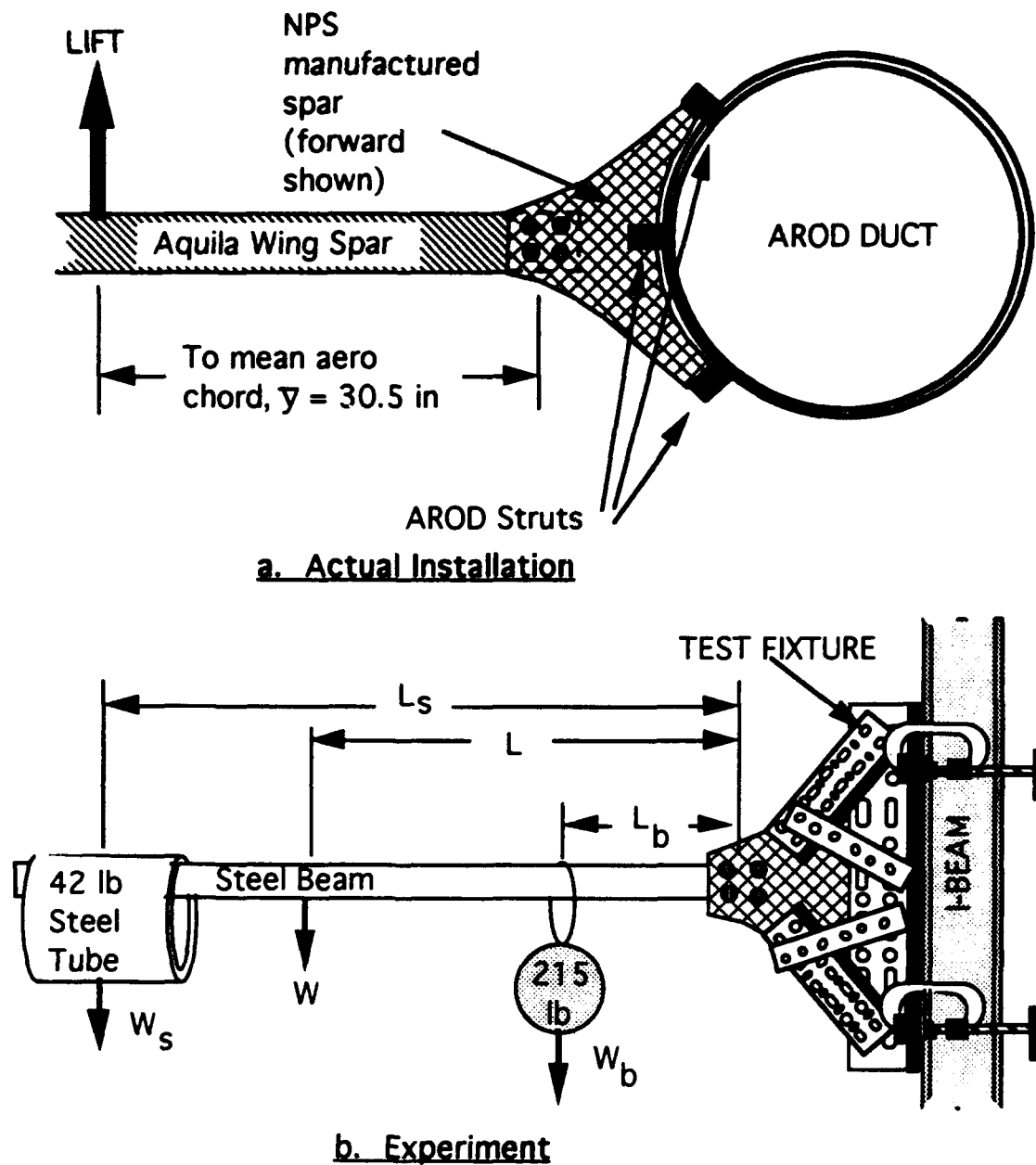


Figure V.3
Archytas Wing Spar Installation and Test

With the combination of tube, beam and bar weights simulating an aerodynamic lift load, the moment supported by the test spar was calculated as follows (refer to Figure V.3):

$$\begin{aligned}\sum Moments &= 0 \\ 215(l_b) + 42(l_s) + W(l) - M_{spar} &= 0 \\ \text{or} \\ M_{spar} &= 215(l_b) + 42(l_s) + W(l)\end{aligned}$$

The loading was placed slowly, i.e. the weights were not dropped on the beam, and were left in position for at least two minutes without any failure of the spar. Failure of the spar was quantified by listening for cracking noises in the vicinity of the spar. Typically, when the load was applied there would be a few small cracking noises as, presumably, a few of the fibers and/or portions of the matrix broke and "settled in". These "micro-failures" were minor and short lived and, if a load was relaxed and re-applied, generally did not reoccur. Failure was generally marked by a slow, continuous series of cracking noises which did not cease, although the time interval between cracks was often on the order of a minute, finally culminating in an actual failure of the whole structure. The time period from application of the load to the actual failure took as long as ten minutes. All of this is to say that the structural testing was considered to be fairly conservative, in that the moment was not rapidly increased in an effort to increase the apparent strength of the component. Table V.II shows the loading sequence for the initial

test of the forward spar. Recall from Table V.I that the goal was to reach an ultimate moment of 3812 in-lbf for this component.

Table V.II
ARCHYTAS FORWARD SPAR TEST (BEAM=16.5 lbf, L=74 in)

L_b (in)(1)	L_s (in)(1)	Notes (M_{spar} in-lbf--Goal=3812)
6	Not applied	2 or 3 small cracking noises ($M=2508$)
6	12	No cracking ($M=3012$)
6	18	10-15 small cracking noises, appeared to come from plate area ($M=3264$)
6	24	Small cracking noises continuous, every 10-15 seconds. Failure after approximately 10 minutes ($M=3516$)

Notes: (1) Refer to Figure V.3 for dimensions and experiment method

The moment at failure was 92 percent of the ultimate, corresponding to a load level of 7.4 g's. Post-experiment analysis of the test spar revealed that the failure may have started at a lower loading level as the laminates separated, but that final failure was partially masked by the test fixture constraining a portion of the

spar. The failure occurred at the juncture of the shear web and spar cap laminates [Ref 11, pp 31] adjacent to the plate that was designed to transmit the loads from the Aquila's wing spar. Figure V.4 depicts the location of this failure.

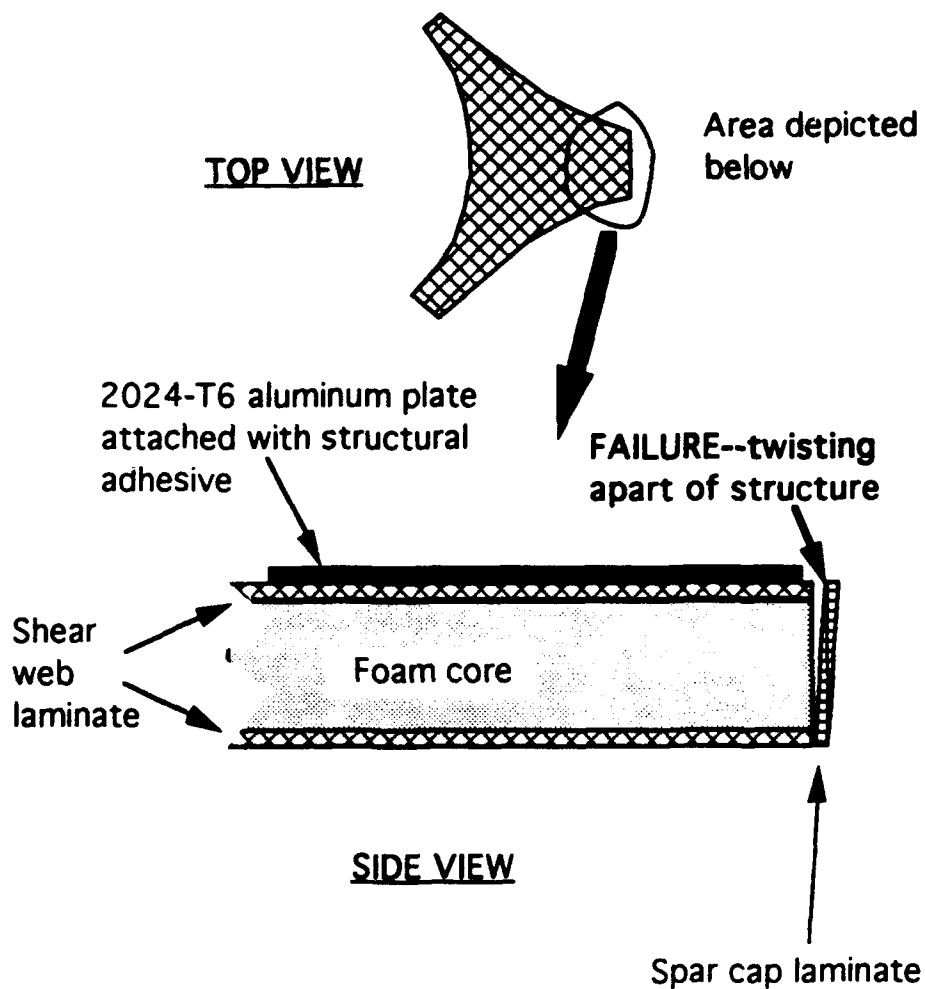


Figure V.4
Archytas First Test Spar Failure Description

2. Redesign of basic spar structure

As a result of the failure witnessed in the first structural test, a modification was made to the basic spar design in an effort to increase its strength. Specifically, the load path between the shear and spar cap laminates, which heretofore had consisted solely of the relatively weak matrix, was strengthened, as depicted in Figure V.5. This modification was made to the tip area of an existing aft spar. These modifications changed the weight of this particular test aft spar from 0.77 to 1.51 lbf, an increase of 49 percent, but it was felt that the weight of a spar built with these modifications incorporated during original construction would not gain as much weight. In any case, the original design was clearly unsatisfactory and in need of modification.

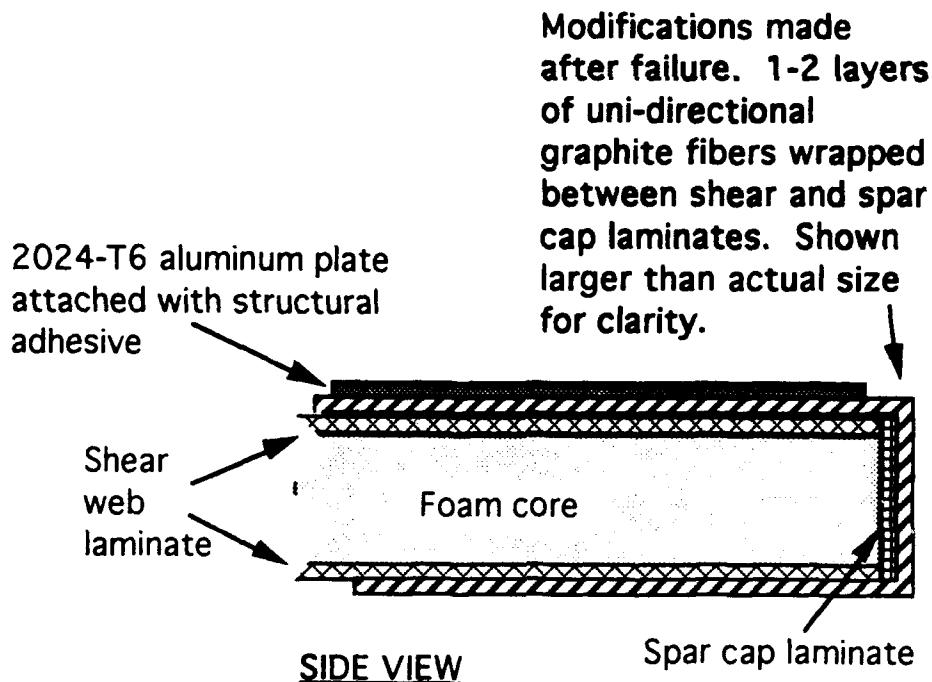


Figure V.5: Modifications Made to Archytas Spar

3. Testing of modified spar

The modified spar was tested in the same way as the original test spar, except that the beam on which the weights were placed was replaced with a shorter version. Table V.III describes the loading pattern. The goal for this test aft spar was to reach an ultimate moment of 8388 in-lbf.

Table V.III

ARCHYTAS MODIFIED AFT SPAR TEST (BEAM=12 lbf, L=37 in)

L_b (in)(1)	L_s (in)(1)	Notes (M_{spar} in-lbf--Goal=8388)
12	36	Nothing noted (M=4536)
12	48	Nothing noted
12	54	Nothing noted (M=5292)
18	Not applied	Nothing noted (M=4314)
18	30	Nothing noted (M=5574)
18	36	Nothing noted
18	42	Small cracking sounds near base of test fixture (M=6078)
18	48	"
18	54	Nothing noted
18	60	Nothing noted (M=6834)
24	Not applied	Nothing noted (M=5604)
24	36	Small cracking sounds near base of test fixture (M=6078)
24	42	As above (M=7368)
24	48	As above (M=7620)
24	54	Failure of spar at attach point to fixture (M=7872--94% of goal)

Notes: (1) Refer to Figure V.3 for dimensions and experiment method

During the testing of this modified spar, cracking sounds were heard and appeared to be coming from the base of the test specimen, where it was held by the test fixture. As shown in Figure V.6, post-test analysis of the spar showed that the modified areas were without permanent deformation and uninjured. Appendix B, Figure B.5 is a photograph of this test spar showing the failure. The failure occurred adjacent to the area that was modified. This area had not been modified because it had been assumed that the test fixture would provide the necessary strength to support the spar, obviating the need to modify the entire test spar. As mentioned, the modified area was unaffected by the 93 percent of ultimate moment, correlating to 7.5 g's. While the results of this second test appeared to shadow the results of the first test it was obvious to test personnel that the modified spar was significantly improved because it did not bend or deform as had the previous design. Because of this confidence in the modified design a decision was made to manufacture a series of new spars using the modified technique and to proceed to the next stage of testing.

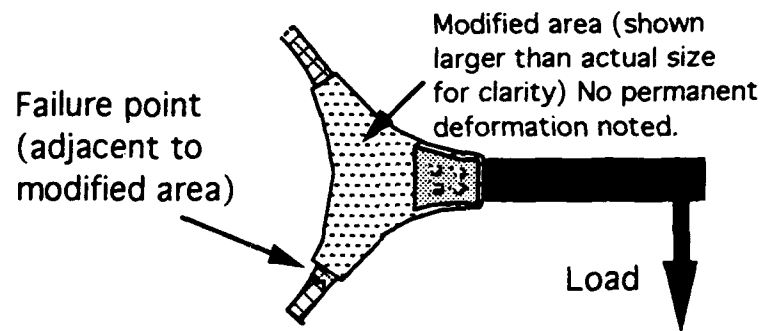


Figure V.6: Archytas Second Spar Test Failure Description

4. Comprehensive structural test

After basic design problems were identified and corrected during the component testing phase, a test was conducted on an entire duct, wing spar, and wing assembly. An AROD duct which had been previously partially damaged was utilized as a Structural Test Vehicle (STV). The damage on the STV was limited to areas not affecting the outcome of structural testing. As depicted in Figure V.7, the STV was a standard AROD duct with a prototype right-hand wing assembly mounted to it. Components included the NPS manufactured wing spars and their attaching hardware as described earlier in this chapter, the canard boom with support hole drilled in the forward spar for it and boom base mounted to the aft spar (see Section VI), and the Aquila wing root bolted to the NPS spars. The STV was assembled using the techniques and materials anticipated for use in the flight article. The beam used for load application was mounted so as to simulate the assumed point lift force, as depicted in Figure V.1; in other words, it was placed five inches in front of the aft spar and eleven inches aft of the forward spar. Similar to the structural tests conducted on individual components, the STV was loaded by a combination of large (215 lbf) and small (42 lbf) weights. Because the wing root ("shoulder") assembly used on this full test was intended for use on the flight article, the decision was made to limit the load applied to the design limit of 5.33 g's or 8128 in-lbf. The loading sequence and comments thereof are contained in Table V.IV.

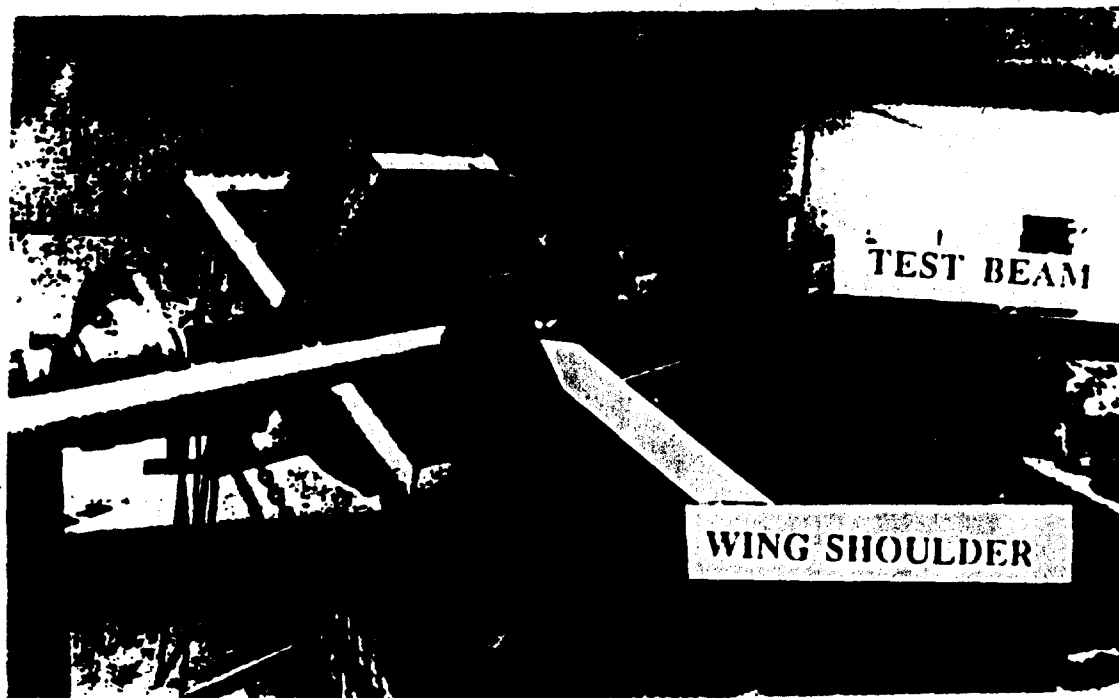


Figure V.7: Archytas full configuration test set-up

Table V.IV

FULL CONFIGURATION STRUCTURAL TEST (BEAM=12 lb, L=46 in)

L_p (in)	L_q (in)	Notes (M_{spar} in-lb; Goal=8128)
12	0	Nothing noted ($M=3132$)
12	24	Small cracking noises heard for first 5-10 seconds ($M=4140$) Appeared to be coming from wing shoulder
12	30	As above
12	36	As above ($M=4643$)
12	42	Small cracking noises lasting 15-20 seconds ($M=4896$)
12	48	Noises continued and wing shoulder was visibly deforming Test suspended ($M=5138$) 63% of goal

The wing shoulder was removed and inspected. As shown in Figure V.8, the wing shoulder had begun ripping at a location adjacent to the wing spar. No failures were noted in the FRL manufactured parts. A decision was made to suspend further testing of the wing shoulder until it could be modified. To determine the strength of the FRL manufactured spars and their attachment with the AROD duct, a test fixture was constructed to take the place of the wing shoulder and allow loading of just these components. This experimental set-up is shown in Figure V.9. Table V.V describes the results of this test. The decision was made to limit the load to design limit (5.33 g) in order to preserve the capability to do testing with a modified shoulder.

Table V.V

ARCHYTAS STRUCTURAL TEST OF FRL SPAR INSTALLATION
(BEAM=12 lbf, L=43 in)

L_b (in)	L_s (in)	Notes (M_{spar} in-lbf--Goal=8128)
12	0	Nothing noted ($M=3096$)
12	18-72	Nothing noted (final $M=6120$)
24	30 to 54	Nothing noted
24	60	GOAL REACHED, test suspended ($M=8196$ --101% of goal)



Figure V.8: Failure of Aquila wing shoulder

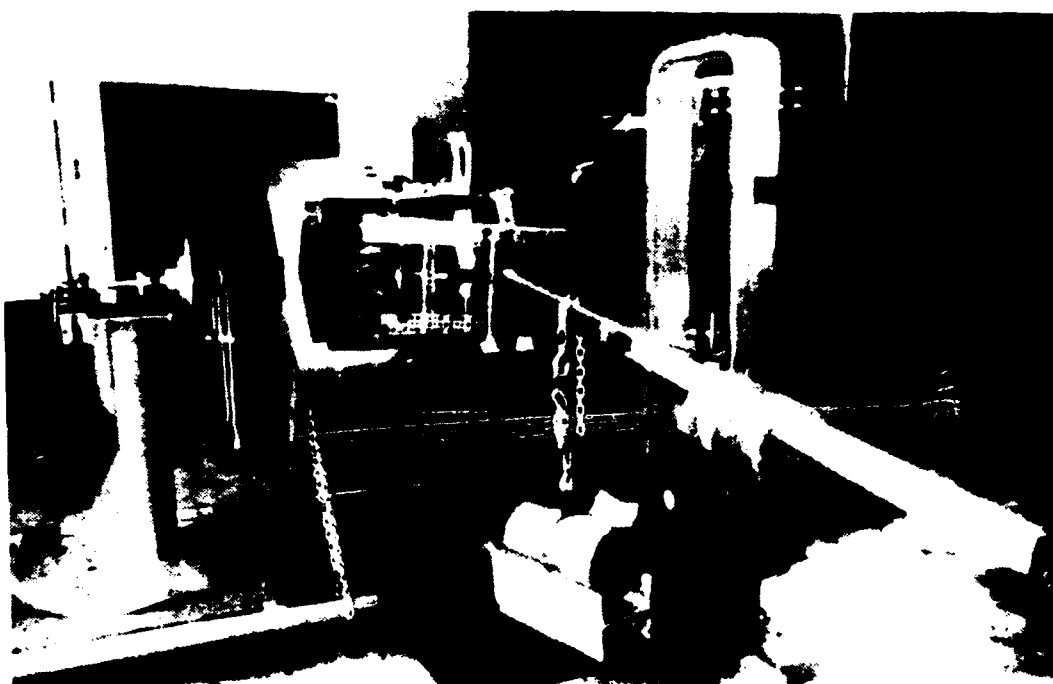


Figure V.9: Structural test of wing spars without wing shoulder

During application of the load, there was approximately five degrees of bending in what would be the wing. When the load was removed, the structure returned to its original position. The spars and attachments were inspected after the test and no cracking, permanent deformation or loss of strength were noted.

VI. CANARD DESIGN, FABRICATION AND TEST

A. GENERAL

After formulating the initial concept of combining the wings from an Aquila with the AROD ducted-fan UAV, the next issue was how longitudinal control and stability would be provided. Use of a conventional, tail-aft design was discarded for several reasons, including too high a center of gravity for takeoff and landing and the structural complexity of building a combination tail and landing gear. The other alternative was the use of a canard. The effort of the present thesis, then, was to design a canard and design, fabricate and test a support structure for the canard, that would have the following characteristics:

- Good static longitudinal stability with a 15 percent static margin, and the aircraft trimmable throughout expected flight range
- Good longitudinal control power for forward flight
- Location of the canard at least one chord length in front of the nearest AROD structure to minimize aerodynamic interference
- Lightweight construction capable of withstanding expected flight loads

The process that resulted in a final canard size and location was iterative in nature. For example, static margin was easily increased by moving the canard forward, but because stronger (heavier) booms

would be required, this added weight to a weight-critical design. The iterative nature of the canard and boom design process was as follows:

(1) The wing was modeled using vortex lattice techniques to determine what moments the canard would be required to counter.

(2) Knowing the wing characteristics, the canard could then be positioned and sized to provide a certain static margin. This was accomplished largely through the creation of a MATLAB program "xplot", which displayed the aircraft's neutral point and center of gravity for a range of canard sizes and locations [Ref. 27]. Note that at this point the canard and boom weight were assigned a nominal value, per linear foot for the boom and per square foot for the canard.

(3) Once the canard location and size were selected, further analysis of the static longitudinal trimmability was carried out through creation of another MATLAB program, named "incidence", whose output of pitching moment versus angle of attack graphically depicted the incidence angles required to fly over a range of speeds, or in other words, the stability and trimmability of the chosen design.

(4) With the canard configuration chosen, the boom was optimized by selecting the lightest tubing size capable of withstanding the expected loads.

(5) Components were then manufactured and tested to assure that they could indeed withstand the expected loads.

B. WING MODELING

The airfoil of the Aquila wing was a modified NACA 23015 section. Modification to the airfoil consisted of a slight reflex at the trailing edge, affecting the last ten percent of the upper surface and 30 percent of the lower surface [Ref. 28]. Table VI.I shows the Aquila airfoil coordinates. Figure VI.1 plots these coordinates as well as the mean camber line, and shows polynomial curve fits for two segments of the mean camber line.

The Aquila wing also incorporated a linear geometric twist of three deg, with the tip at a lower angle of incidence than the root [Ref 28]. A planform view of the basic wing geometry used for analysis is shown in Figure VI.2. The Aquila wing sweep angle of 28 deg was retained for the Archytas design for several reasons. The primary reason was the relative structural simplicity and associated weight savings of mating the Aquila wing spar in-line with the spar manufactured by FRL personnel. Additionally, lower sweep angles had the adverse effect of reducing the static margin for a given center of gravity, causing longitudinal stability and control problems.

Table VI.I
AQUILA WING AIRFOIL COORDINATES (PERCENT OF CHORD)

Station (x/c--percent)	Upper surface (z/c--percent)	Lower surface (z/c--percent)
0	-	0
1.25	3.34	1.54
2.5	4.44	2.25
5	5.89	3.04
7.5	6.90	3.61
10	7.64	4.09
15	8.52	4.84
20	8.92	5.41
25	9.08	5.78
30	9.05	5.96
40	8.59	5.92
50	7.74	5.50
60	6.61	4.81
70	5.25	3.79 (modified)
80	3.73	2.43 (modified)
90	2.26 (modified)	1.00 (modified)
95	1.69 (modified)	0.239 (modified)
100	1.00 (modified)	0.016 (modified)

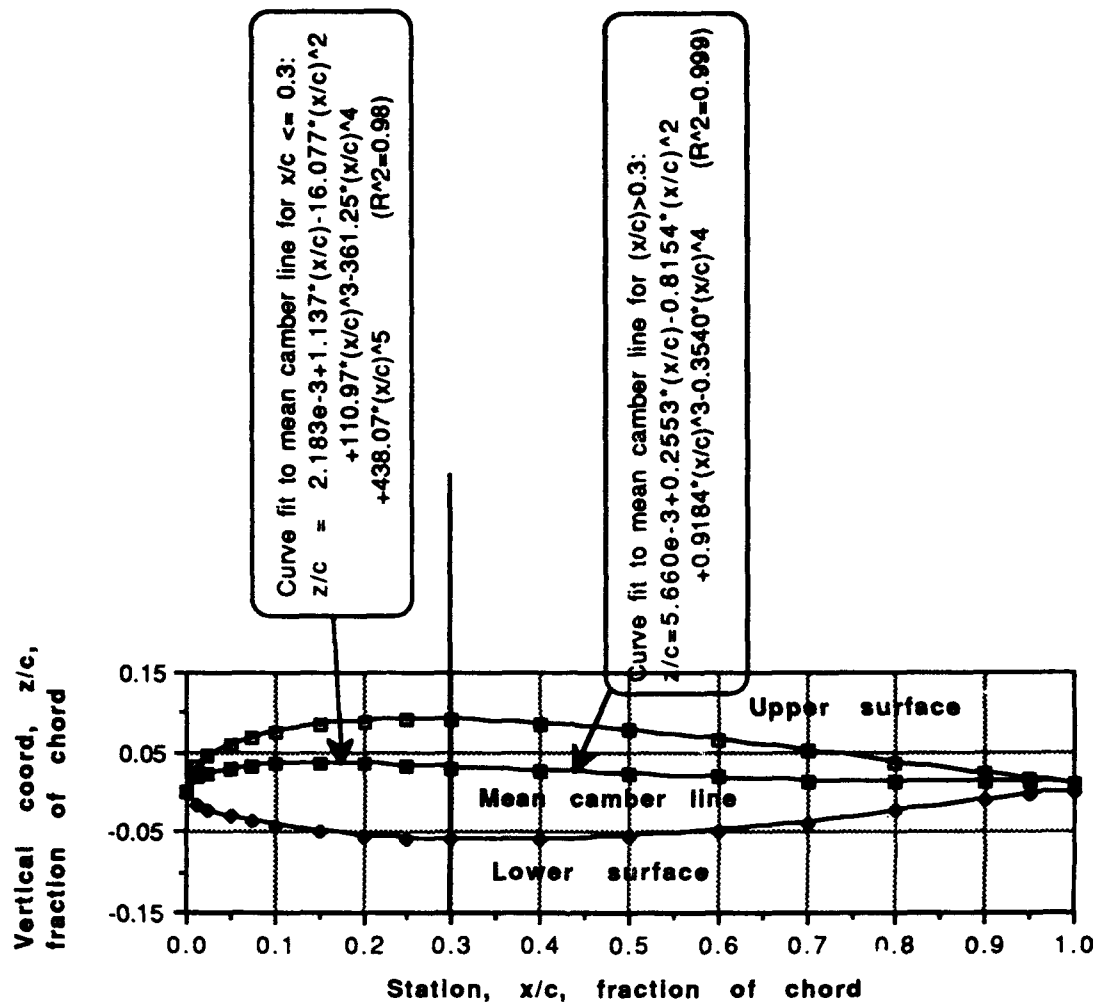


Figure VI.1
 Aquila airfoil, modified NACA 23015
 With Mean Camber Line Curve Fits

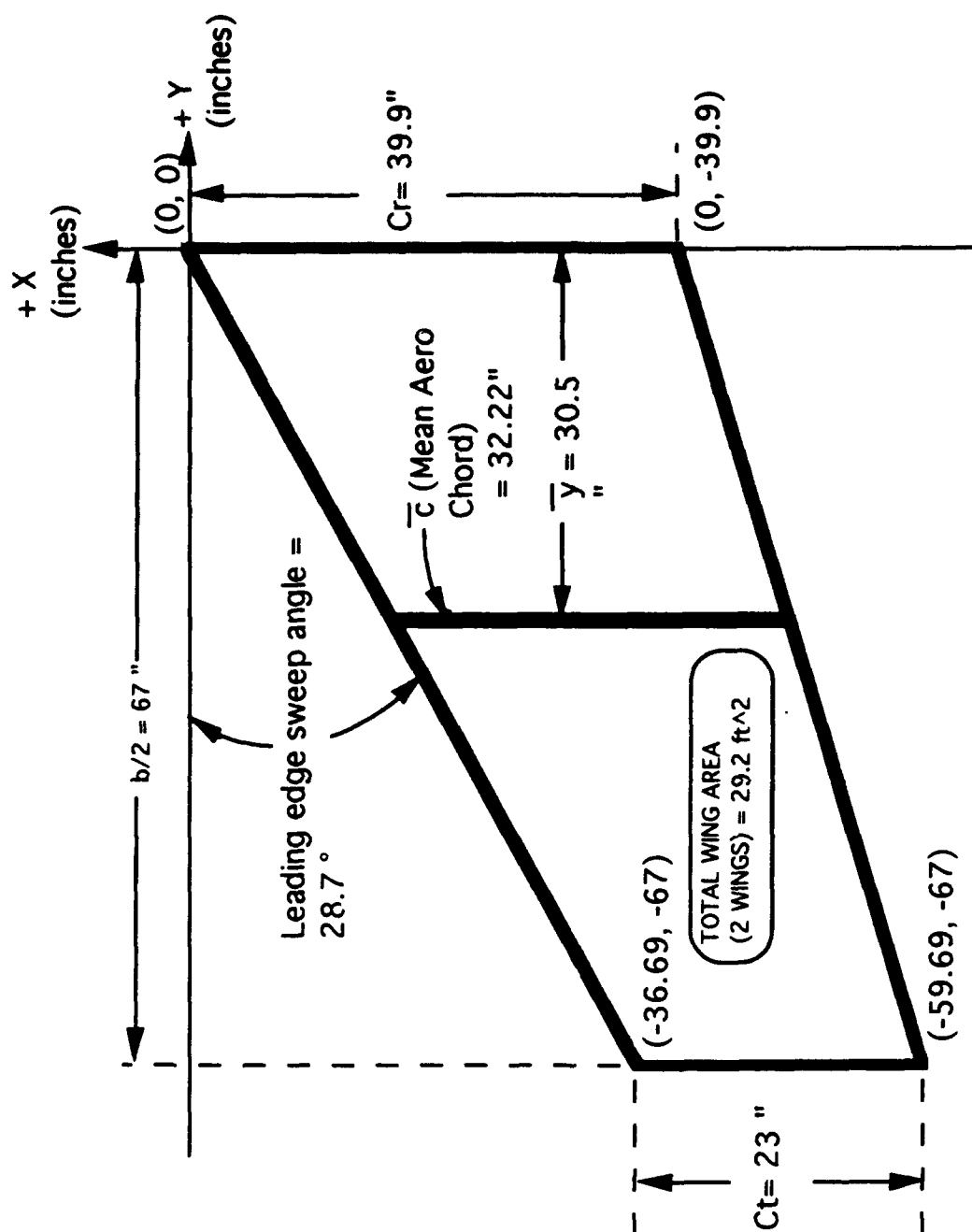


Figure VI.2
Aquila Wing Geometry

An analysis was performed on the basic wing planform using a NASA-developed vortex lattice FORTRAN program, named "SUB", resident on the NPS VAX computer system [Ref 29]. The wing was divided into 100 panels in a ten-by-ten equally spaced grid. A FORTRAN program, named "camber.for" and shown in Appendix C, converted the derivative of the equation for the mean aerodynamic chord, given in Figure VI.1, to a local incidence angle for each of the 100 panels. The output of the program "camber.for" did not include the three deg geometric twist. This twist was calculated manually for each panel. The final input file to program "SUB" is also given in Appendix C. The results of the vortex-lattice analysis are listed in Table VI.II.

Table VI.II
RESULTS OF VORTEX LATTICE ANALYSIS OF AQUILA WING

CHARACTERISTIC	VALUE
Lift curve slope, $C_{L\alpha}$	3.771 per radian 0.06581 per deg
Slope of pitching moment/ C_L curve, $dC_m/dC_L = C_{m_{CL}}$	-0.7578
Intercept of C_m/C_L curve for wing, C_{macwb}	0.00761

C. CANARD SIZING AND LOCATION

1. Static Margin

a. General

With the wing characteristics known, a suitable balancing force, in the form of a canard, could now be designed. A static margin of 15 percent was targeted during the longitudinal stability analysis, to provide a good balance between stability and pitch response [Ref 30]. Figure VI.3 depicts the coordinate system and variables used during the static margin analysis. Note that the variables shown on Figure VI.3 are written in the form used in the static longitudinal stability program "xplot".

b. Computer modelling

The static margin, essentially the distance between the whole aircraft's aerodynamic neutral point and its center of gravity, was determined by creating a MATLAB program named "xplot". The code for this program is shown in Appendix D. The algorithm for this program follows:

(1) The aircraft neutral point was assumed to be due to a combination of two items: the Aquila wing and the to-be-designed canard. As with the simulation effort described in Section VII, no aerodynamic allowance was made for the AROD duct. The following equation was used to define the neutral point [Ref. 31]:

$$X_{ac \text{ aircraft } \bar{c}} = \frac{X_{acwb}}{\bar{c}} + V_H \cdot \frac{a_{c \text{ 3-D}}}{a_{wb}} \left(1 - \frac{\partial \epsilon}{\partial \alpha} \right) \quad (\text{VI.A})$$

where:

$X_{ac \text{ aircraft } \bar{z}}$ \equiv Longitudinal position of aircraft aero center (neutral point), normalized by \bar{c}

X_{acwb} \equiv Aerodynamic center of wing/body combination

\bar{c} \equiv Mean aerodynamic chord of wing (32.2 in)

V_H \equiv Tail volume coefficient

$$= \frac{X_{acc} \cdot S_c}{\bar{c} \cdot S}$$

where:

X_{acc} \equiv Longitudinal position of canard's aero center (user specified in "xplot")

S_c \equiv Area of canard (a vector of values in "xplot")

S \equiv Wing reference area (29.2 ft²)

$a_{c \text{ 3-D}}$ \equiv 3-dimensional lift curve slope of canard

a_{wb} \equiv Lift curve slope of wing/body combination

$\frac{\partial \epsilon}{\partial \alpha}$ \equiv downwash (assumed zero)

(2) With reference to Figure VI.3, allowances were made for the weight and location of the following components: AROD duct including landing gear, Aquila wings (including spars and hardware discussed in Section V), fuel, electronics pod, canard with servo and supporting booms, and an optional ballast box at the tip of the canard's supporting boom. A full description of these components and their weights is contained at the end of program "xplot", Appendix D.

2. Longitudinal trimmability

The purpose of program "xplot", discussed in the preceding section, was to specify the canard size, given a desired static margin

Note: Names of dimensions are those used in the program "sploot". Where dimensions are given these represent constants. If dimensions are not given it represents a user selected dimension or variable.

Dimensions and Labels:

- Canard Chord (cc)** (a vector of lengths from 0 to 18")
- Canard Beam** buried in wing shoulder
- Canard direction** (referenced to duct)
- Quarter Chord of Canard**
- Canard**
- Canard Aero**
- Optional Ballast**
- Ballast**
- Xballast**
- Xacc**
- Ref Line for longitudinal stability**
- Top of Duct**
- Xboom**
- Xboom = 22"**
- Air spar mount**
- Mean Aero Chord, cbar = 32.22"**
- ybar = 30.50"**
- Configuration drawing - not to scale**

FOR ELECTRONICS FOR CRAFTS AND MODELERS FROM THE "ELECTRONICS FOR CRAFTS" COMPANY

75

portion of the analysis a program named "incidence" was written in MATLAB to depict the incidence angles required to trim the Archytas over a range of angles of attack. A printout of the code for program "incidence" is contained in Appendix D. The germane equations were:

$$C_{mo_{aircraft}} = C_{mac_{wb}} - V_H \cdot a_{c\ 3-D} \cdot i_c \quad (VI.B)$$

where:

$C_{mo_{aircraft}}$ = Aircraft pitching moment at zero deg absolute angle of attack

$C_{mac_{wb}}$ = Wing pitching moment coefficient at zero
deg angle of attack (from vortex - lattice analysis)

i_c = canard incidence (measure positive with leading edge down)

and

$$\frac{d(C_{mcg})}{d\alpha_a} = C_{L\alpha} \left[(h - hac_{wb}) - V_H \frac{C_{L\alpha\ canard}}{C_{L\alpha}} \right] \quad (VI.C)$$

where:

$\frac{d(C_{mcg})}{d\alpha_a}$ = Slope of aircraft pitching moment versus absolute angle of attack curve

$C_{L\alpha}$ = Lift curve slope of wing (from vortex lattice)

h = distance from leading edge of mean aerodynamic chord, \bar{c} ,
to center of gravity, normalized by \bar{c}

hac_{wb} = distance from leading edge of \bar{c} to wing/body aerodynamic center,
normalized by \bar{c}

$C_{L\alpha\ canard}$ = Lift curve slope of canard

The program "incidence" simply calculated equations VI.B and VI.C over a range of canard incidence angles, i_c , and displayed the

results on a plot of pitching moment coefficient versus angle of attack. Typical flight angles of attack were calculated for a cruise condition, called "CR" (sea level, standard day, speed of 135 ft/sec, 95 lbf weight), and a slow flight condition, called "PA" for "powered approach" (speed of 59 ft/sec). These angles of attack, 2.3 deg and 10.6 deg respectively, were also plotted by "incidence" to give the user a graphical display of the incidence angles to trim the Archytas over a range of angles of attack, and therefore speeds.

3. Results

In earlier thesis work the electronics pod, containing components for servo control and vehicle stability augmentation, had been located below the engine. Figure VI.4 shows this aft pod location as "configuration 1". The original AROD had the electronics pod located as shown on Figure VI.4 and labelled as "configuration 2". Initial longitudinal stability estimations for the Archytas configuration were made with the electronics pod in the "configuration 1" position. The results showed that an Archytas with ten lbf of electronics that far aft required canard support booms on the order of 8 ft to achieve the 15 percent static margin goal. Even with this long a moment arm for the canard, its chord was less than 3 in (remember that, due to installation reasons, the canard span was considered constrained between the two booms, a distance of 31.5 in). Use of the program "incidence" showed that the aircraft configured with this long boom and small canard required incidence angles beyond ± 20 deg to trim the vehicle over the operational

airspeed range.

It appeared at this point that an aft electronics configuration was not feasible. However, before abandoning the aft pod placement, a tradeoff study was conducted to estimate the amount of ballast required to bring the center of gravity for configuration 1 far enough forward to satisfy stability considerations. The study compared an aft pod (configuration 1), with ballast placed on the tip of the boom, versus a pod placed forward. Multiple executions of programs "xplot" and "incidence" were conducted to achieve similar longitudinal stability and trimmability characteristics. Figure VI.5 shows pitching moment coefficient plots for each of the two different configurations. The two plots on Figure VI.5 are similar in that the chord of the canard for each configuration is about the same, 12 in and the aircraft can be trimmed over the same range of airspeeds with similar incidence angles. But, the similarity ends there in that the aft pod configuration required 7 lbf of ballast! This increased the weight of the vehicle a corresponding amount, thereby reducing the thrust-to-weight ratio by over seven percent, with no added capability, just ballast. As discussed in the simulation section of this thesis, that kind of reduction in thrust to weight would likely prove to be unacceptable. Therefore, the aft pod configuration was abandoned.

The forward pod configuration was then considered in detail. To minimize aerodynamic interference between the pod and the canard, a minimum separation distance of one canard chord

between the two was chosen as a design constraint. Figure VI.6 shows the location of the forward pod configuration and the separation constraint. Program "xplot" and "incidence" were then run for a range of canard locations.

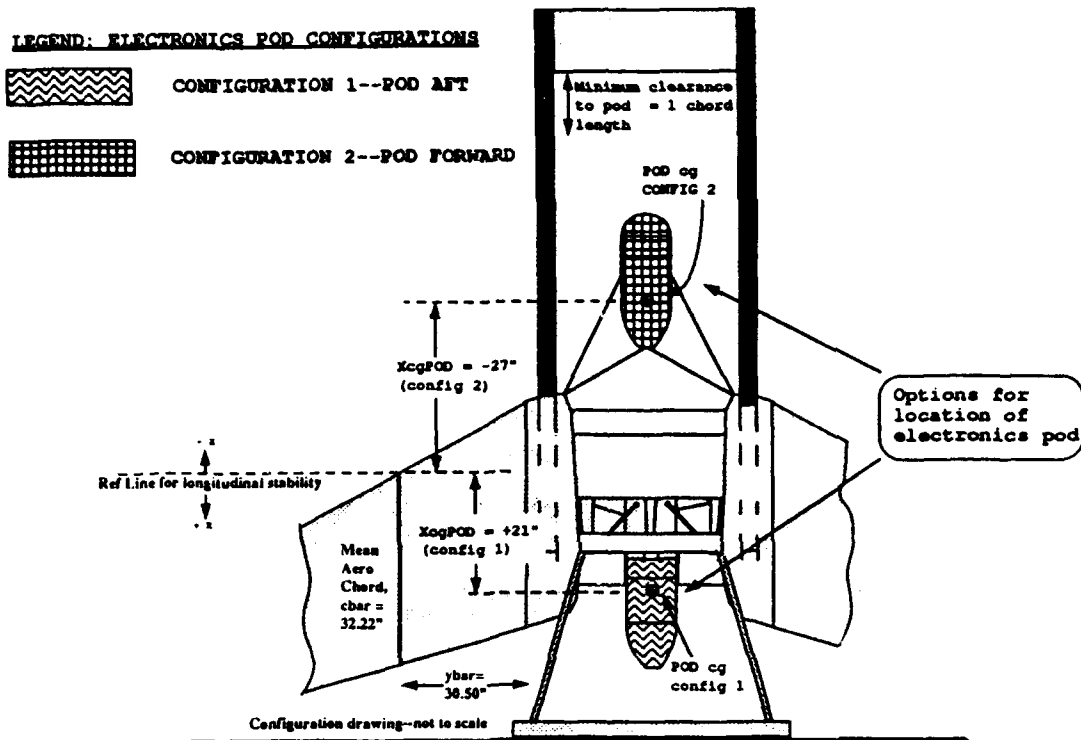


Figure VI.4
Archytas electronics-pod-location options

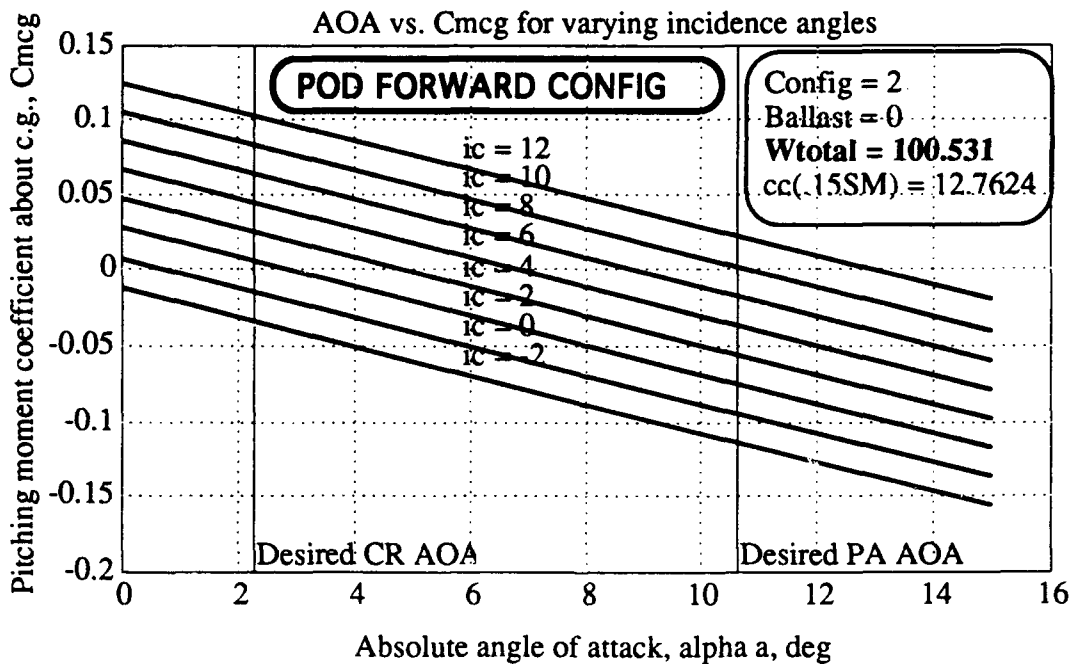
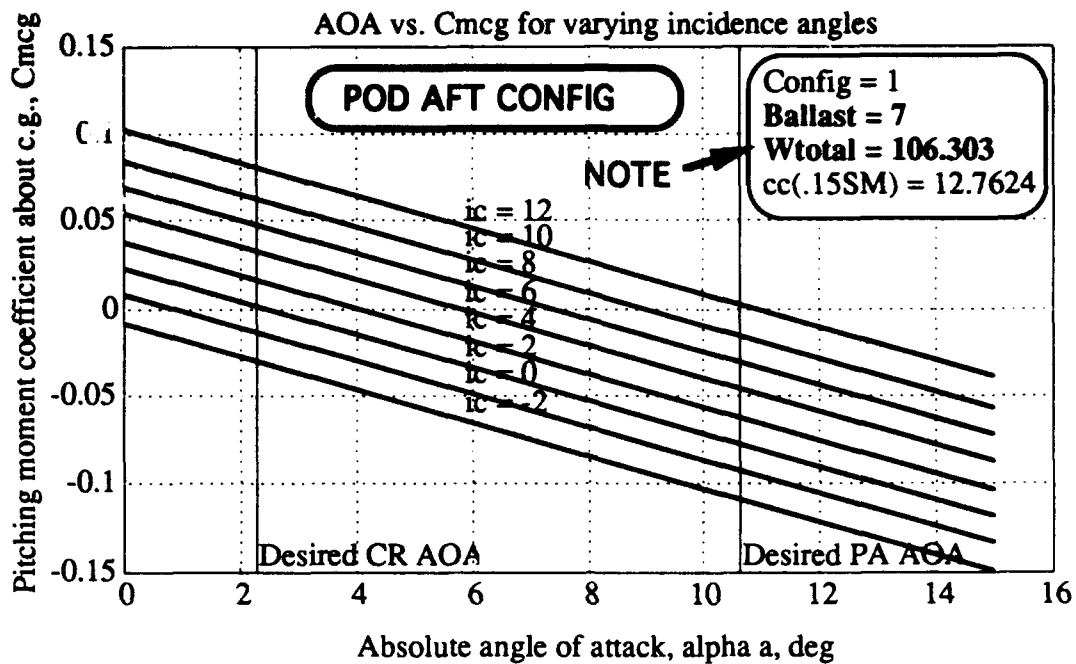


Figure VI.5

Static Longitudinal Stability Comparison Between Pod Configurations

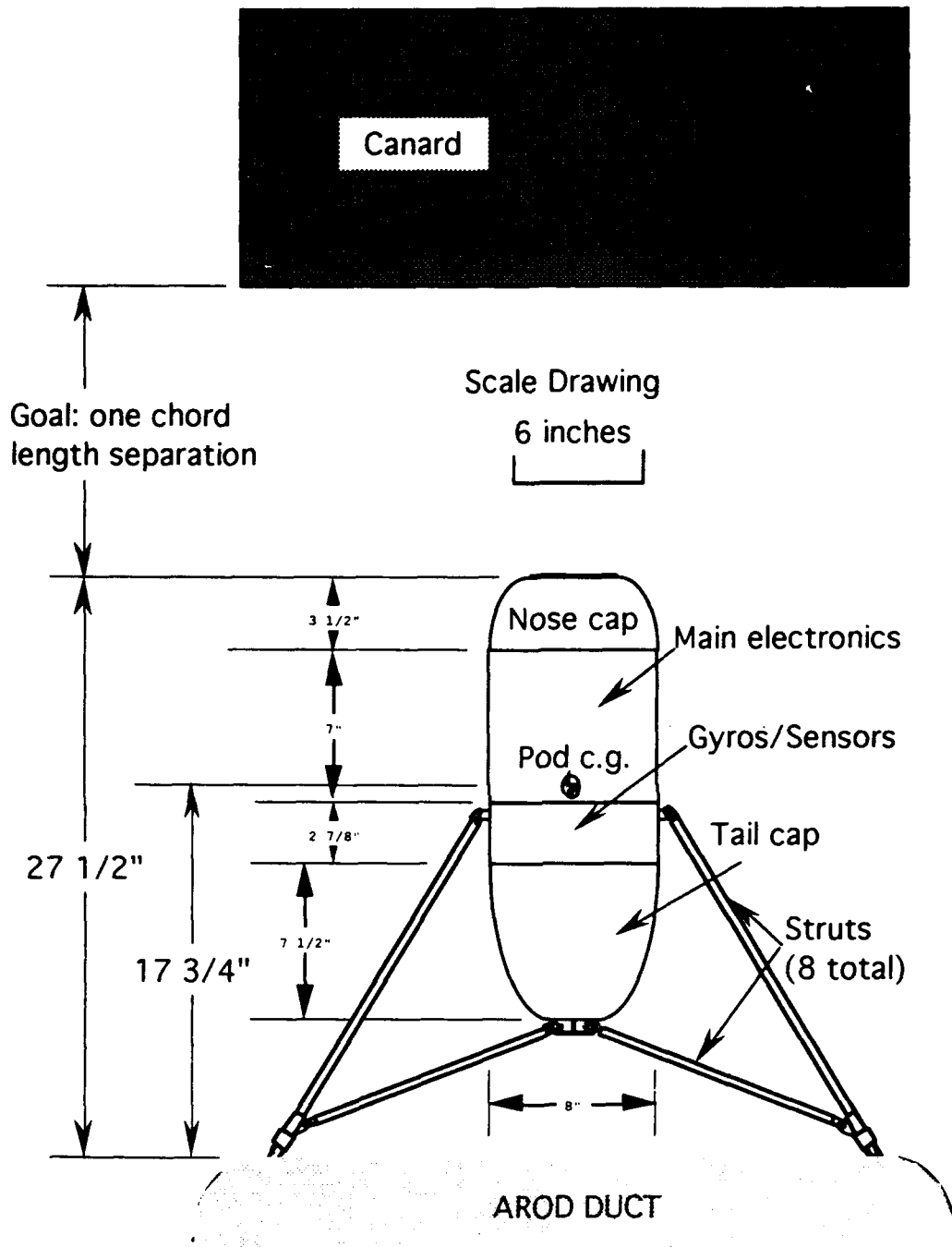


Figure VI.6
Archytas Forward Electronics Pod Configuration--Detail

To review, the constraints and goals at this point were:

- 15 percent static margin (analysis tool: "xplot")
- Minimum weight (analysis tool: "xplot")
- One chord length separation between canard and pod
- Trimmable over flight range (analysis tool: "incidence")
- Canard span limited to 31.5 in by installation restrictions

The result of runs for various canard locations (variable "Canardlocation" in program "xplot") on the two programs is summarized in Figure VI.7. As noted on the figure, with a canard located 52 in in front of the AROD duct entrance, all constraints were satisfied and the weight was minimized. This canard location and size was therefore selected. Figures VI.8 and VI.9 show the results of running programs "xplot" and "incidence" for the selected canard configuration.

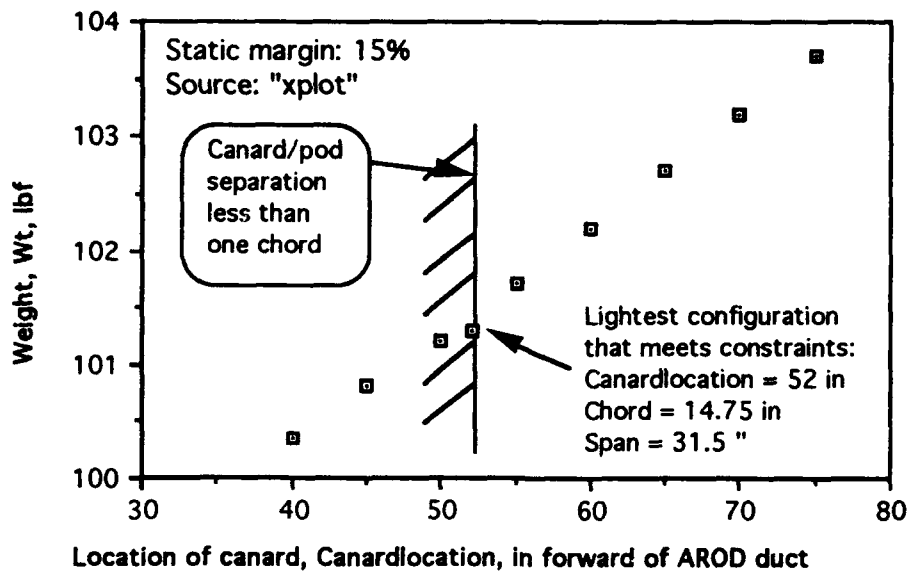


Figure VI.7: Summary of Longitudinal Stability Analysis

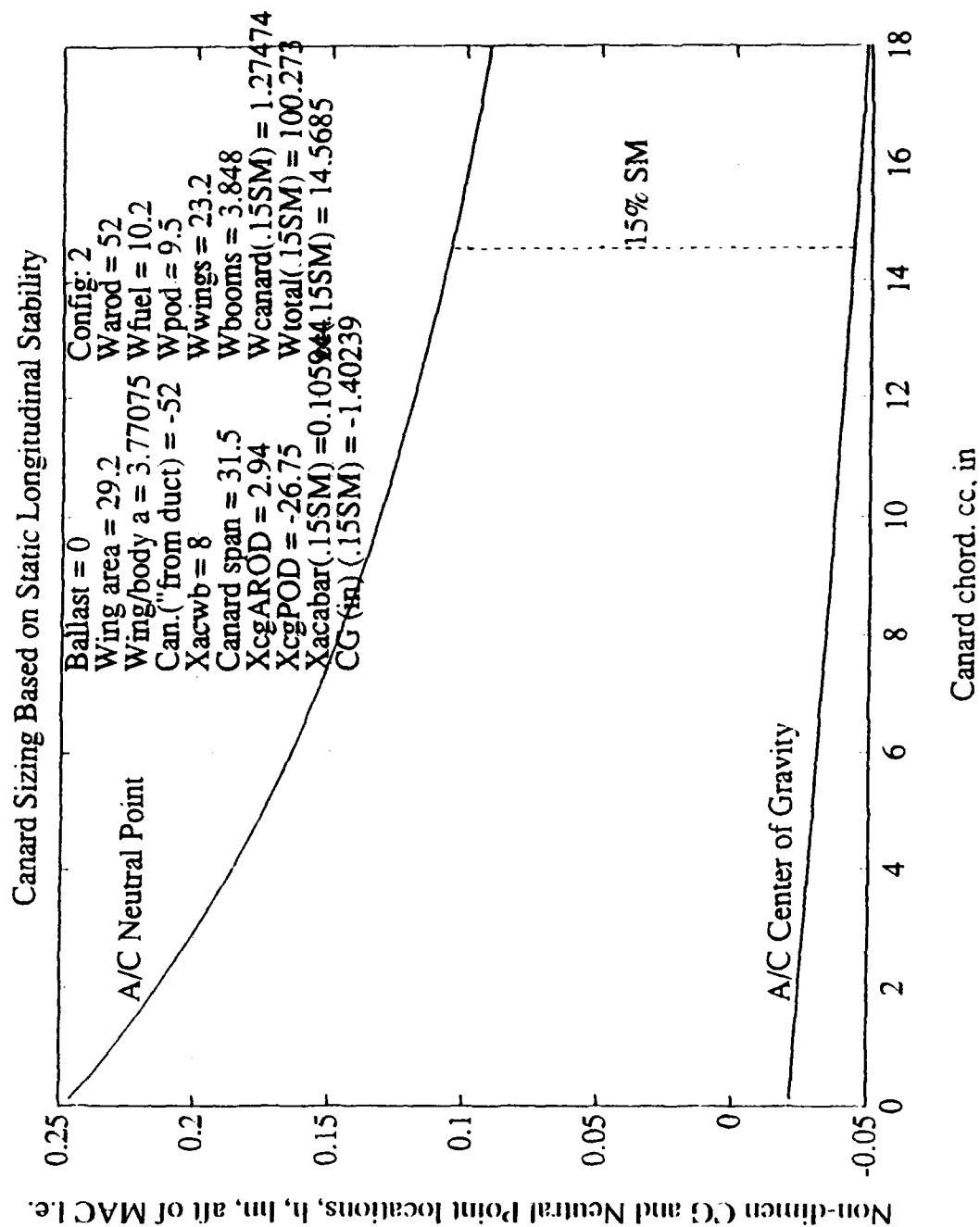


Figure VI.8: Final results from program "xplot"

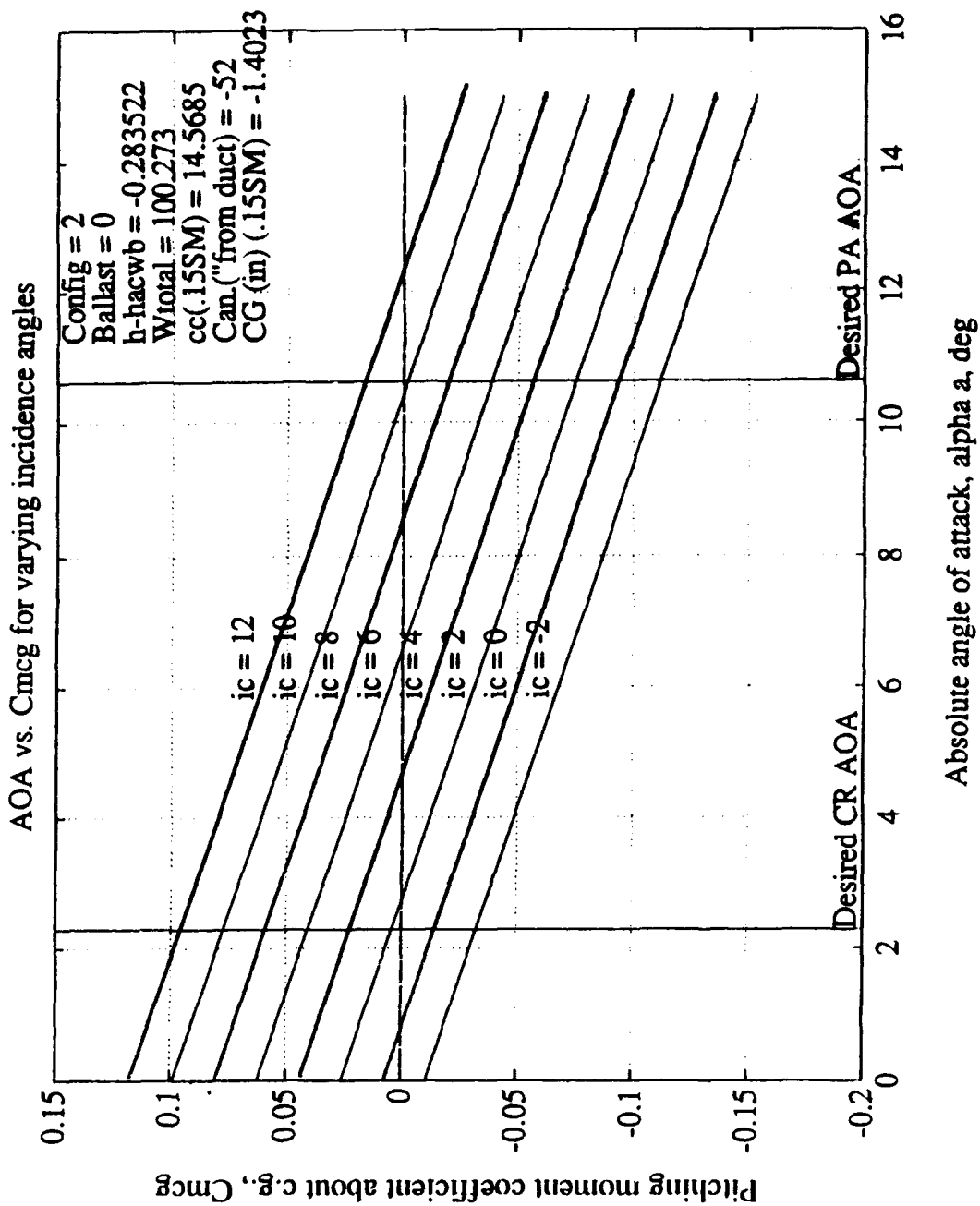


Figure VI.9: Final results from program "incidence"

D. CANARD BOOM STRUCTURAL DESIGN

1. General

Once the canard had been sized, and placed, by the longitudinal stability and control analysis described in previous paragraphs, a final design for the boom to support the canard could be performed. An initial effort was made to manufacture a graphite-epoxy tubular boom in an attempt to minimize weight. Finite element analysis for composite structures was unavailable and so a trial-and-error method ensued. A test boom was manufactured by wrapping graphite in an epoxy matrix around a waxed plastic mandrel. The resulting structure was too flexible and easily crushable and was considered too weak to support expected loads. To prevent delay of other aspects of the project, manufacturing of a composite boom was abandoned in favor of aluminum. A tubular shape was chosen as a good aerodynamic shape and to allow routing of wiring and tubing to the canard servo and planned sensors such as angle of attack and airspeed.

The installation for the canard boom is shown in Figure V.1 and consisted of a support of the boom by a hole in the forward spar and a base for the boom attached to the aft spar. Because the majority of the boom would be forward of the forward wing spar, the boom was modeled as a cantilever tubular beam as shown in Figure VI.10.

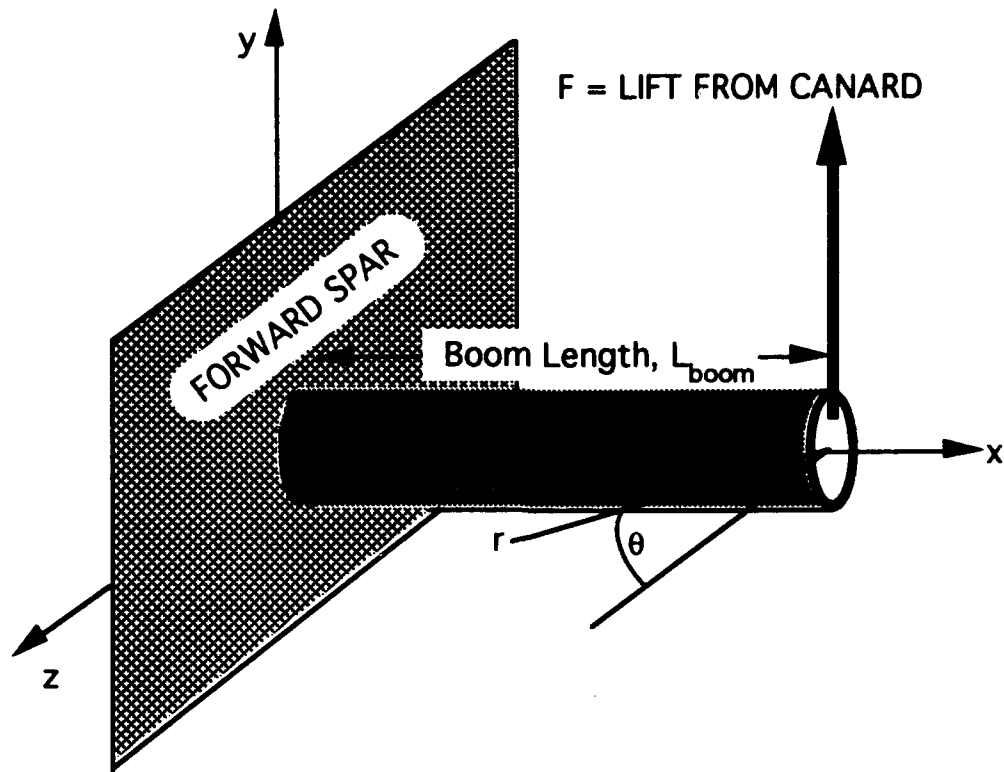


Figure VI.10

Archytas Canard Boom Modeled as Cantilevered Beam

2. Shear stress derivation

Figure VI.11 shows an elemental portion of this tubular beam. Summing forces in the x-direction:

$$(\tau + d\tau) t dx - \tau t dx - \int_A \sigma_x dA + \int_A (\sigma_x + d\sigma_x) dA = 0$$

τ in the first two terms cancels and σ_x from the last two terms cancels.

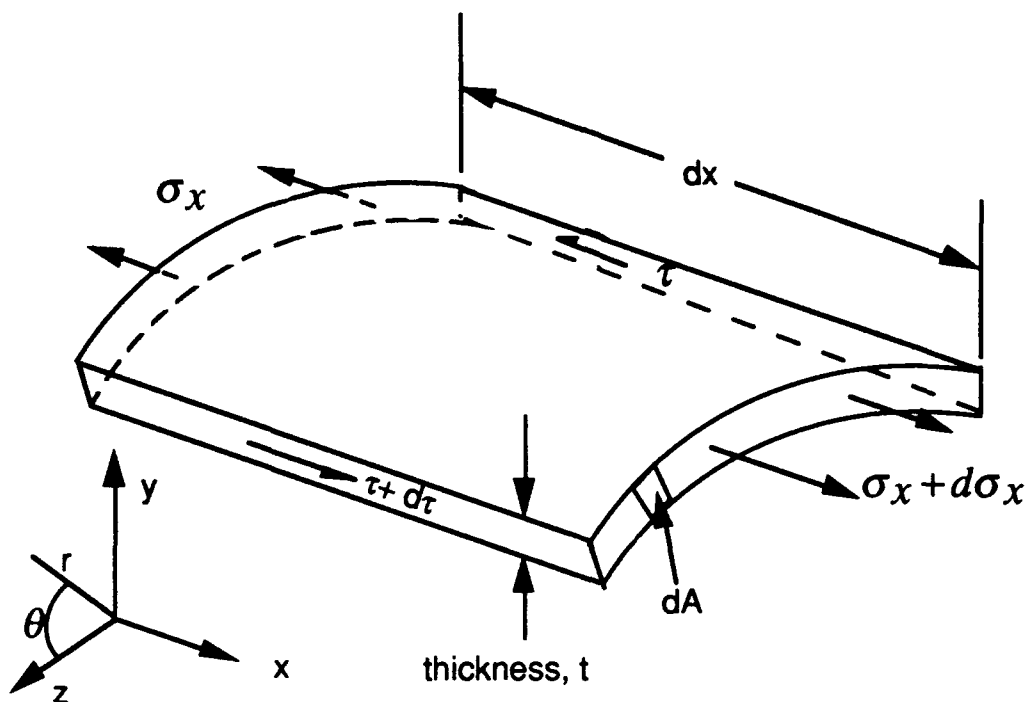


Figure VI.11: Archytas Canard Boom Elemental Portion
With Forces and Coordinate System shown

The following substitutions are then made:

$$\begin{aligned}
 & \text{Not a function of } A \\
 & d\tau t dx + \int_A \left(d\sigma_x \frac{dx}{dx} \right) dA = 0 \\
 & \sigma_x = -\frac{M_z y}{I} \\
 & \frac{d\sigma_x}{dx} = -\frac{d\left(\frac{M_z y}{I}\right)}{dx} \\
 & = \frac{F y}{I} \\
 & M_z = -F x \\
 & \frac{dM_z}{dx} = -F
 \end{aligned}$$

which results in:

$$d\tau t + d\left(\int_A \frac{Fy}{I} dA\right) = 0$$

or:

$$d\tau t + \int_A \frac{Fy}{I} dA = 0$$

Converting to polar coordinates (i.e. $y=r\sin\theta$ and $dA=rdrd\theta$) results in:

$$d\tau t + \frac{F}{I} \int_{\theta}^{\theta+d\theta} r \sin\theta t r dr d\theta = 0$$

Eliminating t from the above equation and removing all non- θ terms from the integral and then evaluating the integral results in:

$$d\tau + \frac{Fr^2}{I} \int_{\theta}^{\theta+d\theta} \sin\theta d\theta = 0$$

(VI.B)

$$d\tau + \frac{Fr^2}{I} [-\cos\theta]_{\theta}^{\theta+d\theta} = 0$$

Consider for a moment the bracketed term to be evaluated:

$$\begin{aligned}
 [-\cos\theta]_{\theta}^{\theta+d\theta} &= -\cos(\theta+d\theta) + \cos\theta \\
 &= -\cos\theta\cos d\theta + \sin\theta\sin d\theta + \cos\theta \\
 \text{(making a small angle assumption:)} & \\
 &= -\cos\theta + \sin\theta d\theta - \cos\theta \\
 &= \sin\theta d\theta
 \end{aligned}
 \tag{VI.C}$$

inserting equation VI.C into VI.B and then solving for $d\tau$ results in:

$$d\tau = -\frac{Fr^2 \sin\theta d\theta}{I}$$

integrating both sides results in:

$$\begin{aligned}
 \int d\tau &= -\int \frac{Fr^2 \sin\theta d\theta}{I} \\
 \tau &= \frac{Fr^2 \cos\theta}{I}
 \end{aligned}$$

the moment of inertia for a tube ($I=\pi r^3 t$) is then inserted, giving the final expression for shear stress:

$$\tau = \frac{F \cos\theta}{\pi r t} \tag{VI.D}$$

3. Tensile stress derivation

Consider next the term σ_x :

$$\sigma_x = -\frac{M_z y}{I}$$

Converting to polar coordinates and substituting $I = \pi r^3 t$ and $M_z = -Fx$ results in the final expression for tensile stress:

$$\sigma_x = -\frac{Fx \sin \theta}{\pi r^2 t} \quad (\text{VI.E})$$

4. Failure criteria

The Von Mises stress criterion was chosen because it is less conservative than the Tresca criterion [Ref 32]. A less conservative approach was considered appropriate because of the unmanned and weight critical nature of the project. A factor of safety was also built in because material analysis was based on the yield stress, not the ultimate stress. Following is the development of the Von Mises stress for the loading shown in Figure VI.10 and developed in previous paragraphs.

$$\begin{aligned} \sigma_{\text{Von Mises}} &\equiv \sigma_{vm} \\ &= (\sigma_x - \cancel{\sigma_y})^2 + (\cancel{\sigma_y} - \cancel{\sigma_z})^2 + (\sigma_x - \cancel{\sigma_z})^2 + 6(\cancel{\sigma_{xy}}^2 + \cancel{\sigma_{yz}}^2 + \cancel{\sigma_{xz}}^2) \\ &= 2\sigma_x^2 + 6\tau^2 \end{aligned}$$

aka: τ

Substituting equations VI.D and VI.E gives the final general expression for Von Mises stress:

$$\sigma_{vm} = \frac{2F^2 x^2 \sin^2 \theta}{\pi^2 r^4 t^2} + \frac{6F^2 \cos^2 \theta}{\pi^2 r^2 t^2} \quad (\text{VI.F})$$


To find the position of the highest Von Mises stress, the derivative of equation VI.F is taken with respect to θ and set equal to zero and constant terms eliminated. The result:

$$\frac{d\sigma_{vm}}{d\theta} = \left(\frac{x^2}{r^2} - 3 \right) (\sin \theta \cos \theta) = 0 \quad (\text{VI.G})$$

Which is satisfied at $\theta = 0, 90, 180$ and 270 degrees--and is termed the first derivative criterion. To determine if each point satisfying the first derivative criterion was a maximum or minimum point, the second derivative of equation VI.F with respect to θ was taken. The result:

$$\frac{d^2\sigma_{vm}}{d\theta^2} = \left(\frac{4F^2}{\pi^2 r^2 t^2} \left(\frac{x^2}{r^2} - 3 \right) \cos 2\theta \right) > \text{or } < \text{ or } = 0?? \quad (\text{VI.H})$$

Always > 0



The maxima will occur when equation VI.H is less than zero. The first factor in equation VI.H is always greater than zero and so is excluded from the analysis.

The second term is less than zero only when

$$(x^2/r^2 - 3) < 0 \quad (VI.I)$$

The largest allowable radius, r , due to physical limitations to the installation of the wing spar on the AROD, was about three inches. A 3.0 in radius substituted satisfies the inequality of equation VI.I only when x is less than 5.2 in, which is clearly an impractically short boom length and therefore the second term of equation VI.H is also excluded from the analysis.

The range of θ that will make equation VI.H less than zero are given as follows:

$\cos 2\theta < 0$ when:

$$45 \text{ degrees} < \theta < 135 \text{ degrees}$$

or

$$225 \text{ degrees} < \theta < 315 \text{ degrees}$$

This range of angles is termed the second derivative criterion. There are only two angles which satisfy both the second and first derivative criterion: 90 and 270 degrees. Substituting 90 or 270 degrees into equation VI.F gives the final expression for the maximum Von Mises stress:

$$\sigma_{vm_{maximum}} = \frac{2F^2x^2}{\pi^2r^4t^2}$$

(VI.J)

5. Canard boom loading model

Figure VI.12 depicts the loading on the canard's support boom and a static diagram of the loads and moment arms involved. The canard lift was assumed to be the maximum lift that an airfoil of the canard's size could generate. This value for maximum lift was calculated as follows:

$$L_{canard} \equiv L_c = 0.5\rho V^2 S_c C_{L_c} = 170 \text{ lb}_f$$

where:

$$\rho = 0.00237688 \text{ slugs/ft}^3 \text{ (std sea level)}$$

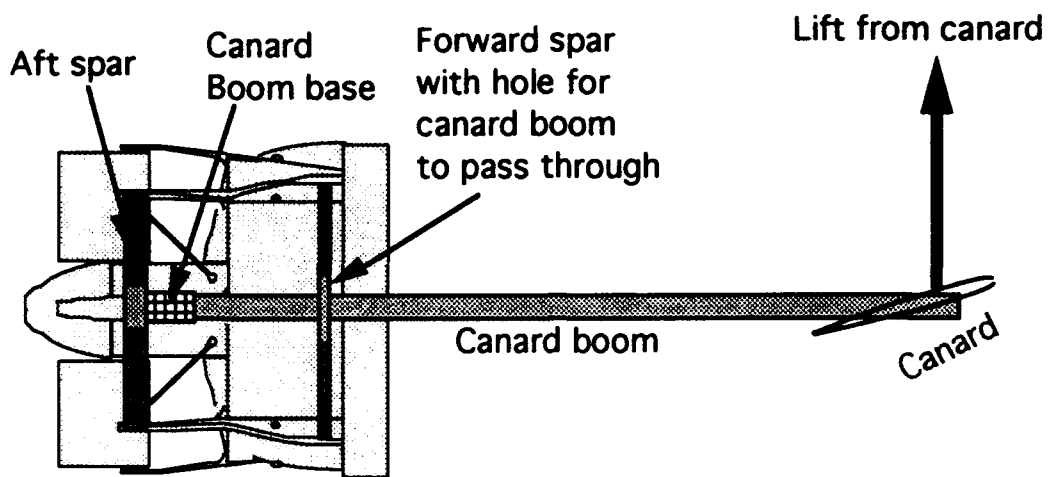
$$V = 100 \text{ knots} = 169 \text{ ft/sec}$$

$$S_c = \text{canard area} = (31.5)(14) \text{ in}^2$$

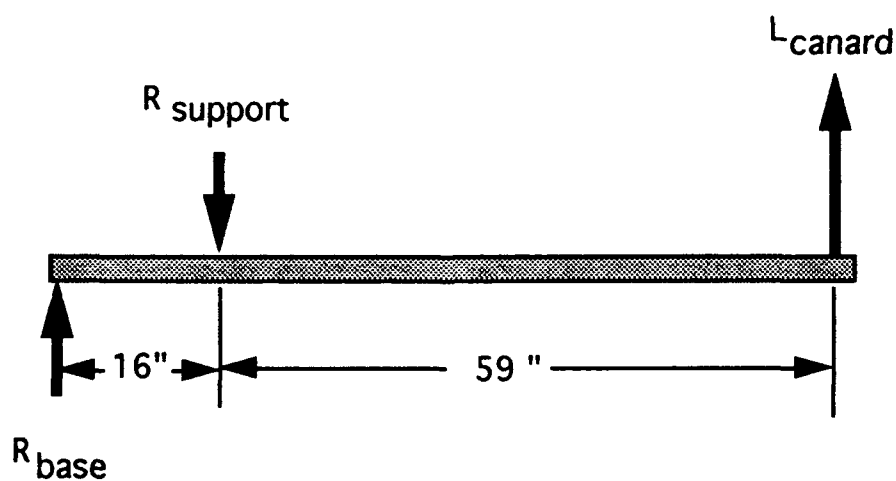
$$C_{L_c} = \text{canard coeff. of lift}$$

$$= C_{L_\alpha} \alpha_{\text{stall}} = (2\pi)(15 \text{ degrees}) \quad (\text{VI.K})$$

The value for velocity came from the simulation work. The canard area was the result of the longitudinal stability analysis. The canard's coefficient of lift was considered as a worst-case scenario.



a. Actual installation



b. Static diagram

Figure VI.12: Archytas Canard-Boom Loading

6. Material selection

Equation VI.J gives the Von Mises stress as a function of the applied force (one half of L_c from equation VI.K--because there are two booms to support the canard's lift), the distance from force application (a maximum value of 59 inches as shown in Figure VI.12), and the radius and thickness of the tube. This equation was implemented on a spreadsheet for 31 commercially available aluminum tubing configurations [Ref. 33]. The spreadsheet is shown in Appendix A, Table A.IV and the Von Mises strength of each of the configurations is shown on Figure VI.13, along with the yield stress values for the two different types of aluminum [Ref. 32]. Configurations which fall below the appropriate yield line are those that "passed" the Von Mises criterion. The configurations that passed this criteria were then compared by weight. The weight per linear foot was calculated simply by knowing a configuration's volume times its density [Ref 32], as shown in Appendix A, Table A.IV. The configuration eventually selected was the lightest one: 6061-T6 aluminum with a 2.5 inch outer diameter and a wall thickness of 0.035 inches, as shown in Figure VI.14.

Prior to purchasing the selected tubing a buckling analysis was conducted. With a thickness ratio, r/t , of 35, the chosen configuration was not considered a "thin walled" structure (the literature focused on tubes with thickness ratios *beginning* at 500) and therefore comparison with empirical information showed that buckling was extremely unlikely [Ref's 34 and 35].

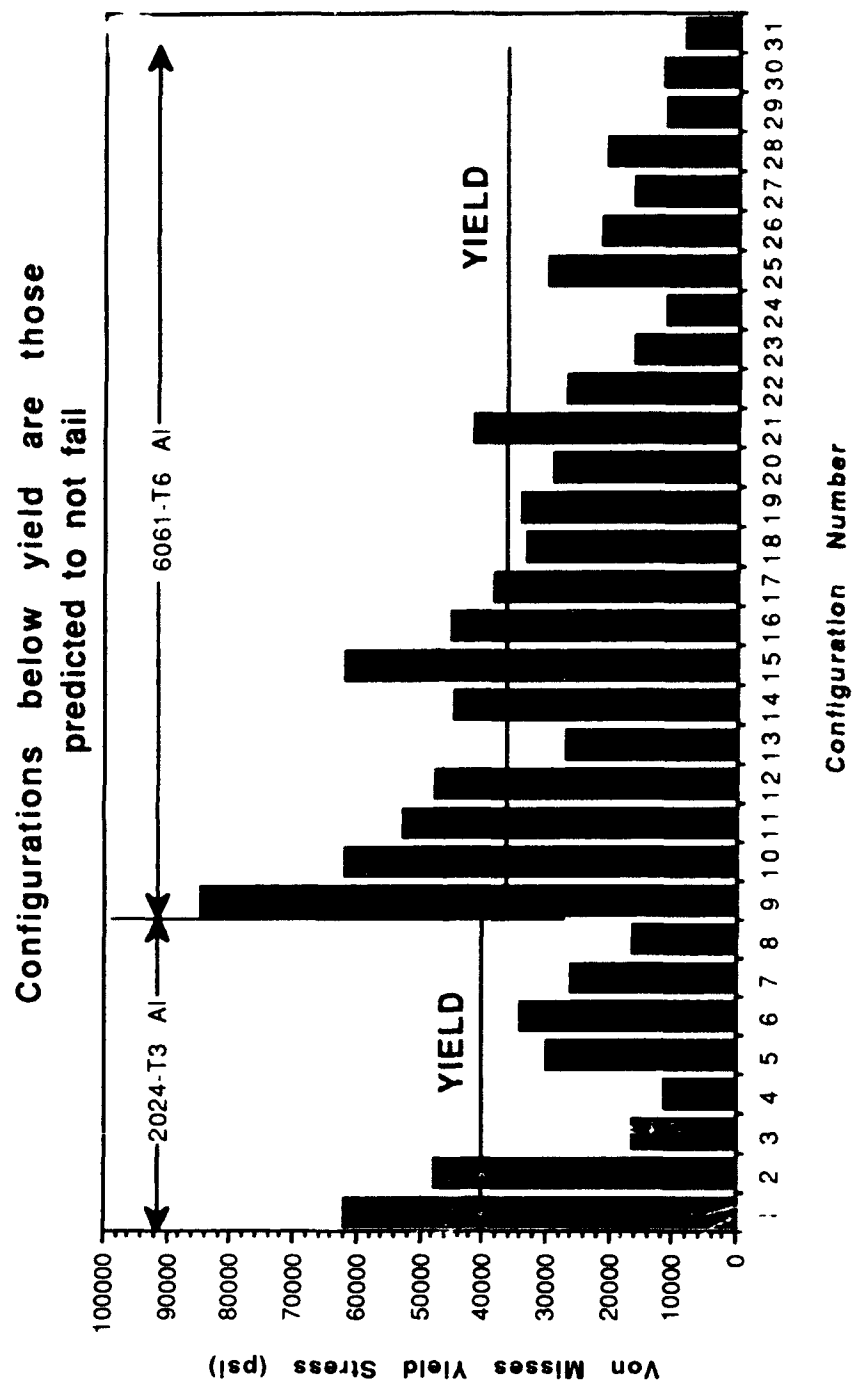


Figure VI.13
Canard support boom strength comparison

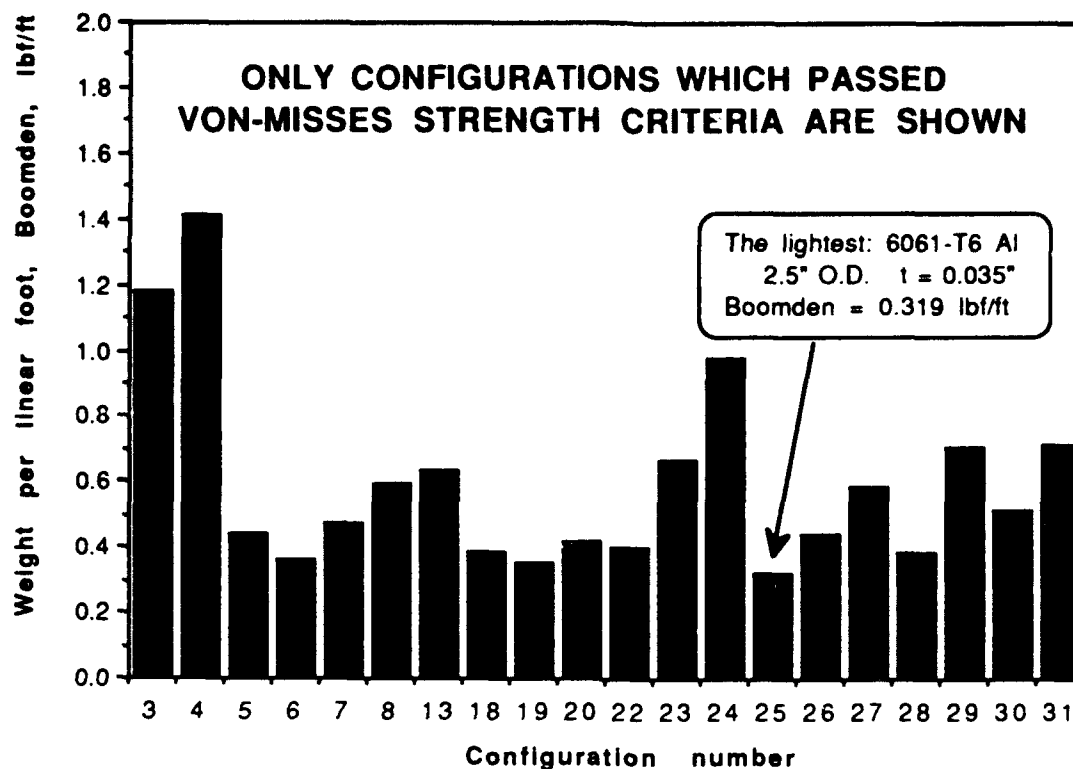


Figure VI.14

Canard Boom Configurations Compared By Weight

7. Structural testing of boom support structure

The canard booms were designed to be supported as shown in Figures VI.10 and VI.1. They were manufactured as specified in reference 21. The strength of these supports, the carry-through hole in the forward spar and the boom base on the aft spar, were each tested. The tests were conducted in a similar manner as that described in Section V for the wing spar. The load was applied

gradually and incrementally using a two weight system. Figure VI.15 shows the test spar in its fixture. The two separate components tested with this one test spar are shown: the canard-boom carry-through hole and the canard-boom base.

With reference to Figure VI.12, a simple statics problem showed that at a design load (canard lift) of 85 lb, the force at the boom base (" R_{base} " of Figure VI.12) would be 228 lb and the support's reaction (" $R_{support}$ " of Figure VI.12) would be 313 lb. The boom base was tested, as shown on the upper portion of Figure VI.16, to 243 percent of the design load without any failure or permanent deformation. Appendix B, Figure B.6 is a photograph of the test of the boom base. The boom's forward-spar carry-through hole was tested, as shown on the lower portion of Figure VI.16, to 207 percent of the design load without any failure or permanent deformation. Appendix B, Figure B.7 is a photograph of the test of the carry-through hole. The boom base was then retested by removing it from the vise shown in Figure VI.15 and adhering it to a test spar with standard epoxy. This test spar was constrained and the test of the boom base repeated with the same results.

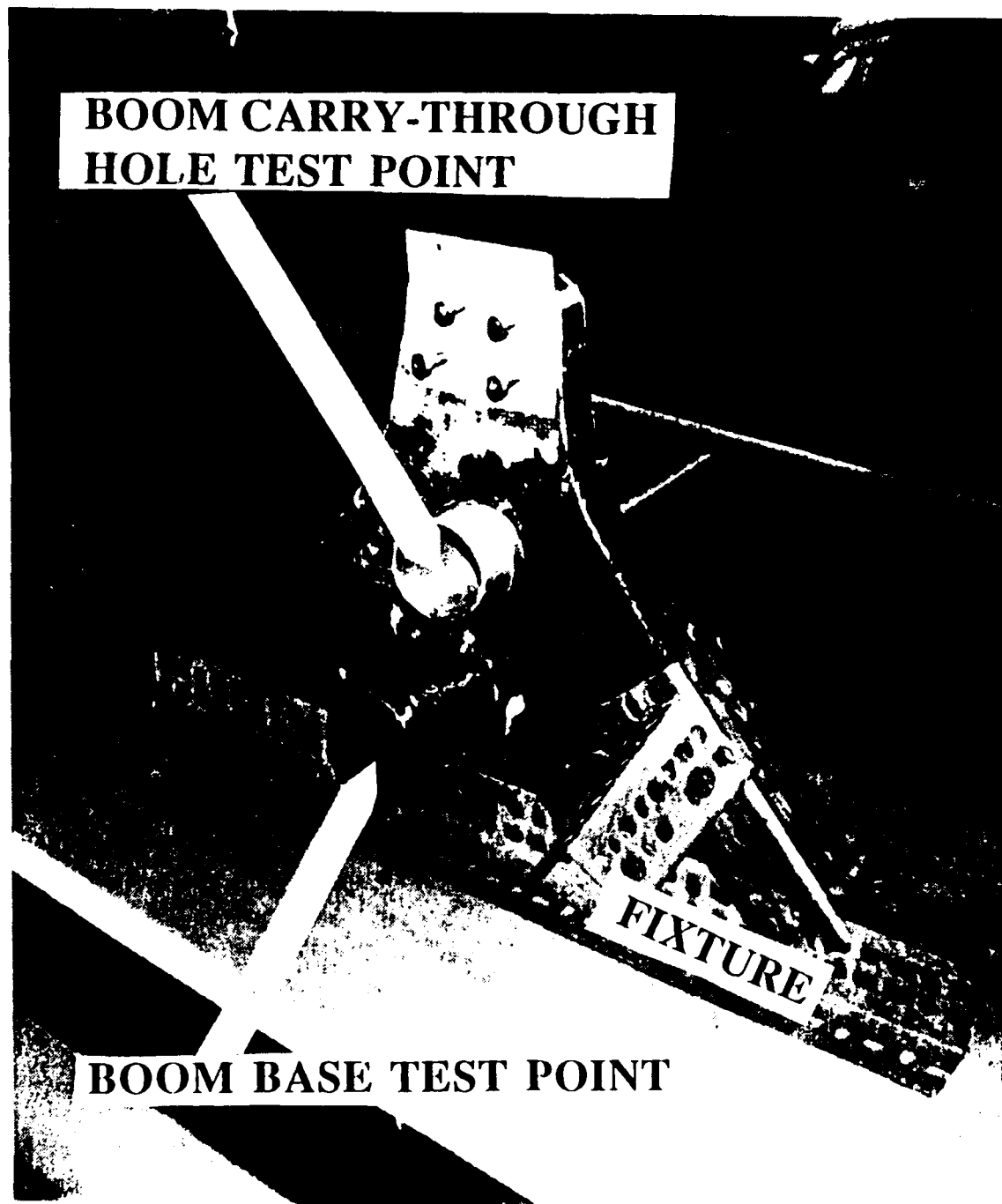
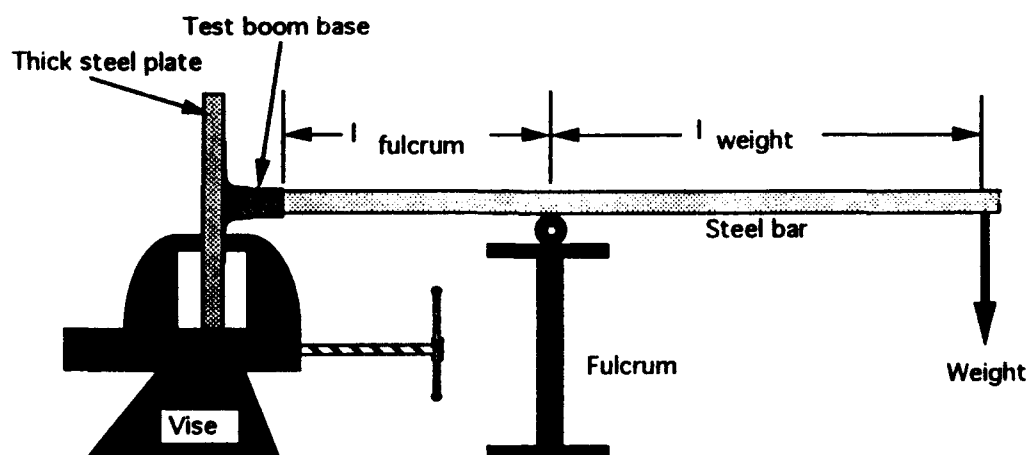
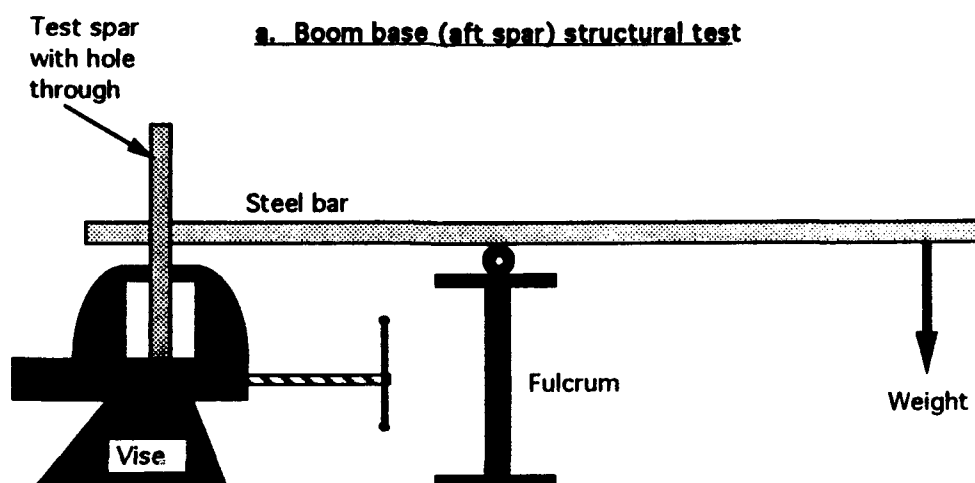


Figure VI.15: Archytas canard-boom carry-through and base test



a. Boom base (aft spar) structural test



b. Boom support hole (forward spar) structural test

Figure VI.16: Archytas canard-boom test set-up

VII. SIMULATION

A. GENERAL

The equations of motion were developed for a three-degree-of-freedom (3-DOF) simulation of Archytas motion--two displacements (downrange and vertical) and one rotation (pitch). The simulation did not address either cross-range displacement or lateral/directional rotations. The simulation program, named AWA1, will be discussed following derivation of the equations of motion and explanation of the modeling of germane forces and moments. Several assumptions made during formulation of the simulation are contained in Appendix E.

B. EQUATIONS OF MOTION--LINEAR MOMENTUM

1. Derivation of equations

Figure VII.1 depicts the general coordinate system and the nomenclature used during formulation of the conservation of linear momentum equations of motion for the Archytas.

With reference to Figure VII.1, the first two equations of motion are simple vector resolutions of the velocity vector into the inertial reference frame:

$$\dot{x} = V \cos \gamma \quad (VII.A)$$

$$\dot{h} = V \sin \gamma \quad (VII.B)$$

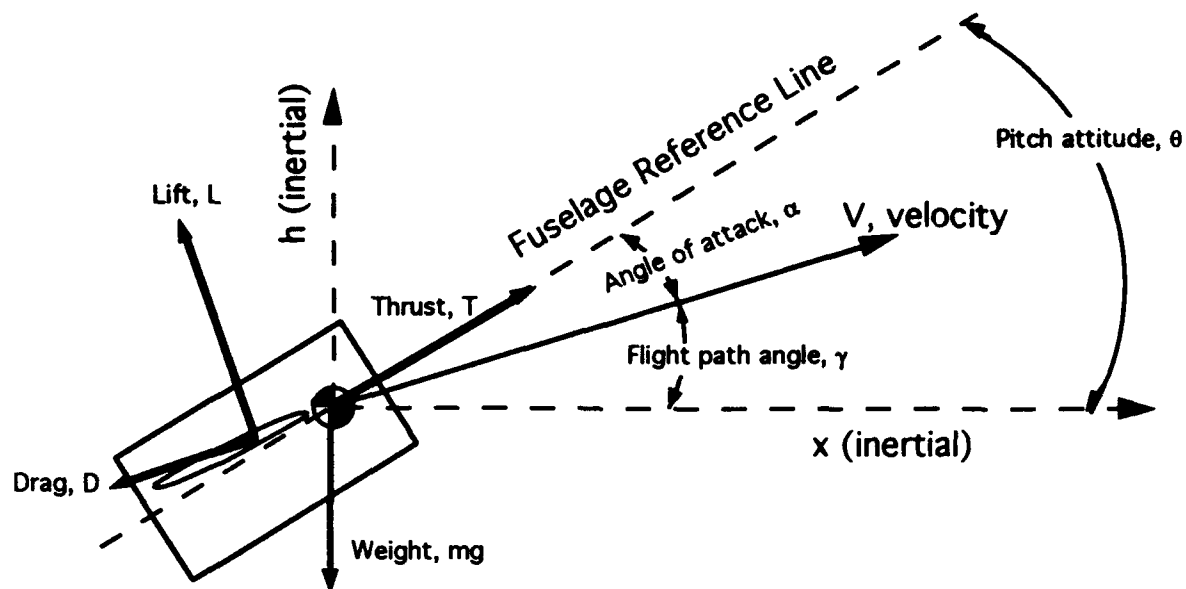


Figure VII: Coordinate System and Nomenclature for Archytas Conservation of Linear Momentum Equations of Motion

The next equation of motion is obtained by applying Newton's second law for conservation of linear momentum along the Velocity vector:

$$\sum F_{\text{along velocity vector}} = (m)(\text{acceleration}_{\text{along velocity vector}})$$

Summing forces and making the following substitution:
 $a = \dot{V}$, results in:

$$T \cos \alpha - D - mg \sin \gamma = m \dot{V}$$

which, when solved for \dot{V} ,

gives:

$$\dot{V} = \frac{T \cos \alpha}{m} - \frac{D}{m} - g \sin \gamma \quad (\text{VII.C})$$

The next equation of motion is obtained also with Newton's second law, this time applied along the vertical inertial axis:

$$\sum F_h = m\ddot{h} \quad (\text{VII.D})$$

Consider for a moment the expression \ddot{h} :

$$\ddot{h} = \frac{d(\dot{h})}{dt}$$

and with $\dot{h} = V \sin \gamma$ (equation VII.B):

$$\begin{aligned} \ddot{h} &= \frac{d(V \sin \gamma)}{dt} \\ &= V \frac{d(\sin \gamma)}{dt} + \sin \gamma \frac{d(V)}{dt} \\ &= V \cos \gamma \dot{\gamma} + \sin \gamma \dot{V} \end{aligned} \quad (\text{VII.E})$$

Substituting equation VII.E into equation VII.D and summing forces:

$$L \cos \gamma - D \sin \theta + T \sin \theta - mg = m(V \cos \gamma \dot{\gamma} + \sin \gamma \dot{V})$$

Solving for $\dot{\gamma}$:

$$\begin{aligned}\dot{\gamma} &= \frac{L \cos \gamma}{mV \cos \gamma} - \frac{D \sin \gamma}{mv \cos \gamma} + \frac{T \sin \theta}{mV \cos \gamma} - \frac{g}{V \cos \gamma} - \frac{\dot{V} \sin \gamma}{V \cos \gamma} \\ &= \frac{L}{mV} - \frac{D \tan \gamma}{mv} + \frac{T \sin \theta}{mV \cos \gamma} - \frac{g}{V \cos \gamma} - \frac{\dot{V} \tan \gamma}{V}\end{aligned}\quad (\text{VII.F})$$

Substitution of the following:

$$\sin \theta = \sin(\gamma + \alpha) = \sin \gamma \cos \alpha + \sin \alpha \cos \gamma$$

in equation VII.F gives:

$$\dot{\gamma} = \frac{L}{mV} - \frac{D \tan \gamma}{mV} + \frac{T(\tan \gamma \cos \alpha + \sin \alpha)}{mV} - \frac{g}{V \cos \gamma} - \frac{\dot{V} \tan \gamma}{V}\quad (\text{VII.G})$$

Equations VII.A,B,C and G, then form four equations of motion for displacement and velocity in two axes. The variables solved for by finite differencing these four equations are as follows:

x = downrange distance

h = height

V = Speed along velocity vector

γ = flight path angle

2. Modeling of linear momentum equation elements

a. Thrust modeling

The thrust is modeled based on engine tests (see Section IV). Data from these tests were used to transform a user input of throttle position (on a scale from 0% for idle to 100% for full power) to engine thrust. Details of the analysis to produce this transformation are contained in Section IV. When plotted, the model appears as shown in Figure VII.2.

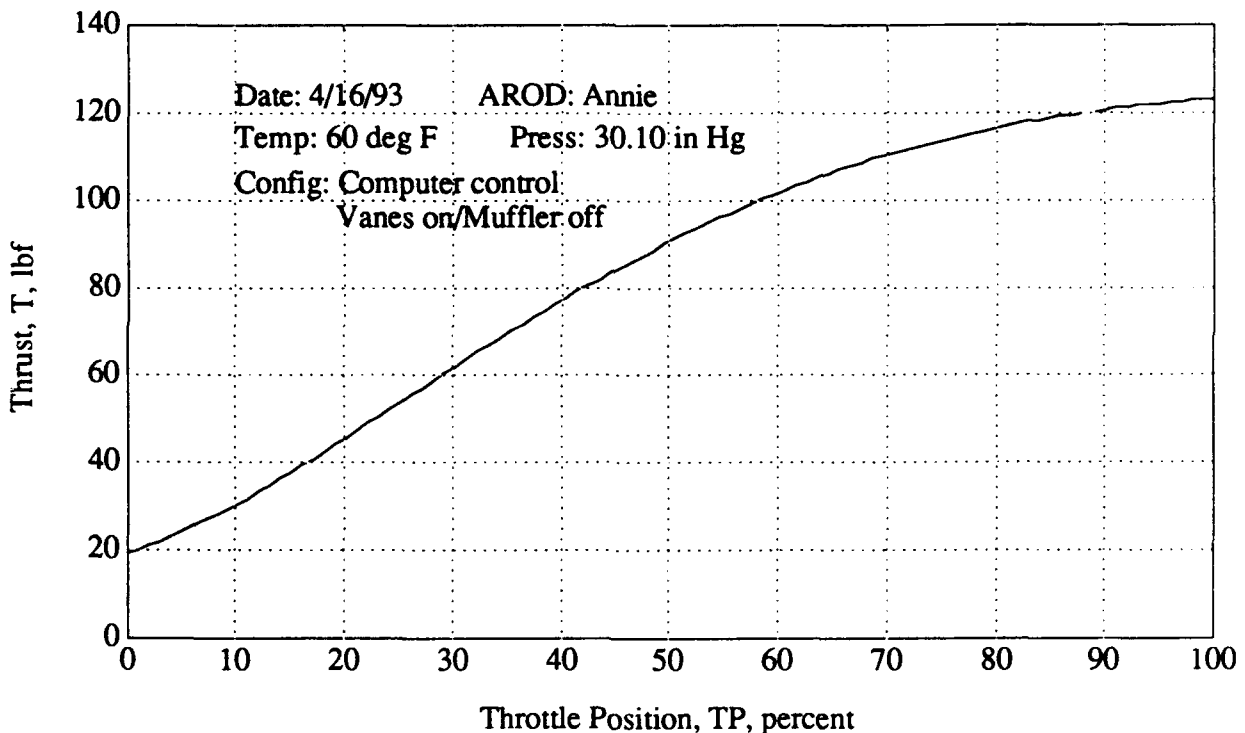


Figure VII.2

Archytas Throttle Position vs. Thrust model

b. Lift modeling

The lift of the wing was modeled as a function of angle of attack. The pre-stall relationship between the trim coefficient of lift and the trim angle of attack was obtained from Aquila wind tunnel tests [Ref. 28]. However, no information was available on the lift curve past the stall angle of attack. In the absence of high-angle-of-attack lift-curve data for the Aquila wing, the post-stall lift versus angle-of-attack relationship was assumed. The relationship between coefficient of lift and angle of attack is graphically depicted on Figure VII.3. This figure has two parts: part (a) shows the lift curve as a function of angle of attack in radians; because no one curve fit would work over the entire range of angles of attack, the lift curve was broken into several sections and polynomial curve fits were developed for each segment. Part (b) is the same plot but with curve fits removed and angle of attack in degrees.

The lift was then calculated from the formula:

$$L = \frac{1}{2} \rho V^2 S C_L$$

where:

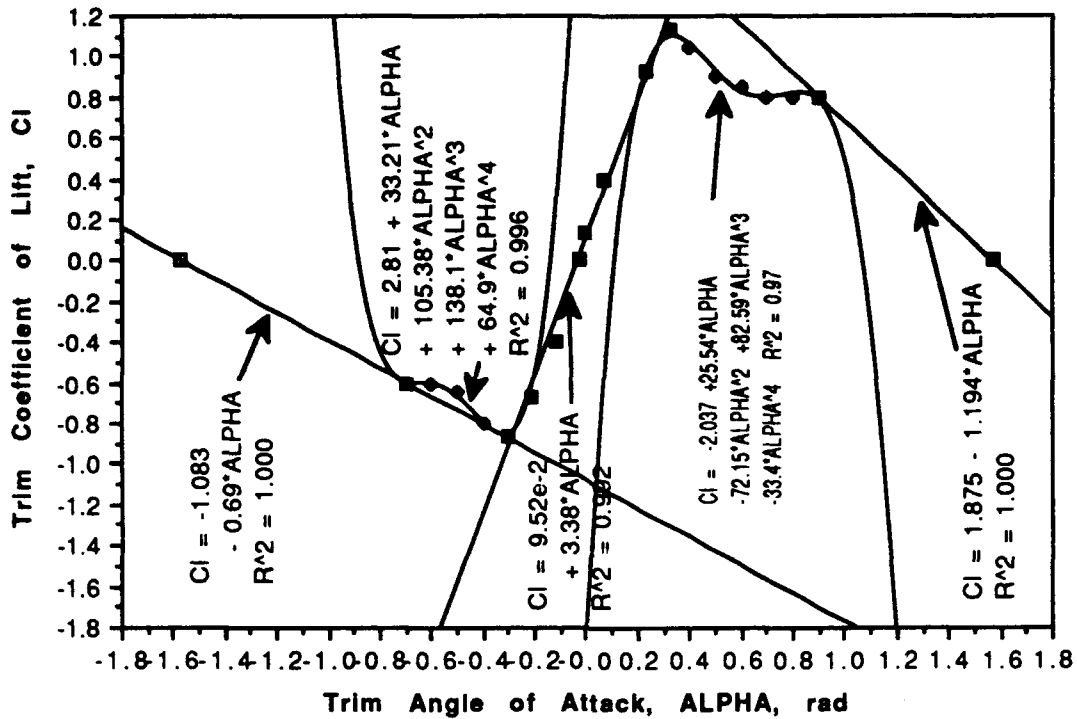
ρ = density

V = speed

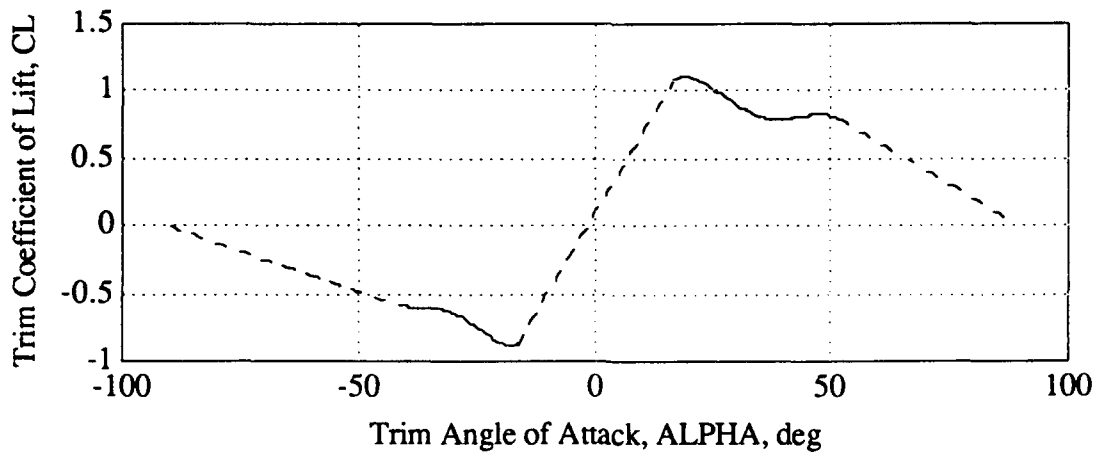
S = reference wing area

C_L = Coefficient of lift

SOURCE: Aquila wind tunnel data for unstalled region; assumed profile for stalled regions.



a. Lift model with curve fits shown



b. Lift model with curve fits removed

Figure VII.3 (two graphs): Archytas Coefficient of Lift Modeling

c. Drag modeling

The coefficient of drag, C_D , is traditionally expressed as a function of the coefficient of lift:

$$C_D = C_{D_0} + KC_L^2 \quad (\text{VII.H})$$

But for the case of a vehicle potentially operating at high angles of attack, such as the Archytas, this equation predicted a decrease in drag at angles of attack beyond stall. Unfortunately this is not the reality and so an alternate model for the coefficient of drag was assumed. The new model assumed that C_D would continue to increase as a second-order function of angle of attack (α). A further assumption was that the relationship between C_D and α would be the same for pre-stall and post-stall regions, allowing use of equation VII.H as follows.

From Figure VII.3a, for angles of attack less than stall, the following relationship exists between the coefficient of lift and angle of attack:

$$C_L = 0.0952 + 3.38\alpha \quad (\text{VII.I})$$

The following constants were used:

$$K = \frac{1}{\pi A Re} = 0.0936 \quad (\text{VII.J})$$

where:

$AR \equiv \text{aspect ratio} = 4.25$

$e \equiv \text{span efficiency factor} = 0.8$

$$C_{Do} = 0.06 \quad (\text{VII.K})$$

Substituting equations VII.I , VII.J and VII.K into VII.H
results in:

$$C_D = 0.0608 + 0.0602\alpha + 1.07\alpha^2 \quad (\text{VII.L})$$

Equation VII.L is graphically depicted in Figure VII.4:

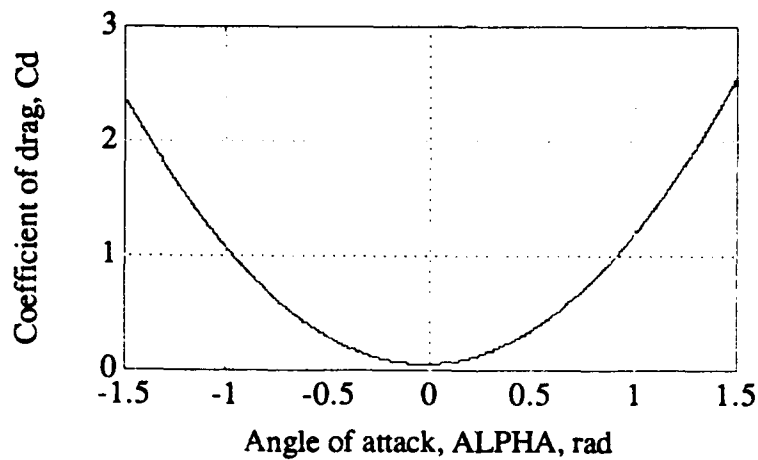


Figure VII.4: Archytas Coefficient of Drag Model

The drag was then modeled traditionally as:

$$D = \frac{1}{2} \rho V^2 S C_D \quad (\text{VII.M})$$

C. EQUATION OF MOTION--ANGULAR MOMENTUM

1. Derivation of equation

Figure VII.5 depicts the general coordinate system and the nomenclature used during formulation of the conservation of angular momentum equation of motion for the Archytas.

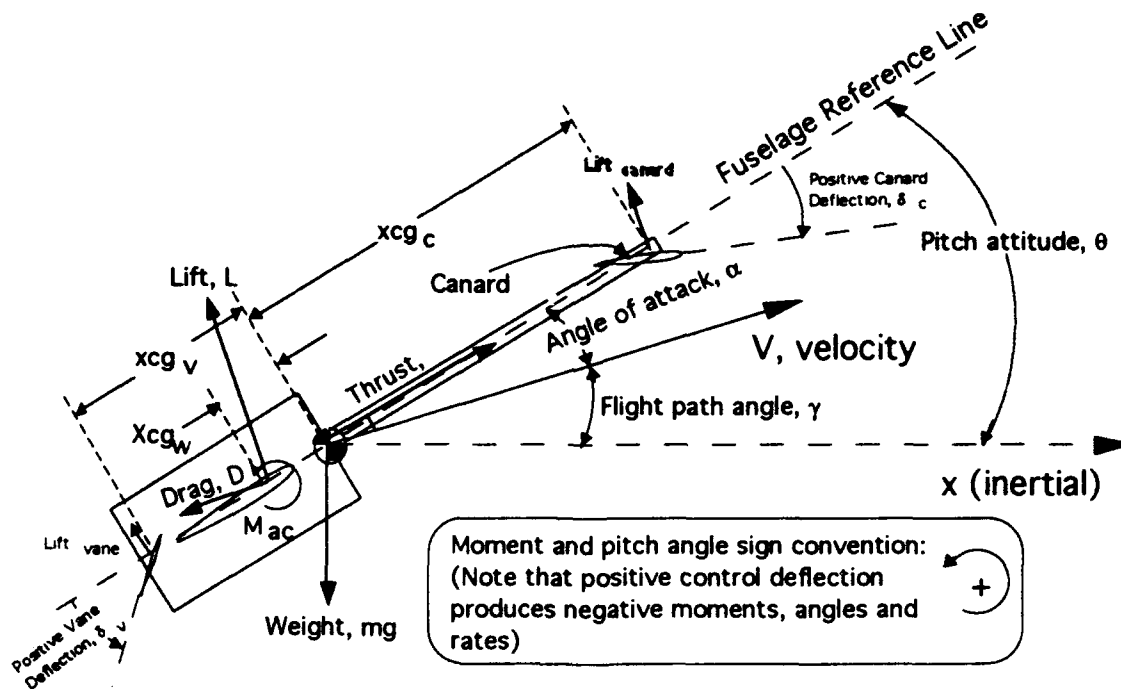


Figure VII.5: Coordinate System and Nomenclature for Archytas
Conservation of Angular Momentum Equations of Motion

With reference to Figure VII.5, the equation of motion for the pitch axis is developed. Applying Newton's second law for conservation of angular momentum:

$$\sum \text{Pitch Moments about c.g.} = (\text{Moment of Inertia}) * (\text{pitch angular acceleration})$$

or,

$$M_{c_g WING} + M_{c_g CANARD} + M_{c_g VANE} + M_{c_g PITCH RATE} = I_{yy} \ddot{\theta} \quad (\text{VII.N})$$

solving equation VII.N for $\ddot{\theta}$ and substituting $\ddot{\theta} = \dot{q}$ results in:

$$\dot{q} = \frac{M_{c_g WING} + M_{c_g CANARD} + M_{c_g VANE} + M_{c_g PITCH RATE}}{I_{yy}} \quad (\text{VII.O})$$

With reference to Figure VII.5, the individual moments are expressed as follows:

$$M_{c_g WING} = M_{\alpha} - (L \cos \alpha)(x c g_W) \quad (\text{VII.Pa})$$

$$M_{c_g CANARD} = (Lift_{CANARD} \cos \alpha)(x c g_C) \quad (\text{VII.Pb})$$

$$M_{c_g VANE} = -(Lift_{VANE})(x c g_V) \quad (\text{VII.Pc})$$

$$M_{c_g PITCH RATE} = -M_q q \quad (\text{VII.Pd})$$

Note that, unlike Section VI's formulation for static longitudinal stability where dimensions forward of the leading edge of the mean aerodynamic chord were negative, distances in equations VII.Pa through VII.Pd are *absolute* distances and the sign of each term is accounted for by the moment convention shown on Figure VII.5.

Substituting equations VII.Pa through VII.Pd into equation VII.O gives an equation of motion for pitch acceleration:

$$\dot{q} = \frac{M_{ac} - (L \cos \alpha)(x_{cg_W}) + (Lift_{CANARD} \cos \alpha)(x_{cg_C}) - (Lift_{VANE})(x_{cg_V}) - M_q q}{I_{yy}}$$

(VII.Q)

Combining equation VII.Q with the following equations, defines pitch angle, rate and angular acceleration.

$$q = \dot{\theta}$$

(VII.R)

$$\theta = \alpha + \gamma$$

(VII.S)

2. Modeling of Angular Momentum Equation Elements

a. Pitching Moment due to wing

The lift of the wing was modeled as previously described (Section VI). With reference to equation VII.Pa, the pitching moment of the wing about the center of gravity was modeled as a function of the moment about the aerodynamic center, taken to be the quarter chord of the mean aerodynamic chord, and

the lift times the distance from the quarter chord to the center of gravity. The moment arm for the lift force, x_{cgw} , was a function of where the wing was installed with respect to the center of gravity. The wing's longitudinal position was limited due to installation constraints.

b. Pitching Moment due to canard deflection

For the simulation, the canard airfoil was assumed to be the same as the main wing, to provide lift as well as longitudinal control. The lifting force of the canard was modeled based on the coefficient of lift versus local canard angle-of-attack relationship shown in Figure VII.6. The canard angle of attack, as shown on Figure VII.6, was a combination of the vehicle's angle of attack and the canard deflection. Changes in this angle due to pitch rate were considered but discounted because, at the highest pitch rate observed during simulation runs, the change in canard angle of attack due to the pitch rate was less than ten percent. At nominal pitch rates this change in local angle of attack was approximately one percent. Additionally, the assumption was made that upwash from the wing had no effect on the canard. This was assumed because the canard was over two chords in front of the wing and the ducted-fan was assumed to negate some of the interaction between the wing and the canard.

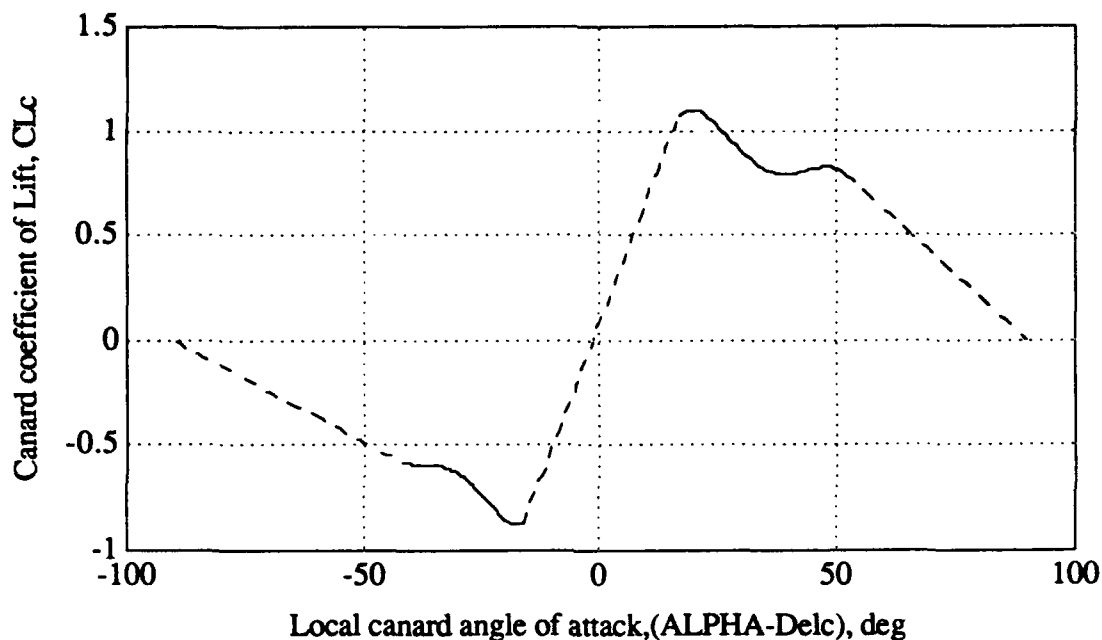


Figure VII.6

Canard coefficient of lift versus local angle-of-attack model

c. Pitching Moment due to vane deflection

The pitching moment due to vane deflection was modeled based on engine test data. These tests produced rolling moment data, which were analyzed to predict pitching moment effectiveness. Details of this analysis are contained in Section IV. As discussed in Section IV, the results of the engine tests and analysis showed essentially no change in control power for thrust levels from approximately 90 to 120 lb (approximate thrust-to-weight ratios of 0.9 to 1.2), which was in agreement with tests performed by the AROD's manufacturer [Ref 18]. Because the thrust levels required during hovering and initial transition were anticipated to be in this

constant-control-power range of 90 to 120 lb and with the assumption that airflow over the vanes would remain approximately constant following transition to horizontal flight, with increases in the local velocity at the vane due to forward flight speed balanced by throttle decrease, control power due to vane deflection was modeled as constant. The relationship between vane deflection and pitching moment, for all speeds and throttle settings, was therefore modeled as shown in Figure VII.7. The vanes are assumed to produce zero moment at zero deflection. As discussed more fully in Section IV, engine tests showed a swirl of the airflow in the vicinity of the vanes, which resulted in some moment being produced by the vanes at zero deflection. This swirl effect, however, was difficult to predict and no tests were performed to analyze the effect of two vanes, deflected in a pitching sense, on the airflow patterns near the vanes. The vane control power, therefore, was referenced to an arbitrary neutral position.

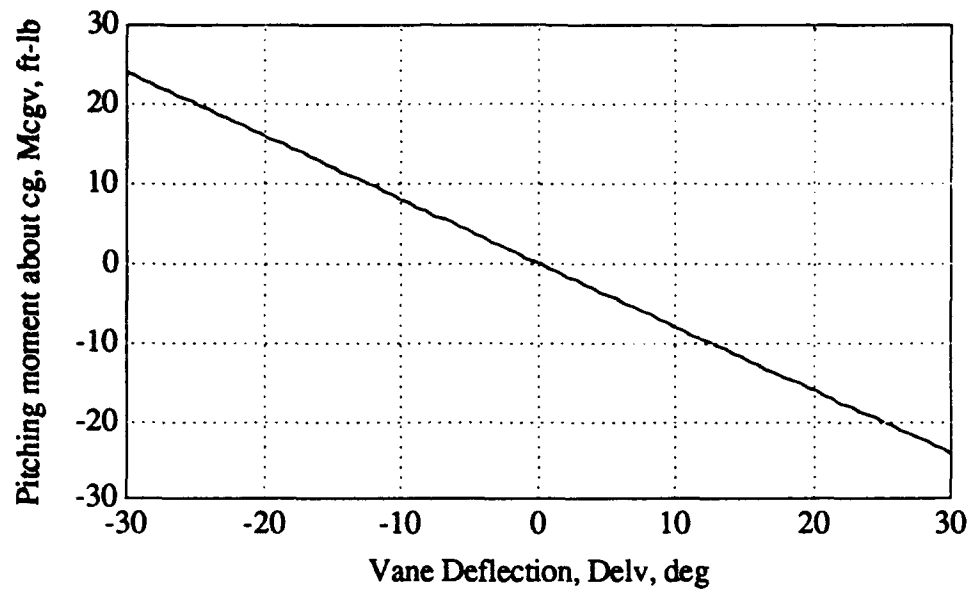


Figure VII.7

Control Vane pitching moment model

d. Pitching moment due to pitch rate

The moment due to pitch rate, also known as pitch damping, was modeled conventionally as per equation VII.Pd, using the dimensional derivative M_q , defined as follows [Ref. 36]:

$$M_q = \frac{C_{mq} \bar{q} S \bar{c}^2}{2V} \quad (\text{VII.T})$$

where:

C_{mq} \equiv pitching moment coefficient due to pitch rate

\bar{q} \equiv dynamic pressure (do not confuse with q , pitch rate)

S \equiv Wing area

\bar{c} \equiv mean aerodynamic chord

V \equiv speed

With no better data available, the value for C_{mq} used was that given for the Aquila airframe of -1.47 per radian. [Ref. 28].

D. COMPUTER CODE

1. Program features

A main program, called "AWA1", and several function programs (similar to subroutines) were written on MATLAB[®] to perform simulation of the three-degree-of-freedom equations of motion. A MACINTOSH[®] IIX computer was used to ease programming, data analysis and processing. The program included the following features:

- Plot of vehicle's downrange and height position as well as pitch angle were graphically displayed in an easily interpretable manner. Data to enable replay of flight were stored and replay was available.
- Initial conditions could be specified by user, or default values were easily input.
- Program was suspended at user's discretion so that changes in control inputs could be made if desired.
- Plots of all stored variables were available for later analysis.
- Vehicle's flight path and all aerodynamic data were stored for later analysis or re-use.

2. Program description

By way of introduction, the programs and their basic functions are listed below:

- "AWA1"--performed variable initialization, file management, numerical differencing, input/output control and overall simulation management.

- "archytas3"--stored aircraft constants, e.g., wing area, canard location relative to center of gravity, pitch damping coefficient.

- "yprimes4"--contained equations of motion VII.A, VII.B, VII.C, and VII.G; calculated the derivatives of downrange position, height, speed, and flight path angle.

- "control3"--contained the model for the conservation of angular momentum, described in equations VII.Q and VII.R. Output was updated pitch angle, rate and acceleration.

- "THROTTLE"--converted user input from throttle position, in percent, to thrust in lbf, based on engine test data.

- "labeller"--provided labels for plots requested by the user.

- "plotter"--provided a series of eight plots of control input and vehicle response. Used following program execution.

- "Movie"--replayed the vehicle's flight path and pitch angle from most recent program execution (or a saved simulation run).

A flowchart of the program and several of its subroutines is given in Appendix F. Appendix G provides a listing of the code for all simulation programs. The basic program scheme, as depicted on the flowchart, was as follows:

1) Aircraft constants were imported from "archytas3".

2) The user was prompted for how many iterations were to be performed, what time increment to use, vehicle weight, control mode (i.e., use vanes or specify a fixed pitch rate) and whether or not the user wanted to suspend the program to make control inputs (if answer to last question was "yes" then user was asked "how many seconds between suspensions?"). The user also had the option of typing "1" which input default values.

3) The user was prompted for vehicle's initial height, speed, pitch attitude and flight path angle.

4) Initial derivatives of the information passed in step 3) were calculated. Initial drag was calculated based on drag model.

5) The output file, called "OUTFILE" which stored virtually all important values, was initialized. This file was updated each time step to allow later plotting of all variables.

6) The following vector of primary variables was defined:

$$\{Y\} = \begin{Bmatrix} x \\ h \\ V \\ \gamma \end{Bmatrix} \equiv \begin{Bmatrix} \text{downrange position} \\ \text{height} \\ \text{speed} \\ \text{flight path angle} \end{Bmatrix}$$

The equations of motion for downrange distance, height, speed and flight path angle were solved using predictor-corrector finite differencing. Euler first forward, half step and Richardson Extrapolation were combined as follows [Ref 37]:

$$Y_{n+1}^{(1)} = Y_n + \Delta t \dot{Y}_n$$

$$Y_{n+\frac{1}{2}}^{(1)} = Y_n + \frac{\Delta t}{2} \dot{Y}_n$$

$$Y_{n+1}^{(2)} = Y_{n+\frac{1}{2}} + \frac{\Delta t}{2} \dot{Y}_{n+\frac{1}{2}}$$

$$Y_{n+1} = 2Y_{n+1}^{(2)} - Y_{n+1}^{(1)}$$

7) The user was presented with a picture of the vehicle's motion, as shown in the sample output, Figure VII.8. This display provided the user with a display of the aircraft's position, displayed as a circle, and also pitch attitude, displayed as a line drawn through the circle. The user also received speed cues by observing the space between successive positions in this constant-time-increment process.

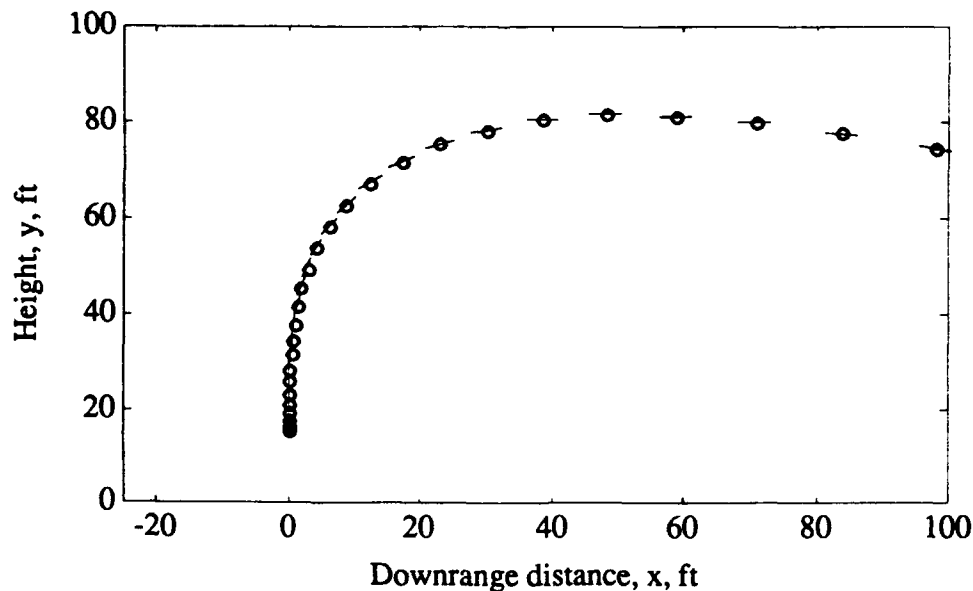


Figure VII.8: Sample Plot From Program AWA1--Continuously Updated Position and Pitch Attitude

8 At user-specified intervals, the user was then allowed to view a plot of any variables desired and to make control input changes. Plots were presented as requested. The user had control over canard and vane deflections and throttle position.

9) The program returned to step 5) and repeated this process until the user-specified program run time had elapsed or the vehicle crashed (height less than zero).

10) Following program execution the user could type "plotter" which provided eight plots on two pages. The plots provided (all versus time except last plot):

- angle of attack
- speed
- pitch attitude
- pitch rate
- canard deflection
- vane deflection
- throttle position
- height versus downrange position

11) The user also could type "Movie" and be presented with a replay of the vehicle's flight path.

12) Ancillary programs included:

- "Mplot"--to produce a plot of all pitching moment equation values versus time. Used for troubleshooting.
- "filesaver"--to save program runs for future analysis
- "resurrect"--to re-load files saved by "filesaver"

E. RESULTS AND DISCUSSION

1. Time step determination

The optimum time step for use during runs of program "AWA1" was determined by varying the time increment, called "DELTAT" in the program, and observing simulation behavior. To speed the simulation a large time step was desirable but too large a time increment destabilized the numerical differencing, producing erroneous results. Time increments of 0.2, 0.1, 0.05 and 0.025 were compared while performing identical maneuvers. In each case, the maneuver was initialized with the vehicle in a vertical attitude at a speed of 1 ft/sec. After allowing the vehicle to accelerate for a few seconds, a gentle pushover transition was initiated. Figure VII.9 depicts a comparison of the vehicle's angle of attack response with varying time increments. As shown in the figure, at time increments of 0.2 and 0.1 the angle-of-attack response showed a tendency to "spike". This was true after any maneuver was initiated. In fact, at a 0.2-sec time increment the simulated vehicle would always depart controlled flight, as defined by angles of attack exceeding 90 deg in one to two seconds. As shown in Figure VII.9, the response was smooth at time increments less than or equal to 0.05 sec. This smoothness was evident during all maneuvers. However, the simulation ran noticeably slower with the 0.025 increment, with no significant differences in response. As a result, 0.05 sec was chosen as the optimum time increment to balance stability of the numerical scheme with program run-time.

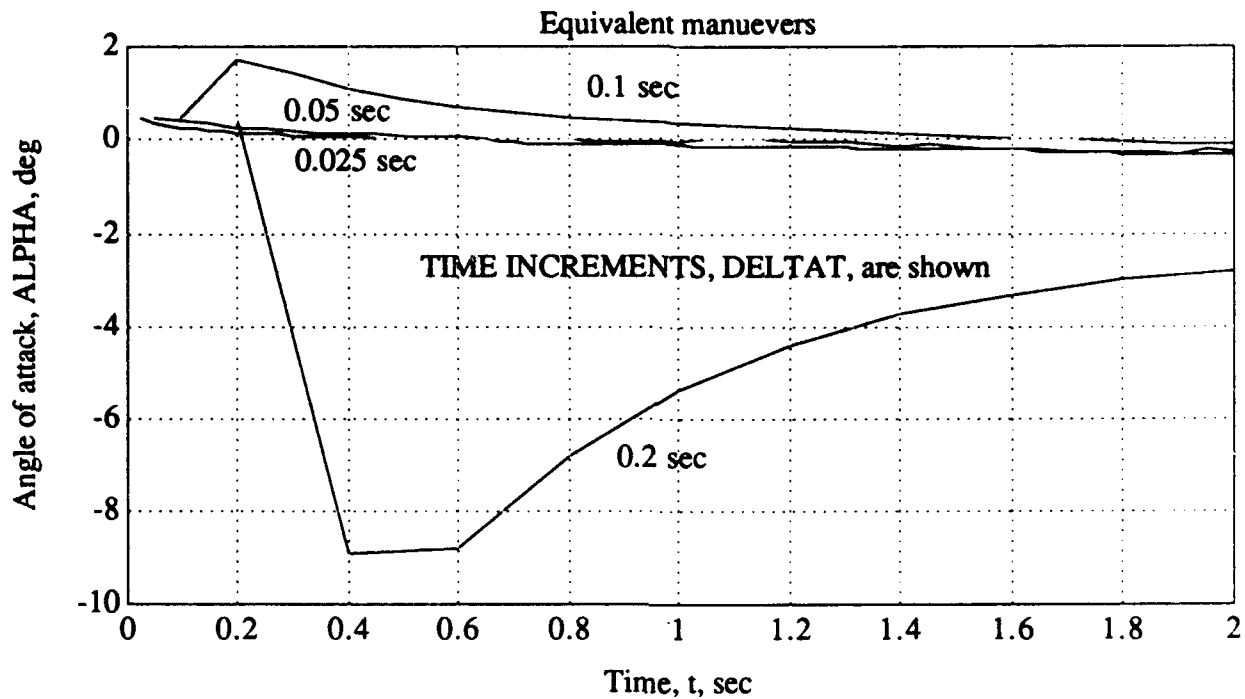


Figure VII.9

Archytas Simulation: Comparison of Time Increments
For Identical Maneuvers

2. Takeoff, transition to forward flight

a. Thrust-to-weight envelope

In order to characterize the effects of increasing weight on the vehicle, simulations were conducted at a range of thrust-to-weight ratios (T/W). In theory, any thrust-to-weight ratio greater than 1.0 is acceptable, given an extremely robust control system and the time to wait for a given flight condition to be reached. However, the reality pilots understand is that more thrust is better; the question is, "how much is enough?". Several assumptions were made

when considering a minimum T/W.

The thrust was assumed to be a constant, as delineated in Section IV, and the weight was varied. Equivalent takeoff maneuvers were simulated at full thrust with weights of 115, 110, 105 and 100 lb, corresponding to T/W values of 1.04, 1.09, 1.14, and 1.2 respectively. The maneuver consisted of starting in a vertical climb at 1 ft/sec, accelerating straight up to 5 ft/sec and then beginning a very gentle "push-over", using 3 deg of vane deflection. The maneuver was considered complete when the vehicle had achieved stable forward flight with less than 10 deg angle of attack.

The figures of merit for this T/W comparison were flight path and angle of attack. Flight paths were compared based on the altitude change from the point the "pushover" was begun. Angle of attack profiles for each T/W level were also compared. It was assumed that high-angle-of-attack (high- α) regions were to be avoided due to the difficult-to-control and unpredictable nature of flying qualities most airplanes exhibit at high α . Angles of attack above 20 deg were considered unacceptable for a vehicle controlled remotely by a person without the proprioceptive and visual cues that the pilot of a manned airplane has.

Of the two figures of merit for this analysis, the angle of attack became the primary parameter for comparison. The flight paths at different T/W were all generally acceptable. In other words, at all T/W, owing to the gentle nature of the pushover, the vehicle did not lose altitude during the transition. The vehicle was

only about 75 feet higher at the highest T/W than it was for a comparable maneuver at the lowest T/W. A comparison of the angle of attack profiles for the various T/W is shown in Figure VII.10. At T/W of less than 1.09 the vehicle exceeded the established angle-of-attack limit.

Because the vehicle weight predicted by the analysis of Section VI was approximately 100 lb, a T/W value of 1.2 was utilized for all subsequent simulations.

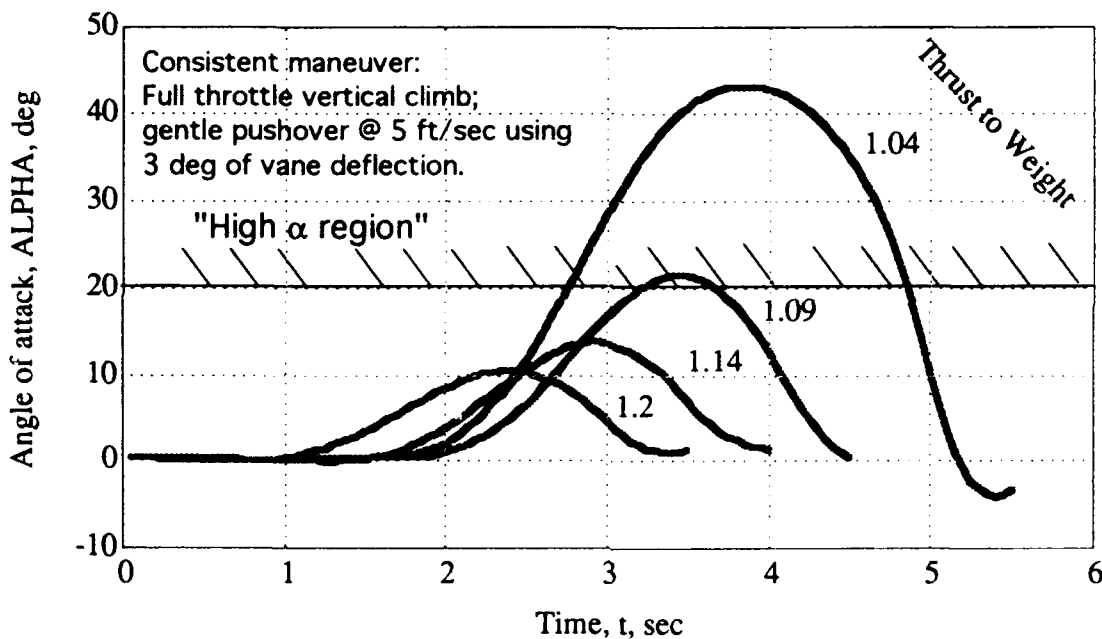


Figure VII.10

Archytas Simulation: Thrust-To-Weight Comparison

b. Takeoff transition tradeoffs

Over 500 runs of program AWA1 were performed for the transition from a hover to horizontal flight and several basic

profiles emerged. These profiles and references for the resulting plots are given in Table VII. For each maneuver the corresponding plots of downrange distance versus height ("X-H PLOT") and time history ("PARAMETER PLOT") are referenced.

Table VII.I
ARCHYTAS SIMULATION: TAKEOFF TRANSITION PROFILES,
DESCRIPTION AND LOCATION OF RESULTS

No.	MANEUVER	DESCRIPTION(1)	X-H PLOT	PARAMETER PLOT
1	Low vane deflection pushover from hover	From hover, 3° Delv until 10° pitch attitude, then pull up.	Figure VII.11	Appendix H, Figure H.1
2	High vane deflection pushover from hover	From hover, 10° Delv until 0° pitch attitude, then pull-up to level flight.	Figure VII.12	Appendix H, Figure H.2
3	Low speed, low altitude climbing gentle pushover	From hover accelerate straight up until V=5 ft/sec, then 3° Delv until 45° pitch attitude then pull-up to level flight.	Figure VII.13	Appendix H, Figure H.3
4	Vertical acceleration to gentle pushover	From hover, accelerate straight up until V=20 ft/sec then 3° Delv until 45° pitch attitude, then accelerate and climb.	Figure VII.14	Appendix H, Figure H.4

Note: (1) "Delv" is vane deflection
(2) "V" is speed

Figures VII.11 through VII.14 depict the results of a particular profile. The pull-up maneuver used consistently was a medium-effort pull-up defined by use of 10 deg of canard deflection and 0 deg of vane deflection. Appendix H, Figures H.1 through H.4, give detailed time histories of several parameters as well as control inputs.

The first profile, in which the vehicle was pushed over using a small vane deflection, was characterized by over 100 ft of altitude loss and an angle of attack that peaked at 15 deg. The second profile, similar to the first except that the vane was deflected about three times as much, was marked by more altitude loss (more than 200 ft) and about the same angle-of-attack response. The third profile involved initiating a gentle pushover while climbing but at a relatively slow speed. The third profile's angle of attack increased both during the initial part of the transition and also during the pull-up. There was a slight loss in altitude from the apex of the transition. The fourth profile, similar to the third except the vehicle was allowed to accelerate to a higher speed prior to pushing over, was characterized by very low angle of attack and a continuous climb requiring less than 75 ft of vertical distance to complete.

The fourth profile was the most repeatable and had the following advantages:

- The angle of attack was low during the entire profile and was easily controlled with slight changes in vane deflection during the initial part of the transition and, as speed built, by canard

deflection during the latter portion. Controlling angle of attack during the other profiles was not as carefree, requiring constant attention to ensure that a high angle of attack region was not entered.

- Altitude required to complete the last profile was well less than 100 ft and it was all altitude *gain* . By contrast, the other profiles involved altitude *losses* up to 200 ft. In particular, performing high-vane-deflection pushovers similar to the first profile generally involved having to climb the vehicle in a hover to an extremely high altitude (up to 500 ft) to ensure enough distance below to complete the maneuver without striking the ground. The altitude required for these high-vane-deflection pushovers was very unpredictable.

Profiles 1, 2, and 3 had no apparent advantages and therefore the fourth profile was recommended.

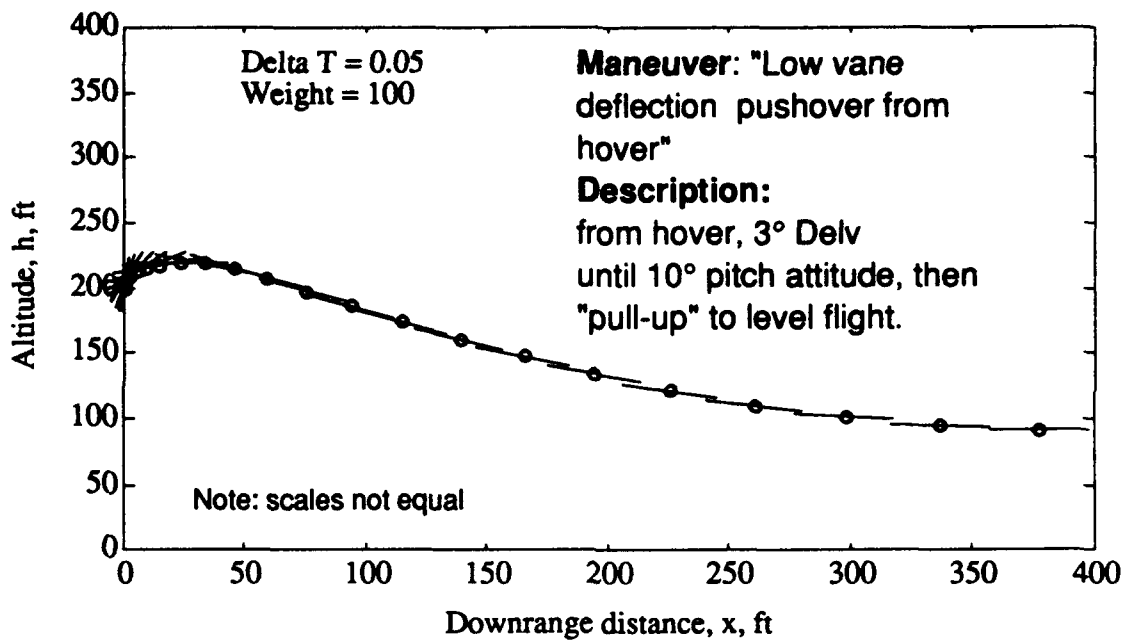


Figure VII.11: Archytas Simulation: Takeoff Transition Profile #1

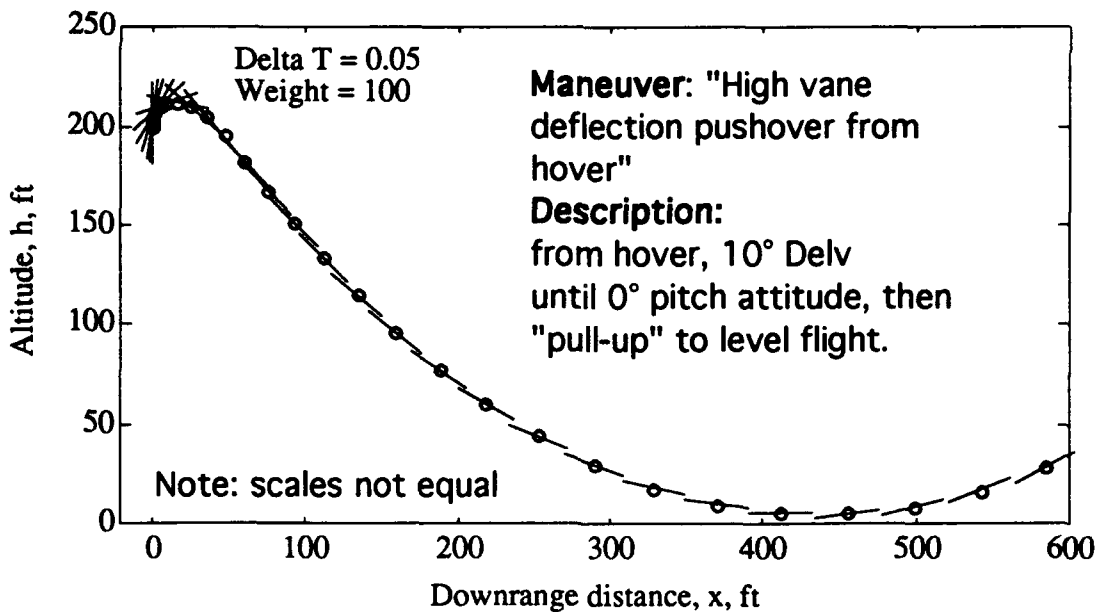


Figure VII.12: Archytas Simulation: Takeoff Transition Profile #2

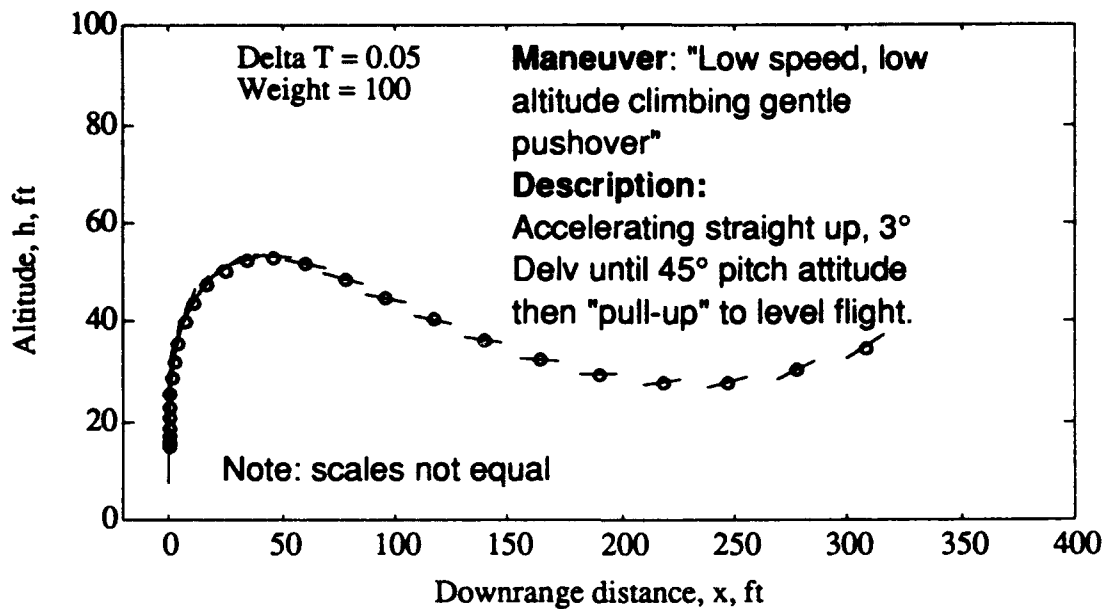


Figure VII.13: Archytas Simulation: Takeoff Transition Profile #3

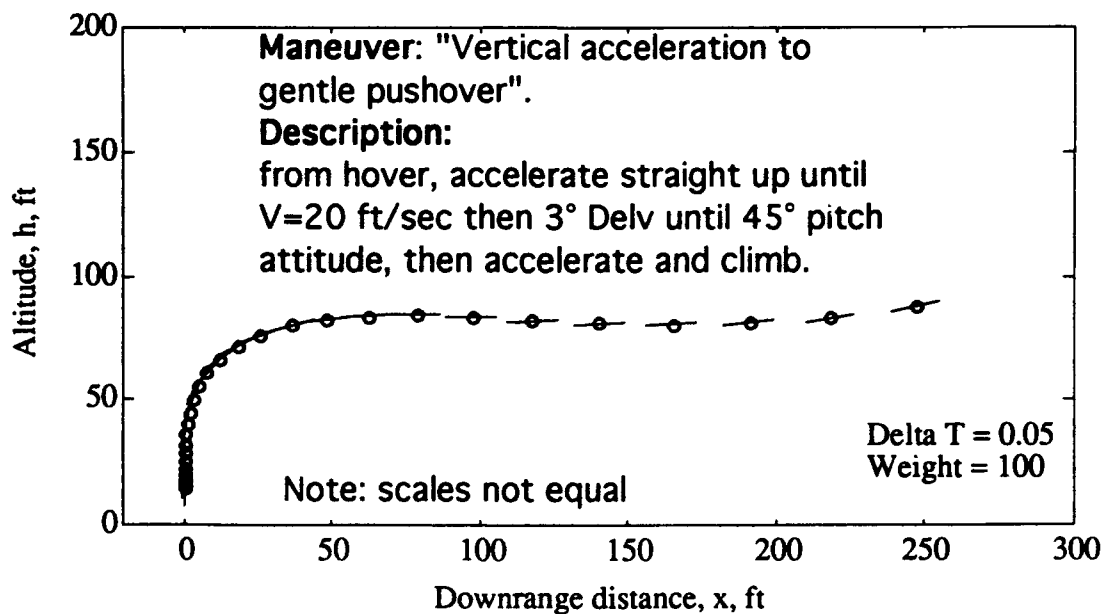


Figure VII.14: Archytas Simulation: Takeoff Transition Profile #4

3. Horizontal flight

a. Trim conditions

The horizontal flight characteristics of the Archytas were simulated at two separate trim conditions listed in Table VII.II. These were considered the standard conditions for all horizontal flight analysis. Condition 1 was considered an average cruise condition for employment of the vehicle and Condition 2 was tested to compare with Aquila data at similar flight conditions.

Table VII.II

ARCHYTAS SIMULATION HORIZONTAL FLIGHT TRIM CONDITIONS

PARAMETER	CONDITION 1	CONDITION 2
Altitude	150 ft	150 ft
Airspeed	153 ft/sec	103 ft/sec
Angle of attack	0.455 deg	3.2 deg
Pitch attitude	0.455 deg	3.2 deg
Canard deflection	-7.2 deg	-9.2 deg
Vane deflection	0	0
Throttle position	24 percent	9.5 percent
Thrust	49.6 lbf	25.5 lbf

b. Cruise flight short period characteristics

The short period characteristics were explored in horizontal flight in Condition 1, as specified by Table VII.II, with a sinusoidal pitch doublet input. Figure VII.15 depicts the input, the response and an expanded view of the response along with the analysis of the dynamics.

c. Predicted short period characteristics

In order to compare the simulation's behavior to that of the Aquila, the short period characteristics of the Archytas were explored in horizontal flight, at a slower speed: Condition 2 as listed in Table VII.II. The simulation was excited by a sinusoidal doublet near the natural frequency. Figure VII.16 depicts the input, the response and an expanded scale view of the response along with analysis of the dynamics. These are compared in Table VII.III to the Aquila's short period characteristics, as derived from wind tunnel data and analytical methods [Ref 38].

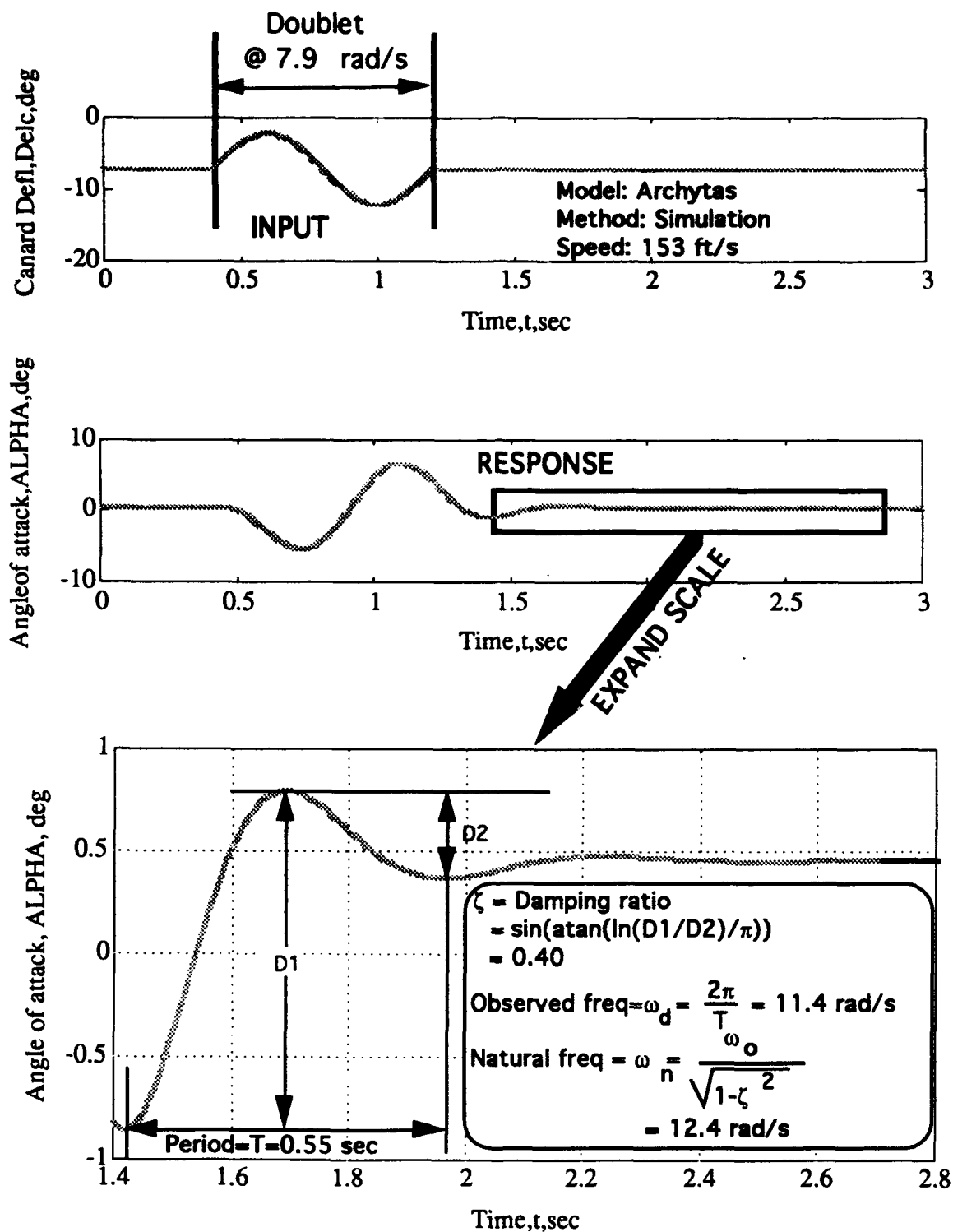


Figure VII.15: Predicted Short Period Response in Cruise Condition 1

Table VII.III
SHORT PERIOD CHARACTERISTICS:
COMPARISON BETWEEN AQUILA AND ARCHYTAS

CHARACTERISTIC	AQUILA ⁽¹⁾	ARCHYTAS ⁽²⁾
Speed (ft/sec)	101	103
Gross weight (lb)	130	100
CG (percent MAC)	21	-6.5
Period (sec)	1.06	0.798
Damping ratio	0.54	0.40
Natural frequency (rad/sec)	5.9	8.57

Notes: (1) Wind tunnel and analytical analysis [Ref 28]

(2) Simulation program AWA1

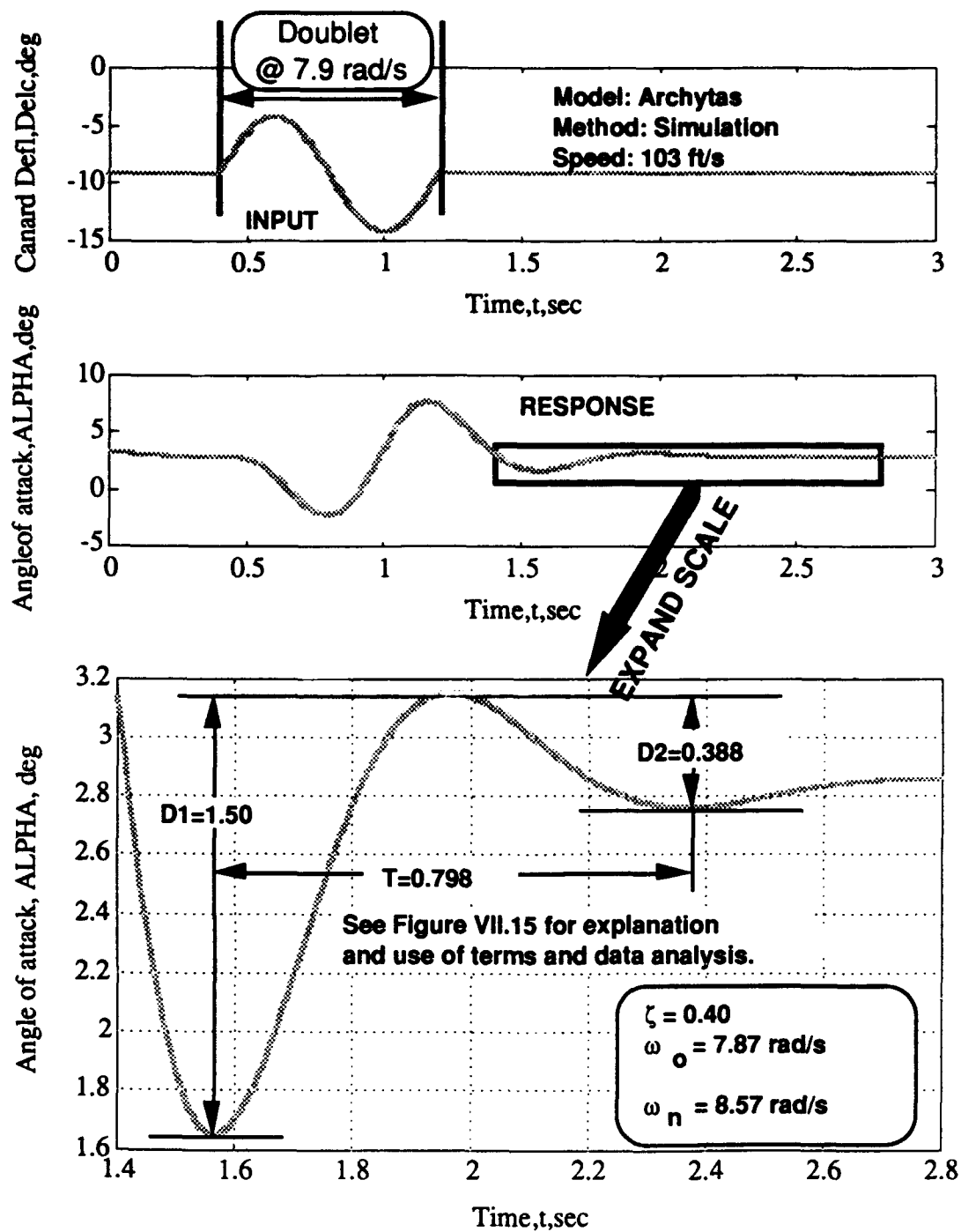


Figure VII.16: Archytas Short Period Response at Condition 2

In view of the use of the Aquila's pitch damping coefficient in the Archytas simulation, the similarity of damping ratios between the two is a favorable indication of simulation fidelity. The difference between the two aircraft's period/frequency, a strong function of the derivative M_{α} , can be attributed to the 15 percent static margin of the Archytas compared to that of the Aquila, which has a static margin on the order of five percent [Ref.28].

d. Long period

The long period or phugoid characteristics of the Archytas were simulated at both trim conditions listed in Table VII.III. The phugoid was excited by slowing the Archytas from a level flight trim condition by approximately 15 ft/sec and then returning the controls to the trim point setting [Ref. 39]. Figure VII.17 depicts the control input, the airspeed response and an expanded plot of the airspeed response with phugoid characteristics. Table VII.IV shows a comparison of phugoid characteristics between Archytas simulation and Aquila.

The simulation's phugoid period was within nine percent of the following approximation for the period [Ref. 36]:

$$\begin{aligned} T_{phugoid} &\cong \sqrt{2}\pi \frac{V}{g} \\ &= \sqrt{2}\pi \frac{104}{32.2} \\ &= 14.34 \end{aligned}$$

The simulation's long period characteristics also compared well to the information available for the similarly shaped

Aquila. The only significant disparity between predictions for the two vehicles involved damping ratio. The difference for the two aircraft's damping ratios, a strong inverse function of the lift-to-drag ratio (L/D), may be explained by either a real or modelled difference in lift or drag. In as much as the lift model was based on a vortex lattice analysis that agreed well with data available for the Aquila, a likely reason for the difference in damping ratio was the drag model. However, both sets of long period characteristics are representative of aircraft flying at the simulation speed and will pose, at worst, only a nuisance to a control system or pilot attempting to counter the phugoid.

Table VII.IV
LONG PERIOD: COMPARISON BETWEEN AQUILA AND ARCHYTAS

CHARACTERISTIC	AQUILA ⁽¹⁾	ARCHYTAS ⁽²⁾
Speed (ft/sec)	101	104
Gross weight (lb)	130	100
CG (percent MAC)	21	-6.5
Period (sec)	15.8	16.9
Damping ratio	0.044	0.16
Natural frequency (rad/sec)	0.37	0.40

Notes: (1) Wind tunnel and analytical analysis [Ref 28]

(2) Simulation program AWA1

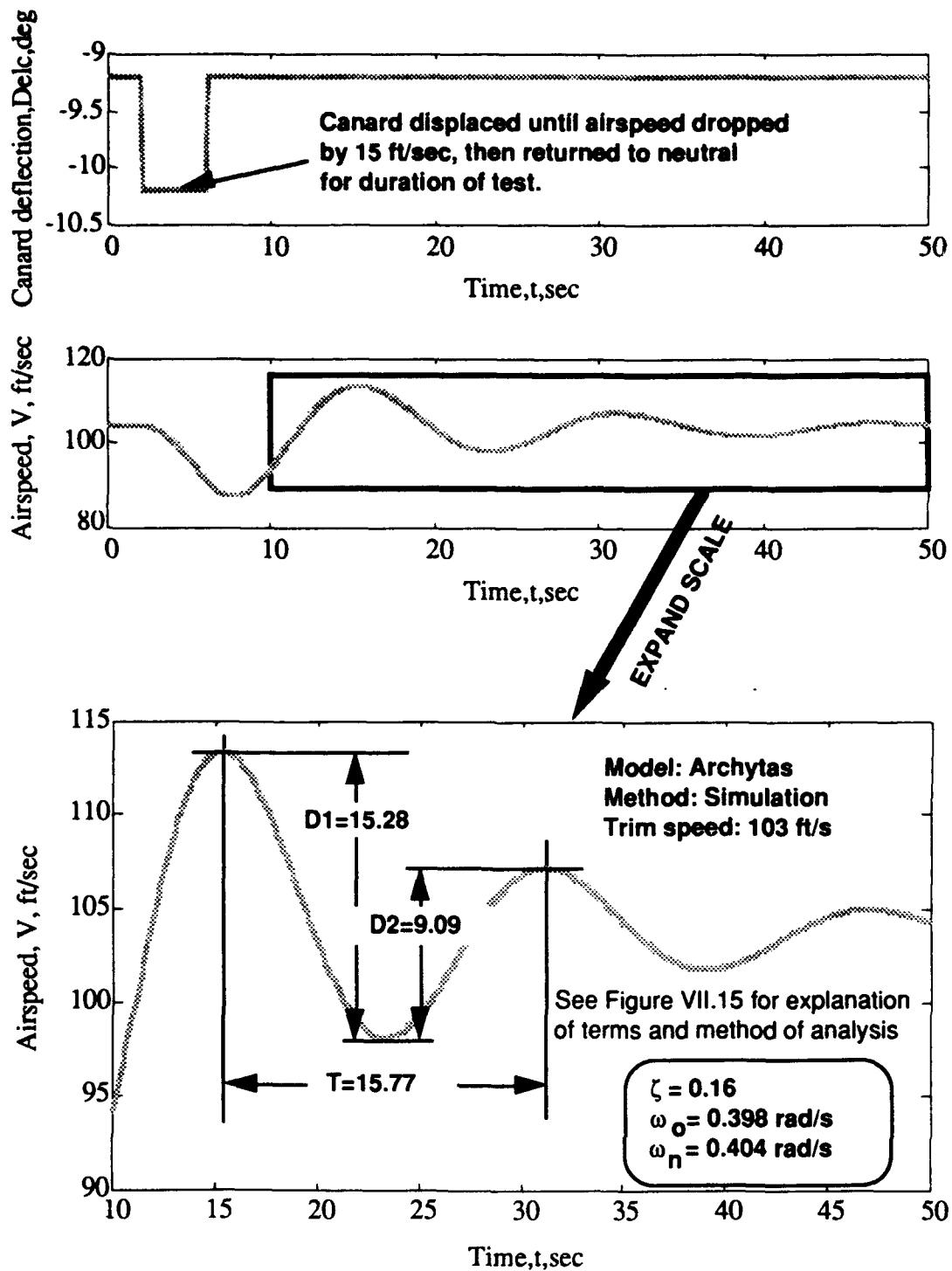


Figure VII.17: Simulation long period response at Condition 1

4. Transition from horizontal flight to vertical landing

a. General

The transition from horizontal flight to a hover, for the purpose of a vertical landing, was evaluated during approximately 150 runs of the simulation program AWA1. Two types of transitions were attempted, described as follows:

- A *level* deceleration to hover parameters. From stabilized horizontal flight, the profile involved attempting to slow the vehicle without gaining altitude while progressively increasing the pitch attitude to 90 degrees. This profile necessitated the ability to generate high angles of attack during the deceleration to avoid gaining altitude as the pitch attitude was increased.

- A "zooming" transition to hover parameters. From stabilized horizontal flight the vehicle's pitch attitude was increased while maintaining unstalled angles of attack. This profile involved a climbing or "zooming" flight path. As the vehicle approached high pitch attitudes, the power was reduced from the level flight setting to allow the vehicle to decelerate. Pitch inputs were then made to capture approximately 90 degrees for both pitch attitude and flight path angle.

For standardization, the vehicle was considered to have entered a hover when the airspeed was less than 0.5 ft/sec, the pitch angle and flight path angle were within 5 degrees of 90 degrees and the pitch rate was less than 2 deg/sec.

b. Level deceleration profile

As is common with canard designs, wherein the canard's aerodynamic loading is higher than the wing's, the Archytas simulation could not be slowed below approximately 65 ft/sec (38 KTAS) in level flight. Attempts to further slow the airspeed resulted in a pitch attitude decrease with an accompanying increase in airspeed and loss of altitude--a classic canard stall. This occurred despite full-effort control inputs for both the canard and the vanes. Figure VII.18 shows a situational plot of an attempt to slow the vehicle with full effective canard and vane deflections. Appendix H, Figure H.5 displays the aircraft response and control inputs for this attempt. The canard was deflected to produce the maximum coefficient of lift for the canard, which occurred at approximately 15 degrees relative angle of attack. As shown on Figure VII.5, the local angle of attack at the canard was a combination of the aircraft's angle of attack and the canard deflection. The vane was deflected to 30 degrees, the maximum effective deflection. As shown in both Figures VII.18 and Appendix H, Figure H.5, the vehicle's pitch attitude simply could not be slowed below the 65 ft/sec range because the canard would stall prior to stalling of the wing. Figure VII.19 shows the balance of moments that prevented the pitch attitude from being increased. This figure shows that the canard and vane, both at maximum effort to pitch the nose up, were countered by the wing's nose down pitch moment. The high nose down pitching moment was due to the aircraft's high static margin coupled with the canard

design. Another characteristic of the level deceleration profile was the large downrange distance used to slow the vehicle.

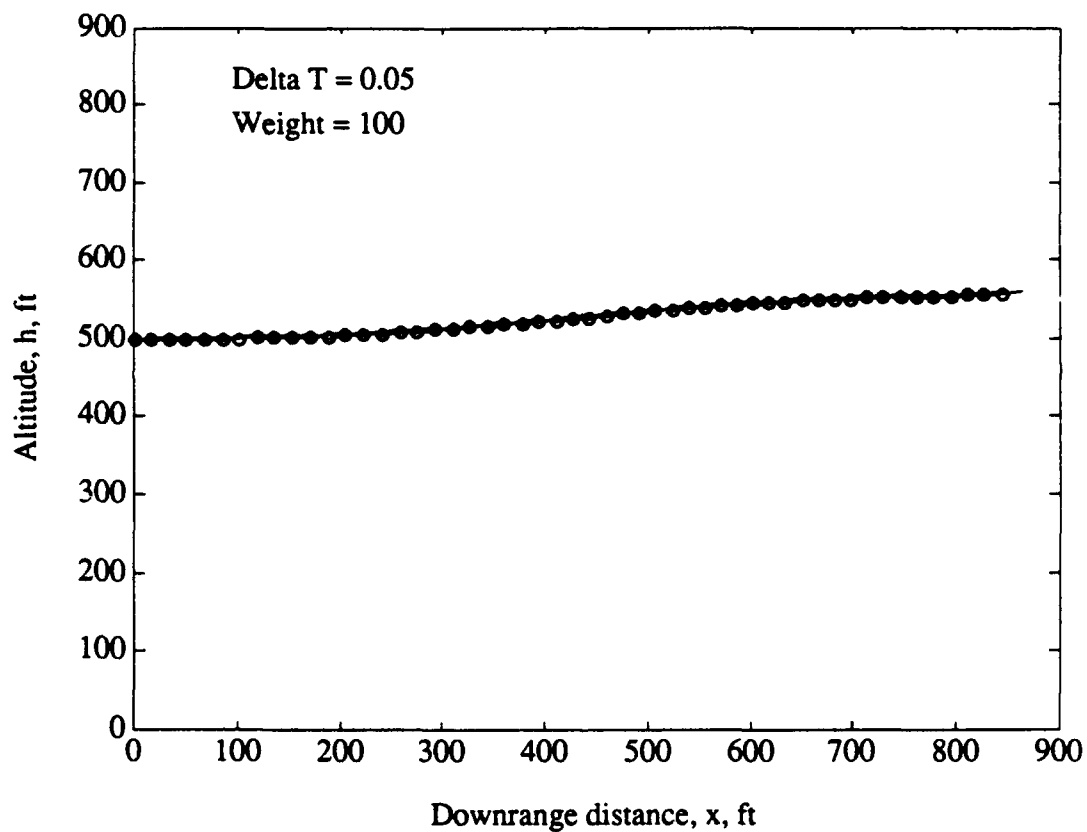


Figure VII.18:Level Deceleration Attempt: Situational Plot

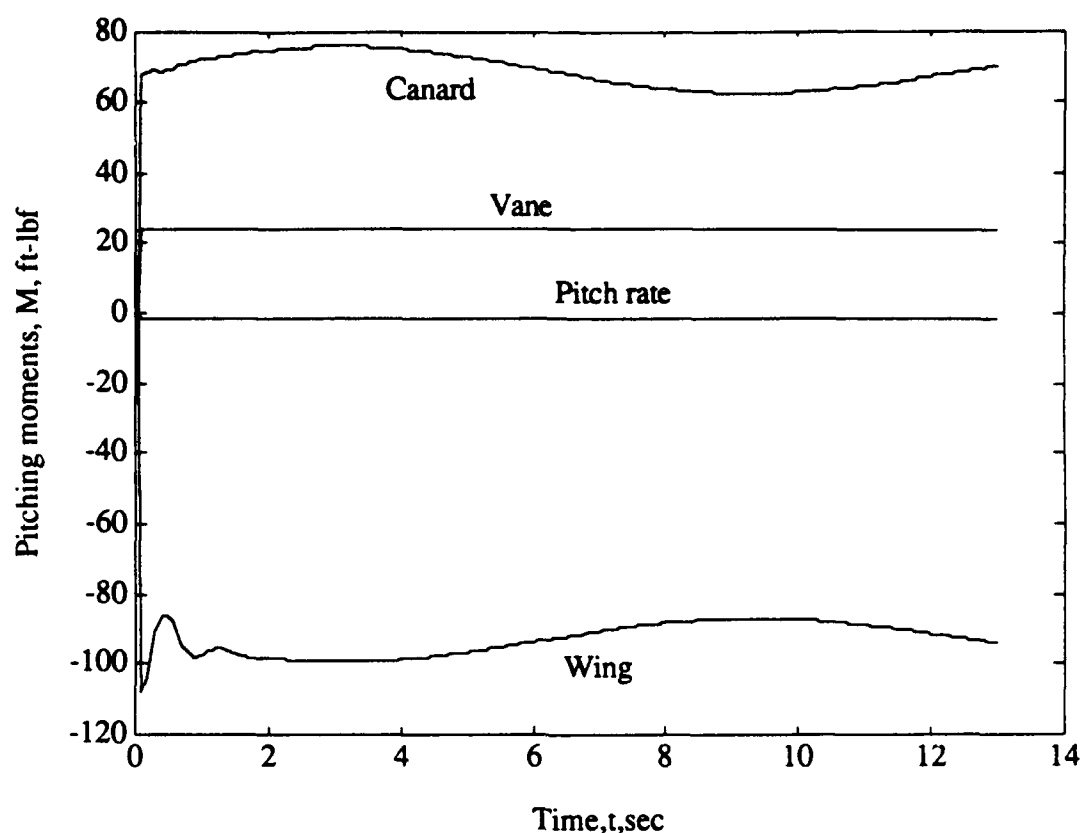


Figure VII.19

Level Deceleration Attempt: Balance of Moments

c. "Zooming" profile

Attempts made using the second type of profile met with success. Figure VII.20 shows a transition first to horizontal flight and then back to a hover. The transition back to a hover began with the vehicle at approximately 70 ft/sec, at which time power was added and the nose raised with canard and vane as the vehicle climbed at angles of attack less than stall. As the pitch attitude

neared 90 degrees power was reduced and an opposite vane/canard input was made to stop the pitch rate. Appendix H, Figure H.6 depicts the aircraft response and control inputs made during this particular run.

The altitude required to perform this type of maneuver varied from 350 to 900 feet, depending on the speed at which the zoom was initiated and the throttle scheduling used.

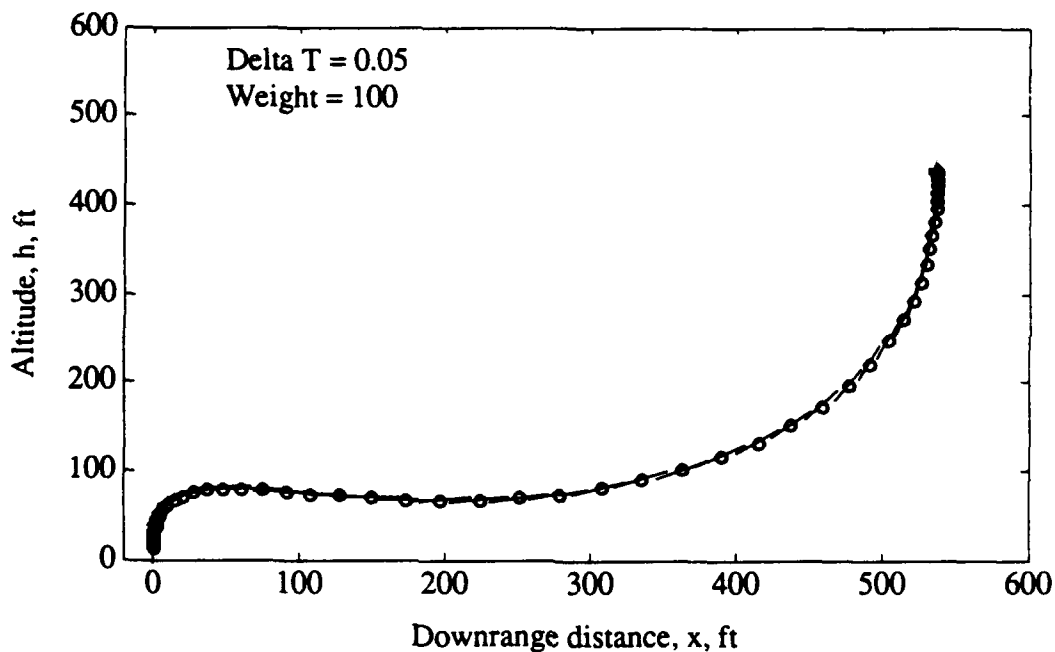


Figure VII.20
Transition to Horizontal Flight
Followed by "Zooming" Transition Back to Hover

VIII. CONCLUSIONS

A. GENERAL

The design and initial fabrication of a Vertical Attitude Takeoff and Landing (VATOL) Unmanned Air Vehicle (UAV) airframe was completed at the Naval Postgraduate School (NPS). The vehicle, called Archytas, was a combination of two existing UAV's--the AROD and Aquila--as well as locally manufactured components, including wing spars and support structure for a canard. The objective of creating Archytas was to provide a proof-of-concept platform for research to explore performance trade-offs and stability augmentation. A three-degree-of-freedom simulation was used as the focus of the design efforts, to validate design decisions made in the fields of propulsion, aerodynamics, structures and flight mechanics. Engine tests were conducted to determine thrust and control power. Structural components were designed, fabricated and then tested, making modifications where necessary to ensure sufficient airframe strength. A longitudinal control system was designed, validated by simulation and tested structurally.

Specific conclusions, by section, follow.

B. SPECIFIC

1. Engine tests

An existing engine test stand was upgraded with improved force and moment measuring devices. The existing engine from the AROD was tested and shown to provide sufficient thrust and longitudinal control power to power the Archytas design. Specifically, thrust and control power were quantified as a function of rpm and throttle position. Additionally, several miscellaneous characteristics were explored including duct blockage, vane movement in the presence of propwash, the speed of the propwash, noise levels, fuel usage and engine dynamics.

2. Wing spar design, fabrication and test

The structural elements to connect the Aquila wings to the AROD duct, including wing spars and associated hardware, were designed, fabricated and tested on an individual basis. These individual tests revealed design deficiencies which were corrected and the components then retested with satisfactory results. A full configuration test was then conducted to simulate the flight loads on an actual vehicle. This full test demonstrated that the basic spar design was sound and identified deficiencies with the Aquila wing root structure.

3. Canard design; support structure fabrication and test

A static longitudinal stability analysis was conducted to choose the size and location of a canard. Detailed weight and balance

analysis as well as aerodynamic modeling dictated a shift in the location of an electronics pod from an aft center of gravity location to a forward one. Canard location and sizing analysis considered trimmability and controllability criteria over the Archytas' expected airspeed range.

Following canard design, a structural analysis of a supporting boom structure was detailed. Empirical analysis of graphite booms was conducted and eventually abandoned in favor of an aluminum tube boom structure with graphite composite support. Aluminum tubing was chosen based on a combined strength and weight comparison. Boom support structural members, boom support hole in forward spar and boom base, were manufactured and tested with favorable results.

4. Simulation

Beginning with conservation of linear and angular momentum equations, a non-linear three-degree-of-freedom simulation program was created. The series of programs that constituted the simulation allowed for analysis of the Archytas' longitudinal flight path and pitch axis. Simulation was used for validation and analysis of a wide variety of issues including: wing location and sizing; canard location and sizing; weight and balance and static margin optimization; vehicle thrust-to-weight ratio analysis; and transition profile prediction and analysis. Additionally, dynamic characteristics for horizontal flight were predicted and compared with theory and Aquila characteristics.

C. ARCHYTAS CONFIGURATION

The airframe that results from the design work of this thesis is the Archytas. With the addition of an avionics suite for command and control, the Archytas will be a Vertical Attitude Takeoff and Landing (VATOL) Unmanned Air Vehicle (UAV) capable of hovering flight, horizontal flight and transition to and from horizontal flight.

IX. RECOMMENDATIONS

A. GENERAL

The Archytas program, comprised of students and professors from several departments at NPS, has so far been marked by a concerted effort to approach testing in a careful manner, often called "build-up" in the test community. This is evident in the testing of individual components and use of low risk platforms, including a remotely controlled car and conventional airplane, for validation of systems. The writer strongly encourages continuation of this laudable approach, particularly as the program enters flight test, with all its potential hazards.

B. SPECIFIC

1. Engine tests

(a) The combination of engine tests and simulation indicated a satisfactory thrust-to-weight ratio for the Archytas. However, if the vehicle's weight rises beyond about 110 lbf, further engine tests may be required to determine optimum thrust conditions. Specifically, a matrix of different blade angles, rpms, and carburetor mixtures could be performed to optimize thrust.

(b) More accurate fuel flow measurements, perhaps by using a commercially available fuel flow sensor, could be taken during future engine tests. Such fuel flow data would be useful in

predicting vehicle range and endurance.

(c) As discussed in thesis work by Lieutenant Commander Moran, several electronics failures were experienced during engine testing [Ref. 16]. Future electronics manufactured *must* be built in a hardy fashion. Redundancy in design is also encouraged where possible.

2. Wing spar design

(a) The spar design manufactured by the FRL appears to be satisfactory. Modifications to the Aquila wing root will be required before a flight article can be assembled. These modifications might include: adding graphite and fiberglass material to the wing root spar to increase its crush strength, thereby allowing the mounting bolts to be tightened more than was feasible during testing; use of skin as structural members; and use of structural adhesive to supplement the present system of bolts and plates.

(b) All design modifications should be tested to determine actual strength. Such tests should eventually include a full configuration test.

(c) The Department of Aeronautics and Astronautics at NPS should have a finite element analysis program capable of performing analysis on composite material intended for manufacture. The Department presently has a program called PAL2 but use of this copy is for educational purposes and is specifically restricted from being used to assist in the design of any components to be manufactured [Ref. 40].

3. Canard design

A canard must be designed and manufactured to sizes specified in this thesis. In view of the fact that canards provide lift for the vehicle, a slightly cambered airfoil, such as a NACA 2412, is recommended. The recommended method of fabrication is hot-wiring of blue foam, then covering the foam with a layer of graphite weave and then a finish layer of fiberglass weave. Structural tests of a sample should be conducted.

4. Simulation

The fidelity of the simulation program may be improved as further information about the Archytas is determined. Appendix E discusses the assumptions made in formulation of the simulation program and is therefore a good source of potential improvements to the program. High-angle-of-attack aerodynamics is perhaps the area that deserves the most attention.

Most simulation runs were made using a thrust-to-weight ratio of 1.2. If the flight article's thrust-to-weight is less, the simulation should be repeated to determine acceptable profiles at a higher weight.

Simulation results indicate several recommended Archytas flying techniques:

- Takeoff transition should be performed by allowing the vehicle to accelerate nearly straight up, allowing speed to build to approximately 20 ft/sec and then *gently* pushing over with vane control. As the pitch attitude reaches 45 deg the vanes may be

relaxed to neutral, and the transition to level flight completed with canard control.

- Short period characteristics in horizontal flight are predicted to have moderate damping and frequency. Care should be taken to avoid excitation of the short period, particularly with inputs near the natural frequency.

- Phugoid characteristics in horizontal flight are predicted to be benign and should present no adverse flying qualities to the Archytas pilot.

- Due to the vehicle's large static margin and its canard design, the transition from horizontal flight to hover will necessarily have to be made using a "zooming" profile. The simulation showed that a deceleration in level flight to a hover will not be possible. The preferred method will be to "zoom" the vehicle from horizontal flight, as shown in section VII.

5. Weight control

Thrust-to-weight ratio in any VTOL design is critical. The weight of candidate components, electronic or otherwise, must be high on the designer's list of priorities and continually stressed to team members. A minimum thrust-to-weight ratio of approximately 1.09 was identified during simulation and, as a result, an absolute maximum weight of 110 lb is recommended. Accurate records should be kept of the weight of all components added to the Archytas to assist in a weight-reduction analysis, in the event the vehicle becomes overweight.

6. Lateral and directional flight mechanics

This thesis essentially ignored the lateral and directional axes of the Archytas. Great care is recommended when considering the areas of horizontal flight directional stability and high-angle-of-attack lateral/directional stability and control. Wind tunnel tests may be useful in determining design requirements in these areas. Specifically, a study should be conducted to determine directional stability in the Archytas' current configuration and then assess the need for addition of a lightweight vertical surface. Active control of sideslip through use of the AROD's vanes, essentially augmented directional stability, is possible but probably would not work well in the event of engine failure.

7. Flight test

The author has some experience in flight test and so a few words on the subject are appropriate. Prior to approving any flight test, including tethered hover, a thorough test plan is recommended. This test plan should include a strong description of *exactly* what tests are to be performed and *exactly* what data are to be taken. The safety of test personnel and bystanders must be thoroughly considered and "what-if" questions asked and answered. A matrix of events, showing the order, description and purpose of each event as well as data required, will be a useful tool. Build-up of events should be considered and specifically addressed, in other words, low-risk events should precede high-risk ones. Checklists for operation of the vehicle and its systems are encouraged as a means of ensuring

standardization and continuity in the project. If possible, the test plan should be reviewed by someone with experience in UAV testing and/or flight test. The test plan should be approved by competent authority prior to the commencement of *any* test plan events and *any deviations* from the test plan must first receive approval from the same authority--the time for creative thinking is as you write the test plan, not as you execute it.

LIST OF REFERENCES

1. Lindenbaum, B., "A Status Review of Non-Helicopter V/STOL Aircraft Development (part 1 of 2)," *Vertiflite*, v. 36, no. 3, pp. 32-43, March/April 1990.
2. Leonard, Lloyd H., "Design Studies of Various Tilting Fuselage Convertible Aircraft," *Proceedings of the 1st Convertible Aircraft Congress*, Philadelphia, PA, Dec 9, 1949, published by Institute of Aeronautical Sciences.
3. David Taylor Research and Development Center Report DTNSRDC-80/018, *A Case for VATOL Flight Demonstration*, by J.C. Martin, pp. 35-45, January 1980.
4. David Taylor Research and Development Center Report ASED-78/08, *An Examination of the Factors Affecting the Thrust Requirements and the Hover and Short Takeoff Performance of Several Jet V/STOL Fighter Concepts.*, by R.E. Kuhn, May 1978.
5. Girard, P.F. and Everett, W.L., "A Test Pilot Report on the X-13 Vertijet and VZ-3RY Vertiplane", *Annals of the New York Academy of Sciences*, v. 107, pp 409-427, March 1963.
6. NASA Report TN D-404, *Hovering and Transition Flight Tests of a 1/5 Scale Model of a Jet Powered Vertical Attitude VTOL Research Airplane*, by Charles Smith, Jr., May 1961.
7. Blanchette, Bryan M., *The Design and Construction of a Shiplaunched VTOL Unmanned Air Vehicle*, Master's Thesis, Naval

Postgraduate School, Monterey, California, June 1990.

8. Ellwood, Jeffrey L., *Design and Construction of a Composite Airframe for UAV Research*, Master's Thesis, Naval Postgraduate School, Monterey, California, June 1990.

9. Brynestad, Mark A., *Investigation of the Flight Control Requirements of a Half-Scale Ducted Fan Unmanned Aerial Vehicle*, Master's Thesis, Naval Postgraduate School, Monterey, California, March 1992.

10. Merz, Paul V., *Development and Test of the Digital Control System for the Archytas Unmanned Air Vehicle*, Master's Thesis, Naval Postgraduate School, December, 1992.

11. Kress, Gregory A., *Preliminary Development of a VTOL Unmanned Air Vehicle for the Close-Range Mission*, Master's Thesis, Naval Postgraduate School, September, 1992.

12. AGARD report No. R-577-70, *V/STOL Handling Qualities, Parts I (Criteria and Discussion) and II (Documentation)*, 1970.

13. Department of the Navy Military Specification MIL-F-83300, *Flying Qualities of Piloted V/STOL aircraft*, 31 DEC 70 updated 26 SEP 1991.

14. David Taylor Research and Development Center Report DTNSRDC/ASED-79/05, *Research and Development Needs of a VATOL Aircraft*, by R.E. Kuhn, May 1979.

15. "AROD Development Status", unpublished manual written by Sandia National Laboratories, held by Naval Postgraduate School Flight Research Laboratory.

16. Moran, Patrick J., *Archytas Ducted-Fan UAV Control Vane Guidance Using Hover Mode Controller*, Master's Thesis, Naval Postgraduate School, Monterey, California, June 1993.
17. Department of the Navy Military Specification MIL-F-8785C, *Flying Qualities of Piloted Airplanes*, 5 November 1980.
18. Weir, Robert J., *Aerodynamic Design Considerations for a Free-Flying Ducted Propeller*, Proceedings of the AIAA Atmospheric Flight Mechanics Conference, pp 420-431, August 15-17, 1988.
19. Kuechenmeister, David, *A High Fidelity Non-linear Simulation of an Autonomous Unmanned Air Vehicle*, Master's Thesis, Naval Postgraduate School, Monterey, California, June 1993.
20. Layton, Donald M., *Helicopter Performance*, Matrix Publications, 1982.
21. Stoney, Robert B., *Archytas Manufacturing Notes*, notes held by Professor R. M. Howard, Naval Postgraduate School, Monterey, California.
22. *Hysol Surface Preparation Guide*, published by the Dexter Aerospace Materials Division, Pittsburg, California.
23. The Boeing Company, *Phosphoric Acid Anodizing*, U.S. Patent Appl.
24. Interview between Doug Shelton, Naval Postgraduate School Physics Department, Monterey, California, and the author, 15 May 1993.
25. Interview between Gary Davis, Hysol Corporation Technical Support, Pittsburg, California, and the author, 12 April 1993.

26. Interview between Kent Knock, Sikorsky Corporation, and the author, 1 April 1993.
27. Roskam, Jan, *Airplane Design, Part VII: Determination of Stability, Control and Performance Characteristics*, Roskam, 1991.
28. U.S. Army Aviation Research and Development Command Report USARTL-TR-78-37A, *Aquila Remotely Piloted Vehicle System Technology Demonstrator (RPV-STD) Program, Volume I--System Description and Capabilities*, by Grover L. Alexander, Lockheed Missiles and Space Company, Sunnyvale, California, April 1979.
29. National Air and Space Administration Technical Report No. TN D-6142, *Vortex-Lattice Fortran Program for Estimating Subsonic Aerodynamic Characteristics of Complex Planforms*, by Richard J. Margason and John E. Lamar, February 1971.
30. Nicolai, Leland M., *Fundamentals of Aircraft Design*, METS, Inc., 1975.
31. Anderson, John D, Jr., *Introduction to Flight*, 3rd ed., McGraw-Hill, 1989.
32. Allen, David H., and Haisler, Walter E., *Introduction to Aerospace Structural Analysis*, John Wiley & Sons, 1985.
33. Wick's Aircraft Supply advertisement, *Trade-a-plane*, Crossville, Tennessee, First February Issue, 1993.
34. Timoshenko, Stephen P., *Theory of Elastic Stability*, McGraw-Hill, 1961.
35. Niu, Michael Chun-Yung, *Airframe Structural Design*, Conmilit Press Ltd.

36. Schmidt, L. V., *Introduction to Aircraft Flight Mechanics*, class notes for flight mechanics class at the Naval Postgraduate School, Monterey, California, July 1992.
37. Bobbitt, Richard B., *Escape Strategies for Turboprop Aircraft in a Microburst Windshear*, Master's Thesis, Naval Postgraduate School, Monterey, California, March 1991.
38. McVernon, J.H., *Stability and Control and Performance Estimates*, LSMC Memo A-R111-11A1 02/03, Lockheed Missiles and Space Company, Inc., Sunnyvale, California, 7 March 1975.
39. U.S. Naval Test Pilot School Flight Test Manual 103, *Fixed Wing Stability and Control, Theory and Flight Test Techniques*, October 1984.
40. Interview between Ed Wu, Professor, Naval Postgraduate School, and the author, 1 April 1993.

APPENDIX A: TABLES
TABLE A.I
AROD THRUST STAND TEST MATRIX

EVENT	THRUST (1)	VANE POSIT(DEG)	DATA (2)	REMARKS
A	-	-	TSG, MSG, etc	CALIBRATE THRUST STAND WITH KNOWN LOADS.
B	-	-	Test Team, Date, AROD number and Configuration (ignition source, etc, etc???)	Prestart. See note (A)
1	0-100% by 10% increments	REMOVED	TS, rpm, T, TSG, M, MSG, Pa, Ta, event number	Warm-up, basic cal. First run up to full power to define 100%, note rpm. and TS, divide into increments. Post: Plot TS and rpm vs. T and decide if any non-linearities exist. If linear, use similar TS's for all events. (1)
2	0-100% by 10%	0/0/0/0	as above + VS, VP	Vanes on warm-up and cal.
3	100%	Vary all in same direction and magnitude	Same as event 2	Attempt to find max thrust vane position--swirl effect. The position for max thrust will be called VPMT
4	100% ON LY	2,3,4: VPMT; 1: VPMT to VPMT+ max available throw in Positive direction, in approximately 5 degree increments <i>for each TS</i> . Repeat in NEGATIVE direction.	As above + distance from center of vane to x-axis of AROD.	To quantify Single vane control power NOTE: discontinue when vane stalls (i.e. thrust falls off)

5	100% ONLY	1/3: VPMT; 2/4: VPMT to VPMT+ max available throw in Positive direction, in approximately 5 degree increments <i>for each TS</i> . Repeat in NEGATIVE direction.	"	Double vane control power: vanes deflected so as to both cause rolling moment in same direction. NOTE: discontinue when vane stalls (i.e. thrust falls off)
6	100% 50% 75%, in that order	Repeat event 5 using all four vanes, AT THREE DIFFERENT THRUST SETTINGS.	"	Total vane control power. NOTE: discontinue when vane stalls (i.e. thrust falls off)
7	100%, chop to 75%	VPMT	rpm initial, rpm final, T initial and final, TS initial and final, TIME between rpm initial and final.	Attempt to characterize thrust response during engine deceleration. Qualitatively determine if the spool down sounds linear.
8	75% max rate power application to 100%	VPMT	"	Attempt to characterize thrust response during engine acceleration. Qualitatively determine if the spool up sounds linear.

NOTES: (A) Prior to start up check all AROD and thrust stand components for security. Ensure fire extinguisher is available. Brief test team on: Noise, FOD, and prop arc hazards.

(1) Initially computer input value for throttle setting (TS) will be used to increment engine power. Following initial runs a decision will be made concerning linearity of TS vs. T (Thrust). If feasible, TS will be used for follow-on events.

(2) Abbreviations:

TS: Computer input Throttle Setting

rpm: Revolutions per minute

T: Thrust reading in LB read directly from scale.

TSG: Thrust Scale geometry, i.e. Moment arm, slider location sufficient to calculate actual thrust.

M: Rolling moment reading in lb read directly from Moment scale.

MSG: Moment Scale geometry, i.e. Moment arm, slider location sufficient to calculate actual Moment.

Pa: Ambient pressure

Ta: Ambient temperature

VS: Vane positions for each vane as input from computer.

TABLE A.2
AROD ENGINE TESTS: 4/16/93

Purpose of Test	Run # (note 1)	Event # (2)	Conditions (note 3)	TS	RPM	T, M	Moment ft-lbf	VS	VP1-A, deg
1 Thrust check	117	New	Mufflers On	M	7595	116.0	Gauge stop		15/6/7/15
2 Mufflers on vs.	118	New	Mufflers On	M	5000		Gauge stop		
3 mufflers off.	119	New	Mufflers Off	M	7595	123.0	Gauge stop		
4	121	New	Mufflers Off	H	7595	123.0	Gauge stop		
5	122	New	Mufflers Off	H	3191	25.0	Gauge stop		4/4/5/4
6 Baseline Thrust	11	2	Mufflers Off	K	3000	21.0	Gauge stop	106	0/0/0/0
7 with Vases On	12	2	Mufflers Off	K	4000	28.0	Gauge stop	106	0/0/0/0
8 and CP VP	13	2	Mufflers Off	K	5000	47.0	Gauge stop	106	0/0/0/0
9 command	14	2	Mufflers Off	K	6000	84.0	Gauge stop	106	0/0/0/0
10	15	2	Mufflers Off	K	6369	90.0	Gauge stop	106	5/0/4/2
11	16	2	Mufflers Off	K	6367	100.0	Gauge stop	106	5/0/4/2
12	17	2	Mufflers Off	K	7143	106.0	Gauge stop	106	5/0/4/2
13	18	2	Mufflers Off	K	7317	115.0	Gauge stop	106	5/0/4/2
14	19	2	Mufflers Off	K	7538	119.0	Gauge stop	106	5/0/4/2
15	20	2	Mufflers Off	K	7595	120.0	Gauge stop	106	5/0/4/2
16 All Vase Control	45	6	Mufflers Off	K	7595	117.0	Gauge stop	106	4/-1/10/10
17 Power (test)	49	6	Mufflers Off	K	7595	117.0	Gauge stop	106	11/7/12/15
18 constant group	50	6	Mufflers Off	K	7595	116.0	Gauge stop	106	17/15/17/20
19 break-up it	51	6	Mufflers Off	K	7595	112.0	Gauge stop	89	20/19/20/25
20 turned into on	52	6	Mufflers Off	K	7595	108.0	Gauge stop	83	25/28/25/30
21 attempt to change	53	6	Mufflers Off	K	7595	106.5	Gauge stop	78	28/28/29/28
22 scenario thrust	54	6	Mufflers Off	K	7595	104.0	Gauge stop	72	30/30/30/31
23 change with	55	6	Mufflers Off	K	7595	118.5	Gauge stop	111	-3/-6/-3/-5
24 vane calibration	56	6	Mufflers Off	K	7595	116.0	Gauge stop	117	-10/-14/-10/-11
25 and also vane	57	6	Mufflers Off	K	7595	116.0	Gauge stop	123	-16/-20/-17/-17
26 (baseline)	58	6	Mufflers Off	K	7595	112.5	Gauge stop	129	-21/-25/-24/-24
27	59	6	Mufflers Off	K	7595	111.0	Gauge stop	134	-25/-30/-30/-26
28	60	6	Mufflers Off	K	7595	104.5	Gauge stop	140	-30/-35/-34/-31
29 Thrust with	1	1	Mufflers Off	M	3190	21.0	Gauge stop		
30 vane off.	2	1	Mufflers Off	M	3490	28.0	Gauge stop		
31 (Bussings effect)	3	1	Mufflers Off	M	4725	46.0	Gauge stop		
32	4	1	Mufflers Off	M	6125	78.0	Gauge stop		
33	123	1	Mufflers Off	M	63	4915	Gauge stop		
34	124	1	Mufflers Off	M	63	4915	Gauge stop		
35	125	1	Mufflers Off	M	66	4777	Gauge stop		
36	126	1	Mufflers Off	M	73	5217	Gauge stop		
37	5	1	Mufflers Off	M	78	5714	Gauge stop		
38	6	1	Mufflers Off	M	8422	96.0	Gauge stop		
39	7	1	Mufflers Off	M	100	107.0	Gauge stop		
40	8	1	Mufflers Off	M	110	114.0	Gauge stop		
41	9	1	Mufflers Off	M	120	119.0	Gauge stop		
42					130	120.0	Gauge stop		

NOTES:
41 (1) Chronological order
42 (2) See April 93 test matrix
43 (3) Temp day F and Press at Hg
44 "H": 5600.14
45 "K": 6090.10
46 "M": 5800.10
47 "W": 5800.10
48 -AROD coming external power
49 supply, external 1 quart
50 fuel tank, mufflers off.
51 -Computer control of vane and
52 throttle.
53 -AROD name Auto

TABLE A.3
AROD ENGINE TESTS: 4/27/93

Purpose of Test	Run # (note 1)	Event # (2)	Temp/Press (3)	RPM	T, Bt	M, Bt (5)	Vane #1	Vane #2	Vane #3	Vane #4	NOTES
1 DOUBLE VANE	35	5	59/30.09	7540	120.0	-8	0	2	0	0	5 (1) Shown in chronological order.
2 CONTROL POWER	36	5	59/30.09	7540	125.0	-5	0	6	0	0	10 error.
3	37	5	59/30.09	7540	121.0	-3	0	14	0	0	15 (2) From April 93 test matrix
4	38	5	58/30.08	7540	120.5	-2	0	17	0	0	20 (3) Temperature in deg F
5	39	5	59/30.09	7540	119.0	0	0	21	0	0	25 Pressure in "Hg (KMH)
6	40	5	59/30.09	7540	119.0	0	0	25	0	0	25 (4) See figure XX
7	41	5	59/30.09	7540	118.5	5	0	30	0	0	30 (5) This is the last read at
8	42	5	59/30.09	7540	124.0	-11	0	-5	0	0	5 lbs gauge. To correct to
9	43	5	59/30.09	7540	121.5	-15	0	-10	0	0	-10 moment in H-b, multiply
10	44	5	59/30.09	7540	121.0	-20	0	-16	0	0	-18 by 9/12.
11	45	5	59/30.09	7540	121.0	-22	0	-21	0	0	-20
12	46	5	59/30.09	7540	119.0	-22	0	-25	0	0	-24 GENERAL NOTES:
13	47	5	59/30.09	7540	118.5	-29	0	-30	0	0	-30 -Date: 27 Apr 93
14 ALL VANE	48	6	60/30.09	7520	119.5	-7	5	8	5	10	5 -Test Team: Sunny/Melissa
15 CONTROL POWER	49	6	60/30.09	7520	119.0	0	10	9	10	10	10 -AROD engine: external power
16 WITH 100% THROTTLE	50	6	60/30.09	7520	115.0	3	15	17	15	15	20 fuel tank, mufflers off
17	51	6	60/30.09	7520	113.0	9	21	20	20	20	25 -Vane and throttle control
18	52	6	60/30.09	7520	113.0	10	25	25	25	25	30 vs Fuel/RAC set
19	53	6	60/30.09	7520	112.0	20	30	30	30	30	30 -AROD name: Aroce
20	54	6	60/30.09	7520	123.0	-10	-5	-5	-5	-5	-5
21	55	6	60/30.09	7520	121.0	-17	-11	-10	-10	-10	-10
22	56	6	60/30.09	7520	119.0	-25	-15	-15	-17	-14	-14
23	57	6	60/30.09	7520	117.5	-32	-20	-20	-20	-20	-20
24	58	6	60/30.09	7520	113.0	-35	-25	-25	-25	-25	-25
25	59	6	60/30.09	7520	111.0	-30	-30	-30	-32	-30	-30
26	60	6	60/30.09	6590	89.0	-5	0	0	0	4	4
27 ALL VANE	61	4	60/30.09	6590	89.0	-2	5	6	5	10	10
28 CONTROL POWER	62	4	60/30.09	6590	89.0	0	10	11	10	15	15
29 WITH REDUCED THROTTLE	63	4	60/30.09	6590	89.0	5	14	16	15	15	15
30	64	4	60/30.09	6590	86.0	7	20	20	20	20	20
31 (-75% THRUST)	65	4	60/30.09	6590	86.0	11	25	24	25	25	25
32	66	4	60/30.09	6590	83.0	16	30	28	27	30	30
33	67	4	60/30.09	6590	90.0	-10	-3	-3	0	-2	-2
34	68	4	60/30.09	6590	89.0	-15	-8	-10	-5	-10	-10
35	69	4	60/30.09	6590	89.0	-20	-16	-17	-15	-15	-15
36	70	4	60/30.09	6590	86.0	-25	-20	-22	-20	-20	-20
37	71	4	60/30.09	6590	84.0	-25	-26	-26	-25	-25	-25
38	72	4	60/30.09	6590	82.0	-25	-30	-30	-30	-30	-30
39	73	4	60/30.09	6590	112.0	-6	0	0	0	5	5
40 ALL VANE	74	4	61/30.09	7240	111.5	-5	5	6	5	10	10
41 CONTROL POWER	75	4	61/30.09	7240	109.0	1	10	12	10	15	15
42 WITH REDUCED THROTTLE	76	4	61/30.09	7240	107.5	4	15	16	15	15	15
43	77	4	61/30.09	7240	107.0	10	21	20	20	20	20
44 (-50% THRUST)	78	4	61/30.09	7240	104.0	13	25	25	25	30	30
45	79	4	61/30.09	7240	102.0	17	30	30	30	30	30
46	80	4	61/30.09	7240	112.0	-8	-3	-3	0	0	0
47	81	4	61/30.09	7240	111.0	-17	-11	-10	-10	-10	-10
48	82	4	61/30.09	7240	108.0	-23	-15	-16	-15	-15	-15
49	83	4	61/30.09	7240	105.0	-26	-20	-20	-20	-20	-20
50	84	4	61/30.09	7240	104.0	-31	-24	-25	-25	-25	-25
51	85	4	61/30.09	7240	102.0	-37	-30	-30	-30	-30	-30
52	86	4	61/30.09	7240	102.0	-37	-30	-30	-30	-30	-30

TABLE A.4
COMMERCIALLY AVAILABLE ALUMINUM TUBE CONFIGURATIONS
AND STRUCTURAL ANALYSIS SPREADSHEET

Force applied= length of boom	8.5 5g	Note: if changed, show change in Von Mises Yield Stress formula		Note: if changed, show change in Von Mises Yield Stress formula				
Configuration	Material	Outer Diameter(OD)	Wall thickness (t)	Mean radius	Von Mises Yield Stress (psi)	Below Yield?	Density (lbm-in ³)	Weight (lb-ft)
1	2024-T3	1.51	0.049	0.7255	61894.22811	No	0.11	0.2680
2	2024-T3	1.51	0.065	0.7175	47704.99967	No	0.11	0.3516
3	2024-T3	1.51	0.25	0.625	16346.35857	Yes	0.11	1.1781
4	2024-T3	1.75	0.25	0.75	11351.6379	Yes	0.11	1.4137
5	2024-T3	1.875	0.065	0.905	29985.44854	Yes	0.11	0.4435
6	2024-T3	2	0.049	0.975	34235.00827	Yes	0.11	0.3604
7	2024-T3	2	0.065	0.9675	26236.49155	Yes	0.11	0.4742
8	2024-T3	2.5	0.065	1.2175	16567.98788	Yes	0.11	0.5967
9	6061-T6	1.51	0.035	0.7325	85003.68676	No	0.098	0.1894
10	6061-T6	1.51	0.049	0.7225	61894.2281	No	0.098	0.2627
11	6061-T6	1.51	0.058	0.721	52944.70608	No	0.098	0.3090
12	6061-T6	1.51	0.065	0.7175	47704.99967	No	0.098	0.3446
13	6061-T6	1.51	0.125	0.6875	27018.7745	Yes	0.098	0.6350
14	6061-T6	1.625	0.058	0.7835	44834.78273	No	0.098	0.3358
15	6061-T6	1.75	0.035	0.8575	62027.56934	No	0.098	0.2218
16	6061-T6	1.75	0.049	0.8505	45037.71504	No	0.098	0.3079
17	6061-T6	1.75	0.058	0.846	38434.95832	No	0.098	0.3626
18	6061-T6	1.875	0.058	0.9085	33345.95859	Yes	0.098	0.3893
19	6061-T6	2	0.049	0.975	34235.00827	Yes	0.098	0.3532
20	6061-T6	2	0.058	0.971	29191.37898	Yes	0.098	0.4161
21	6061-T6	2.125	0.035	1.045	41765.78489	No	0.098	0.2703
22	6061-T6	2.25	0.049	1.1005	26899.54232	Yes	0.098	0.3984
23	6061-T6	2.25	0.083	1.0835	16382.68727	Yes	0.098	0.6645
24	6061-T6	2.25	0.125	1.0625	11312.35887	Yes	0.098	0.9814
25	6061-T6	2.5	0.035	1.2325	30024.73372	Yes	0.098	0.3187
26	6061-T6	2.5	0.049	1.225	21891.93795	Yes	0.098	0.4437
27	6061-T6	2.5	0.065	1.2175	16567.98788	Yes	0.098	0.5847
28	6061-T6	3	0.035	1.4825	20752.17477	Yes	0.098	0.3834
29	6061-T6	3	0.065	1.4675	11403.84979	Yes	0.098	0.7048
30	6061-T6	4	0.035	1.9825	11604.50522	Yes	0.098	0.5127
31	6061-T6	4	0.049	1.975	8347.778493	Yes	0.098	0.7153

For graphic depiction of results, see the following figures:
"Strength Comparison" and
"Weight Comparison"

For graphic depiction of results, see the following figures:

"Strength Comparison" and
"Weight Comparison"

APPENDIX B: PHOTOGRAPHS OF FABRICATION AND TEST

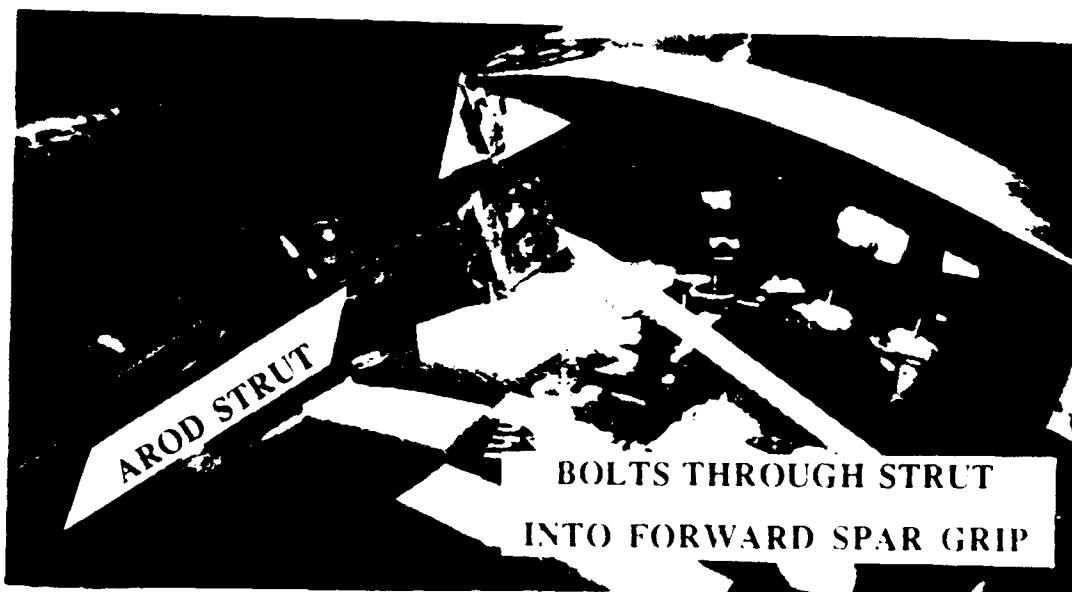


Figure B.1: Archytas construction detail: through-strut bolts

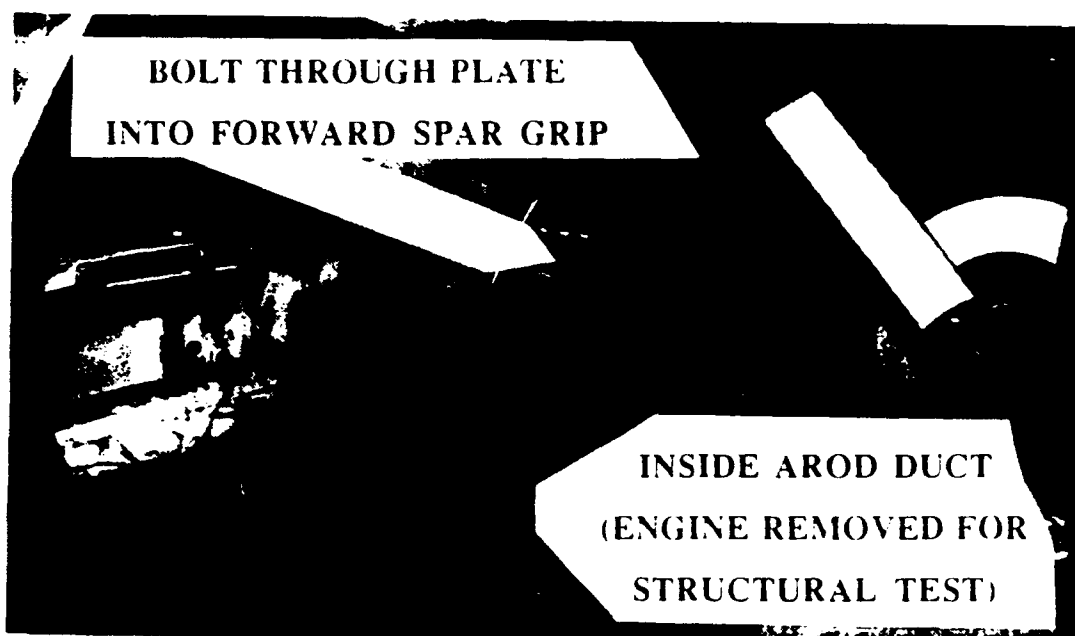


Figure B.2: Archytas construction detail: plate on inside of duct

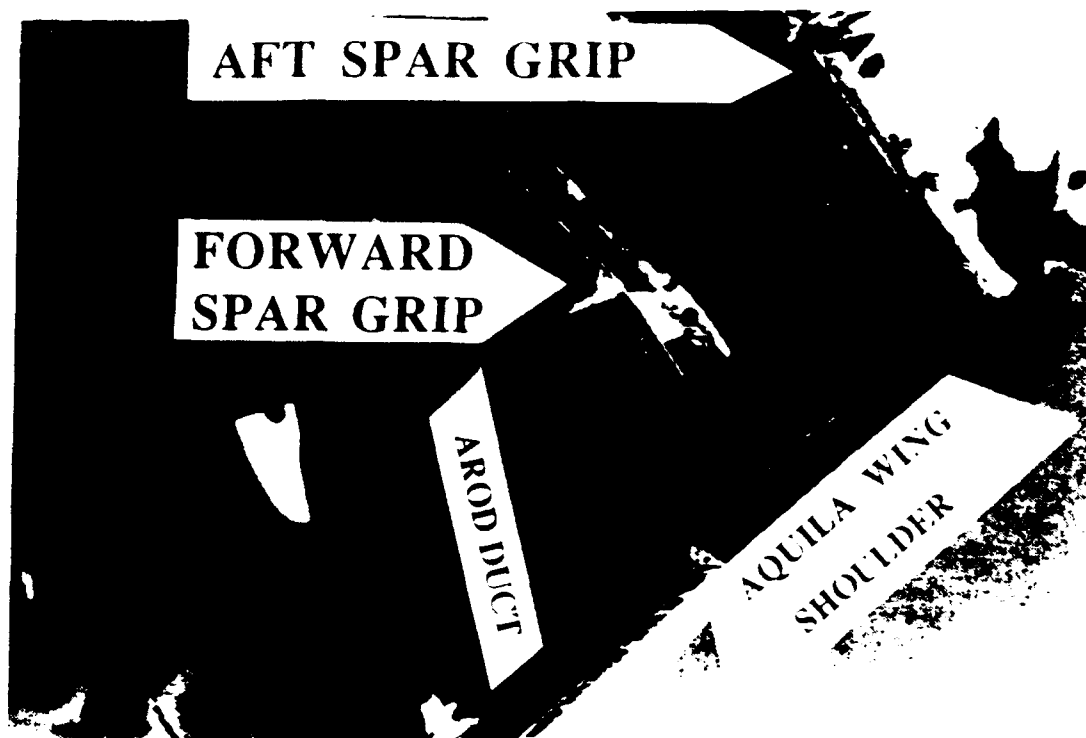


Figure B.3: Archytas construction detail: spar grip plates

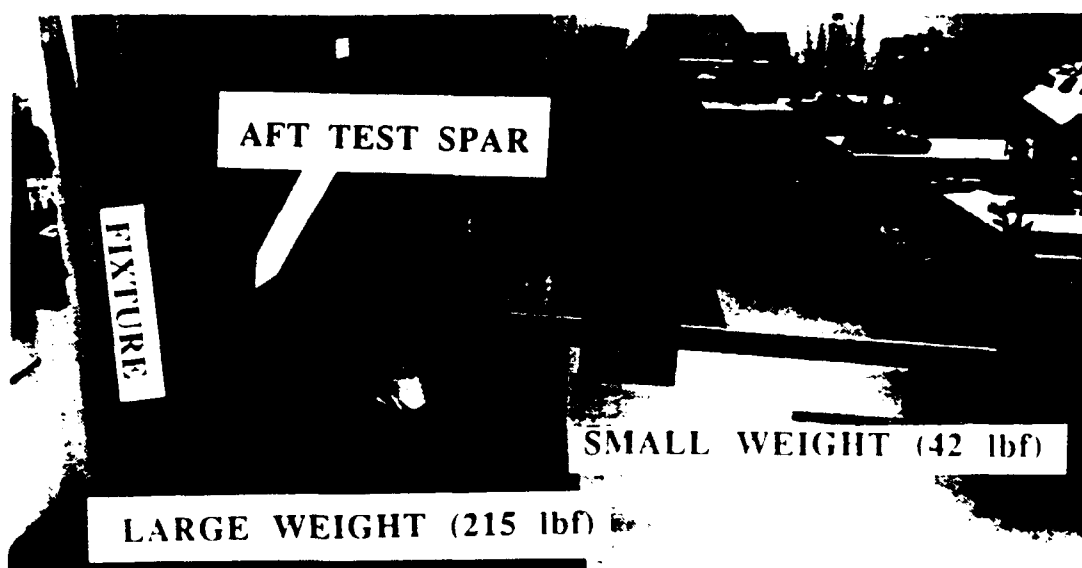


Figure B.4: Archytas structural test: individual spar



Figure B.5

Archytas structural test results: Aft spar failure



Figure 3. Boom base test specimen.

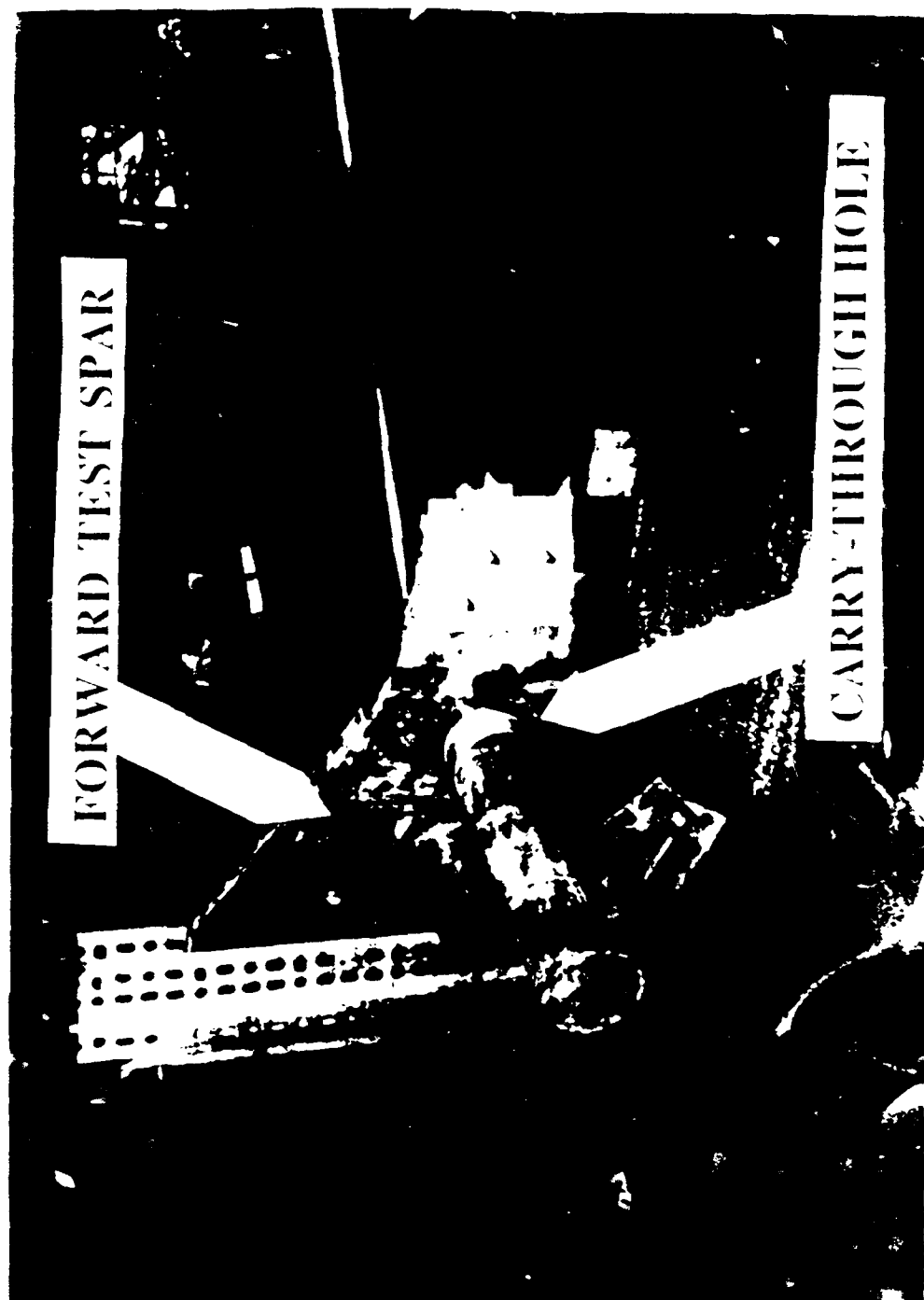


Fig. 1. Ship's hull structure with test spar and carry-through hole.

```

C PROGRAM "CAMBER", MODIFIED FROM PROGRAM OF SAME NAME AS USED IN AE3501
C THIS VERSION INCLUDES THE DERIVATIVE OF THE AQUILA UAV'S MEAN CAMBER
C LINE. NOTE: THIS IS FOR THE UNTWISTED AIRFOIL. THE ACTUAL AIRFOIL
C HAS THREE DEGREES OF GEOMETRIC TWIST AS SPECIFIED IN AD-A068 (REPORT
C ON AQUILA).

```

```

C LDR R.B. STONEY      NPS      WRITTEN: DEC 1992
C

```

```

*****
* THIS PROGRAM ALLOWS YOU TO INPUT THE CONTROL POINTS OF THE VORTEX PANELS
* AND FIND THE RESULTING AOA'S FOR A GIVEN CAMBER DISTRIBUTION. THIS FILE
* MAY BE EASILY MODIFIED FOR DIFFERENT DISTRIBUTION EQUATIONS.
*****

```

```

PROGRAM CAMBER
REAL Y(120),XC(120),ZC(120),DZC(120),ALP(120),XQ(120),XTO(120)
OPEN (UNIT=20,FILE='CAMBER.IN',STATUS='UNKNOWN')
OPEN (UNIT=21,FILE='CAMBER.OUT',STATUS='UNKNOWN')
PRINT *, 'INPUT THE NUMBER OF CONTROL POINTS ON PLANFORM:'
PRINT *, '(CHORDWISE TIMES SPANWISE STATIONS)'
READ *, N
PRINT *, 'INPUT THE Y-COORDINATE OF THE WING ROOT'
PRINT *, '0.0 IF PLANFORM IS WING ONLY:'
READ *, YCORD
DO I=1,N
  READ(20,*) XQ(I),XTO(I),Y(I)
  IF(Y(I) .LT. YCORD) THEN
    NDATA = I
  END IF
  PRINT *, Y(I),YCORD,NDATA,N
END DO
CORD = 0.0
NPANEL = 0
NSTART = 1
DO 10 I=1,NDATA
  CORD = CORD + 2*ABS(XTO(I)-XQ(I))
  PRINT*, I,CORD,Y(I+1),Y(I)
  NPANEL = NPANEL + 1
  IF(Y(I+1).EQ. Y(I)) GOTO 10
  XLE=XQ(NSTART)-(XTO(NSTART)-XQ(NSTART))/2.0
  DO J=NSTART,NSTART+NPANEL-1
    PRINT*, J,NSTART,NPANEL,CORD
    XC(J) = ABS((XTO(J)-XLE))/CORD
    C *****AQUILA AIRFOIL*****
    IF(XC(J) .LE. .3) THEN
      DZC(J)= 1.1372-32.154*XC(J)+332.91*XC(J)**2
      + -1445.0*XC(J)**3+2190.35*XC(J)**4
      ALP(J)= ATAN(DZC(J))
    ELSE
      DZC(J)= 0.25532-1.63078*XC(J)+2.75505*XC(J)**2
      + -1.41616*XC(J)**3
      ALP(J)= ATAN(DZC(J))
    END IF
  END DO
  NSTART=J
  NPANEL = 0
  CORD = 0.0
10  CONTINUE
  DO I = NDATA+1,N
    ALP(I) = 0.0
  END DO
C REMEMBER THE SLOPE = -AOA
  WRITE(21,20) (-ALP(I),I=1,N)
20  FORMAT(8F10.4)
END

```

1.0	1.0	32.22	4215.6				
3.0	0.0	0.0	0.0				
0.0	0.0	0.0	0.0				
-36.69	-67.0	0.0	0.0				
-59.69	-67.0	0.0	0.0				
-39.92	0.0						
1	10.0	11.0	0.0	1.0			
0.0579	-0.0156	0.0533	0.0434	0.0494	0.0407	0.0257	0.0130
0.0110	0.0282	-0.0527	-0.0104	0.0585	0.0486	0.0546	0.0459
0.0309	0.0182	0.0162	0.0334	-0.0474	-0.0051	0.0638	0.0539
0.0599	0.0512	0.0362	0.0235	0.0215	0.0387	-0.0422	0.0001
0.0690	0.0591	0.0651	0.0564	0.0414	0.0287	0.0267	0.0439
-0.0370	0.0053	0.0262	0.0643	0.0703	0.0616	0.0466	0.0339
0.0319	0.0491	-0.0317	0.0106	0.0795	0.0696	0.0756	0.0669
0.0519	0.0392	0.0372	0.0544	-0.0265	0.0156	0.0847	0.0748
0.0808	0.0721	0.0571	0.0444	0.0424	0.0596	-0.0213	0.0210
0.0899	0.0800	0.0860	0.0773	0.0623	0.0496	0.0476	0.0648
-0.0160	0.0263	0.0952	0.0853	0.0913	0.0826	0.0676	0.0549
0.0529	0.0701	-0.0108	0.0315	0.1004	0.0905	0.0965	0.0878
0.0728	0.0601	0.0581	0.0753				

```

%=====
%-----Program "xplot"-----
%=====
%
% Bob Stoney 3/24/93 Naval Postgraduate School
% A program to implement a survey of static longitudinal stability using
% formulas contained in Anderson's text, specifically eq'n 7.30 on pg 386
% This program analyzes a CANARD design, the Archytas UAV
% being developed at NPGS. The basic idea is to plot both the center
% of gravity and aerodynamic center versus canard CHORD (which is simply
% the canard AREA divided by it's span...in the archytas configuration
% the span is considered a constraint (to fit the canard between the "goalpost"
% canard booms). Where the lines cross is zero static longitudinal stability
% and to the left of the intersection is varying degrees of static margin.
% (items marked with "*****" are those that will be frequently changed by user)
% (items marked with @@@@@@ are those that are a vector)
% "FRL" is fuselage reference line, the leading edge of the mean aero chord
% (negative is forward), which is 9 inches aft of the top of the AROD duct.
% For the center of gravity portion, the following items' weights are accounted
% for: The AROD, the wings and hardware, the electronics, the canard boom, and
% the canard itself. See the end of the program listing for a definition of the
% weights.
clear
clc
hold off

%*****
%-----Solicit input from user for configuration:-----
%*****
disp('Input config (1=aft pod;2=forward pod)')
CONFIG=input(' ');

%*****
%-----Set up vector of Canard chords to calculate Xcg and Xac:-----
%*****
n=100; % number of increments of canard chord.
cc=linspace(.01,1.5,n); % Canard chord in feet @@@@

%*****
%-----AERODYNAMIC CENTER PORTION-----
%*****
% Uses equation 7.30 on pg 386 of Anderson's "Intro to Flight"
disp('Input the "Canardlocation"--the distance in inches from the duct to')
disp('canard c/4. REMEMBER: forward is negative....enter negative number')
ans1=input(' ');

```



```

        ac15=ac3d(i); % Cl alpha at 15% SM
        Sc15=Sc(i); % Canard area at 15% SM
        Cancd15=cc(i); % Canard chord at 15% SM
        Wcanard15=Wcanard(i); %the WT of the canard when SM=15% (put on plot)
        WTOTAL15=WTOTAL(i); % the total weight when SM=15% (put on plot)
    elseif abs(SM(i)-0.1)<=0.001, % to identify 10% static margin value
        SM10=SM(i); % The 10% static margin values
        Xacabar10=Xacabar(i); % "
        XcgTOTALbar10=XcgTOTALbar(i); % "
        cc10=cc(i)*12; % "
        plotflag10=1; % to enable polyline plot later
        ac10=ac3d(i); % Cl alpha at 10% SM
        Sc10=Sc(i); % Canard area at 10% SM
        Wcanard10=Wcanard(i); %the WT of the canard when SM=10% (put on plot)
        WTOTAL10=WTOTAL(i); % the total weight when SM=10% (put on plot)
    elseif abs(SM(i)-0.05)<=0.001, % to identify 5% static margin
        SM5=SM(i); % The 5% static margin values
        Xacabar5=Xacabar(i); % "
        XcgTOTALbar5=XcgTOTALbar(i); % "
        cc5=cc(i)*12; % " (converted to inches, like plot)
        plotflag5=1; % to enable polyline plot later
        ac5=ac3d(i); % Cl alpha at 5% SM
        Sc5=Sc(i); % Canard area at 5% SM
    end %if
end %for

%-----COMPARE CG AND AERO CENTER ON A PLOT-----
%-----
plot(cc*12,Xacabar,'-',cc*12,XcgTOTALbar,'-')
grid;xlabel('Canard chord, cc, in');
ylabel('Non-dimen CG and Neutral Point locations, h, hn, aft of MAC l.e.')
title('Canard Sizing Based on Static Longitudinal Stability')
if plotflag5==1,
    hold on
    X5=[cc5 cc5]; % for polyline function
    Y5=[Xacabar5 XcgTOTALbar5]; % "
    polyline(X5,Y5,'--') % draw 5% static margin line
    texty=(Xacabar5-XcgTOTALbar5)/2+XcgTOTALbar5;
    text(cc5,texty,'5% SM') % put label on 5% SM line
end %if
if plotflag10==1,
    hold on
    X10=[cc10 cc10]; % for polyline function
    Y10=[Xacabar10 XcgTOTALbar10]; % "
    polyline(X10,Y10,'--') % plot 10% static margin line
    texty=(Xacabar10-XcgTOTALbar10)/2+XcgTOTALbar10;
    text(cc10,texty,'10% SM') % put label on 10% SM line
end %if

```

```

if plotflag15==1,
    hold on
    X15=[cc15 cc15]; % for polyline function
    Y15=[Xacabar15 XcgTOTALbar15]; % "
    polyline(X15,Y15,'—') % plot 15% static margin line
    texty=(Xacabar15-XcgTOTALbar15)/2+XcgTOTALbar15;
    text(cc15,texty,'15% SM') % put label on 15% SM line
end %if

* Plotting "niceties":
text(cc(10)*12,Xacabar(10),'A/C Neutral Point')
text(cc(10)*12,XcgTOTALbar(10),'A/C Center of Gravity')

Ltop=sprintf('Ballast = %g',Wballast);text(.45,.9,Ltop,'sc')
L1=sprintf('Wing area = %g',S);text(.45,.87,L1,'sc')
L2=sprintf('Wing/body a = %g',awb);text(.45,.84,L2,'sc')
L3=sprintf('Can. ("from duct) = %g',Canardlocation*12);text(.45,.81,L3,'sc')
L4=sprintf('Xacwb = %g',Xacwb*12);text(.45,.78,L4,'sc')
L5=sprintf('Canard span = %g',bc*12);text(.45,.75,L5,'sc')
L6=sprintf('XcgAROD = %g',XcgAROD*12);text(.45,.72,L6,'sc')
L7=sprintf('XcgPOD = %g',XcgPOD*12);text(.45,.69,L7,'sc')
if plotflag15==1,
    L8=sprintf('Xacabar(.15SM) = %g',Xacabar15);text(.45,.66,L8,'sc')
    L9=sprintf('CG (in) (.15SM) = %g',XcgTOTALbar15*cbar*12);
        text(.45,.63,L9,'sc')
elseif plotflag10==1,
    L8=sprintf('Xacabar(.10SM) = %g',Xacabar10);text(.45,.66,L8,'sc')
end

Rtop=sprintf('Config: %g',CONFIG);text(.7,.90,Rtop,'sc')
R1=sprintf('Warod = %g',Warod);text(.7,.87,R1,'sc')
R2=sprintf('Wfuel = %g',Wfuel);text(.7,.84,R2,'sc')
R3=sprintf('Wpod = %g',Wpod);text(.7,.81,R3,'sc')
R4=sprintf('Wwings = %g',Wwings);text(.7,.78,R4,'sc')
R5=sprintf('Wbooms = %g',Wbooms);text(.7,.75,R5,'sc')
if plotflag15==1,
    R6=sprintf('Wcanard(.15SM) = %g',Wcanard15);text(.7,.72,R6,'sc')
    R7=sprintf('Wtotal(.15SM) = %g',WTOTAL15);text(.7,.69,R7,'sc')
    R8=sprintf('cc(.15SM) = %g',cc15);text(.7,.66,R8,'sc')
elseif plotflag10==1,
    R6=sprintf('Wcanard(.1SM) = %g',Wcanard10);text(.7,.72,R6,'sc')
    R7=sprintf('Wtotal(.1SM) = %g',WTOTAL10);text(.7,.69,R7,'sc')
end
if plotflag10==1,
    R9=sprintf('cc(.10SM) = %g',cc10);text(.7,.63,R9,'sc')
end

```



```

% POD WEIGHT includes (4/4/93):
% • Frame (that holds circuit cards); skin (4" ring, 8" ring, 8" cap)
% • Electronics: 3 ~7" cards (fiber optic card removed); 1 MHz DC-DC converter;
% 6 black power supplies in tray; complete gyro/acclerometer package
% • Board that smooths generator output (the one with the big
% orange capacitor).
% • For forward mounting includes bullet supports (4), front cap (with fan and
% other electronics.
% WEIGHT: Aft mount: 10 lb      Forward mount: 11.72 lb
% Local CG: is 5 inches aft of forward lip of gyro section skin.
% See also: Figure entitled "Electronics pod dimensions--Forward pod config"
% (A MacDraw document)

```

```

% WINGS weight includes (2/7/93):
% • RH Aquila wing w/o hardware, RH shoulder; RH tip

% • Forward test spar, with 4 plates for holding end and 2 plates for
% attaching to shoulder's spar, plus 8 bolts to put it all together.
% • Aft test spar, with aft grips (grip weight estimated).
% TOTAL weight of two wings with associated components: 23.2 lb

```

```

=====
%-----END Program "xplot"-----
=====

```


APPENDIX E

ASSUMPTIONS USED IN SIMULATION PROGRAM

A. GENERAL

This appendix contains many of the assumptions made during formulation of the AWA-series 3 DOF simulation programs. The format of this appendix is informal, stating the assumption, its location in the program, justifying information and, in some cases, suggestions for further refining the assumption. The order of the assumptions roughly follows the order reached in the program AWA1.

B. ASSUMPTIONS

(1) ASSUMPTION: Wing area= 29.2 ft^2

LOCATION: archytas3 function

JUSTIFICATION: From vortex lattice, Aquila documentation and actual measurement of the wing.

SUGGESTIONS FOR REFINEMENT: The duct will certainly add to the effective wing area--ducts are well known for their capability to provide lift. A study of duct aero might provide a better estimate for S.

(2) ASSUMPTION: $C_{do}=.06$

LOCATION: archytas function

JUSTIFICATION: Prof Howard's estimate.

SUGGESTIONS FOR REFINEMENT: Should account for fan, shroud, etc. Wind tunnel test

(3) ASSUMPTION: $I_{yy}=7.4 \text{ slugs-ft}^2$

LOCATION: archytas function

JUSTIFICATION: Aquila's was 10.4 according to ref 8. Reduced it 25% for lighter archytas

SUGGESTIONS FOR REFINEMENT: calculate using swing/time period method

(4) ASSUMPTION: $C_{mq}=-1.47$

LOCATION: archytas function, used in control function for pitch damping

JUSTIFICATION: This is Aquilas C_{mq} , as per Aquila documentation.

SUGGESTIONS FOR REFINEMENT: Vortex lattice program, using canard and shroud.

(5) ASSUMPTION: Canard and vane deflections are step inputs, no oscillations, no time constant.

LOCATION: user input

JUSTIFICATION: probably not true. Depends on servos.

SUGGESTIONS FOR REFINEMENT: once flight quality servos are obtained they could be tested under load to determine fidelity and time constant. May need to be modeled as a noise vector in the state equations. Note: LCDR Moran and CAPT Kuechenmeister have modeled the servo response for their thesis work.

(6) ASSUMPTION: Sea level, standard day density

LOCATION: main program

JUSTIFICATION: simple, probably good for Monterey operations.

SUGGESTIONS FOR REFINEMENT: could modify program for temp affects

(7) ASSUMPTION: Aircraft coefficient of lift beyond stall as per profile discussed in Section VI.

LOCATION: main program, after "Ydot vector initialization" block and again in iteration.

JUSTIFICATION:

SUGGESTIONS FOR REFINEMENT: I could find no high alpha information during my literature search for similar low sweep angle configurations. Wind tunnel tests would further refine this or a more thorough lit search.

(8) ASSUMPTION: Drag model at high alpha is an assumed profile.

LOCATION: main program

JUSTIFICATION: Drag varying as the square of α matches well with the pre-stall region and seemed reasonable for the post stall region (i.e. drag kept going up, quickly, past stall).

SUGGESTIONS FOR REFINEMENT: Wind tunnel/lit search/CFD. Account for entire vehicle.

(9) ASSUMPTION: Canard pitch authority is simply based on a C_l vs α (using overall vehicle α and an extrapolated NACA 0009 airfoil times dynamic pressure (same as vehicle's) times distance to c.g.

LOCATION: control function

JUSTIFICATION: Good first approximation. No downwash to wing from canard is probably a good approximation in that the duct may ingest the wake of the canard.

SUGGESTIONS FOR REFINEMENT: Modify airfoil characteristics once configuration is known. Wind tunnel force measurement for C_l vs. α and flow visualization for canard--wing downwash (and flow energization) effects. Lit search?

(10) ASSUMPTION: No contribution to pitching moment from $\dot{\alpha}$ or \dot{q}

LOCATION: control function

JUSTIFICATION: neglected. Is often neglected in conventionally configured aircraft where the effect would be more expected (i.e.

time lag of downwash transport) so I neglected it here, feeling that the canard's contribution to downwash over the wing would be small.

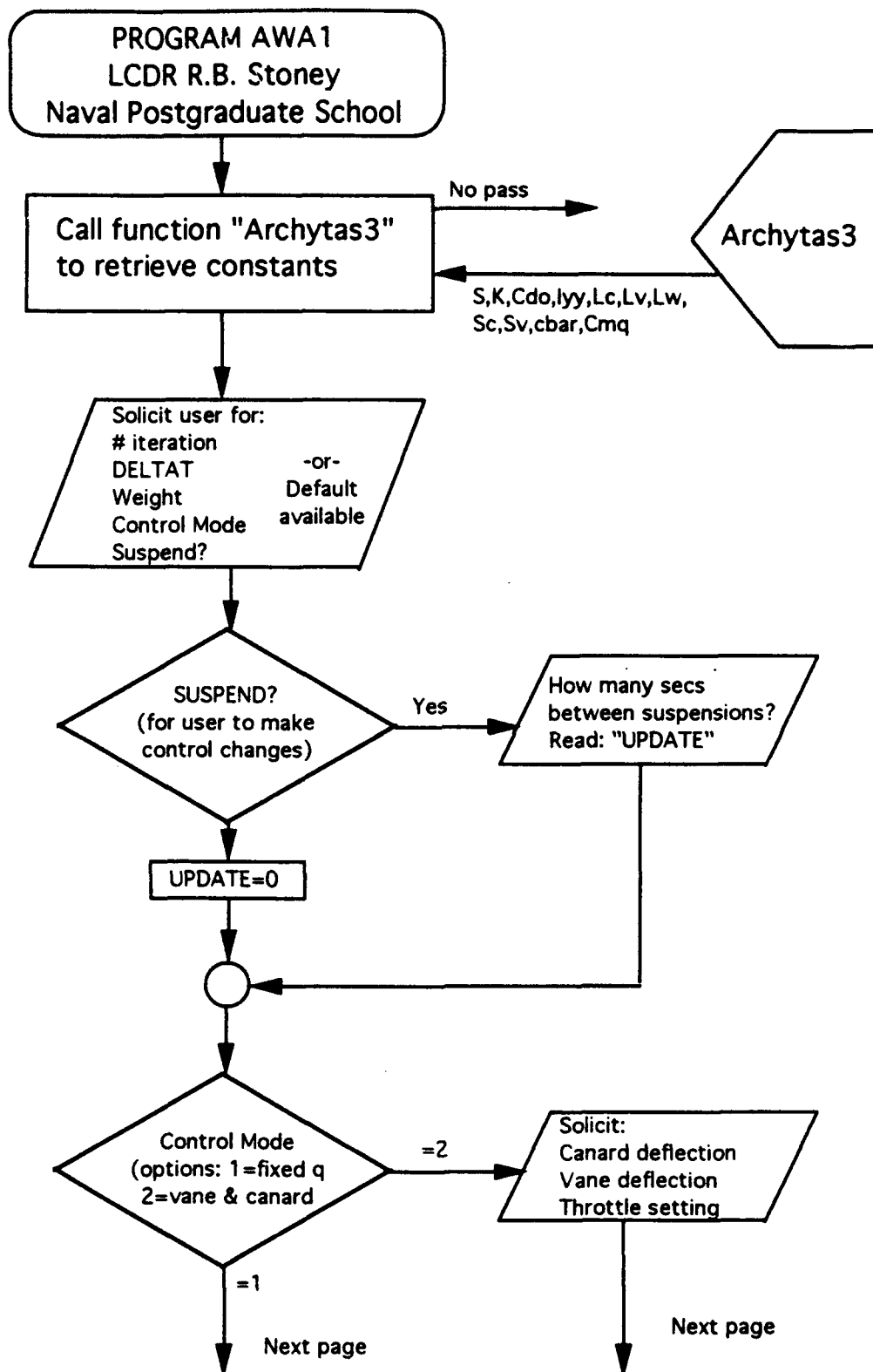
SUGGESTIONS FOR REFINEMENT:

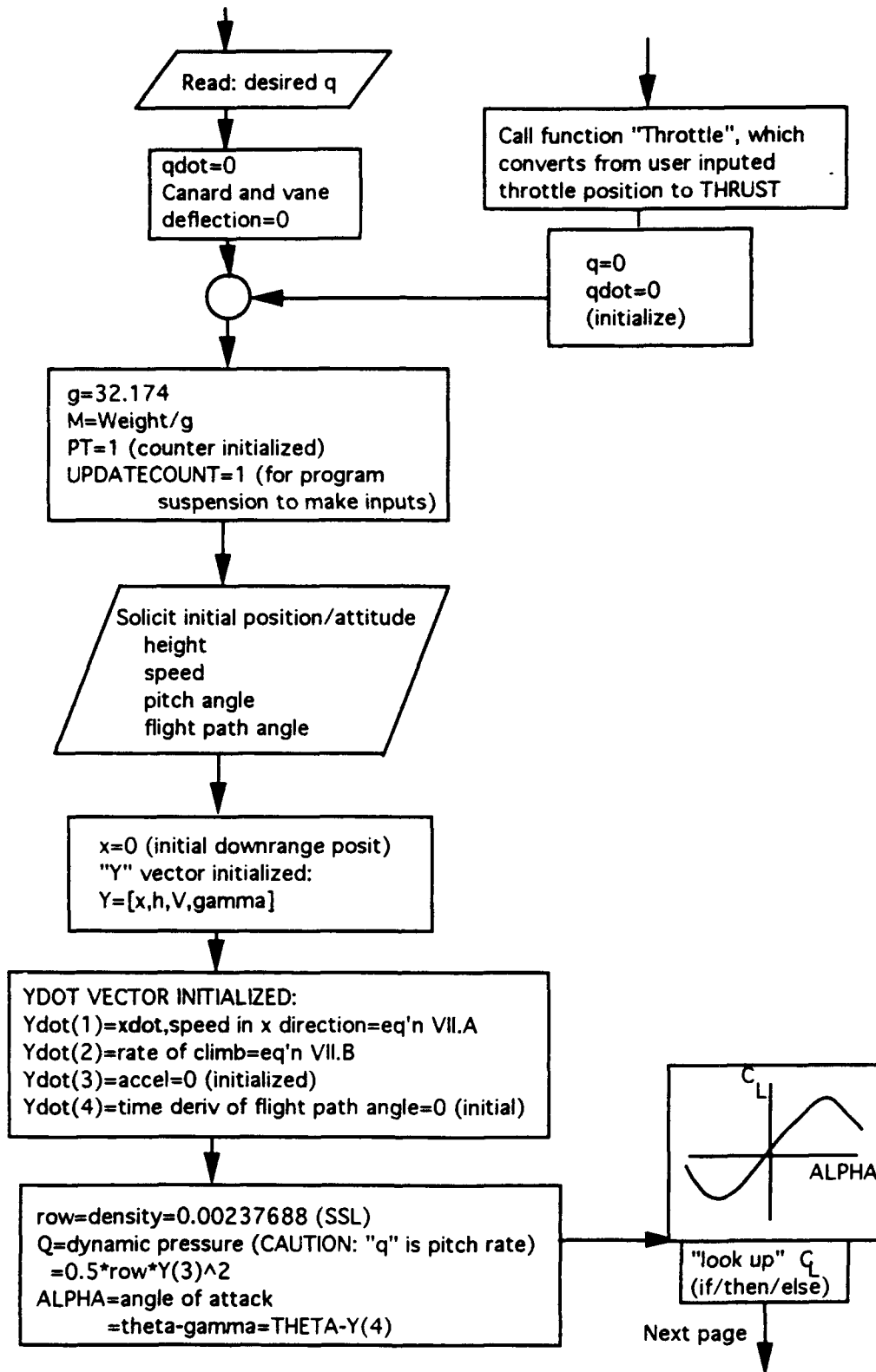
(11) ASSUMPTION: Gyroscopic effects not considered

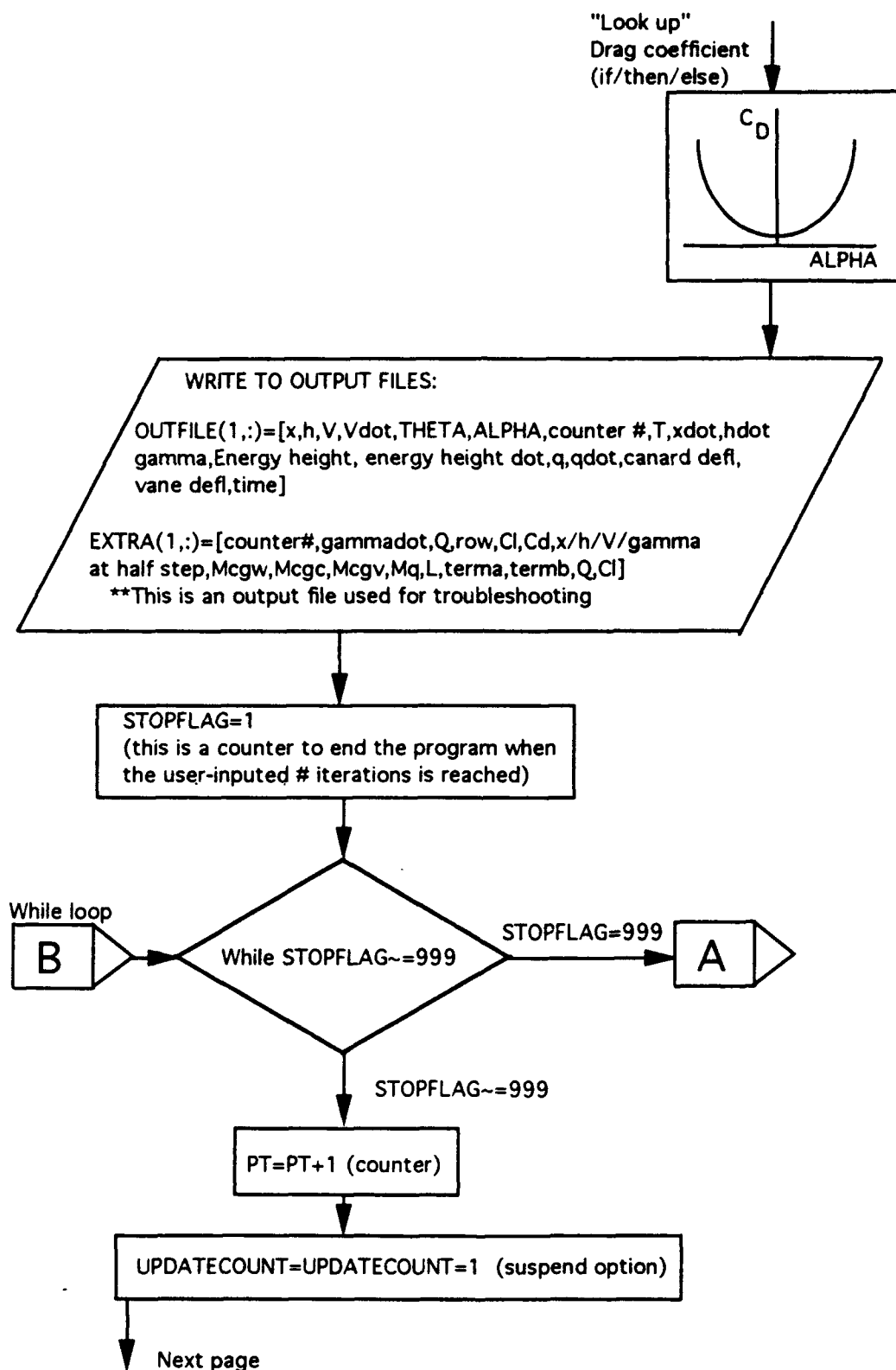
LOCATION:

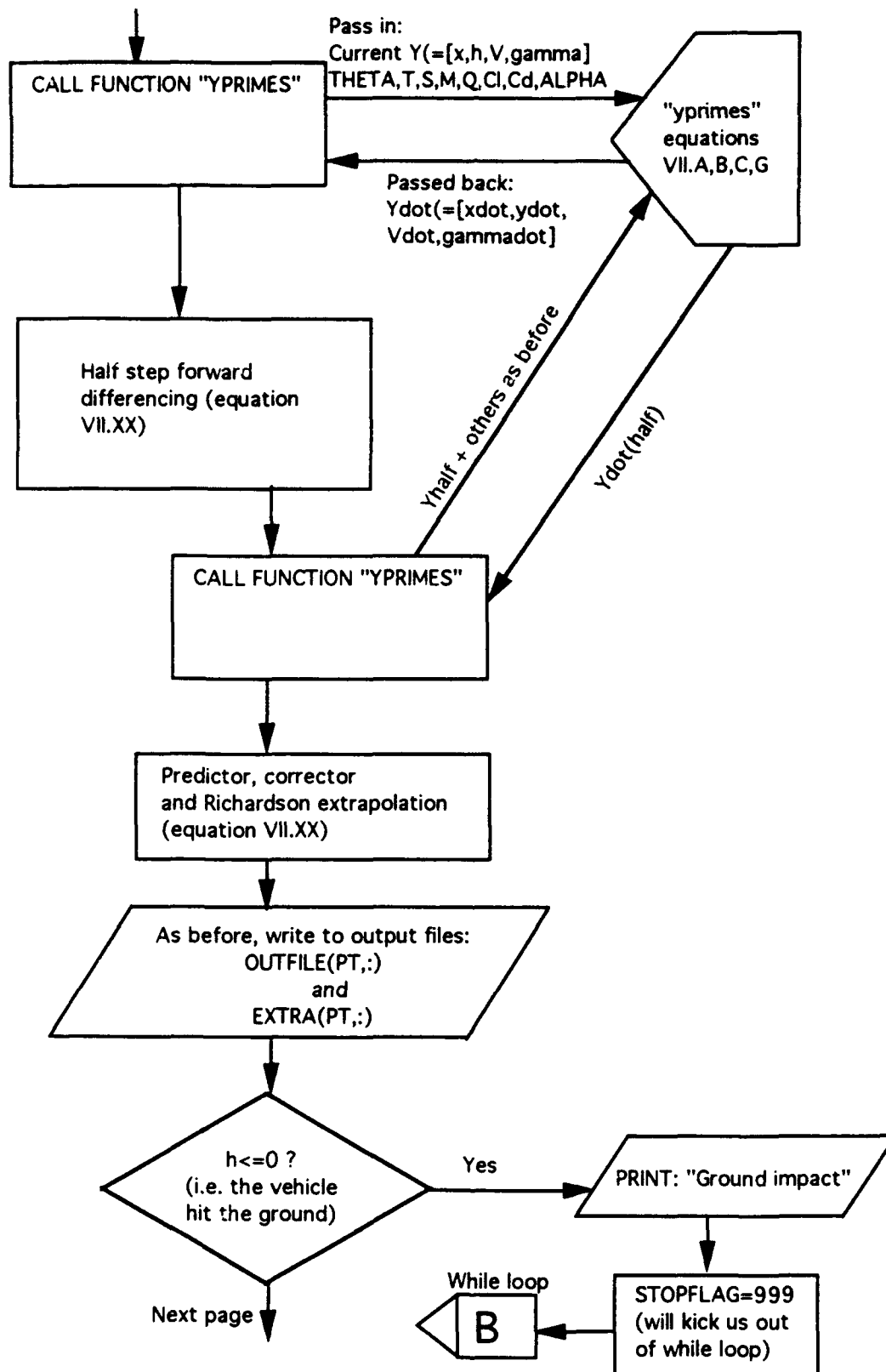
JUSTIFICATION:

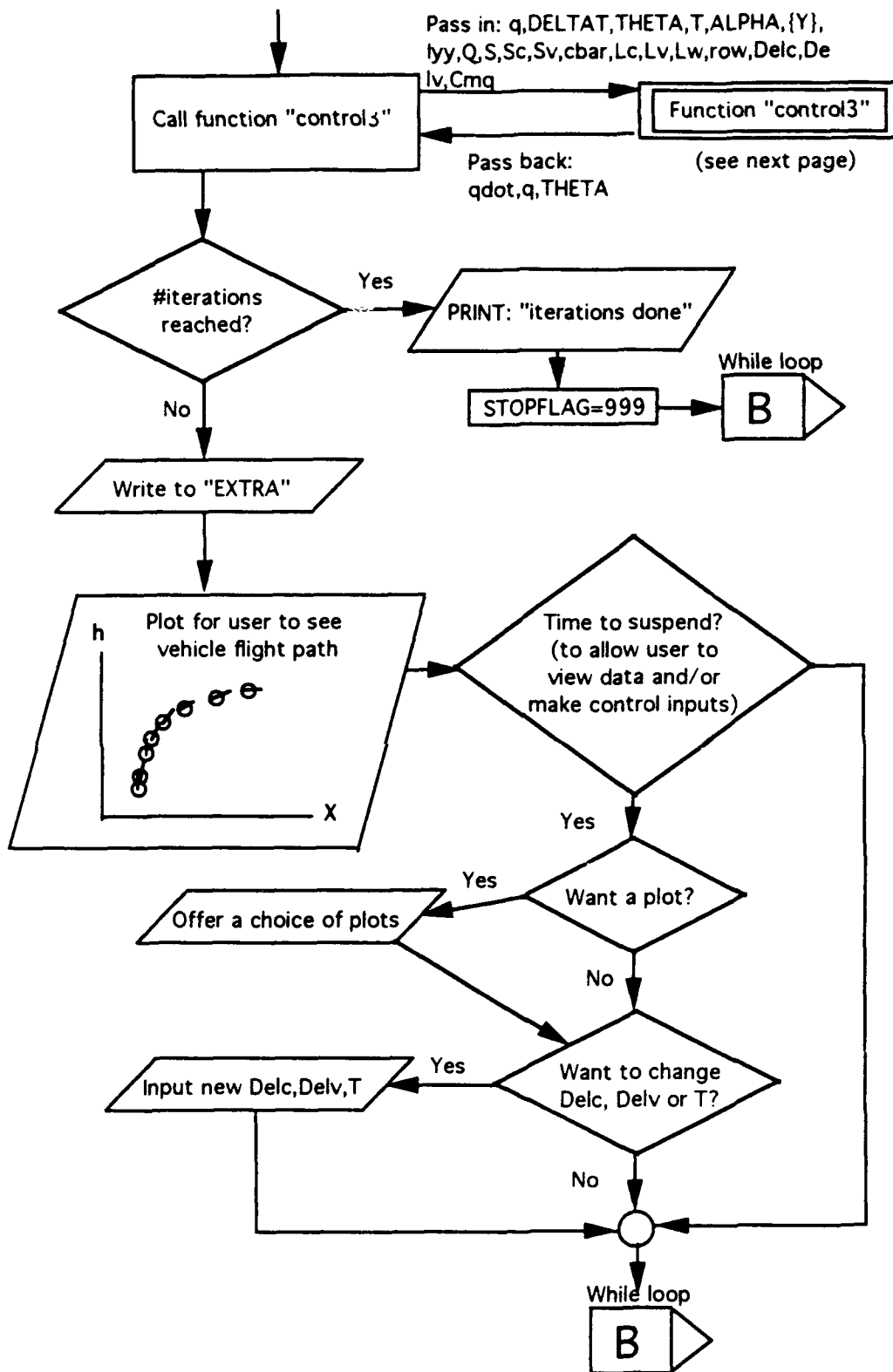
SUGGESTIONS FOR REFINEMENT: Model them. CAPT Kuechenmeister has done this in his thesis work.

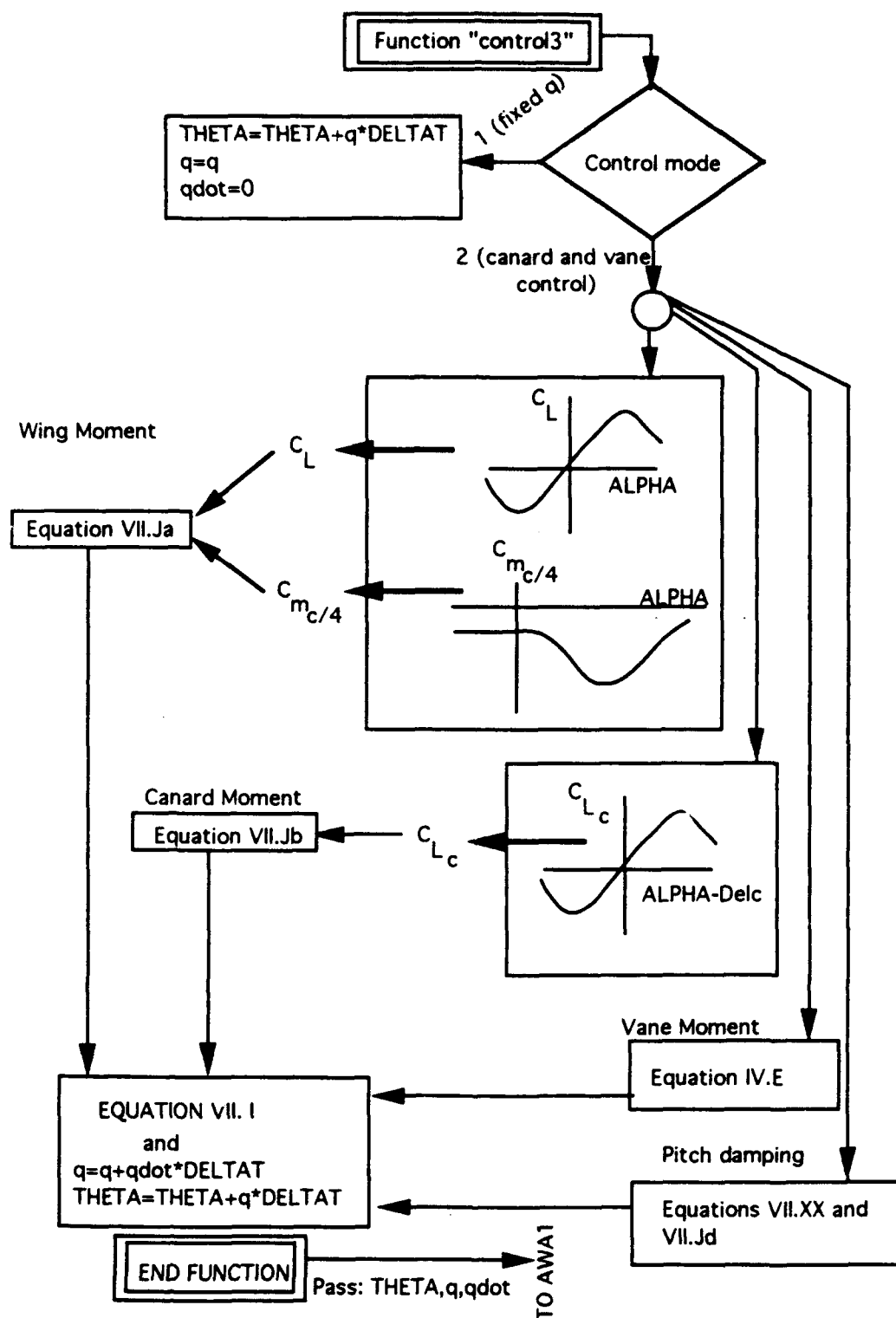


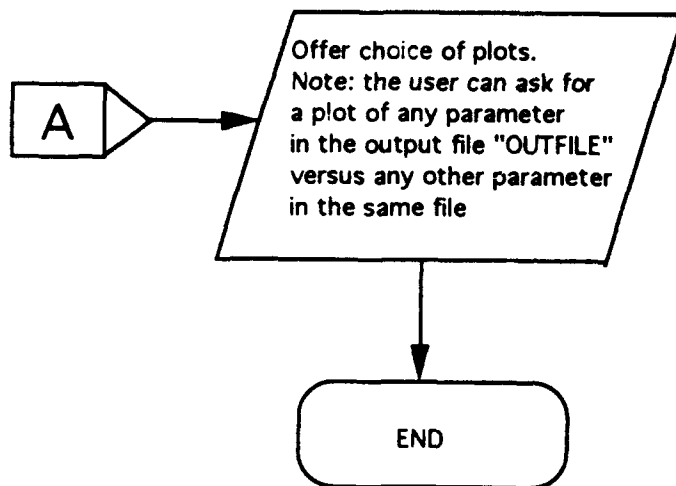












After running AWA1, the user may then run:

"Plotter"--gives 8 plots of the most important info

"Movie"--replays the run

```

%-----
%-----PROGRAM "AWA1"-----
%-----

% LCDR Bob Stoney, Naval Postgraduate School, Monterey
% Written for APPLE MACINTOSH ©
% Last update: 12 MAY 93 (Throttle model and vane model updated)
%               29 May 93 (PROFILE question added at beginning of program
%               to optimize continuously updated plot for different
%               flight profiles (hover versus horizontal flight))

% Three degree of freedom (pitch, x, z) simulation for ARCHYTAS Vertical
% Attitude Takeoff and Landing (VATOL) UAV. Includes improvements over PMS3,
% in that the equations of motion (contained in "yprime4" and "control3" do not
% have any small angle assumptions. Also incorporates autoscaling plot feature
% for continuously updated downrange distance vs. height plot.
% Thanks to Colin Cooper (aka "Mr MATLAB") of the EC department for help with
% making the graphics look nice.
% Note: "*****" means an area open to further programming (may be
% accompanied by amplifying information concerning work to be done)

clear      % Clear all variables from system--wipe the slate clean
clc        % Clear the command window
clf        % Clear the graph window
hold off   % To release any previous graph settings

%-----
% PROGRAM SCHEME
% The algorithm is performed as follows:          (line 30)
%   • Aircraft constants--gathers needed constants for particular aircraft
%     from a function.
%   • Starting values--initializes model's position, orientation and velocity
%   • Iteration--Utilizes predictor and corrector to increment desired
%     quantities.
%       Predictor--first guess at the solution of the governing Dif EQ's
%       Corrector--Corrected solutions to the governing Dif EQ's
%   • Output file management--sets up a matrix of the most important
%     quantities, which are recorded at each iteration.
%   • Aircraft control--Uses a function to control system inputs.
%   • Final output--To let the user extract desired information.

```



```

%-----Block to set flag ("UPDATE") to alert program to periodically
%-----halt program for view/control...or will allow uninterrupted run
    if SUSPEND==1, % (line 90)
        disp('Input the #secs between suspensions');
        UPDATE=input(' '); % Time period between view/control
    elseif SUSPEND==0,
        UPDATE=0;
    else
        disp('You did not enter a 0 or 1 for suspend option—default is 0')
        UPDATE=0;
    end
%-----End UPDATE set loop-----

%-----Control input block----- (line 101)
    if CONIMODE==1, % Constant pitch rate mode (mostly for troubleshooting)
        disp('Input the desired pitch rate in deg/sec (down is neg) and TP')
        qdeg=input(' ');
        q=qdeg(1)*pi/180; % Pitch rate converted to rad/sec
        qdot=0; % Because constant pitch rate
        Delc=0; % Canard angle set to 0 for output file
        Delv=0; % Vane angle set to 0 for output file
        TP=qdeg(2); % Throttle position in percent
    else,
        if CONIMODE~=2,
            disp('Your input for control mode was not 1 or 2..default is 2');
        else
            disp('Input as row vector initial canard deflection (LE down is +),')
            disp('Vane deflection (TE down is +) and Throttle position ')
            disp('(percent—0 is idle 100 is full throttle): [Delc, Delv,TP]')
            disp('OR TYPE 1 FOR DEFAULT: [-2 0 100]') % see default loop below
            CONTINIT=input(' ');
            if CONTINIT==1,
                Delc=-2*pi/180; % Default canard deflection in rad(line 120)
                Delv=0; % Default vane deflection in rad
                TP=100; % Default throttle position in percent
            else
                Delc=CONTINIT(1)*pi/180; % Canard deflection converted to rad
                Delv=CONTINIT(2)*pi/180; % Vane deflection converted to rad
                TP=CONTINIT(3); % Throttle position in percent
            end %CONTINIT==1?
            q=0; % Pitch rate set to 0 for first entry in output file
            qdot=0; % Pitch accel set to 0 for first entry in output file
        end %CONIMODE~=2?
    end %CONIMODE if,else
    [T]=THROTTLE(TP); % call function that converts Throttle position to thrust
%-----End Control input block-----

```

```

q=32.174;
M=Wt/g;      %Mass in slugs
PT=1;        % Counter
UPDATECOUNT=1; % Counter for program's option to suspend run for view/input
ROW=0.00237688; % Density in slugs/ft^3

%-----The Y vector (comprised of 4 elements that constitute the dependent
%variables in the differential equations) is as follows:
% Y(1)=x position in ft, Y(2)=height in ft, Y(3)=Velocity ft/sec,
% Y(4)=gamma (flight path angle in radians). Or: [Y]=[x,h,V,gamma]Transpose
% This vector will be overwritten throughout the program, with required values
% (line 145)
% being retained in the OUTFILE matrix (to be introduced below).
disp(' ')
disp('Input as row vector (deg) [hi,Vi,gamma(i)--deg,and theta(i)--deg]')
disp('Note: Vi must not be zero or a DIVIDE BY ZERO error will occur. ');
disp('OR TYPE 1 FOR DEFAULT: [15 .5 89.5 90]')
INITIAL2=input(' ');
Y(1)=0;      %Initial x position in ft
if INITIAL2==1, % i.e. default selected by user.
    INITIAL2(1)=15; Y(2)=INITIAL2(1); % These are all spelled out
    INITIAL2(2)=0.5; Y(3)=INITIAL2(2); % because they are used in a
    INITIAL2(3)=89.5; Y(4)=INITIAL2(3)*pi/180; % configuration definition later
    INITIAL2(4)=90; THETA=INITIAL2(4)*pi/180;
else
    Y(2)=INITIAL2(1); % Initial height in ft
    Y(3)=INITIAL2(2); % Initial velocity in ft/sec
    if INITIAL2(3)>89.5 & INITIAL2(3)<90.5,
        INITIAL2(3)=89.5; % to prevent instability in numerical scheme due to
        % singularity in gamma dot equation contained in function "yprimes"
    end
    Y(4)=INITIAL2(3)*pi/180; % Initial flight path angle in rad
    THETA=INITIAL2(4)*pi/180; % Initial Pitch attitude in rad
end % Default if loop
%-----End Y vector initialization-----

%-----YDOT vector initialization-----
%-----The YDOT vector is as follows:
% YDOT(1)=Groundspeed in ft/s, YDOT(2)=Rate of climb in ft/s,
% YDOT(3)=Acceleration along velocity vector in ft/s^2
% YDOT(4)=time rate of change of flight path angle in radians/sec
% Or: [YDOT]=[Xdot,Hdot,Vdot,gamma dot]transpose
% This vector will be overwritten throughout the program, with required values
% being retained in the OUTFILE matrix (to be introduced below).
YDOT(1)=Y(3)*cos(Y(4)); %Initial groundspeed in ft/s
YDOT(2)=Y(3)*sin(Y(4)); % Initial rate of climb in ft/s
YDOT(3)=0.0; % Initial acceleration along vel vector in ft/s^2

```

```

YDOT(4)=0.0;      % Initial flt path angle rate in rad/sec
%-----End Ydot vector initialization-----

% Record configuration:
CONFIG=[Wt, DELTAT, INITIAL2(1), INITIAL2(2), INITIAL2(3), INITIAL2(4)];

Q=0.5*ROW*Y(3)^2;      % Dynamic pressure
ALPHA=THETA-Y(4);      % AOA in radians
% From "Final Archytas Cl vs. AOA" plot:
  if (ALPHA<=-1.57) | (ALPHA>=1.57),
    CL=0;
    disp('Warning: WING aoa greater than +/- 90 deg')
  elseif ALPHA>-1.57 & ALPHA<-0.72,
    CL=-1.083-0.69*ALPHA;
  elseif ALPHA>=-0.72 & ALPHA<=-0.285,
    CL=2.81+33.21*ALPHA+105.38*ALPHA^2+138.1*ALPHA^3+64.9*ALPHA^4;
  elseif ALPHA>=-0.285 & ALPHA<=0.29,
    CL=9.52e-2+3.38*ALPHA;
  elseif ALPHA>0.29 & ALPHA<0.9,
    CL=-2.037+25.54*ALPHA-72.15*ALPHA^2+82.59*ALPHA^3-33.4*ALPHA^4;
  elseif ALPHA>=0.9 & ALPHA<1.57,
    CL=1.875-1.194*ALPHA;
  end

CD=0.0608+0.0543*ALPHA+0.910*ALPHA^2; % Coefficient of drag as fcn of aoa
% for post-stall drag increases which CD=f(CL^2) doesn't account for.
Es=Y(3)^2/(2*g)+Y(2); % Energy height
Esdot=Y(3)*YDOT(3)/g+YDOT(2); % Time rate of change of specific energy—for

%-----BEGIN FILE MANAGEMENT-----
% The outfile consists of the following:
%   OUTFILE(row#, :)= [X, H, V, Vdot, Theta, Alpha, Counter#, Thrust, Groundspeed, Rate
%   of climb, flight path angle, energy height, time rate of change
%   of Eng Ht, pitch rate, pitch accel, canard defl, vane defl, time, TP]
OUTFILE(1, :)= [Y(1), Y(2), Y(3), YDOT(3), THETA*180/pi, ALPHA*180/pi, PT, T, ...
YDOT(1), YDOT(2), Y(4)*180/pi, Es, Esdot, q*180/pi, qdot*180/pi, Delc*180/pi, ...
Delv*180/pi, DELTAT*PT, TP]; % Note continuation marks (...)
EXTRA(PT, :)= [PT, YDOT(4), Q, ROW, CL, CD, 0, 0, 0, 0, 0, 0, 0, 0, 0, 0];
% Troubleshooting info (0's for some items 'cause undefined so far)
XHPCOUNTER=0; % Used in continuously update x-h plot

```

```

%
%-----Iteration-----
%
STOPFLAG=1;
while STOPFLAG~=999,          % i.e. terminates loop when STOPFLAG=999 (assigned)
    PT=PT+1;                  % Increment counter
    UPDATECOUNT=UPDATECOUNT+1; % Increment "suspend" option counter
    XHPLOT_COUNTER=XHPLOT_COUNTER+1; % Used in continuously update x-h plot
    ALPHA=THETA-Y(4);          %AOA in radians
% Predictor and intermediate values
    [YDOT]=yprimes4(Y,THETA,T,S,M,Q,CL,CD,ALPHA); % Call to the D.Eqn Function

    for i=1:4,
        Y1(i)=Y(i)+DELTAT*YDOT(i); %Euler first step forward predictor
        YHALF(i)=Y(i)+DELTAT/2*YDOT(i); % Euler half step forward predictor
    end %end for

% Corrector and new value formulation
    [YDOT]=yprimes4(YHALF,THETA,T,S,M,Q,CL,CD,ALPHA);
    for i=1:4,
        Y2(i)=YHALF(i)+DELTAT/2*YDOT(i); %Richardson extrapolation
        Y(i)=2*Y2(i)-Y1(i); %Correction made
    end %end for
    Es=Y(3)^2/(2*g)+Y(2); %Energy height
    Estdot=Y(3)*YDOT(3)/g+YDOT(2); %New TRC of energy height
    Q=0.5*ROW*Y(3)^2; % Dynamic pressure
    ALPHA=THETA-Y(4); %AOA in radians
% From "Final Archytas Cl vs. AOA" plot:
    if (ALPHA<=-1.57) | (ALPHA>=1.57),
        CL=0;
        disp('Warning: WING aoa exceeds +/- 90 deg')
    elseif ALPHA>-1.57 & ALPHA<-0.72,
        CL=-1.083-0.69*ALPHA;
    elseif ALPHA>=-0.72 & ALPHA<=-0.285,
        CL=2.81+33.21*ALPHA+105.38*ALPHA^2+138.1*ALPHA^3+64.9*ALPHA^4;
    elseif ALPHA>=-0.285 & ALPHA<=0.29,
        CL=9.52e-2+3.38*ALPHA;
    elseif ALPHA>0.29 & ALPHA<0.9,
        CL=-2.037+25.54*ALPHA-72.15*ALPHA^2+82.59*ALPHA^3-33.4*ALPHA^4;
    elseif ALPHA>=0.9 & ALPHA<1.57,
        CL=1.875-1.194*ALPHA;
    end

    CD=0.0608+0.0543*ALPHA+0.910*ALPHA^2; % Coefficient of drag as fcn of aoa
    % for post-stall drag increases which CD=f(CL^2) doesn't account for.

```



```

%-----Output file update (add latest iteration)-----
OUTFILE(PT,:)=[Y(1),Y(2),Y(3),YDOT(3),THETA*180/pi,ALPHA*180/pi,PT,T,...
YDOT(1),YDOT(2),Y(4)*180/pi,Es,Escdot,q*180/pi,qdot*180/pi,Delc*180/pi,...
Delv*180/pi DELTAT*PT,TP];

%-----Aircraft control-----
% ***Constant q or Delc/Delv control, depending on CONTMODE selection***
if Y(2)<=0 %Stops @ ground impact
    disp('Ground Impact--and that is bad')
    STOPFLAG=999; %Stops while loop
end %end if

[THETA,q,qdot,Mcgw,Mcgc,Mcgv,Mq,L,Q,CL]=control4(q,DELTAT,...
THETA,T,ALPHA,Y,Iyy,Q,S,Sc,Sv,Cbar,Lc,Lv,Lw,ROW,Delc,Delv,Cmq,CONTMODE);
%Call control function
if PT==ITERS, % i.e. if # of iterations is through
    STOPFLAG=999; % Kicks out of while loop
    disp('All iterations completed')
end %end if
EXTRA(PT,:)=[PT,YDOT(4),Q,ROW,CL,CD,YHALF(1),YHALF(2),YHALF(3),.....
YHALF(4),Mcgw,Mcgc,Mcgv,Mq,L,Q,CL];
% Extra info for troubleshooting

%XXXXXXXXXXXXXXXXXXXXXXXXXXXXXXXXXXXXXXXXXXXXXXXXXXXXXXXXXXXXXXXXXXXXXXXXXXXX
% -----Continuously updated plot for user reference-----
%XXXXXXXXXXXXXXXXXXXXXXXXXXXXXXXXXXXXXXXXXXXXXXXXXXXXXXXXXXXXXXXXXXXXXXXXXXXX
TIME=.05; % Put in here so that the plot wouldn't update every time step...slow
%-----
%-----PROFILE 1 (takeoff trans) SECTION OF CONTINUOUS PLOT-----
%-----
if PROFILE==1, % i.e. takeoff transition

% This plot places a circle ("polymark") at the vehicle's x/h position and
% draws a line ("polyline") at an angle corresponding to a/c's pitch attitude.
if (XHPLCOUNTER*DELTAT)>=TIME, % i.e. causes this plot to update every TIME
    if ((Y(1)<100 & Y(2)<100) & L1==1), % This if loop sets plot axes for updated
        hold off
        V=[-25,100,0,100];axis(V); % Axis limits (xmin, xmax, ymin, ymax)
        plot(OUTFILE(:,1),OUTFILE(:,2),'o')
        xlabel('Downrange distance, x, ft');ylabel('Height, y, ft')
        L1=0; % set the plot flag to zero to prevent redrawing of plot
        hold on
    elseif (((Y(1)>=100 & Y(1)<200) | (Y(2)>=100 & Y(2)<200)) & L2==1),
        hold off
        V=[-25,200,0,200];axis(V); % Axis limits (xmin, xmax, ymin, ymax)
        plot(OUTFILE(:,1),OUTFILE(:,2),'o')
        xlabel('Downrange distance, x, ft');ylabel('Height, y, ft')
        L2=0;
        hold on
    end
end

```

```

elseif ((Y(1)>=200 & Y(1)<400) | (Y(2)>=200 & Y(2)<400)) & (L3==1),
    hold off
    V=[-25,400,0,400]; axis(V); % Axis limits (xmin, xmax, ymin, ymax)
    plot(OUTFILE(:,1),OUTFILE(:,2),'o')
    xlabel('Downrange distance, x, ft');ylabel('Height, y, ft')
    L3=0;
    hold on
elseif (((Y(1)>=400) | (Y(2)>=400)) & (L4==1)),
    hold off
    V=[-25,1000,0,1000]; axis(V); % Axis limits (xmin, xmax, ymin, ymax)
    plot(OUTFILE(:,1),OUTFILE(:,2),'o')
    xlabel('Downrange distance, x, ft');ylabel('Height, y, ft')
    L4=0;
    hold on
elseif (((Y(1)>=1000) | (Y(2)>=1000)) & (L5==1)),
    hold off
    V=[0,2000,0,2000]; axis(V); % Axis limits (xmin, xmax, ymin, ymax)
    plot(OUTFILE(:,1),OUTFILE(:,2),'o')
    xlabel('Downrange distance, x, ft');ylabel('Height, y, ft')
    L5=0;
    hold on
end % end if
%plot(OUTFILE(:,1),OUTFILE(:,2))
polymark(OUTFILE(PT,1),OUTFILE(PT,2),'o')
dx=((V(2)-V(1))/50)*cos(THETA);dy=((V(4)-V(3))/50)*sin(THETA);
polyline([OUTFILE(PT,1)-dx OUTFILE(PT,1)+dx],[OUTFILE(PT,2)-dy ...
    OUTFILE(PT,2)+dy],'-w') % This shows the vehicle's pitch attitude
XHPLOTCOUNTER=0; % To reset

end % end if for "(XHPLOTCOUNTER*DELTAT)>=0.1"
%-----
%-----PROFILE 2 (horiz. or landing transition) SECTION OF CONTINUOUS PLOT-----
%-----
elseif PROFILE==2, % i.e. horizontal flight optimized display
if (XHPLOTCOUNTER*DELTAT)>=TIME, % i.e. causes this plot to update every TIME
if Y(3)>=40, % Velocity > 40? If so, leaves "big picture plot", otherwise
    % focuses on vehicle for control to hover....
    if ((Y(1)<1000 & Y(2)<1000) & L1==1)
        hold off
        V=[-25,1000,0,1000];axis(V); % Axis limits (xmin, xmax, ymin, ymax)
        plot(OUTFILE(:,1),OUTFILE(:,2),'o')
        xlabel('Downrange distance, x, ft');ylabel('Height, y, ft')
        L1=0; % set the plot flag to zero to prevent redrawing of plot

        hold on

```

```

elseif ((Y(1)>=1000 & Y(1)<2000) | (Y(2)>=1000 & Y(2)<2000)) & L2==1),
    hold off
    V=[-25,2000,0,2000];axis(V);    % Axis limits (xmin, xmax, ymin, ymax)
    plot(OUTFILE(:,1),OUTFILE(:,2),'o')
    xlabel('Downrange distance, x, ft');ylabel('Height, y, ft')
    L2=0 ;
    hold on
elseif ((Y(1)>=2000 & Y(1)<4000) | (Y(2)>=2000 & Y(2)<4000)) & (L3==1)),
    hold off
    V=[-25,4000,0,4000]; axis(V);    % Axis limits (xmin, xmax, ymin, ymax)
    plot(OUTFILE(:,1),OUTFILE(:,2),'o')
    xlabel('Downrange distance, x, ft');ylabel('Height, y, ft')
    L3=0;
    hold on
end    %for this if: "if ((Y(1)<1000 & Y(2)<1000) & L1==1)"
elseif (Y(3)<40) & (L4==1),
    hold off
    V=[Y(1)-100,Y(1)+100,0,1.5*Y(2)]; axis(V); % x +/- 100 and 0 to 1.5height
    plot(OUTFILE(:,1),OUTFILE(:,2),'o')
    xlabel('Downrange distance, x, ft');ylabel('Height, y, ft')
    L4=0;
    hold on
end    % end if for Airspeed > 40? (has elseif too)
polymark(OUTFILE(PT,1),OUTFILE(PT,2),'o')
dx=((V(2)-V(1))/50)*cos(THETA);dy=((V(4)-V(3))/50)*sin(THETA);
polyline([OUTFILE(PT,1)-dx OUTFILE(PT,1)+dx],[OUTFILE(PT,2)-dy ...
    OUTFILE(PT,2)+dy],'-w')    % This shows the vehicle's pitch attitude
XHPLCOUNTER=0;    % To reset (will allow plot to work in another .1 sec
end    % end if for "(XHPLCOUNTER*DELTAT)>=0.1"
end    % if for which PROFILE

%%%%%%%%%%%%%%%%%%%%%%%%%%%%%%%%%%%%%%%%%%%%%%%%%%%%%%%%%%%%%%%%%%%%%%%%
% -----END Continuously updated plot for user reference-----
%%%%%%%%%%%%%%%%%%%%%%%%%%%%%%%%%%%%%%%%%%%%%%%%%%%%%%%%%%%%%%%%%%%%%%%%

%-----Suspend loop (to view progress/update control)-----
if UPDATECOUNT*DELTAT>=UPDATE,    % i.e. "Time to suspend?"
    UPDATECOUNT=0;                %reset it for next suspend
    ans=input('Program suspended, want a plot? 1=yes 0=no');
    while ans~=0,
        hold off;
        axis([1 2 3 4]);axis;
        L1=1;L2=1;L3=1;L4=1;

```

```

disp('These are the quantities stored:')
disp('1: X posit   6: Alpha      11: Flt Path Angle  16: Delc')
disp('2: height    7: Point#     12: Energy Ht (Es)  17: Delv')
disp('3: speed     8: Thrust      13: Esdot         18: time')
disp('4: Accel     9: Groundspd  14: q             19: Thr1 Posit')
disp('5: Theta    10:Rate of Cl  15: qdot  ')
    % Ask user for desired x and y plot values:
xanswer=input('Type #for what you want on x-axis');
yanswer=input('Type #for what you want on y-axis');
if xanswer<1 | xanswer>19 | yanswer<1 | yanswer>19, % (i.e. misentry)
    xanswer=18;yanswer=18; % just plots time vs. time as error indication
end
plot(OUTFILE(:,xanswer).OUTFILE(:,yanswer))
[XLABEL,YLABEL]=labeler(xanswer, yanswer);
xlabel(XLABEL);ylabel(YLABEL);
title(['Weight: ',num2str(Wt),'lbf'])
pause
    % Ask user if they want another plot:
ans=input('Another plot? 0=NO');
end % end suspend while loop
if CONTIMODE==2,
MAT2=[Delc*180/pi,Delv*180/pi,TP];
disp('Present values for Delc,Delv (in deg) & TP:');
disp(MAT2)
ans2=input('Want to change these settings? 0=No');
if ans2~=0,
    NEWCONT=input('Enter as row matrix, new [Delc(deg),Delv(deg),TP(%)]');
    NEWCONTsize=size(NEWCONT);
    check=NEWCONTsize(2);
    if check~=3,
        disp('You misentered the new Control—default is previous input')
    else,
        Delc=NEWCONT(1)*pi/180;
        Delv=NEWCONT(2)*pi/180;
        TP=NEWCONT(3);

        end % this if block prevents program termination by user misentry.
    end %ans 2 if
elseif CONTIMODE==1,
    disp('Present value for pitch rate (deg/sec) & TP:')
    disp(q*180/pi);disp(T);
    ans3=input('Would you like to change? 0=no');
    if ans3~=0,
        NEWQT=input('Input new q, in deg/sec (down is neg) & TP as [ ]')
        q=NEWQT(1)*pi/180;
        TP=NEWQT(2);
    end % ans3 if
end % CONTIMODE=2 or 1?
[T]=THROTTLE(TP); % call to function "THROTTLE"
end % end new control input if loop
end % end suspend if loop
%-----End SUSPEND loop block-----

```

```

end      %end the iteration while loop
% Display configuration to user:
disp('Configuration:')
format compact
disp('  Weight      Delta T      hi      Vi      Gammai      Thetai      ')
disp(CONFIG)
format short

%-----Final Output-----
ans1=input('Want a plot? 1=yes 0=no');      %Kick out flag
while ans1~=0,
    hold off;
    axis([1 2 3 4]);axis;
    L1=1;L2=1;L3=1;L4=1;
    disp('These are the quantities stored:')
    disp('1: X posit   6: Alpha      11: Flt Path Angle  16: Delc')
    disp('2: height    7: Point#     12: Energy Ht (Es)  17: Delv')
    disp('3: speed     8: Thrust      13: Esdot         18: time')
    disp('4: Accel     9: Groundspd  14: q             19: Thr1 Posit')

    disp('5: Theta    10:Rate of Cl  15: qdot  ')
    % Ask user for desired x and y plot values
    xanswer=input('Type #for what you want on x-axis');
    yanswer=input('Type #for what you want on y-axis');
    disp('Note: will have to add own axis labels, etc') %*****at this point
    plot(OUTFILE(:,xanswer),OUTFILE(:,yanswer))
    [XLABEL,YLABEL]=labeler(xanswer, yanswer);
    xlabel(XLABEL);ylabel(YLABEL);
    title(['Weight: ',num2str(Wt),'lbf'])
    pause
    % Ask user if they want another plot:
    ans1=input('Another plot? 0=NO');
end      % this while loop

%-----Final instructions (help for storing and retrieving data)-----
disp('Recommended commands to save data:')
disp('>>filename=OUTFILE;')
disp('>>filenameC=CONFIG: (to keep a record of the configuration)')
disp('>>save filename filename;')
disp('>>save filenameC filenameC;')
disp('Then, when you want to use it again:')
disp('>>load filename or filenameC (filename is a 18 by #iters matrix for a
particular set of conditions—specified on filenameC')
% NOTE: also useful are programs "filesaver" and "resurrect"

%---NOTE: See also "AWA assumptions" (Microsoft word document)

%-----
%-----END PROGRAM "AWA1"-----
%-----

```

```

=====
%-----Function archytas3-----
=====
function[S,K,CDo,Iyy,Lc,Lv,Lw,Sc,Sv,Cbar,Cmq,xcg]=archytas3();
% Aircraft data function *****Note these are all WAGS at this point***
% Used by program PMS3
% LCDR Bob Stoney
% Last update: 8 May 93
S=29.2;           % Wing Area in ft^2
e=0.8;           % Efficiency factor
AR=4.25;         % Aspect ratio (vortex lattice output)
K=1/(pi*AR*e);   % Constant for CD calculation (CD=CDo+K(CL^2))
CDo=0.06;        % Rick's guess
Iyy=7.4;         % Moment of inertia (slugs-ft^2) Aquila=10.4 rept AD-A068 345
Lc=4.66;         % Absolute Distance in ft from canard's aero center to a/c c.g.
Lv=1.5;          % Distance in ft from Vane's aero center to a/c c.g. ***Refine
Lw=0.758;        % Distance in ft from wing's aero ctr to a/c c.g. (From program
                  % "Xplot")
%*****CHECK Sc!!!!!!31.5"X12"=2.6 ft^2*****
Sc=2.6;          % Area of canard in ft^2 (From program "Xplot")
Sv=1.111;        % Area of two (2!!) vanes in ft^2 (Each is 8" by 10")
CR=3.33;         % Root Chord in ft
Ct=1.92;         % Tip chord in ft
lambda=Ct/CR;    % Taper ratio
Cbar=2/3*CR*(1 + lambda^2/(1+lambda)); % MAC
Cmq=-1.47;       % Pitch damping (1/rad) Ref: Aquila rept AD-A068 345*****
=====
%-----END archytas3-----
=====

```

```

%=====
%-----function "THROTTLE"-----
%=====

% A companion program to "ANA1", the 3 DOF simulator.
% This function receives the user input throttle position (TP) (in %—0=idle,
% 100=full throttle) and converts it into thrust (T) in lbf, based on data from
% engine tests on 4/16/93 and shown curve fit on the cricket graph file
% "Thrust vs. TP"

% Bob Stoney, Naval Postgraduate School, created: 5/12/93
% Last update: 5/12/93

function[T]=THROTTLE(TP);

flag=1;
while flag==1,
    if TP>100 | TP<0,
        disp('THE THROTTLE POSITION YOU INPUT WAS <0 OR >100, RE-INPUT 0-100')
        TP=input(' ');
        flag=1;
    else
        T=21.215-.40269*TP+.10932*TP^2-2.1907e-3*TP^3+1.7515e-5*TP^4-5.1479e-8*TP^5;
        flag=0;    % i.e. will kick us out of while loop and back to main prog.
    end    % TP out of bounds if loop
end

%=====
%-----end program "THROTTLE"-----
%=====

```

```

=====
function "yprimes4"
=====

% LCDR Bob Stoney, NPGS.
% Contains the equations defining conservation of linear momentum,
% used in program AWA-series
% Written: Aug 92
% Last update: 4 May 93

% Improvement over previous editions:
% gamma dot equation (YDOT(4)) doesn't have the small angle assumption of
% previous programs.
% See AWA1 for description of this function

function [YDOT]=yprimes4(Y,THETA,T,S,M,Q,CL,CD,ALPHA) % [passed out] (passed in)

% The ydot vector is as follows: [xdot, hdot, vdot, gammadot]
%
% This function calculates the y solutions to the coupled system equations:
YDOT(1)=Y(3)*cos(Y(4));
YDOT(2)=Y(3)*sin(Y(4));
    D=Q*S*CD;      % Drag
    g=32.174;      % gravitational constant
YDOT(3)=T*cos(THETA-Y(4))/M-D/M-g*sin(Y(4));
    L=Q*S*CL;      % Lift
    TERM1=(L-D*tan(Y(4)))/(M*Y(3));
    TERM2=T*(tan(Y(4))*cos(ALPHA)+sin(ALPHA))/(M*Y(3));
    TERM3=-g/(Y(3)*cos(Y(4)));
    TERM4=-YDOT(3)*tan(Y(4))/Y(3);
YDOT(4)=TERM1+TERM2+TERM3+TERM4;

=====
end function "yprimes4"
=====

```



```

%=====
%-----Function control4-----
%=====

% LCDR Bob Stoney. Last update: 12 May 93. (vane control power re-modeled based
% on engine test data).
% This function is for aircraft control. It is essentially a model of Newton's
% second law applied to conservation of angular momentum around the pitch axis.
% This function is a companion to AWAL, a point mass simulator for the Archytas

% Change over control3: Improved Vane control power model
% and Cl vs. AOA model.

% CAUTION: "Q" is dynamic pressure. "q" is pitch rate.

function[THETAOUT,qout,qdotout,Mcgw,Mcgc,Mcgv,Mq,L,Q,CL]=control4...
    (q,DELTAT,THETA,T,ALPHA,Y,Iyy,Q,S,Sc,Sv,.....
    Cbar,Lc,Lv,Lw,ROW,Delc,Delv,Cmq,CONTIMODE);

% -----Constant pitch rate section:
if CONTIMODE==1,
    THETAOUT=THETA+q*DELTAT;% Note: for CONTIMODE=1 q,qdot have already been
                           % specified
    qout=q;
    qdotout=0;           % Constant pitch rate.
    Mcgw=0;              % These effects not included. Passed for troubleshooting.
    Mcgc=0;              % These effects not included. Passed for troubleshooting.
    Mcgv=0;              % These effects not included. Passed for troubleshooting.
    Mq=0;                % These effects not included. Passed for troubleshooting.

%-----Using canard and vane control:-----
else, %i.e. if Delc and Delv specified

% ---Wing contribution:
% LIFT:
% From "Final Archytas Cl vs. AOA" plot:
    if (ALPHA<=-1.57) | (ALPHA>=1.57),
        CL=0;
        disp('Warning: WING aoa greater than +/- 90 deg')
    elseif ALPHA>-1.57 & ALPHA<-0.72,
        CL=-1.083-0.69*ALPHA;
    elseif ALPHA>=-0.72 & ALPHA<=-0.285,
        CL=2.81+33.21*ALPHA+105.38*ALPHA^2+138.1*ALPHA^3+64.9*ALPHA^4;
    elseif ALPHA>=-0.285 & ALPHA<=0.29,
        CL=9.52e-2+3.38*ALPHA;

```

```

elseif ALPHA>0.29 & ALPHA<0.9,
    CL=2.037+25.54*ALPHA-72.15*ALPHA^2+82.59*ALPHA^3-33.4*ALPHA^4;
elseif ALPHA>=0.9 & ALPHA<1.57,
    CL=1.875-1.194*ALPHA;
end

% Cmac contribution: (Ref: NACA2412 in Anderson.)
Cmac=0.05;

% Add Lift and Cmac contributions:

L=Q*S*CL;
Mcgw= -L*cos(ALPHA)*Lw + Cmac*Q*S*Cbar;

%---Canard contribution: %Presently using fit from main wing to show high aoa.
% From "Final Archytas Cl vs. AOA" plot:
if ((ALPHA-Delc)<=-1.57) | ((ALPHA-Delc)>=1.57),
    Clc=0;
    disp('Warning: Canard aoa greater than +/- 90 deg')
elseif (ALPHA-Delc)>1.57 & (ALPHA-Delc)<-0.72,
    Clc=1.083-0.69*(ALPHA-Delc);
elseif (ALPHA-Delc)>=0.72 & (ALPHA-Delc)<=0.285,
    Clc=2.81+33.21*(ALPHA-Delc)+105.38*(ALPHA-Delc)^2...
        +138.1*(ALPHA-Delc)^3+64.9*(ALPHA-Delc)^4;
elseif (ALPHA-Delc)>0.285 & (ALPHA-Delc)<=0.29,
    Clc=9.52e-2+3.38*(ALPHA-Delc);
elseif (ALPHA-Delc)>0.29 & (ALPHA-Delc)<0.9,
    Clc=2.037+25.54*(ALPHA-Delc)-72.15*(ALPHA-Delc)^2...
        +82.59*(ALPHA-Delc)^3-33.4*(ALPHA-Delc)^4;
elseif (ALPHA-Delc)>0.9 & (ALPHA-Delc)<1.57,
    Clc=1.875-1.194*(ALPHA-Delc);
end %end if for Clc loop
Mcgc=Q*Sc*Clc*Lc*cos(ALPHA);

%---Vane contribution:
% Note: "Delv", the vane deflection, is assumed to be 0 at 0 control
% power. Any deviation, plus or minus, produces a pitching moment.
Vanemodel=2; % Used to compare the two different types of
    % vane control power models. 1="old"--NACA0009 data with
    % velocity measurements from engine tests. 2="new"--moment
    % data from engine tests (only applies for 90-120 lb but left
    % as is for now) converted to pitch direction.
    % NOTE: Vanemodel=2 was used for all runs used for analysis in the thesis

```

```

if Vanemodel==1,
    if (Delv)<=-.56,
        Clv=0;
        disp('Warning: Vane local aca less than -.56 (low end)')
    elseif ((Delv)>-.56) & ((Delv)<=.23),
        Clv=1.0419+22.5*(Delv)+67.754*(Delv)^2+56.417*(Delv)^3;
    elseif ((Delv)>.23 & ((Delv)<.2),
        Clv=2.2772e-20+5.8809*(Delv);
    elseif (Delv)>=.2 & (Delv)<.65,
        Clv=-3.2096e-2+12.433*(Delv)...
            -37.257*(Delv)^2+27.979*(Delv)^3;
    elseif (Delv)>.65,
        Clv=0; %***Beyond specified alpha there's no lift***
        disp('Warning:Vane local aca gtr .65 (high end)')
    end %end if for Clv loop
    % From Thrust tests, the following relationships apply to convert
    % from thrust to rpm and then to velocity at the vane (Vv) (ft/sec):
    RPM=1771.2+78.657*T-0.26205*T^2;
    Vv=36.47-2.016e-3*RPM+1.867e-6*RPM^2; % f(AOA,V?)****
    Mcgv=-Lv*0.5*ROW*W^2*Sv*Clv; % Pitching Moment due to vane
elseif Vanemodel==2,
    Newvanelift=2*(0.267*Delv*180/pi); % must convert to degrees
    % 'cause that's how curve was fit.
    Mcgv=-Newvanelift*Lv;
end % if for vanemodel type
%---Pitch damping:
Mq=Qnq*Q*S*Cbar^2/(2*Iyy*Y(3));

%---Total: Pitch acceleration (by conservation of angular momentum):
qdotout=(Mcgw+Mqgc+Mcgv)/Iyy+Mq*q; %q dot to send to main program
qout=q+qdotout*DELTAT; %q to send to main program

%-----

THETAOUT=THETA+qout*DELTAT; %pitch angle to send to main program
end %end if

% See also: AWA assumptions (Microsoft word document)
%=====
%-----END control 4-----
%=====

```

```
%=====Function "labeler"=====
```

```
% This function provides axis labelling for AWA series of programs.
% LCDR Bob Stoney, Naval Postgraduate School
% Last update: 12 MAY 93 (addition of throttle position)
```

```
function(XLABEL,YLABEL)=labeler(xanswer,yanswer)
    % The pass in list contains xanswer and yanswer, which is what
    % the user asked to be plotted on an x-y plot. The pass out
    % variables XLABEL and YLABEL are text strings to be placed on
    % the desired plot.
if xanswer==1,
    XLABEL='Downrange distance, x, ft';
elseif xanswer==2,
    XLABEL='Height, y, ft';
elseif xanswer==3,
    XLABEL='Speed, V, ft/sec';
elseif xanswer==4,
    XLABEL='Acceleration, Vdot, ft/sec^2';
elseif xanswer==5,
    XLABEL='Pitch attitude, theta, deg';
elseif xanswer==6,
    XLABEL='Angle of attack, alpha, deg';
elseif xanswer==7,
    XLABEL='Point number of iteration';
elseif xanswer==8,
    XLABEL='Thrust, T, lbf';
elseif xanswer==9,
    XLABEL='Groundspeed, ft/sec';
elseif xanswer==10,
    XLABEL='Rate of Climb, ft/sec';
elseif xanswer==11,
    XLABEL='Flt path angle, gamma, deg';
elseif xanswer==12,
    XLABEL='Energy height, Es, ft';
elseif xanswer==13,
    XLABEL='Es dot, ft/sec';
elseif xanswer==14,
    XLABEL='Pitch rate, q, deg/sec';
elseif xanswer==15,
    XLABEL='Pitch acceleration, qdot, deg/sec^2';
elseif xanswer==16,
    XLABEL='Canard deflection (TE down +), Delc, deg';
elseif xanswer==17,
    XLABEL='Vane deflection (TE up +), Delv, deg';
```

```

elseif xanswer==18,
    XLABEL='Time, t, sec';
elseif xanswer==19,
    XLABEL='Throttle position, TP, percent';
end    % end if loop for XLABEL

% -----Y axis label:-----
if yanswer==1,
    YLABEL='Downrange distance, x, ft';
elseif yanswer==2,
    YLABEL='Height, y, ft';
elseif yanswer==3,
    YLABEL='Speed, V, ft/sec';
elseif yanswer==4,
    YLABEL='Acceleration, Vdot, ft/sec^2';
elseif yanswer==5,
    YLABEL='Pitch attitude, theta, deg';
elseif yanswer==6,
    YLABEL='Angle of attack, alpha, deg';
elseif yanswer==7,
    YLABEL='Point number of iteration';
elseif yanswer==8,
    YLABEL='Thrust, T, lbf';
elseif yanswer==9,
    YLABEL='Groundspeed, ft/sec';
elseif yanswer==10,
    YLABEL='Rate of Climb, ft/sec';
elseif yanswer==11,
    YLABEL='Flt path angle, gamma, deg';
elseif yanswer==12,
    YLABEL='Energy height, Es, ft';
elseif yanswer==13,
    YLABEL='Es dot, ft/sec';
elseif yanswer==14,
    YLABEL='Pitch rate, q, deg/sec';
elseif yanswer==15,
    YLABEL='Pitch acceleration, qdot, deg/sec^2';
elseif yanswer==16,
    YLABEL='Canard deflection (TE down +), Delc, deg';
elseif yanswer==17,
    YLABEL='Vane deflection (TE up +), Delv, deg';
elseif yanswer==18,
    YLABEL='Time, t, sec';
elseif yanswer==19,
    YLABEL='Throttle position, TP, percent';
end    % end if loop for XLABEL

%=====
%=====end function "labeler"=====
%=====

```

```

%=====
%-----misc. program "plotter"-----
%=====
% Program used in conjunction with the AWA series programs.
% Uses subplot to plot most important parameters on a two
% sheets of paper.
% To use, simply type plotter at the MATLAB command carrot >>
% LCDR Bob Stoney, NPGS
% Created 12 SEP 92
clc
hold off
%-----Aircraft parameters: Alpha, speed, theta, q-----
subplot(221),plot(OUTFILE(:,18),OUTFILE(:,6))
xlabel('Time, t, sec');ylabel('Angle of attack, alpha, deg');grid
title(['Weight=',num2str(Wt),' lbf'])
subplot(222),plot(OUTFILE(:,18),OUTFILE(:,3))
xlabel('Time, t, sec');ylabel('Speed, V, ft/sec');grid
subplot(223),plot(OUTFILE(:,18),OUTFILE(:,5))
xlabel('Time, t, sec');ylabel('Pitch attitude, theta, deg');grid
subplot(224),plot(OUTFILE(:,18),OUTFILE(:,14))
xlabel('Time, t, sec');ylabel('Pitch rate, q, deg/sec');grid
pause
cla
hold off
%-----Control parameters: Canard, vane, thrust, and x vs. h-----
subplot(221),plot(OUTFILE(:,18),OUTFILE(:,16))
xlabel('Time, t, sec');ylabel('Canard defl., Delc, deg');grid
title(['Weight=',num2str(Wt),' lbf'])
subplot(222),plot(OUTFILE(:,18),OUTFILE(:,17))
xlabel('Time, t, sec');ylabel('Vane deflection, Delv, deg');grid
subplot(223),plot(OUTFILE(:,18),OUTFILE(:,19))
xlabel('Time, t, sec');ylabel('Throttle posit, TP, %');grid
subplot(224),plot(OUTFILE(:,1),OUTFILE(:,2))
xlabel('Downrange distance, x, ft');ylabel('Height, h, ft');grid
pause
hold off

%=====
%-----end program "plotter"-----
%=====

```

```

=====
%-----misc. program "Movie"-----
=====

% 'Movie' LCDR Bob Stoney, NPS. 1 March 93
% Last update: 30 May 93
% Companion program to AWAL that shows the vehicle's position and pitch
% attitude during the most recent run.

clc
hold off

ans1=size(KEEPMARK);
ansla=ans1(1);

disp('What axes would you like on the movie? [xmin, xmax, ymin, ymax]')
disp('Enter 1 for default to last axis used on AWAL run.')
movieaxis=input(' ');
if movieaxis==1,
    axis(V); % i.e. DEFAULT
else,
    axis([movieaxis(1),movieaxis(2),movieaxis(3),movieaxis(4)]);
        % Axis limits ([xmin, xmax, ymin, ymax])
end
plot(OUTFILE(1,1),OUTFILE(1,2),'o')
xlabel('Downrange distance, x, ft');ylabel('Altitude, h, ft')
L1=sprintf('Delta T = %g',DELTAT);text(.2,.85,L1,'sc')
L2=sprintf('Weight = %g',Wt);text(.2,.8,L2,'sc')

STEPSIZE=5; % Interval of plotting the vehicle's position and pitch attitude

for PT=1:STEPSIZE:ansla;
    % Scale the pitch attitude to the last scale used by main program
    XScaler=(Vkeep(ansla,2)-Vkeep(ansla,1))/(Vkeep(PT,2)-Vkeep(PT,1));
        %to scale pitch attitude line in x direction to last plot coordinates
    dx=KEEPdxdy(PT,1)*XScaler;
    YScaler=(Vkeep(ansla,4)-Vkeep(ansla,3))/(Vkeep(PT,4)-Vkeep(PT,3));
        %to scale pitch attitude line in y direction to last plot coordinates
    dy=KEEPdxdy(PT,2)*YScaler;
    % end scaling
    polymark(OUTFILE(PT,1),OUTFILE(PT,2),'o')
    polyline([OUTFILE(PT,1)-dx OUTFILE(PT,1)+dx]...
        .{OUTFILE(PT,2)-dy OUTFILE(PT,2)+dy},'-w')
        % This shows the vehicle's pitch attitude
end

=====
%-----end program "Movie"-----
=====

```

```

%=====
%-----misc. program "Mplot"-----
%=====

% -----Program Mplot-----
% Program to aid in troubleshooting the control function.
% Simply generates a plot of the Moments about the cg
% due to Wing, canard, vane and pitch damping vs. time.
% Also shows (on another plot) the theta, q and qdot results of
% the control function.
% To use: type "Mplot" at the command carrot.
% LCDR Bob Stoney
% Created 13 SEP 92
clc
hold off
subplot(211)
plot(OUTFILE(:,18),EXTRA(:,11),'-',OUTFILE(:,18),EXTRA(:,12),'--',....
      OUTFILE(:,18),EXTRA(:,13),'*',OUTFILE(:,18),EXTRA(:,14),'o')
xlabel('Time,t,sec');ylabel('MWing- C- V* q oo');grid
title(['Weight=',num2str(Wt),' lbf'])
subplot(212)
plot(OUTFILE(:,18),OUTFILE(:,5),'-',OUTFILE(:,18),OUTFILE(:,14),'--',....
      OUTFILE(:,18),OUTFILE(:,15),':')
xlabel('Time,t,sec');ylabel('theta- q- qdot..');grid
title(['Weight=',num2str(Wt),' lbf'])
pause
%=====
%-----end program "Mplot"-----
%=====

```


%
%-----misc. program "filesaver"-----
%

% "filesaver"...this program is used to save information from
% program AWAl.
% LCDR R.B. Stoney, Naval Postgraduate School
% May 1993

R27=OUTFILE;
R27E=EXTRA;
R27C=CONFIG;
save R27 R27;
save R27E R27E;
save R27C R27C;

```
%=====
%-----misc. program "resurrect"-----
%=====
```

```
% "resurrect"....a program to load the results of a run of program
% AWAI that were saved. See also "filesaver"
% LCDR R.B. Stoney, Naval Postgraduate School
% May 1993
% user: change the number on each line for the appropriate file
% Note: can use "save workspace" if desired but that takes up a LOT
% of memory
```

```
load R24      % "OUTFILE" matrix
load R24C     % "CONFIG" matrix
load R24E     % the "EXTRA" matrix
OUTFILE=R24;
Wt=R24C(1);
disp('File number R24 has been recovered')
```

```
%=====
%-----end program "resurrect"-----
%=====
```

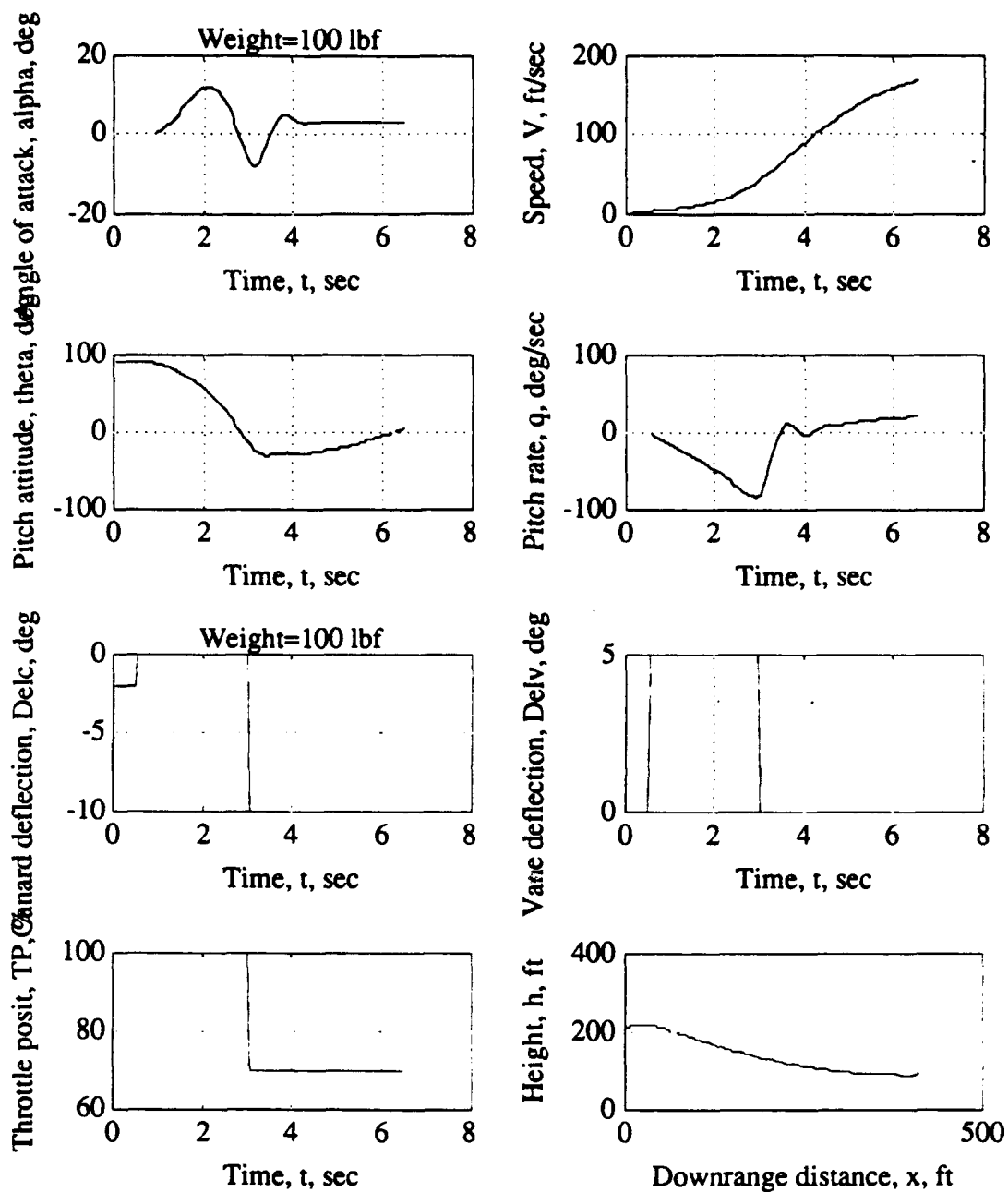


Figure H.1
Archytas simulation "Low vane deflection pushover from hover"

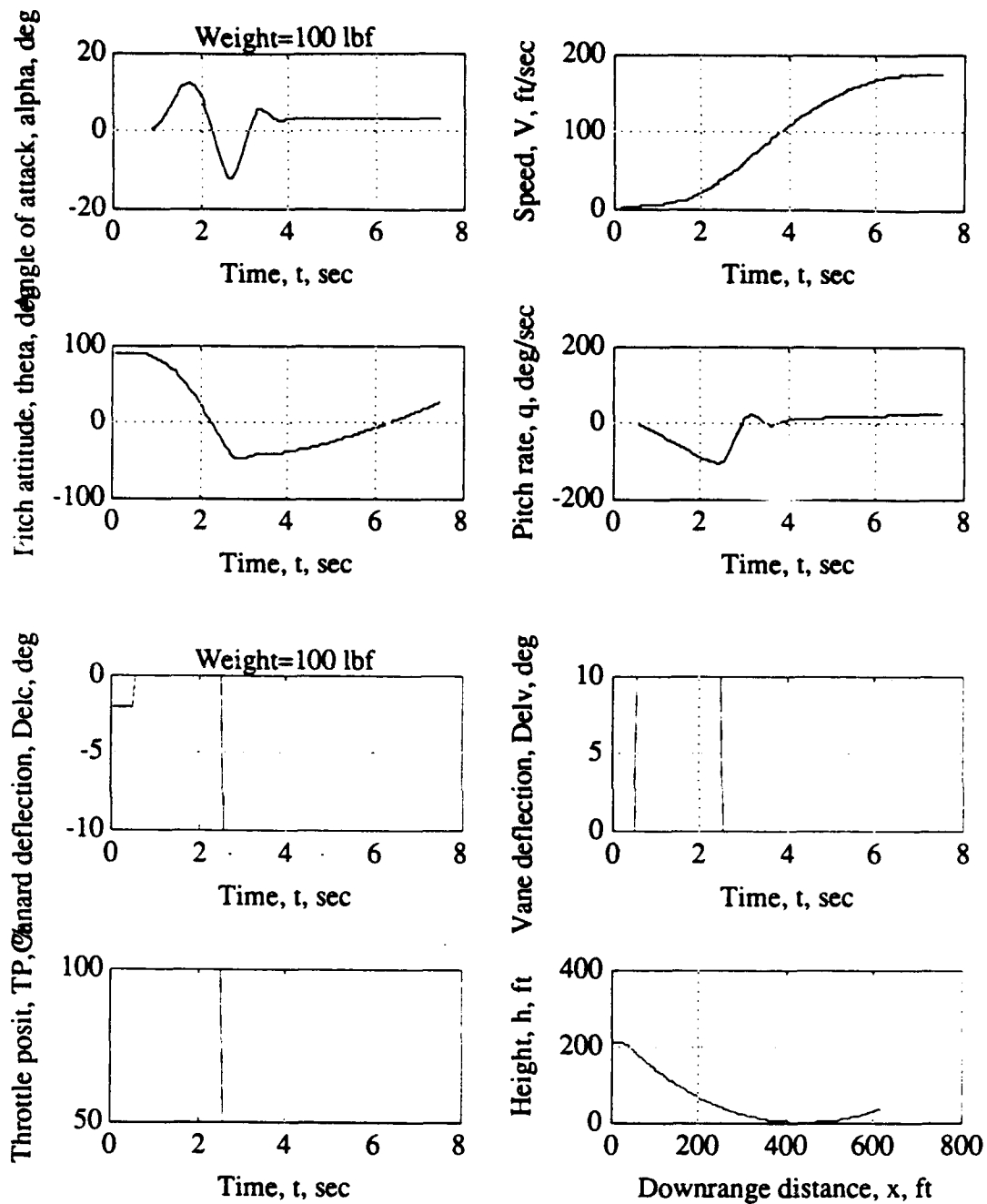


Figure H.2
Archytas simulation: "High vane deflection pushover from hover"

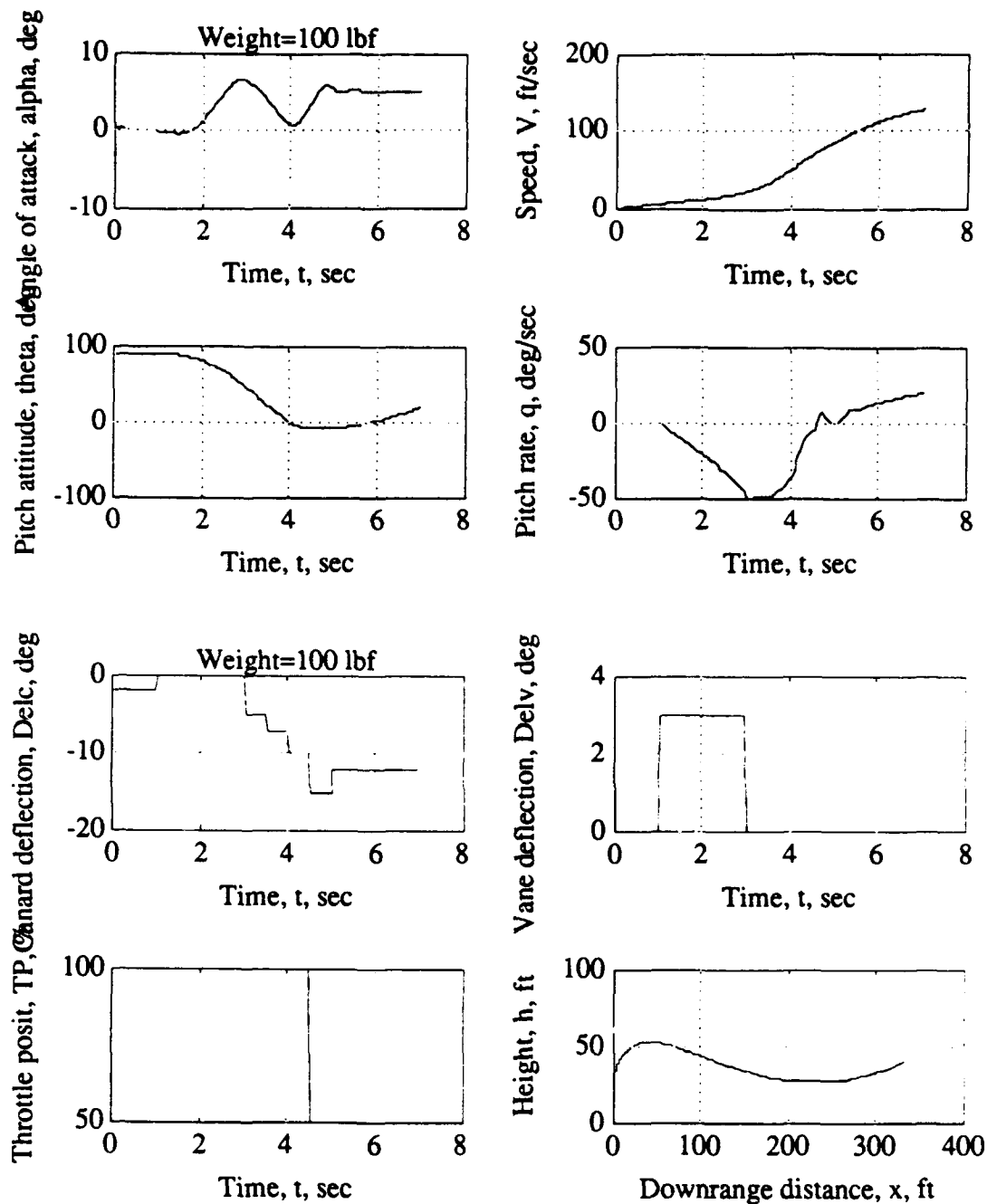


Figure H.3
Archytas simulation: "Low speed, low altitude climbing gentle pushover"

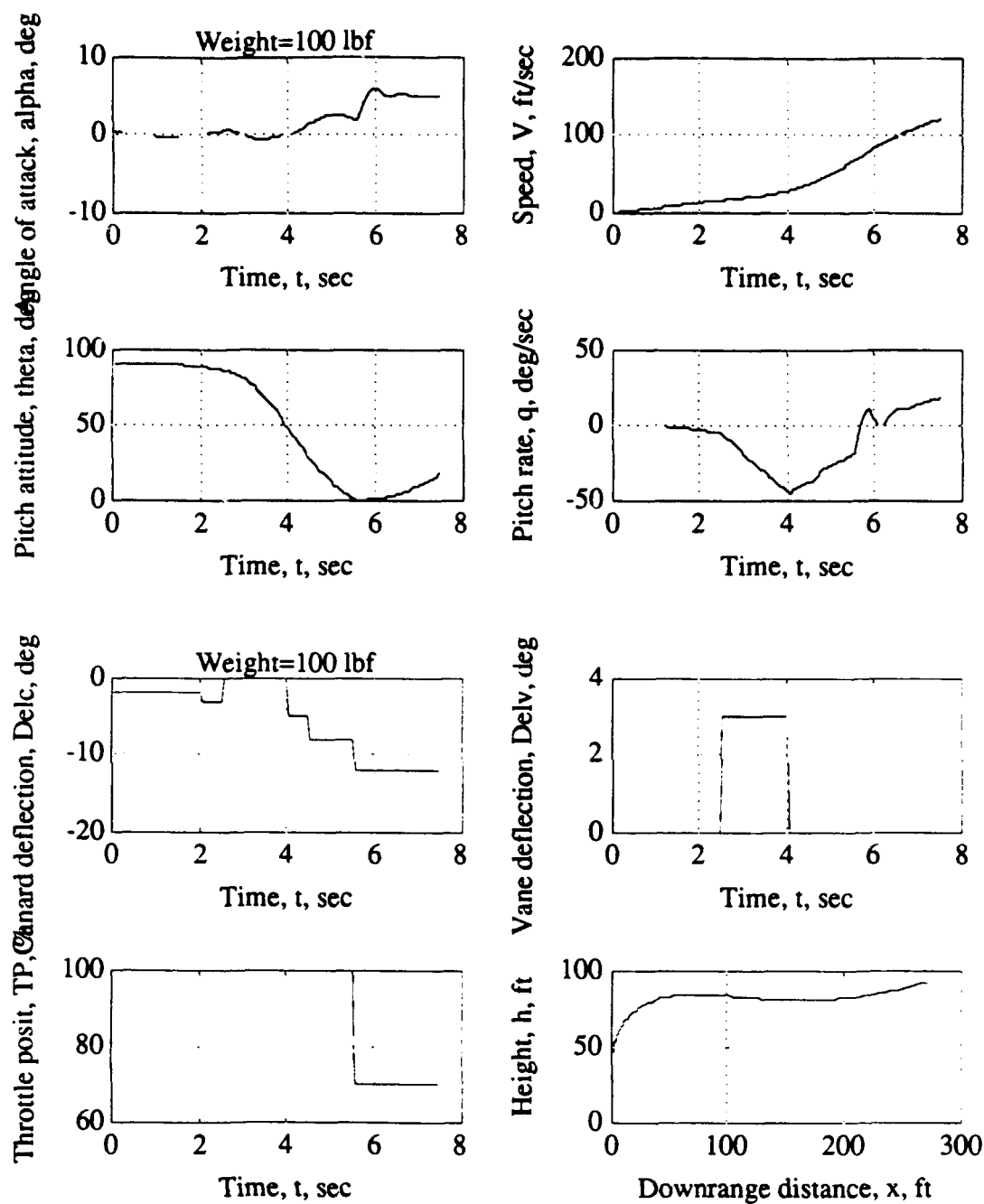


Figure H.4
Archytas simulation: "Vertical acceleration to gentle pushover"

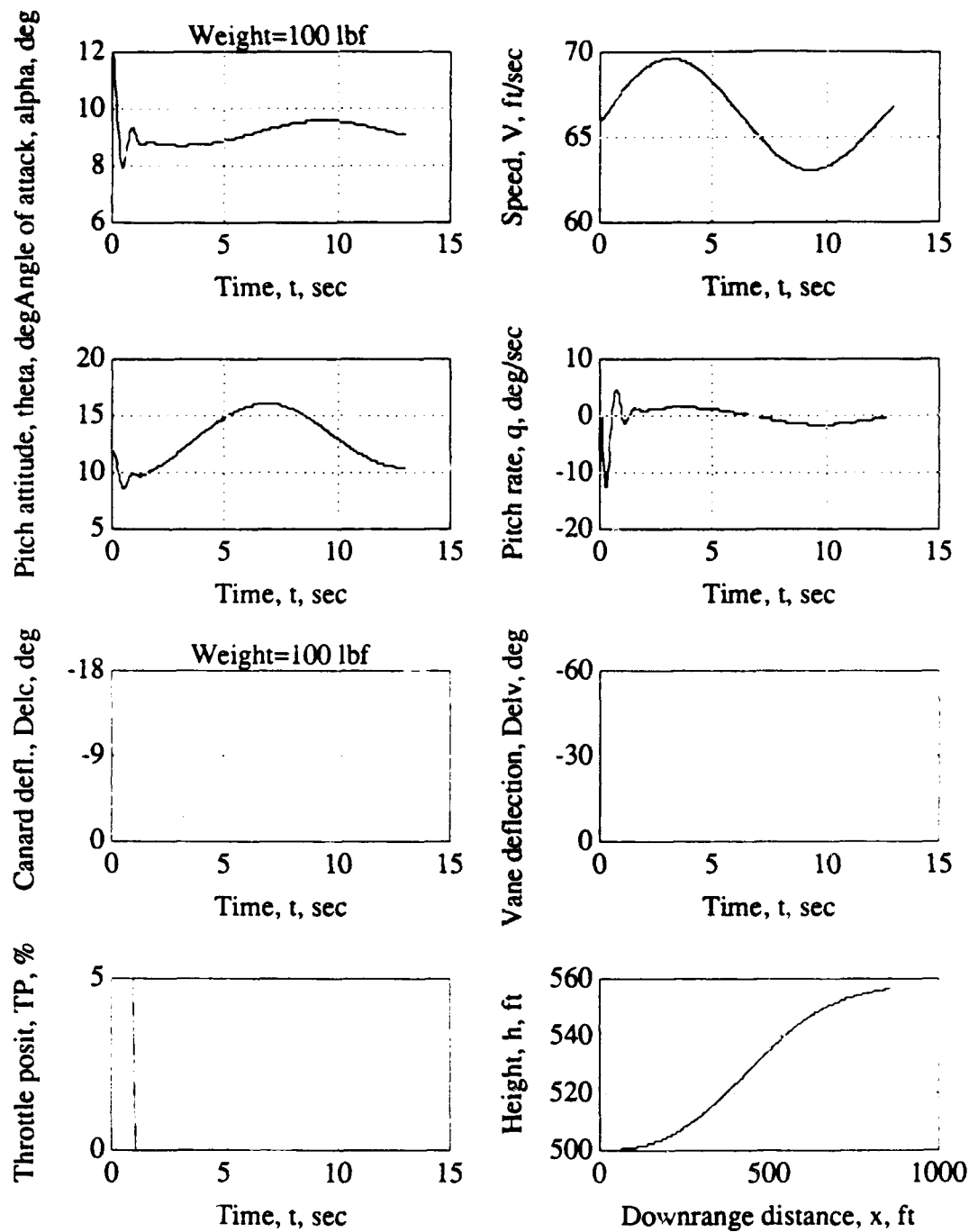


Figure H.5
 Archytas simulation: maximum effort slow flight, unsuccessful
 attempt
 at level transition from horizontal flight to hover

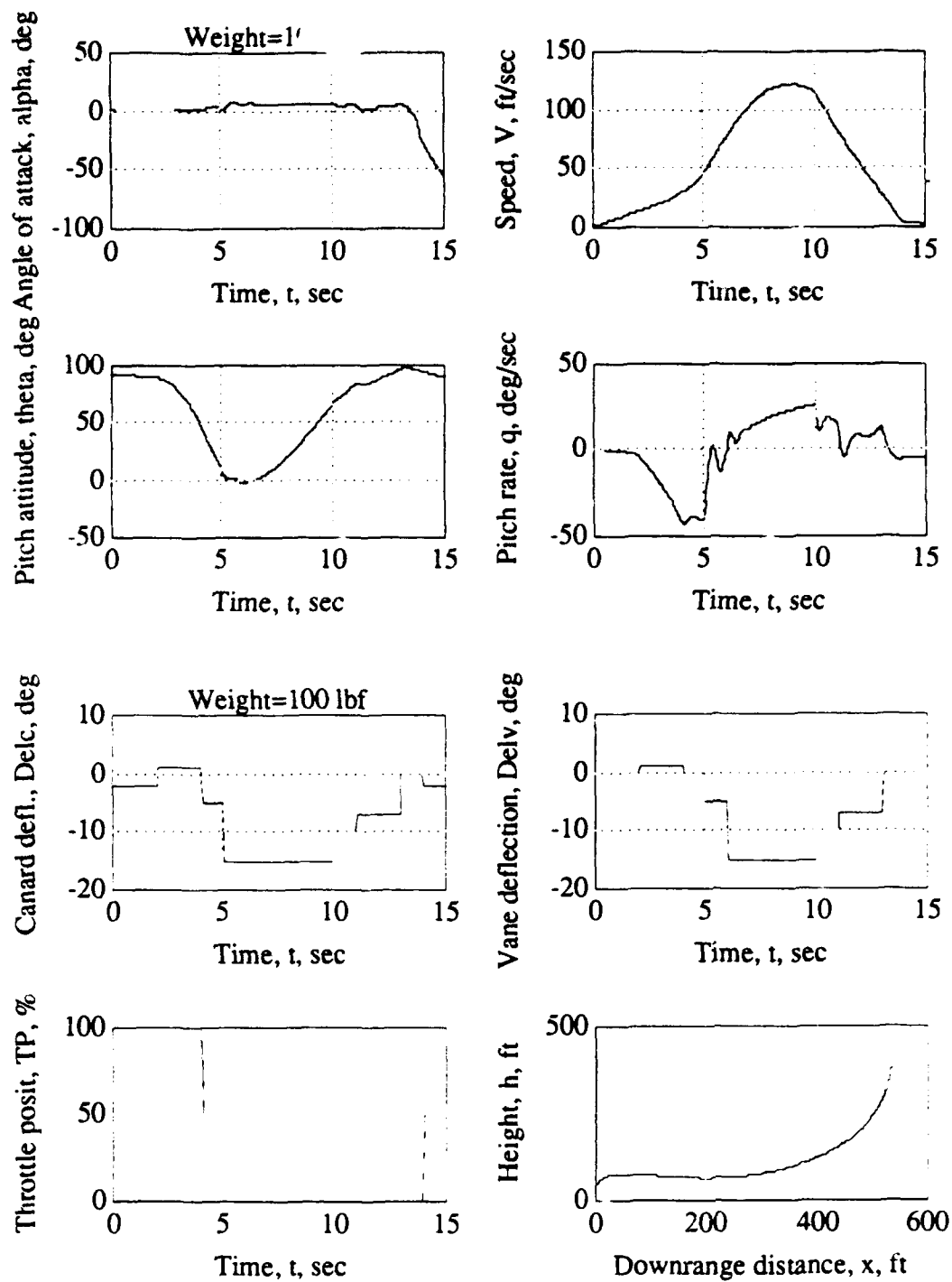


Figure H.6
Archytas simulation: Transition to horizontal flight
followed by "zooming" transition back to hover

INITIAL DISTRIBUTION LIST

	No. Copies
1. Defense Technical Information Center Cameron Station Alexandria, Virginia 22304-6145	2
2. Library, Code 52 Naval Postgraduate School Monterey, California 93943-5002	2
3. Chairman Department of Aeronautics and Astronautics Code AA Naval Postgraduate School Monterey, California 93943-5000	1
4. Walter L. Dixon Unmanned Aerial Vehicle Joint Projects Office Naval Air Systems Command PEO(CU)-UD3 Washington, D.C. 20361-1014	1
5. Mr. Rick J. Foch Naval Research Lab Code 5712 4555 Overlook Ave, S.W. Washington D.C. 20375	1
6. Mr. Doug Murphy Naval Command, Control and Ocean Surveillance Center NRaD, Code 53 San Diego, California 92152-5000	1
7. Mr. Barth Shenk WL/FIMGD Wright-Patterson AFB, Ohio 45433	1
8. Prof. Rick Howard Department of Aeronautics and Astronautics Code AA/Ho Naval Postgraduate School Monterey, California 93943-5000	2
9. Mr. William E. Stoney 4646 O'Connor Court Irving, Texas 75062	1

10. Lieutenant Commander Robert Stoney
Naval Air Systems Command (AIR-09P1)
Washington, D.C. 20361-0903

2